



City Research Online

City, University of London Institutional Repository

Citation: Bejarano Monroy, M. G. (2019). A novel approach to bioelectrical impedance plethysmography for the assessment of arterial and venous circulatory problems in the forearm. (Unpublished Doctoral thesis, City, University of London)

This is the accepted version of the paper.

This version of the publication may differ from the final published version.

Permanent repository link: <https://openaccess.city.ac.uk/id/eprint/24064/>

Link to published version:

Copyright: City Research Online aims to make research outputs of City, University of London available to a wider audience. Copyright and Moral Rights remain with the author(s) and/or copyright holders. URLs from City Research Online may be freely distributed and linked to.

Reuse: Copies of full items can be used for personal research or study, educational, or not-for-profit purposes without prior permission or charge. Provided that the authors, title and full bibliographic details are credited, a hyperlink and/or URL is given for the original metadata page and the content is not changed in any way.

A Novel Approach to Bioelectrical Impedance Plethysmography for the Assessment of Arterial and Venous Circulatory Problems in the Forearm



Mario Guiovanni Bejarano Monroy

School of Mathematics, Computer Science & Engineering
City, University of London

This dissertation is submitted for the degree of
Doctor of Philosophy

December 2019

For my wife [REDACTED] who never gave up on me and was my most significant support during all this time, without her, this work would not be possible. I also dedicate this to my loving family back in Colombia my father [REDACTED] my mother [REDACTED] and my sister [REDACTED] who have been a continue source of inspiration and encouragement.

For our baby, love and strength must come together when you need support. Never give up, keep trying and trying until you achieve your goals. The key of success is perseverance.

Acknowledgements

I would like to express my gratitude to my supervisor Dr. Iasonas Triantis for his continuous support, guidance, knowledge, expert advice, patience and encouragement throughout the period of my research.

I would also convey my thanks and appreciation to my second supervisor Prof. Panayiotis Kyriacou, for sharing his knowledge and experience to complete the experimental procedures to get significant results.

I would like to acknowledge The School of Mathematics, Computer Science and Engineering at City, University of London for financial assistance for this research work. Thanks to its studentship I was able to complete this research, but it is also important to recognise the significant amount of money that the school invested in the new laboratories and equipment which additionally helped me to complete my research

Special appreciation to my family, beginning with my wife [REDACTED] my father [REDACTED] [REDACTED] my mother [REDACTED], my sister [REDACTED] and my parents-in-law [REDACTED] Thank you for their love, help, support and encouragement to complete this work. I am indebted to my parents for all their sacrifices made to secure my education.

Thanks to my friends and colleagues in the Research Centre for Biomedical Engineering for all their advice and sharing and learning knowledge amid this time. Your remarks, comments and feedback were entirely helpful to complete this work. Special gratefulness to my friend [REDACTED] who was always there, to listen, to assist and give any advice when needed.

Mario Guiovanni Bejarano Monroy



Declaration

I hereby declare that the work presented in this thesis is my own work. Any idea, result, or illustration originating from other subjects' work has been acknowledged in the text by referencing to the original author. This thesis has never been published or submitted elsewhere for obtaining an academic degree or professional qualification.

I grant power of discretion to the Librarian at City University of London to allow the thesis to be copied in whole or in part without further reference to the author. This permission covers only single copies made for study purposes, subject to normal conditions of acknowledgement.

Mario Guiovanni Bejarano Monroy

December 2019

Abstract

Peripheral vascular disease (PVD) and/or peripheral arterial disease (PAD) are sicknesses known to inadequate delivery of either arterial or venous blood towards the extremities. Such sickness may trigger complications owing to the lack of transport of oxygen and nutrients, thus causing hypoxic events that may eventually prompt to ischaemic tissue or even the loss of the compromised limb. One of the most prominent indicators of prosperous health is blood volume and flow. The basic information within these health parameters may show cardiovascular problems or the advance of further complications related to other diseases like diabetes. In clinical setting, there effective methods to measure these parameters like Doppler ultrasound, photoplethysmography or venous occlusion plethysmography.

These methods take measurements from either single vessels and/or small volume of tissue. However, it is difficult to establish a relation between the obstruction of arterial and/or venous circulation and the amount of blood received by the tissue. Bioelectrical impedance plethysmography (iPG) measures blood changes by driving a small amount of AC current into the body and after measuring the potential created by fluids flowing through tissue. This technique apart from taking measures within defined volumes of tissue, it is easy to use as only needs four electrodes on the skin.

Hence, a bespoke bioelectrical impedance device including hardware and software was built ready to measure changes in blood volume/flow in the upper limbs. The system was assessed in an in-vivo controlled environment with 8 participants. The blood flow towards their left arms was altered by constricting the upper arm with a cuff at three levels: 1) below venous pressure 2) amongst venous and arterial pressure and 3) during total occlusion. Simultaneously, measurements from various instruments like ECG, Doppler ultrasound, laser Doppler flowmetry and PPG were taken and compared to the measurements obtained from the iPG instrument and defining its correlation with the impedimetric signal.

The results from the experiments showed that the bioelectrical impedance signal changed in basal and arterial pulses showing specific characteristics for each kind of occlusion. The data indicated that it is possible to differentiate between a venous and arterial occlusion by examining both components of the impedance signal. The impedance during venous occlusion dropped in average 0.658 ± 0.230 % from the baseline. On the other hand, during arterial occlusion the base impedance dropped in a higher rate approximately 1.13 ± 0.82 %, indicating a differentiator during both type of blood flow disruption. Furthermore, the impedance plethysmography waveform morphology also reshaped during these occlusive periods. The whole waveform during artificial venous obstruction increased in magnitude, the systolic peak rose 31.80 %, the dicrotic notch 47.73 % and the diastolic point 31.92 %, where the value of the latter was higher than the dicrotic notch point. In contrast, in the time of partial arterial occlusion the waveform also increased in size at all these points, but its shape was altered. The impedance magnitude at the diastolic point went below the ones at the dicrotic notch. These fluctuations provided additional further information that it might be possible to differentiate amongst venous and arterial occlusions. By consolidating the data obtained by the iPG device, it is possible to produce an index ratio between the basal impedance and these three reference points which may help to identify early circulatory problems in the arterial and/or venous systems.

Table of contents

List of figures	xvii
List of tables	xxi
Nomenclature	xxiii
1 Introduction	1
1.1 Methods for measuring blood flow and volume	1
1.1.1 Bioelectrical impedance plethysmography	3
1.1.2 The need of a method to assess arterial and venous problems	5
1.2 Motivation of the thesis and project aims	6
1.3 Novelty and contribution of the thesis	7
1.4 Work done	7
1.5 Organisation of the thesis	8
2 Principles of Plethysmography and Plethysmographic Methods	11
2.1 Origin of the plethysmography signal in the circulatory system	12
2.2 Problems derived from poor blood delivery	16
2.2.1 Ischaemia	16
2.2.2 Hypoxia	17
2.3 Diseases derived from poor blood delivery	18
2.3.1 Peripheral vascular disease	18
2.3.2 Compartment syndrome	19
2.3.3 Diabetic foot infection	20
2.3.4 Upper extremity venous occlusion	20

Table of contents

2.4	Clinical assessment of peripheral vascular diseases	21
2.5	Methods to measure blood flow and volume	23
2.5.1	Doppler ultrasound	23
2.5.2	Optical methods measuring blood volume and flow	25
2.5.2.1	Photoplethysmography	26
2.5.2.2	Laser Doppler Flowmetry	27
2.5.2.3	Laser speckle contrast imaging (LSCI)	28
2.5.3	Additional methods to measure limb plethysmography and blood flow	30
2.5.3.1	Air/Water plethysmography	30
2.5.3.2	Strain gauge plethysmography	31
2.5.3.3	Bioelectrical Impedance plethysmography	32
2.5.4	Comparison of the different methods	34
2.6	Conclusion	37
3	Bioelectrical impedance plethysmography	39
3.1	Electrical current in the human body	40
3.2	Electrical impedance principle	42
3.3	Current distribution in conductors (Geselowitz theorem)	45
3.4	Electrode-skin interface	47
3.4.1	Analysis of tetrapolar electrode configuration	49
3.5	Bioelectrical impedance	51
3.5.1	Mathematical representation of electrical impedance	55
3.6	State of the art of commercial bioelectrical impedance devices	56
3.7	Basic components of a bioelectrical impedance device	59
3.7.1	Methods of measuring bioelectrical impedance	61
3.8	The principle of bioelectrical impedance plethysmography	64
3.8.1	Alternative applications of impedance plethysmography	66
3.9	Impedance plethysmography in the forearm	68
3.9.1	Blood contribution to impedance	71
3.9.2	Impedance plethysmography waveforms	73
3.9.2.1	Basal impedance	73
3.9.2.2	Venous occlusion plethysmography	75
3.9.2.3	Arterial pulse amplitude	75
3.10	Conclusion	76

4	Method and protocols	77
4.1	Design of a bioelectrical impedance plethysmography device	77
4.1.1	Electrodes topology and location	78
4.1.2	Bioelectrical impedance device modules	79
4.1.2.1	Power supply module	80
4.1.2.2	Direct digital synthesis (DDS) module	82
4.1.2.3	Differential amplifier gain module	82
4.1.2.4	Modified Howland Amplifier module	83
4.1.2.5	Current and voltage sensing module	85
4.1.2.6	Envelope detection and AC extraction circuit module	86
4.2	Experimental Procedure	87
4.2.1	Instruments set-up	88
4.2.2	Physiological measurements	90
4.2.3	Experimental protocol	91
4.2.3.1	Blood flow occlusion protocol	92
4.3	Data processing	94
4.3.1	Data conversion	95
4.3.1.1	Calculation of the basal impedance value	95
4.3.1.2	Calculation of the Arterial Pulse Amplitude value	97
4.3.1.3	Converting ultrasound to flow	98
4.3.1.4	Converting LDF	100
4.3.1.5	Volume and flow calculation beat by beat from iPG signal	101
4.4	Conclusion	103
5	Investigation of changes of the basal impedance signal	105
5.1	Basal impedance measurements during baseline	105
5.1.1	Deviation of the basal impedance from baseline	109
5.1.2	Confidence interval of the basal impedance baseline	110
5.2	Change of basal impedance during occlusions	111
5.2.1	Basal impedance shift during venous occlusion	112
5.2.2	Basal impedance change during partial arterial occlusion	115
5.2.3	Basal impedance variation during total occlusion	119
5.3	Conclusion	123

Table of contents

6	Research of the shape changes of the arterial pulses during proximal occlusions	125
6.1	Reference points and algorithm for the arterial pulse amplitude analysis . . .	126
6.2	Changes of the plethysmography waveform during different occlusions . . .	129
6.2.1	Plethysmography waveform change during venous occlusion	129
6.2.1.1	Changes in systolic peak (Point A)	129
6.2.1.2	Changes in diastolic peak (Point B)	131
6.2.1.3	Changes in diastolic peak (Point C)	132
6.2.2	Plethysmography waveform change during partial arterial occlusion	132
6.2.2.1	Changes in systolic peak (Point A)	134
6.2.2.2	Changes in diastolic peak (Point B)	134
6.2.2.3	Changes in diastolic peak (Point C)	135
6.2.3	Plethysmography waveform variation during total occlusion	136
6.3	Novel evaluation of blood obstructions using iPG baseline over APA waveforms	138
6.3.1	Analysis of the novel index ratio between the three different levels of occlusion	142
6.4	Conclusions	145
7	Quantification and correlation of iPG, Doppler Ultrasound, LDF and PPG	147
7.1	Quantification of the measurements of the devices	148
7.1.1	Measurements from the ECG device	148
7.1.2	Blood flow calculation from arterial pulses signal	149
7.1.2.1	Blood flow quantification and analysis during occlusion .	152
7.1.3	Blood flow estimation from Doppler ultrasound instrument	154
7.1.3.1	Blood flow estimation from Doppler Ultrasound instrument	155
7.1.4	Measurements from Laser Doppler Flowmetry	156
7.1.5	Measurements from the PPG Red-light signal	158
7.1.5.1	Changes in the DC component of the signal	160
7.1.5.2	Changes in the AC component of the signal	161
7.2	Correlations of the iPG amplitude wave and Doppler ultrasound, PPG and LDF	162
7.2.1	Analysis of the heartbeat detection in the frequency domain	163
7.2.2	Correlation between iPG and Doppler ultrasound	165
7.2.3	Correlation between iPG and PPG	168
7.2.4	Correlation between iPG and LDF	171
7.3	Summary of the changes and correlations	173
7.4	Conclusion	174

8	General conclusion and future work	177
8.1	Future work	179
8.1.1	Improvements of the iPG device	179
8.1.2	Waveform analysis under different conditions	180
	References	181
	Appendix A Final assembly circuit	199
	Appendix B Schematics of the iPG instrument	201
	Appendix C Arduino program to control DDS AD5930	219

List of figures

1.1	Basic bioelectrical impedance illustration	3
2.1	Common pressures in different parts of the systemic and pulmonary circulation	13
2.2	Common flow and volume waveforms	15
2.3	Doppler ultrasound instrument	24
2.4	Doppler technique to measure flow	24
2.5	PPG sensors placements as transmission and reflectance modes	26
2.6	Laser Doppler flowmetry theory overview	28
2.7	Setup of a Laser speckle contrast imaging	29
2.8	Air plethysmography method	31
2.9	Strain gauge plethysmography	32
3.1	Threshold current sensation vs. frequency	40
3.2	Schematic representation of electrical impedance	42
3.3	Complex representation of impedance	43
3.4	Impedance waveforms	44
3.5	Volume conductor with 4 electrodes	46
3.6	Equivalent circuit of the electrode-tissue interface	48
3.7	Tetrapolar electrodes position and equivalent circuit	50
3.8	Cell permeability and conductivity distribution	52
3.9	Electrical model of the cell	53
3.10	Dielectric response of a cell against frequency	54
3.11	Block diagram of a common bioelectrical impedance device	59
3.12	Circuit of stray capacitances at the output of the current source	60
3.13	Two compartment cylinder model	64

List of figures

3.14	Pulse wave velocity between two different points using bioelectrical impedance	69
3.15	Electrodes distribution in tetrapolar configuration	70
3.16	Impedance plethysmography waveform from an AC source	72
3.17	Impedance plethysmography waveforms	74
4.1	Bioelectrical impedance device design concept	79
4.2	Block diagram of the bioelectrical impedance plethysmography device	81
4.3	Modified Howland circuit schematic	83
4.4	Current sensing circuit schematic	85
4.5	Envelope detection circuit schematic	86
4.6	Instruments position in the forearm during the experiment procedure	89
4.7	Pressure levels applied to the arm and description of regions during the experiment	94
4.8	Matlab application graphic user interface	96
4.9	APA waveform representation.	101
5.1	Measurements of the basal impedance during the whole study	107
5.2	Mean basal impedance box plot	108
5.3	Percentile change of baseline impedance	109
5.4	Confidence interval of the baseline impedance	111
5.5	Impedance change during venous occlusion	113
5.6	Percentile variation of impedance during venous occlusion	113
5.7	Impedance change rate per 10 heartbeats during venous occlusion	115
5.8	Impedance change during partial arterial occlusion	117
5.9	Percentile variation of impedance during partial arterial occlusion	117
5.10	Impedance change rate per 10 heartbeats during partial arterial occlusion	119
5.11	Impedance change during total occlusion	121
5.12	Percentile variation of impedance during total occlusion	121
5.13	Impedance change rate per 10 heartbeats during total occlusion	122
6.1	Marker points in an iPG waveform	127
6.2	Plethysmography waveform of the participant seven between baseline and venous occlusion	130
6.3	Changes of the impedance peak values during baseline, venous occlusion and return to baseline for points A,B and C.	130

6.4	Plethysmography waveform of the participant seven between baseline and partial arterial occlusion	133
6.5	Changes of the impedance peak values during baseline, partial arterial occlusion and return to baseline for points A,B and C.	133
6.6	Plethysmography waveform of the participant seven between baseline and total occlusion	137
6.7	Changes of the impedance peak values during baseline, total occlusion and return to baseline for points A,B and C.	137
6.8	Representation of the novel index ratio of the impedance plethysmography waveform during the whole experiment	141
6.9	Bar graph of the index ratio i_z for every point during every occlusion	143
7.1	ECG measurement acquired by the system	148
7.2	Blood flow calculated from the impedance plethysmography waveform during the whole experiment	150
7.3	Blood flow calculated from Doppler ultrasound device all along the experiment	154
7.4	Results of the LDF in BPU	157
7.5	PPG red wavelength measurements, AC and DC components	159
7.6	Fequency components of the signals acquired	164
7.7	Bland and Altman plot of the relation between Doppler ultrasound and iPG	167
7.8	Bland and Altman plot of the relation between PPG and iPG	170
7.9	Bland and Altman plot of the relation between LDF and iPG	172
A.1	Assembly of the bioelectrical impedance device	200
B.1	Top-up view of the power supply	202
B.2	Schematic of the 12 V voltage regulator	203
B.3	Schematic of the -12 V voltage regulator	204
B.4	Schematic of the 5 V voltage regulator	205
B.5	Schematic of the Power supply of the DDS	206
B.6	Direct digital synthesis circuit schematic	207
B.7	Schematic of the differential gain amplifier circuit	208
B.8	Positive power supply (6 V) for the differential amplifier	209
B.9	Negative power supply (−6 V) for the differential amplifier	210
B.10	Positive power supply (5 V) for the modified Howland circuit	211
B.11	Negative power supply (−5 V) for the modified Howland circuit	212

List of figures

B.12 Schematic of the differential gain amplifier circuit	213
B.13 Schematic of the voltage sense circuit	214
B.14 Top-up schematic of the envelope detector circuits	215
B.15 Envelope detector of the current channel	216
B.16 Envelope detector of the voltage channels	218

List of tables

1.1	Comparative table of techniques/methods that measure blood volume/flow	4
2.1	Hypoxia classification	17
2.2	Leriche-Fontaine classification	22
2.3	Comparison of the different methods to measure bioelectrical impedance	35
3.1	Effect of electric current in the human body	41
3.2	Commercial devices for measuring bioelectrical impedance plethysmography	58
3.3	Comparison of the different methods to measure bioelectrical impedance	62
4.1	Components of the Power Supply and its functions	80
4.2	Instruments used during the study and measurements taken	88
4.3	Participants' age, sex and forearm measurements	90
4.4	Participants' forearm dimensions and initial total volume	91
4.5	Participants' blood pressure and occlusion levels	93
5.1	Mean and range of the impedance change for each participant	110
5.2	Statistical analysis of the percentile change of impedance during venous occlusion	114
5.3	Statistical analysis of the percentile change of impedance during partial arterial occlusion	118
5.4	Statistical analysis of the percentile change of impedance during total occlusion	122
6.1	Markers on the APA waveform	127
6.2	Total amount of iPG waves detected by the algorithm	128

List of tables

6.3	Change of amplitude of the waveform at point A during the transition baseline-venous occlusion-baseline.	131
6.4	Change of amplitude of the waveform at point B during the transition baseline-venous occlusion-baseline.	131
6.5	Change of amplitude of the waveform at point C during the transition baseline-venous occlusion-baseline.	132
6.6	Change of amplitude of the waveform at point A during the transition baseline-partial arterial occlusion-baseline.	134
6.7	Change of amplitude of the waveform at point B during the transition baseline-partial arterial occlusion-baseline.	135
6.8	Change of amplitude of the waveform at point C during the transition baseline-partial arterial occlusion-baseline.	136
6.9	Index ratio i_Z for baseline, venous occlusion, partial arterial occlusion and total occlusion	144
7.1	Median blood flow calculated from the iPG APA waveform	152
7.2	Mean blood flow calculated from the Doppler Ultrasound	156
7.3	Calculated median perfusion index (BPU) from the LDF device	158
7.4	Mean peak value of the PPG DC signal for all participants in all regions . . .	160
7.5	Mean peak value of the PPG AC signal for all participants in all regions . . .	161
7.6	Peak frequency obtained from Fast Fourier Transform	165
7.7	Summary of the change of clinical values during occlusion of the different instruments	173

Nomenclature

Greek Symbols

ε	Permittivity of a material
ϕ	Angular phase shift / Potential field
μ	Viscosity of a medium
π	$\simeq 3.14\dots$
ρ	Resistivity of a material / Blood resistivity $\simeq 150 \Omega \text{cm}^{-1}$
σ	Conductivity of a material
θ	Angle of incidence
ω	Angular frequency in radians, equivalent to 2π

Acronyms / Abbreviations

ABI	Ankle-Brachial index
AC	Analogue Current
ADC	Analogue to digital converter
ALS	Amyotrophic lateral sclerosis
APA	Arterial pulse amplitude
ATP	Adenosine Triphosphate

Nomenclature

BA	Bland and Altman analysis
BIA	Bioelectrical impedance analysis
BI	Basal impedance
BLM	Bilayer lipid membrane
BPU	Blood Perfusion Unit
C	Speed of sound
CCD	Charge Coupled Device
CLI	Critical Limb Ischaemia
CMMR	Common Mode Rejection
CO	Cardiac output
CVI	Chronic peripheral venous insufficiency
CVP	Central venous pressure
DAQ	Data Acquisition Card
DC	Direct Current
DDS	Direct Digital Synthesis
DGA	Differential Gain Amplifier
DLC	Dual layer capacitance
DSP	Digital signal processors
DU	Doppler ultrasound
DVT	Deep vein thrombosis
ECG	Electrocardiography
FFT	Fast Fourier Transform
ECW	Extracellular water

EIS	Electrical impedance spectroscopy
EM	Electromagnetic
FFM	Free-fat mass
GND	Ground Point
GSR	Galvanic impedance response
GUI	Graphic User Interface
Hb	Haemoglobin
HPF	High-Pass Filter
ICG	Impedance cardiography
IC	Integral Circuit
ICW	Intracellular water
IEC	International Electrotechnical Commission
In-Amp	Instrumentation Amplifier
iPG	Impedance Plethysmography
LDF	Laser Doppler Flowmetry
LED	Light emitting diode
PCB	Printed Circuit Board
LSCI	Laser speckle contrast imaging
LVM	LabVIEW Measurement file format
MHC	Modified Howland Circuit
NIRS	Near-infrared spectroscopy
Op-Amp	Operational Amplifier
PAD	Peripheral Arterial Disease

Nomenclature

PAO	Partial arterial occlusion
PDF	Probability density function
PI	Perfusion Index
PPG	Photoplethysmography
PTT	Pulse transit time
PVD	Peripheral vascular disease
PVT	Proximal vein thrombosis
PWV	Pulse Wave Velocity
RBC	Red Blood Cells
RBI	Resting baseline impedance
RC	Resistor Capacitor
RF	Radio frequency
RMS	Root mean square
SGP	Strain gauge plethysmography
SPI	Serial Peripheral Interface Bus
SPST	Single Pole Single Throw
SVR	Systemic vascular resistance
SV	Stroke Volume
TBW	Total body water
TO	Total Occlusion
USB	Universal Serial Bus
VOP	Venous occlusion plethysmography
VO	Venous occlusion

Introduction

Peripheral vascular disease (PVD) and/or peripheral arterial disease (PAD) [1] are illnesses that affects blood vessels when these narrow, block or spasm. It could affect both either veins or arteries, thus the two different names. This blood circulation disorder can be attributed to hereditary factors or lifestyle choices; when combined with other risk factors such as diabetes or smoking, the chances of contracting the disease increase drastically, making frequent clinical visits for diagnostic tests imperative. An inadequate delivery of blood towards the extremities may trigger complications owing to the lack of transport of oxygen and nutrients, thus causing hypoxic events that may eventually lead to ischaemic tissue. If left untreated, this illness may result in the loss of the compromised limb.

Blood volume and flow [2] is one of the most valuable indicators of good health not only in extremities but in the general body. The underlying information within these health parameters may indicate cardiovascular problems or the progress of further complications pertaining to other diseases such as diabetes. Currently, there are methods that can measure changes of blood flow or volume in the extremities. However, most of these techniques estimate the instant flow or change of volume in a vessel or in a small volume of tissue. The information provided by these instruments is valuable but it misses to judge good perfusion towards vast amount of tissue, like in large muscles.

1.1 Methods for measuring blood flow and volume

Blood delivery towards a limb can be estimated by measuring either the change of blood volume or flow rate. In the clinical setting, both parameters are widely-used aid methods to examine critical problems in the periphery [3, 4]. In this regard, one of the most popular

Introduction

ways is instruments based on the Doppler technique. The instruments can be applied using ultrasound [5] or optical [6] methods which, blood volume/flow can be estimated. One of the disadvantages of the Doppler method is that necessitates specific skills to place the sensor correctly, often leading to erroneous outcomes if the sensor is even slightly misplaced. Moreover, it measures a single point only, focusing on an artery, vein or micro-circulation.

Devices involving optical techniques are widely available to measure changes of volume, also known as plethysmography. Moreover, optical sensors can uncover useful information about the absorption of oxygen in the deep tissue within an area of the body [7]. Qualitatively, blood flow rate can be estimated when using light in the near-infrared spectrum (NIRS) [8–11] or the speed of movement of red cells with Laser Doppler techniques [6, 12]. The use of light is quite useful in home or low resource setting, although its penetration can be quite superficial around the muscle tissue [13]. The lack of depth is one of the main limitations of this method; furthermore, the volume of the tissue being monitored is quite small or shallow [13]. Moreover, it is not feasible to accommodate large volumes or deep tissue measurements. New approaches including NIRS and optical imaging techniques look promising in the context of overcoming these drawbacks. Indeed, a system referred to as Laser speckle contrast imaging (LSCI) is a suitable candidate to estimate blood circulation to a more comprehensive area of tissue with an adequate representation on a screen [14]. However, the signal obtained is merely from the surface of the skin. Having a measurement from over a large would reduce the need for multiple and accurate point measurements, thereby obviating the need of a skilled user for such a diagnostic device.

Venous occlusion plethysmography (VOP) is another known method to assess circulatory problems in the periphery. This technique is primarily used to examine issues in the venous system by occluding on the upper section of the extremity. Performing this action blocks the return of venous blood into the heart by increasing the volume of the limb. By measuring and analysing this enlargement, it becomes possible to gather information about blood flow and the health of the veins in that specific part of the body [15]. Thus, this method requires two devices one that blocks veins like a pneumatic cuff, and an instrument to measure plethysmography. The latter can be achieved by availing different technologies such as the chambers of air/water or strain gauges. Nonetheless, using a chamber to measure plethysmography in a home setting can be quite cumbersome. Positioning the arm in a tight cylinder filled with air or water and using the other hand to accommodate other instruments is incongruous with the principle of usability of a home device. Meanwhile strain gauges could be another viable option, but some sensors are filled with mercury, which is highly toxic. Some strain gauges can use another type of electrodes, but they are just confined to

1.1 Methods for measuring blood flow and volume

a small volume of tissue. Additionally, there are instances where a pressure cuff cannot be used in a patient. For instance, people with a ulnar nerve compression [16] and superficial phlebitis [17]. In such special cases, it is imperative to monitor changes of blood without obstructing the normal blood flow towards the extremity.

1.1.1 Bioelectrical impedance plethysmography

Bioelectrical impedance denotes a technique that can perform plethysmography measurement and also detects arterial pulses waveform. In entirety, this method is called bioelectrical impedance plethysmography, or simply impedance plethysmography (iPG). It measures the changes of blood volume by injecting a tiny amount of AC current into the body and subsequently measuring the potential created by blood flow [18] as shown on figure 1.1. One of the advantages of this technique is that it can measure a larger volume of tissue, as opposed to a single vessel or superficial body part. A pair of electrodes is enough to drive current, with another couple measuring the voltage drop in any part of the body. Using the measurement of current and potential, it is possible to calculate the impedance of the segment of the body contained within these electrodes. The table 1.1 provides a more descriptive information about the type of measurements that the method can provide as well as advantages and disadvantages.

The data sourced from bioelectrical impedance plethysmography is quite rich and informative about circulatory problems. From this technology, different methods have been developed to estimate plethysmography, blood flow and cardiac output. Some of these methods may require the use of venous occlusion plethysmography or an analysis of the arterial pulse waveform. Regardless of the technique, iPG has proven to be a useful tool to investigate circulatory problems in the extremities [18–24]

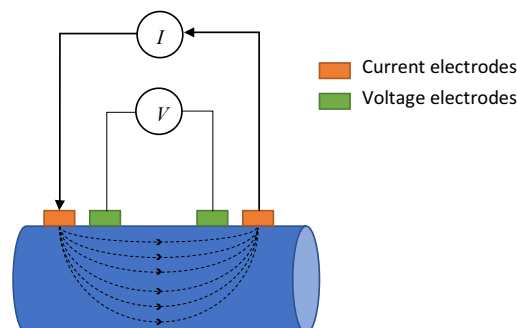


Figure 1.1 Bioelectrical impedance plethysmography measures changes in volume. The cylinder represents a section of limb. Taking a measurement requires electrical current and manuring the potential through it.

Table 1.1 Advantage and disadvantages of technologies or methods that measure blood volume or flow

Instrument/Technique	Measure	Advantage	Disadvantage
Doppler Ultrasound and Optical	<ul style="list-style-type: none"> • Blood velocity • Instant blood flow estimation 	<ul style="list-style-type: none"> • Non-invasive • Portable • Low energy consumption 	<ul style="list-style-type: none"> • Skilled operation • Single vessel measurement • Low depth penetration
Photoplethysmography (PPG)	<ul style="list-style-type: none"> • Blood volume • NIRS (blood flow estimation) 	<ul style="list-style-type: none"> • Non-invasive • Easy to use • High fidelity 	<ul style="list-style-type: none"> • Small volume of tissue measurement • Localised measurement
Venous occlusion plethysmography	<ul style="list-style-type: none"> • Changes of blood volume • Blood flow estimation 	<ul style="list-style-type: none"> • Non-invasive 	<ul style="list-style-type: none"> • Requires multiple instruments • Cumbersome • Skill operation
Bioelectrical Impedance	<ul style="list-style-type: none"> • Blood volume • Blood flow estimation 	<ul style="list-style-type: none"> • Non-invasive • Portable • Low energy consumption • Easy to use • Measures large volumes of tissue 	<ul style="list-style-type: none"> • Signal close to noise floor

1.1.2 The need of a method to assess arterial and venous problems

Measuring the amount of blood that flows into a known volume of tissue allows understanding if this is being perfused properly [20–22]. If variations in the delivery of arterial or return of venous blood were detected, it will be possible to minimise the time on assessing a patient and recommend a treatment to follow. As can be seen in table 1.1 there are methods that are used to detect changes in blood in specific vessels or concealed volumes of tissue. This kind of measurements only provide information of arterial flow and/or microcirculatory changes. However, there is not a single device technique that provides data to analyse the changes of arterial or venous blood in a larger volume of tissue continuously.

Providing information on which circulatory path might be blocked will allow taking preventive measurements when a population falls within recognised risk factors. Hence, monitoring changes of either circulation continuously not only provides early diagnostic but also detecting variations in tissue health might grant early pointers in the progress of a circulatory illness. The combination of detecting disturbance on the circulation, indicating if the problem is located in either arterial or venous path and the health of the perfused tissue would be of vital importance accelerating the implementation of corrective actions before any complication. For this reason, a system that continuously monitors and detects changes of blood or volume would provide further actionable information in order to facilitate better decisions for preventive treatments.

Bioelectrical impedance has been acknowledged to give information about the health of tissue by correlating total impedance with the healthiness of tissue. Different experimental settings demonstrated that changes in the basal impedance are related to perfusion of tissue. If the tissue is not properly nourished with blood, its basal impedance tends to increase as there are not enough ions to promote electric conduction. Additionally, bioelectrical impedance also contains a waveform that is synchronous with arterial pulsations. This signal is known to be related to the amount of blood being pumped through the volume of tissue being sensed. Previous studies demonstrated a correlation between the impedimetric signal amplitude and blood flow, indicating that bioelectrical impedance can quantify tissue perfusion. Moreover, the analysis of the waveform morphology has been used in previous studies to analyse the development of lymphedema in a female population.

Hitherto, most of the efforts have been centred in analysing the basal and arterial amplitude impedance separately. In this project, a novel method to analyse the combination of both signals is presented. For this, a bioelectrical impedance device was built to gather basal and arterial pulses from an upper extremity. An experiment with healthy volunteers was

Introduction

performed where their arterial and venous circulation was limited evaluating the performance of the method and compared with other instruments. A full analysis of the basal and are trials pulses is presented, including algorithms that analyse the changes of signal morphology characteristic of each kind of blood flow restriction. Finally, a ratio between basal and amplitude pulses is presented showing that changes in the wave format are an indication of possible arterial or venous blockage.

1.2 Motivation of the thesis and project aims

Bioelectrical impedance plethysmography has the potential to provide further information about the general health of a large volume of tissue and blood circulation, something that is beyond the scope of other methods. This technique has also been proven to be useful in research and medical settings, particularly when measuring plethysmography and blood flow. However, using this technology to quantify a relationship between poor circulation and the health of the tissue remains an uncommon phenomenon. In principle, an instrument such as this should be simple to use, safe for patients and likely portable for low resources area use. In this dissertation, I am presenting a novel method to use a bioelectrical impedance plethysmography device that has the potential to meet the conditions previously mentioned. This enables this technique to be used in either home or any remote area where there is no access to more than one instrument. The results derived from the experimental work not only highlight a portable, non-invasive, effective and potentially cheap instrument but also show the way forward to differentiate changes in arterial and venous circulation by analysing waveforms.

The main aim of this project is to use the bioelectrical impedance plethysmography waveforms to identify low perfusion in tissue caused by circulatory blockages. For this, the basal impedance signal is used to pinpoint changes in blood circulating through a large volume of tissue. Additionally, this study presents arterial pulses shape analysis which may indicate blockages in either arterial or basal circulation. Combining the information from these two signals provide a numeric quantification that indicates low perfusion or circulatory impediment.

The other main aim is to design and implement a bioelectrical impedance device for capturing the aforementioned waveforms within the forearm's common impedance range. The apparatus able to continuously monitor blood changes safely and straightforward which may enable its use in low setting resources places or even at home.

1.3 Novelty and contribution of the thesis

Although some instruments are focused on measuring either overall tissue impedance (including blood), to assess perfusion levels [20–22] or only arterial pulses [23–28], the proposed method, to the best of the author’s knowledge, is the first one that distinguishes whether low perfusion in tissue is due to restriction of arterial or venous blood. This is achieved through combining impedance measurements of basal values and arterial pulses. This thesis has been structured to present both impedimetric signals. Chapter 5 analyses the basal impedance of all the study participants. By isolating the basal readings during the measurements, the errors produced by the instrument were analysed. The results obtained from here were used as the denominator for the novel index shown in this work. Chapter 6 focuses on the study of the arterial pulses, identifying three inflection points of the plethysmographic waveform to determine alterations compared to baseline conditions. The method shows that an increase in arterial peaks pulses are early indicators of possible arterial blood restriction, whereas additional changes in the dicrotic notch and diastolic pulse amplitude impedance may be a clue of possible circulatory blockage. Although arterial pulses amplitude has been previously used to analyse haemodynamic factors on female population with lymphedema [29] or the quantification of blood flow [23–28], the analysis of the full waveform morphology has not been adopted before in studying alterations on arterial or venous circulation.

Further to the novelty of distinguishing between arterial and venous occlusions, the work presented here is the first one to introduce an index that combines the basal and pulsing measurements to give a numerical value that classifies the severity of occlusion. The section 6.3 described in full detail of how this index ratio is calculated.

Assessing the aforementioned novel aspects of this new method was only achievable through the use of custom made instrumentation and electronics. Although basal limb impedance has been used for studying tissue health and blood flow [23–28], in some instances, this was previously carried out using commercial instrumentation that was originally designed for other impedimetric applications (e.g. cardiothoracic impedance [30, 31]) rather than through an application specific device, such as the one developed here, presented in Chapter 4.

1.4 Work done

In order to gather the signals required by the study, a bioelectrical impedance device, including hardware, software and algorithms, has been developed as part of the work for this thesis.

Introduction

This device was needed as the instruments available in the laboratory were not able to take readings continuously. More important, the devices at one's fingertips were designed for industrial applications but not for medical purposes. Therefore, this device was designed with the aim of getting basal impedance and the arterial pulses contained within it in a human arm.

Bioelectrical impedance is calculated as a ratio between alternating current (AC) driven to a material and the alternating voltage produced by it. Section 4.1 describes in more detail how bioelectrical impedance is computed and how this interfaces with tissue. As a brief introduction, the instrument must provide a continuous sinusoidal current which is driven into the body by a pair of electrodes, a second pair of electrodes placed nearby measures the potential caused by the interaction of the current and the tissue components. With this in mind, the instrument was designed and manufactured as a modular system, where every PCB board performs a specific task - for instance, wave generation, current injection and sensing. The instrument while in operation uninterruptedly measures the two signals produced by the instrument (current and voltage peak value) which are needed for further off-line processing. A USB DAQ card and a custom software application developed in LabView [32] were used to capture and display the waveforms emitted by the instrument. The application interface also controls some parameters of the apparatus, such as frequency and trigger of the wave generator. Another program developed in Matlab [33] post-process all the captured data. In this application a custom graphic user interface was created to compare windowed data, apply filters, obtain statistical data and detect peaks and valleys. Chapter 4 illustrates the full instrument design including designs and algorithms used.

From the data analysis standpoint, different mathematical equations and algorithms were applied in Matlab to convert the information recorded into meaningful clinical units like flow rate. Chapter 7.2 shows the data quantification of the instruments used in the experiment. In there, the Doppler ultrasound sources to arterial flow; the PPG signal the changes in volume and the laser Doppler flowmetry the cell movement in the microcirculatory bed. Furthermore, this chapter presents the correlational analysis of the tailor-made bioelectrical impedance device and the other instrument, providing an understanding of the main contributors to the impedimetric signal.

1.5 Organisation of the thesis

The thesis has been organised in different chapters covering clinical and technical background. The chapter 2 will cover the origin of the plethysmographic signal and the clinical problems

derived from not monitoring it on patients at risk. Later on, this chapter will elaborate on some of the different instruments available to measure changes in blood flow and volume. Some of the methods covered include Doppler ultrasound, optical techniques and plethysmography covering bioelectrical impedance.

Meanwhile, chapter 3 will describe, in an in-depth manner, how bioelectrical impedance works and the different techniques to measure it. It includes an explanation of the ionic conduction in the human body, electrodes positioning, mathematical representations and the methods to measure bioelectrical impedance including mono and multi-frequency. Finally, the chapter will describe the principles and the kind of signals that can be obtained from a bioelectrical impedance plethysmography device on the forearm, including basal impedance, venous occlusion plethysmography and the arterial pulse amplitude.

Chapter 4 will explain the works performed towards the development of the bioelectrical impedance plethysmography device and the experimental procedure to gather data from the participant's left arm. Some detail of the electrical characteristics of the bespoke impedance device will be explained, including the frequency of operation and maximum current delivery, but more details will be found in the Appendix sections. The experimental protocol will be explained, including instruments placement and the different levels of pressure applied to the cuff in the upper arm in order to alter the blood flow to the forearm. Finally, the algorithms and mathematical formulas will be presented to show how to convert data to clinical units, including the ones from the bioelectrical impedance method.

The following chapters elaborate on the analysis of the signals obtained. Chapters 5 will analyse the basal impedance of all the participants. By isolating the basal readings during the experiments, the errors produced by the instrument were analysed. Furthermore, the effects of occlusion on the basal impedance during the three different kinds of occlusion - below systolic pressure, in between systolic and diastolic and during total occlusion - were also described. Chapter 6 will focus on the analysis of the waveform shape of the arterial pulses during the experiment, including the changes occurring in three different points within the plethysmographic waveform. The novel method denominated impedance index ratio is introduced to identify possible circulatory obstruction in the arterial or venous path.

Meanwhile, chapters 7.2 will illustrate the data correlation between the additional instruments and the designed bioelectrical impedance plethysmography (iPG) device. Here, the signals from iPG at different levels of occlusion will be correlated with the arterial flow of Doppler ultrasound, changes in amplitude pulses in PPG and the movement of red cells in laser Doppler flowmetry.

Introduction

Finally, chapter 8 will comprise of a general conclusion and achievements of the performance of the bioelectrical impedance plethysmography device, the merits of the novel index ratio and how it correlates with the measurements from other instruments. Furthermore, additional work is proposed to investigate further into the morphological changes of impedimetric arterial pulses under other physiological triggers.

Chapter 2

Principles of Plethysmography and Plethysmographic Methods

Measuring the changes of blood in extremities provides the clinical community with valuable information about the overall health of a patient. Estimating immediate changes of blood volume within a limb offers insightful data on the wellness of "highways" that transport oxygen and nutrient to these tissues via the vasculature. Some diseases are attributed to problems in either the micro or macro vasculature. For instance, some of the disorders may include cardiovascular disease, peripheral vascular disease, diabetes and Raynaud's syndrome. In the absence of adequate blood supply, these tissues are liable to become ischaemic (*isch* in Greek means to stop or block, which *emia* implies blood flow). If severely compromised, it can even lead to necrosis (death of tissue). In medicine, the clinician always attempts to salvage tissue whenever is possible. Therefore, measuring the progression of disease or acute problems with the vasculature (in the extremities) can help clinicians decide on the optimal line of treatment, which may include a bypass graft or in extreme cases, amputation.

This chapter presents the principles involved in the generation of a plethysmographic signal. It also cover the methods available to measure changes of arterial blood or micro-circulation.

2.1 Origin of the plethysmography signal in the circulatory system

The origin of the word plethysmography originates from two Greek words *plethysmos* which means population and *grapho* which is the word for writing [34] and is an instrument used to record changes of blood volume or blood flow during every heart cycle. From the circulatory standpoint, a plethysmographic signal forms when blood cell pushes through the circulatory systems generating a pulsating waveform synchronous with the heart's cycle [35].

A plethysmography device produces an output waveform that is synchronous to the heart cycle. The shape of the signal is similar to an arterial pressure waveform. In fact, the plethysmography plot represents the volume of the arterial vasculature that related to the amplitude of the arterial pulse. This waveform gives vital insights into the pulse velocity and indications of possible circulatory obstruction.

The circulatory system divides in systematic or peripheral circulation and pulmonary circulation. The human body entails a closed circulatory system where blood vessels are the main paths to move blood. In this sense, the heart works as a pump transporting blood to all the tissues around the body. The primary function of the circulatory system is to carry oxygen and nutrients to every cell in the body. It also collects the final by-product of the entire metabolic process. Blood flows through the vessels that form a complex, elastic tubular network which reaches all cells of the body. The arteries are capable of carrying oxygenated blood, whereas the veins return de-oxygenated blood [36].

Blood is transported from the arterial to venous circulation within the capillaries. Meanwhile plasma passes through capillaries that are only about a cell's thickness in diameter. Subsequently, an increase of blood pressure expels interstitial fluid out of the capillary walls. In the end, some part of this fluid returns to the capillaries, with the rest flowing into lymphatic vessels [37].

The amount of blood cells in tissue relates to the amount of blood flow and the dilation/contraction of the surrounding vessels. For blood to flow, there should be a differential in pressure between arterial and venous pressure. Because the heart pumps blood in a rhythmic way, the blood pressure changes accordingly. When blood comes out of the left ventricle into the aorta, the highest blood pressure forms at this point with an average 100 mmHg. Then blood flows towards the large arteries where pressure varies between systolic pressure commonly around 120 mmHg and diastolic pressure in roughly 80 mmHg. Figure 2.1

2.1 Origin of the plethysmography signal in the circulatory system

shows in more detail the different pressures in different parts of the systemic and pulmonary circulation.

As blood flows through the systemic system, the pressure in the arteriolar capillaries is around 35 mmHg and 10 mmHg in the venous end. The average functional pressure of the vascular bed is 17 mmHg, which is high enough to allow the exchange of nutrients between tissue and blood. At the end of the systemic circulation in the inferior and superior venae cavae, the pressure falls to nearly 0 mmHg where blood pours back in the right atrium of the heart.

On the other hand, the pressures in the pulmonary circulation are lower in comparison. The pulmonary artery systolic pressure is around 25 mmHg and diastolic pressures averages about 8 mmHg. The pulmonary capillary pressure averages 7 mmHg which is adequate to allow gas exchange in the lungs.

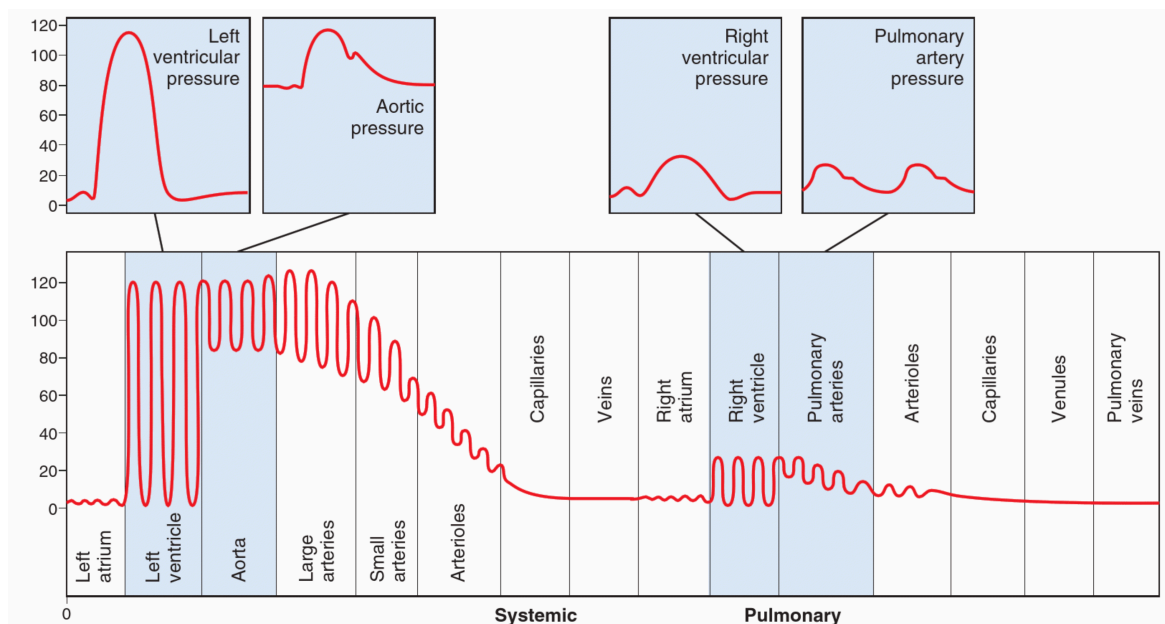


Figure 2.1 Common pressures in different parts of the systemic and pulmonary circulation of a person laying in horizontal position. Figure adapted from [37].

The circulatory systems is quite complex to go more in deep but there are three basic principles that describe the whole process and how is controlled [37]:

1. *Blood flow is delivered according to the needs of the tissue.* Depending of the level of activity, tissue requires more nutrients to operate. Hence, a larger supply of blood is required but heart alone cannot cope with the whole demand. For this, micro-vessels reduce or increase the amount of blood into the tissue by changing its cross sectional diameter. Controlled by the central nervous system these micro-vessels can contract

Principles of Plethysmography and Plethysmographic Methods

and dilate according to the tissue needs, thus manipulating the amount of blood passing by the surrounding fibres.

- Total cardiac output is equivalent to the sum of all the local tissue flows.* The total blood coming in and out of tissue must be equal to zero. All the arterial blood pushed into any tissue must return to the heart via the veins. Hence, the heart works as a dual pump, pushing out arterial and collecting venous blood. As explained before, the heart can react to the needs of blood in tissue by increasing its pumping frequency. This is also controlled by special nerve signals that trigger the heart to pump the required amounts of blood.
- Arterial pressure is regulated independently from either local blood flow control or cardiac output control.* The human body always tries to keep the arterial pressure to a minimum value. For this, a complex network of special nerves operates to maintain this arterial pressure to a level where red blood cells can be passed through tissue. For example, if a trauma occurs and arterial pressure falls below 100 mmHg then (a) the nervous system send signals to increase the heart's pumping force (b) same signals contract large venous reservoirs to send more blood back to the heart and (c) the arterioles that transport blood into tissue contract increasing the amount of blood contained in large arteries resulting in an increase of the arterial pressure.

Plethysmography in the circulation aims to measure the changes of volume of blood caused by the increase of pressure against vessels walls in any part of the body. Due to the heart's pumping effect, blood components move through vessels which diameter increases slightly in major arteries and veins. For instance, according to the elastic constant of the aorta, when its inner pressure is 100 mmHg the diameter of the vessels distend about 5% [38]. Therefore, this additional diameter increments the total amount of blood cells during the systolic peak.

A plethysmographic waveform forms by the effect of the blood being pushed all the way through the circulatory system. The forwarding-going pressure wave is transmitted all the way from the heart's left ventricle to the periphery creating the systolic peak. The diastolic waveform forms from pressure waves being transmitted from the aorta to small arteries in the periphery [39]. Regardless of the method, the plethysmography waveform seems to have similar shape as described in figure 2.2, where systolic peak, dicrotic notch and diastolic peak can be identified.

Figure 2.2 shows the comparative waveforms between flow measured with an ultrasound instrument and the instrument produced by it in an upper limb. A normal blood flow waveform

2.1 Origin of the plethysmography signal in the circulatory system

contains three different phases during a cardiac cycle. The systolic peak reference the point after the ejection of blood from the heart. The reverse diastolic flow is an indicative of healthy blood flowing trough a limb, any absence on these valley may indicate arterial problems [40, 41]. Finally the forward diastolic flow peak completes the waveform. This change of flow also traduces in a change in volume which is compared in the same figure. The time that the pressure takes to travel from generates the systolic peak seen on the figure. The dicrotic notch is generated when the aorta valve closes, this point in the waveform is synchronous with the reverse diastolic flow. The diastolic peak which is in phase with the forward diastolic flow is caused by the recoil effect of the elastic wall in arteries that propel slightly blood forward.

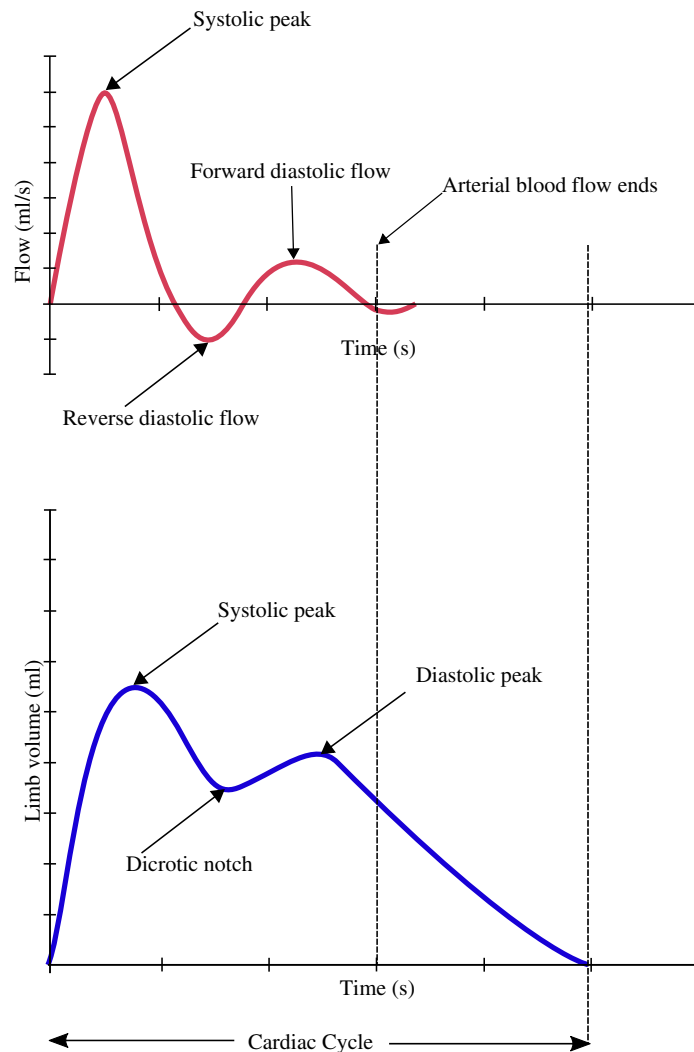


Figure 2.2 Common triphasic flow waveform and volume change waveform. The most common peaks and valleys are marked as systolic peak, dicrotic notch and diastolic peaks. Figure adapted from [40, 42].

2.2 Problems derived from poor blood delivery

The plethysmography waveform indicates the amount of blood volume in any part of the body which is key in the metabolic process. In the human body, blood requires different paths to circulate blood which carries oxygenated and deoxygenated blood. Arteries transport arterial blood (oxygenated blood) flowing from the heart through the lungs. Meanwhile, veins are used to return venous blood (deoxygenated blood) into the heart and back to the lungs [37].

More in detail, the blood in humans comprises of plasma and specialised cells. Approximately half of its volume is made up of plasma, which consists mostly of salt and water. In fact, it is quite similar to seawater, albeit with a lower concentration of ions. Some other ions present in significant numbers include sodium (Na), chloride (Cl^-) and bicarbonate (HCO_3^-). Additionally, traces of calcium, magnesium, copper, potassium and zinc are also found. The remaining half volume includes red blood cells (erythrocytes) which transport oxygen (O_2), white blood cells (leukocytes or monocytes) that are in charge of the immunological response and platelets (thrombocytes) which aid in the clotting process [37, 43].

The red blood cells are key to move around oxygen and nutrients. These cells contain Haemoglobin (Hb) which gives the red colour to the blood, it has a high affinity to oxygen that is an essential component in one's metabolic process. Oxygen is required for the chemical reactions that eventually convert biochemical energy created by nutrients coming from food into cellular energy known as coenzyme or adenosine triphosphate (ATP). As a result of these reactions, a waste product is released from the cell and collected by the blood. Part of this byproduct includes carbon dioxide (CO_2) collected by haemoglobin that also has a high affinity to transport this molecule.

2.2.1 Ischaemia

It is clear that human cells cannot survive without oxygen and other nutrients for more than a few minutes [44]. A restriction in the blood flow delivering any of these basic cell's fuels might have critical consequences to one's well being. Ischaemia is one of the harmful consequences of the insufficient supply of blood to tissue. This medical ailment develops when one of the main vessels restrict the flow of red blood cells due to any sort of blockage, all the tissues below that blocked path will suffer from the starvation of oxygen and other critical nutrients. In general, ischaemia signifies a major cause of disability, cardiovascular morbidity and mortality around the globe [45].

2.2 Problems derived from poor blood delivery

Different causes could account for the blockage of an artery; these can include internal or external factors. Section 2.3 describes more in depth some of the illnesses that may develop ischaemia. For instance in limbs, peripheral arterial disease (PAD) could evolve into critical limb ischaemia (CLI), whereby the patient could lose their limb in the absence of timely medical intervention. The diagnosis of this type of diseases starts when symptoms start to manifest, which for some cases could be already to late. One of the first manifestations is that the patient experiences continuous pain at the extremity, even at rest [1].

2.2.2 Hypoxia

Hypoxia is one of the consequences of not delivering properly oxygenated blood to an organ. As explain in the previous section, an occlusion of a main vessel may result on a reduction of red blood cells volume, as a result this may lead to tissue *hypoxia* (reduced oxygen) or *anoxia* (absence of oxygen). ischaemia always lead to hypoxia; but hypoxia can occur without ischaemia. Marie et al. [46] have classified this illness in four different kinds depending on its cause as shown in table 2.1.

Table 2.1 Hypoxia classification according to Marie et al. [46]

Disease	Condition	Causes
Anaemic Hypoxia	Poor O_2 delivery to tissue	<ul style="list-style-type: none">• Small count of RBCs and abnormal or inadequate Hb levels
Ischaemic (stagnant) hypoxia	Blood circulation is reduced or blocked	<ul style="list-style-type: none">• Congestive heart failure that may cause body-wide hypoxia• Emboli or thrombi blocking oxygen supply to the tissue distal from the occlusion.
Histotoxic hypoxia	Metabolic poisoning (i.e. ingestion of cyanide)	<ul style="list-style-type: none">• The cell is unable to use O_2 for metabolic purposes, even though there is an appropriate amount of O_2 being delivered by the body
Hypoxemic hypoxia	Decrease in the arterial oxygen partial pressure (PO_2)	<ul style="list-style-type: none">• Imbalance in the ventilation-perfusion coupling mechanism• Poor ventilation attributed to pulmonary disease and breathing air with a low O_2 content.• Carbon monoxide (CO) poisoning as it has 200 times more affinity with Hb than O_2. Thus, in scenarios that involve high concentrations of CO, such as fires, this could easily lead to death.

2.3 Diseases derived from poor blood delivery

There are different illnesses that may lead to the development of either ischaemic or hypoxic tissue derived from internal or external causes. The study presented in this document focuses on a method to detect either arterial or venous blockage caused by diseases affecting the limbs. Hence, the following sections describe some of the most common disorders associated with poor blood delivery towards the periphery of the body.

2.3.1 Peripheral vascular disease

Peripheral vascular disease (PVD), also known as peripheral arterial disease (PAD) is a disease that causes the reduction of blood towards a limb. This illness is a progressive vascular condition caused by the blockage, narrowing, or spasms in a blood vessel (arteries, veins or lymphatic vessels), thereby, altering the blood circulation to and from upper or lower extremities. It most commonly affects the lower limbs, particularly most distally, which explains the derivation of its name as *peripheral* because it mostly affects the periphery of a body. It affects 5 % of people over 50 and between 12 % to 20 % of people over 65 years old. To some extent, it is more common in men than women. People with certain risk factors are more likely to suffer PVD such as patients with diabetes or smokers, as some studies have demonstrated [47–51]. Patients with diabetes are more likely to develop occlusion of large arteries in the lower extremities that also could lead to gangrene and ulcers. In contrast, smokers may present intermittent claudication, in other words, pain, cramp, numbness or sense of muscle fatigue.

Different factors could cause the narrowing of the blood vessels. The most common cause of PVD is atherosclerosis [36], which in short is the deposit of fatty material on the arterial walls. Accumulation of cholesterol builds a plaque that reduces the blood flow within the vessels. This in turn, lessens the transport of O_2 and nutrients as explained previously in section 2.2. Moreover, this uneven deposit increases the chances of clots to form on the artery walls reducing the internal size of the vessel and increasing the risk of obstructing a major artery.

Different risk factors are contributing to the development of this illness. Some can be inherited; others are based on lifestyle choices. The combination of two or more of the following risks may exacerbate the complications from PVD, such as smoking and diabetes [47, 48, 51]. To elaborate further, some of the documented risk factors are:

- Age (especially over 50)

2.3 Diseases derived from poor blood delivery

- Family history (high blood pressure, high cholesterol or PVD)
- Diabetes
- Smoking
- Obesity
- Infections
- Coronary artery disease
- Injury to vessels
- Physical inactivity
- High blood pressure
- Autoimmune diseases
- Nutritional deficiencies
- High blood cholesterol
- Emboli from other locations in the body
- Inflammation of the blood vessels

During the first stages of the illness, symptoms are unnoticeable, which makes the condition difficult to diagnose. The most common presentation occurs when the illness has progressed to the extent of causing pain. However, performing a qualitative assessment of the extremity might help to diagnose the illness at earlier stages. This assessment makes use of helpful indicators such as coldness of the extremity to touch, poor skin condition (thinning, shining or brittle), poor nail health (thickening or opaque nails), hair loss in the extremity, reduced pulse sensation (in the extremity), impotence, infections or injuries that do not get healed properly, insufficient muscle condition (numbness, weakness or heaviness), pain while walking and stopping at rest, local skin discolouration (pale, blue or dark red) and restricted mobility [52, 53]. Table 2.2 describes one of the methods to damage caused by the obstruction of a main vessel.

2.3.2 Compartment syndrome

All the muscles, blood vessels and nerves are contained within a tissue known as fascia. When the pressure in a limb within this compartments increases owing to bleeding or swelling, it could lead to total or partial restriction of micro-vascular blood flow [54]. Some cases may present with rapid discolouration and blistering of the affected limb, which is commonly associated with oedema, cyanosis and severe pain [55]. Hence, it can lead ultimately to venous hypertension and loss of blood plasma. If the arterial flow is reduced, it may also cause severe ailments such as gangrene, limb loss or even death [56]. This syndrome can

be catalogued as acute when it is caused by an injury, accident or medical emergency and chronic when it occurs gradually during any sports activity.

The most common method to diagnose this illness is Doppler sonography [55]. Nevertheless, detecting foot compartment syndrome could be challenging as opposed to other parts of the body because its symptoms and indicators are less reliable [57].

2.3.3 Diabetic foot infection

Diabetes can develop into further health complications like the absence of blood supply towards an extremity. Some of the most common problems that diabetic patients are required to deal with are diabetic foot infection, which is a clinical syndrome characterised by local findings of inflammation or purulence in a person suffering from diabetes. This disease also leads to a decrease in peripheral circulation, vascular disease and loss of nerve sensation, ending up in the formation chronic ischaemic ulcers and bacterial infection. Diabetes is the leading cause of lower extremity amputation in developed countries, and is responsible for 60 % of these amputations [58]. Currently, Doppler ultrasound flowmetry remains one of the primary tools to diagnose the advance of diabetes foot infection. New techniques that are aimed to follow up the progress of this illness have been researched, such as bioelectrical impedance [59], planar pressure analysis [60], image technique analysis [54], near infrared [61] and electronic noses [62]. Until now, no medical advancement has taken place which allows the detection of this problem at an early stage before the occurrence of ulceration. With regard to bioelectrical impedance technology used in this study, previous studies have focused on the detection of ischaemia of the sole of the feet, signifying a good correlation with laser Doppler flowmetry [59].

2.3.4 Upper extremity venous occlusion

Upper extremity venous occlusion, also known as Paget-von Schrötter Syndrome, upper extremity deep vein thrombosis (DVT), axillo-subclavian vein thrombosis and effort thrombosis is a condition that primary affects mostly young people (below 40 years old) due to practising repetitive tasks. Nonetheless, in the secondary type of the disease, it can develop in the elderly population after medical procedures like the implant of cardiac pacemakers [63]. This disease is caused by the narrowing, blocking or pinching of the vein coming from the arm to the chest. People who perform heavy and repetitive tasks with their upper arms, like swimmers or house painters, are at higher risk of contract this type of illness [64]. It has been noticed that the exaggerated use of their arms thickens the upper muscles. As a result, it

2.4 Clinical assessment of peripheral vascular diseases

can squeeze the vein above the first rib that collects the blood coming from the arm causing a reduction in the blood flowing towards the chest.

The obstruction of venous blood in the upper arm is normally acute. However, some of the initial symptoms are discomfort, pain, swelling and reddish or bluish discolouration of the arm. The treatment of this disease may require a surgical procedure to open the vein segment and maintaining open using balloon angioplasty. Blood clots may also form as a secondary effect of the disease, therefore it is common to prescribe anticoagulants to prevent or dissolve any clots in acute cases and post-surgery [63, 64].

2.4 Clinical assessment of peripheral vascular diseases

The initial assessment of the diseases described in the previous section focuses on qualitative inspection of the affected extremity. The medical practitioner inspects patients with this method but in many cases, symptoms are already noticeable which may indicate some sort of tissue damage. Although this technique seems to be effective to control the progression of the ailment, it may miss early stages of the disease, at the right moment when it could be treated more effectively. The development and evolution of these illnesses are quite complex because it can be also asymptomatic, thus further tests might be required to confirm the diagnosis.

Clinically, there are different methods to assess the development of the illnesses affected by the low flow of blood. Some scales of qualitative evaluation have been developed, such as the Rutherford classification, the Leriche-Fontaine classification, and the TACS II classification of femoral and popliteal lesions [52, 65]. Following any of these procedures, health practitioners perform a visual inspection and a survey, which aims to reveal any indication of pain when walking as well as discoloration and skin wounds. This makes it possible to determine the severity of the damage derived from an arterial occlusion.

Table 2.2 illustrates the Leriche-Fountain classification which is one of the methods commonly used by the clinical personnel. This classification considers 5 stages to evaluate the progression of the illness. As shown by this table, there are various levels of stratifying the severity of this disease in accordance with the symptoms and pathophysiology which can vary from asymptomatic stages up to the development of necrotic tissue.

Upon a qualitative or physical examination, and the classification of the illness's progression, additional tests may help in ascertaining the severity of the arterial occlusion. In some cases, sophisticated medical equipment may be needed to fully complement the diagnosis of the patient, which some of these are described in the next section. Nevertheless, additional

Principles of Plethysmography and Plethysmographic Methods

Table 2.2 Leriche-Fontaine classification

Stages	Symptoms	Pathophysiology	Pathophysiological classification
Stage I	Asymptomatic or effort pain	Relative hypoxia	Silent Arteriopathy
Stage II A	Effort pain Pain free walking distance > 200 m	Relative hypoxia	Stabilized Arteriopathy Non-Invalidant claudication
Stage III A	Rest Pain Ankle arterial pressure > 50 mmHg	Cutaneous hypoxia Tissue acidosis Ischemic neuritis	Instable arteriopathy Invalidant claudication
Stage III B	Rest pain Ankle arterial pressure < 50 mmHg	Cutaneous hypoxia Tissue acidosis Ischemic neuritis	Instable arteriopathy Invalidant claudication
Stage IV	Trophic lesions Necrosis or Gangrene	Cutaneous hypoxia Tissue acidosis	Necrosis Evolutive arteriopathy

medical procedures have come into place where clinical practitioners use common medical devices to try to indicate the location of the blockage. The following shows some of the therapeutic methods that do not require bulky or cumbersome devices in a clinical setting.

- **Ankle-brachial index (ABI):** This is the ratio of the differential measurement of systolic blood pressure measured at the ankle to the measurement undertaken at the brachial artery [66]. This necessitates a comparison in blood pressure between the arm and the ankle, as well as recording the ankle's blood flow using a Doppler ultrasound instrument.
- **Treadmill exercise test:** Under this method, the patient needs to walk or run in order to monitor the circulation during exercise. Pain or problems experienced during the test are recorded to examine the severity of the obstruction.
- **Reactive hyperaemia test:** This test refers to a temporary increase (*hyper*) of blood flow (*emia*) of the extremity. It is usually performed on people who are not able to walk on a treadmill. In this case, the person remains in a supine position after which, comparative measurements of blood flow are taken using a Doppler ultrasound instrument on the thighs and ankles. Subsequently, an occlusion is applied on the limb to compare any decrease in the flow rate between both the sites.

2.5 Methods to measure blood flow and volume

It is clear that complementing qualitative with a quantitative method would provide further physiological data which increases the chances of detecting any circulatory problem at an early stage of the disease. Blood flow obstructions in the limbs can be quite complex to diagnose as may affect different parts of the circulatory path. As described in this document, some of these illnesses affect the arterial circulation, venous return or even the microcirculation. Different technologies have been developed aiming to identify circulatory issues in localised areas of the body. However, currently, to have the whole picture of the development of circulatory diseases affecting tissue in the limbs require to combine one or more technologies, which makes it less efficient and requires extra training for clinicians.

Nowadays the measurement of blood volume or flow can be performed with non-invasive techniques. There are different kind of portable technologies that can be used in medical devices as a single source of information or combined with other methods to get a proper clinical diagnosis. Moreover, there are several variations of a single technique in order to assess the blood volume or flow. For instance, Doppler technique can be implemented using either light or sound waves. It also can be used as a continued monitor or diagnostics image technique.

The following list of equipment describes the methods or instruments that can measure blood volume or flow in an extremity. It must be taken into consideration that devices that measure blood volume measure changes of blood in defined volumes of tissue, whereas blood flow is usually restricted to single blood vessel measurement. However, this list is confined to devices that are portable, and need minimum assistance from a specialist. Diagnostic imaging techniques do impart high accuracy, but they are confined to a clinical setting.

2.5.1 Doppler ultrasound

The widely used ultrasound method can be applied on different fields such as diagnostic imaging, localising tissues and the most common blood flow measurement at a single vessel. Currently, it is commonly used in medical practice when measuring the blood flow in different part of the body, such as in the brachial or femoral arteries [67] as shown in figure 2.3.

From the technical viewpoint, this method derives from the *Doppler effect* principle, which describes the relationship between the frequency of a source and its velocity relative to its source [69]. This method operates on any wavelength above the ultrasound spectrum (above 20 kHz). Conventional equipment operates in the range of 2 MHz to 15 MHz [70].



Figure 2.3 Doppler ultrasound instrument used measuring blood flow in femoral artery [68]

The principle behind this technique in terms of medical use was the propagation of ultrasound waves through the tissue. The Doppler method measures the velocity of particles in a liquid solution using the frequency shift of backscattered ultrasound [5, 36]. In other words, if an electromagnetic wave is transmitted at a fixed frequency and is reflected by a moving body, the frequency of the received signal will be shifted (see Figure 2.4) [67, 70, 69, 71]. A device using this principle can detect moving blood cells within a vessel. When an erythrocyte passes through a vessel under the electromagnetic beam, a frequency shift occurs, which is proportional to the blood flow velocity [72].

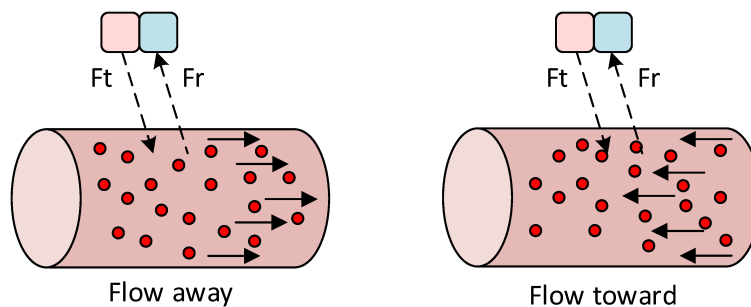


Figure 2.4 Representation of the Doppler technique measuring blood flow. The cylinder represents the vessel; the red dots are the RBCs. The F_t and F_r are the frequencies of transmission and reception of the sensor. The phase shift between both signals change according to the movement of the particles.

Estimating blood flow based on this principle requires the measurement of arterial diameter and the blood velocity. Using these parameters, it becomes possible to calculate the blood flow by multiplying the blood's mean velocity (cm s^{-1}) by the cross-sectional area of the artery in cm^2 , before multiplying it by 60 seconds to express the value in millilitres per minute (ml min^{-1}) [67].

2.5 Methods to measure blood flow and volume

Some of its advantages include non-invasiveness, the ability to measure velocity continuously, portability (and hand-held), and less energy consumption, which makes it an excellent choice for low clinical setting use. However, this method is not without its share of disadvantages. First, the operator requires some skill to be able to locate the artery accurately. Some instruments provide a sound feedback pertaining to the flow velocity of the artery. However, there are different levels of sound or pitch in order to identify the right vessel correctly. Second, it is recommended to use a low insonation angles ($\sim 60^\circ$) for limiting the number of errors [73] which also require steady hands from the operator. Third, it is effective when the limb and the artery remain in a fixed position; it is quite sensitive to motion. Lastly, as mentioned previously, it requires measuring the arterial diameter to convert velocity into flow, which marks a significant disadvantage because the only way to measure this parameter accurately is by making use of imaging methods [74] but this could be quite an arduous task in a home setting.

2.5.2 Optical methods measuring blood volume and flow

Light is one of the most common electromagnetic energies applied on the field of medicine. Using optical methods makes it possible to estimate blood flow by measuring volume changes or by applying complex imaging techniques. One of the key features of this method is its mostly non-invasive or inclusive contact-less for some applications. Furthermore, optical imaging techniques are advantageous in that they offer a high resolution; they are also cost effective when compared to magnetic resonance imaging (MRI) or positron emission tomography (PET), apart from being a non-ionising source [70].

It is one of the most popular methods to monitor continuously volume changes using the principle of optical absorption of the arterial blood. In principle, it requires a coherent light source provided by a laser/light emitting diode (LED) set to a specific wavelength in accordance to the application. The light propagates due to the transport of individual photons, which under the area of influence, may be absorbed or scattered [75].

This method is so popular that it is used in mostly every clinical setting as well as for personal use. The latter has become extensively available owing to the use of activity monitors that utilise optical methods, such as one employed in the Apple Watch [76]. This makes it clear that this method can be applied to home settings owing to its versatility and portability. The following application describes the methods to estimate the rate of flow.

2.5.2.1 Photoplethysmography

Photoplethysmography or PPG measures change of blood volume using light as the emitting source. Nowadays, it is one of the most popular methods in the parlance of medical applications. It is non-invasive and can accommodate a wide range of light wavelengths to obtain a plethysmography graph. It is widely used for the purpose of monitoring heart rate, oxygen saturation, peripheral arterial pressure and peripheral microcirculation after skin grafting, drug ingestion, burns or revascularization [7].

There are two different techniques to obtain the readings. One is transmission-mode (see figure 2.5a.) which works by placing the tissue of interest (i.e. finger, toe or ear lobe) between the light emitting diode (LED) and the photoreceptor (PD). The other is in the PPG reflectance-mode (see figure 2.5b) by placing the LED next to the photoelectric cell over the surface of the tissue. PPG leverages the AC component of the signal for arterial pulse detection and the DC component for venous evaluation [77]. It also uses different kinds of wavelengths to avoid interference from external sources of light. The underlying principle behind PPG detects the degree of attenuation of backscatter light from the superficial layers of skin about 1.5 mm to 2 mm [7, 13, 78]. The amount of reflected light varies in accordance with the total number of RBC's in the cutaneous micro-circulation, which alters the wavelength during each cardiac cycle. This method provides valuable insights based on the waveform analysis into the initial diagnostics of peripheral arterial disease (PAD) [79–81] and chronic peripheral venous insufficiency (CVI) [82, 83].

One of the biggest disadvantages of PPG is that it only measures a small volume of tissue at a given point in time. Therefore, it is not possible to get a spatial distribution of the blood volume change over a significant portion of the skin [84]. Additionally, skin pigmentation has proven to be a factor of error and nail polish [85]. Also, light scattering in tissue makes it impossible to estimate its complete penetration in the skin. Therefore, it is not possible to calculate the volume of tissue being measured.



(a) Placement of LED and photodetector in transmission mode (b) Placement of LED and photodetector in reflectance mode

Figure 2.5 PPG light emitter placement and receptor according to the mode, transmission and reflectance

2.5.2.2 Laser Doppler Flowmetry

LDF refers to a non-invasive optical method to estimate the blood perfusion within the microcirculatory bed under the skin. This device uses the same Doppler principle described in section 2.5.1. However, as the name suggests, it uses a beam of light as the electromagnetic source. It requires a laser diode emitting a wavelength commonly between 633 nm (red) and 780 nm (near-infrared) with an intensity of close to 1 mW [6]. A flexible fibre optic delivers and detects the light applied to a roughly 1 mm³ of tissue. Subsequently, the light scatters by tissue as well as the moving blood cells. Scattering by way of a moving blood cell with haemoglobin produces a frequency shift, whereas scattering from stationary tissue yields the opposite results. The velocity of the red blood cell passing through the beam is equivalent to the frequency shift.

An analysis of the backscattered light provides crucial information on blood cell velocity given by the frequency of Doppler shift [6, 12], and the fraction of the backscattered light that is Doppler shifted is proportional to the total volume of moving blood cells concentrated within the tissue [12]. As a result, an index of red blood cells flow is calculated from the product of mean Doppler shift and the fraction of light that is Doppler shifted [12]. This blood perfusion index is also called flux. Figure 2.6 overviews the laser doppler flowmetry theory, whereas additional details behind this principal are illustrated described in the works of Fredriksson et al. [6].

Some instruments can monitor blood flow in absolute blood flow units. However, some doubts persist about this quantification because the value is premised on an empirical calibration correlated to other methods [86]. Another drawback is that the measurement is quite superficial; the penetration of the wavelength used by LDF is quite shallow. For instance, light in the wavelength of 840 nm only penetrates up to 2.5 mm [13], with the total volume of tissue being studied being quite small - at about 0.1 mm³ or less [14]. Therefore, location remains a key component in the context of obtaining a proper measurement as an area with a good amount of capillaries equals to a greater blood flow distribution around the surface of the skin. Thus, more blood particles can be detected without having to go deeper into the tissue.

This method can be used within a home setting as well; it is portable, easy to locate and battery operated. Nonetheless, it does suffer from some shortcomings. Firstly, the measurement is affected by temperature in that it is recommended to have a stable room temperature. Secondly, it is vulnerable to motion artefact, and the probe must be attached firmly [6].

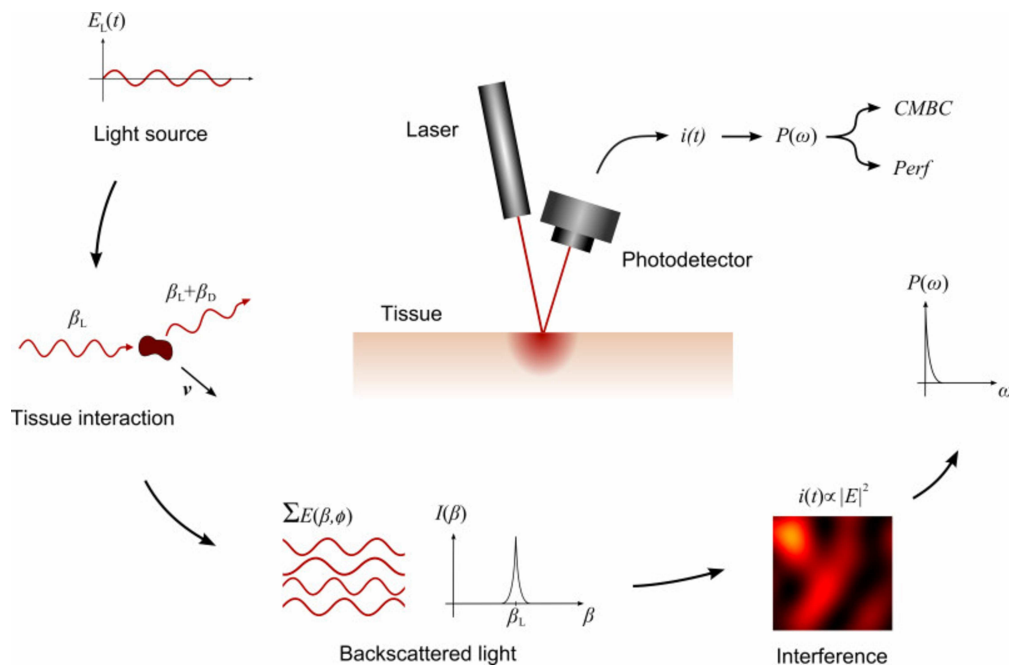


Figure 2.6 The electromagnetic wave is emitted by light $E_L(t)$, the interaction with a red blood tissue produce backscatter light β_L . The photodetector detects the light and process the frequencies of the backscattered light that produces a power spectral density $P(\omega)$ that allows to estimate the concentration of moving blood cells (CMBC) and the perfusion index (*Perf*). This image has been copied from [6] to explain the theory behind LDF

2.5.2.3 Laser speckle contrast imaging (LSCI)

The Laser speckle laser is a fairly new technique that is still being studied. Some medical applications under this method have measured cerebral blood flow [87], microcirculatory research [88], dentistry [89] and wound assessment [90] to name a few. This method can be catalogued as an imaging technique because it requires processing of images in order to obtain a coherent result.

The set-up of a LSCI instrument is a fairly simple process, but the processing behind it can be quite complicated. Figure 2.7 illustrates a common experimental procedure. A coherent (laser) light beam illuminates a sample recorded by a CCD (Charge Coupled Device) camera. A custom software captures the speckle pattern, which is then processed by a computer and displayed as an image [70, 91, 92]. The software controls the camera's exposure time, amount of pixels, local contrast area as well as the option of colours to code the contrast.

Speckle images are generated by the interference pattern produced by the laser beam scattered on a rough surface, which is a random intensity distribution pattern created by the random refractive index fluctuations of the sample. This speckle pattern can only be explained by statistics [93]. As is the case with LDF, stationary tissue produces a constant intensity contrast; however, scattering from moving particles like blood cells produce fluctuations in

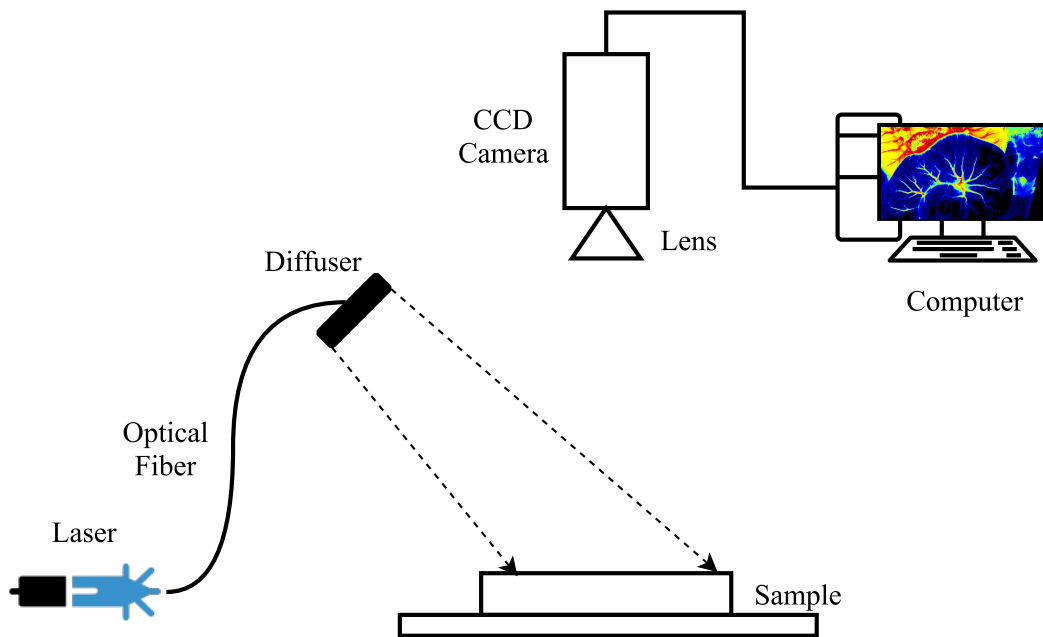


Figure 2.7 A LSCI device requires a laser illuminating a surface, a CCD camera and a computer for the statistical analysis of the images. Image retrieved from [91]

the intensity of the speckle pattern [91]. These fluctuations end up reducing the local speckle contrast; hence the contrast value is inversely proportional to the blood flow speed.

LCSI can be used within a home setting. Some of the advantages of the device are as follows: it is portable and can probably be battery operated if a mobile device replaces the computer. No exogenous material is required to produce a high spatial-temporal resolution image [92], thus making it completely non-invasive. The image generated is easy to decipher even for non-experts.

A technical improvement with Doppler techniques is that area is confined to the focal distance of the camera, whereas Doppler targets a single point measurement. However, there are some disadvantages of this method. For instance, the image is merely a representation of the surface vasculature; it is not possible to monitor the blood flow of large vessels. Although studies are being performed in order to quantify regional blood flow, this method continues to be a qualitative method until the statistics behind it are better-understood [92].

2.5.3 Additional methods to measure limb plethysmography and blood flow

The methods described in the previous section can measure either blood flow in a single vessel like in Doppler ultrasound (see section 2.5.1), single-cell velocity or plethysmography over the skin with optical methods (see section 2.5.2.1). Nevertheless, these techniques cannot provide perfusion details of a large volume of tissue, like in the whole forearm.

If one wants to measure the changes of blood volume in substantial sections of the body, other techniques are required to assess the blood coming in and out from the limb. Hence, different approaches have been developed to diagnose vascular problems in the extremities. Venous occlusion plethysmography (VOP) is one of the methods accepted by the clinical community. This technique has been around for more than 100 years, providing valuable insights into the behaviour and extent of the vascular endothelium in health and disease [94]. It requires the measurement of plethysmography to evaluate the patient's vascular response. Additionally, the blood flow rate could be derived from the change of volume of the limb when used in conjunction with other instruments.

The principle behind VOP is that a pneumatic cuff is inflated around the upper arm or thigh below diastolic pressure, commonly about 40 mmHg to 50 mmHg. Thus, the arterial inflow continues toward the limb even as the venous outflow is blocked [67, 94]. As a result, the blood pooling effect swells the limb and raises its volume. The blood flow rate is calculated as linear hikes of the limb's volume over time, which is believed to be proportional to the rate of arterial inflow [67, 95]. Plethysmographic methods then measure the increase of volume in the limb. In a clinical setting, there are different techniques available to take this measurement. The following section describes some of the methods available, including pros and cons.

2.5.3.1 Air/Water plethysmography

Air/water plethysmography is not a common method to measure a limb's change of volume. This method has more relevance in the research environment than in clinical setting. According to Chuah et al. [42], it measures plethysmography without the need of venous occlusion. This approach encloses the limb in a special chamber with transducers and calibration devices connected through orifices. The arm is introduced into the case using a tight rubber sleeve to ensure that the instrument is airtight. The plethysmography pulsations are detected by measuring the displacement of the surrounding air/water with a sensor connected to the

2.5 Methods to measure blood flow and volume

chamber; this also moves the rubber diaphragm whereby a Doppler ultrasound transducer measures the extent of displacement.

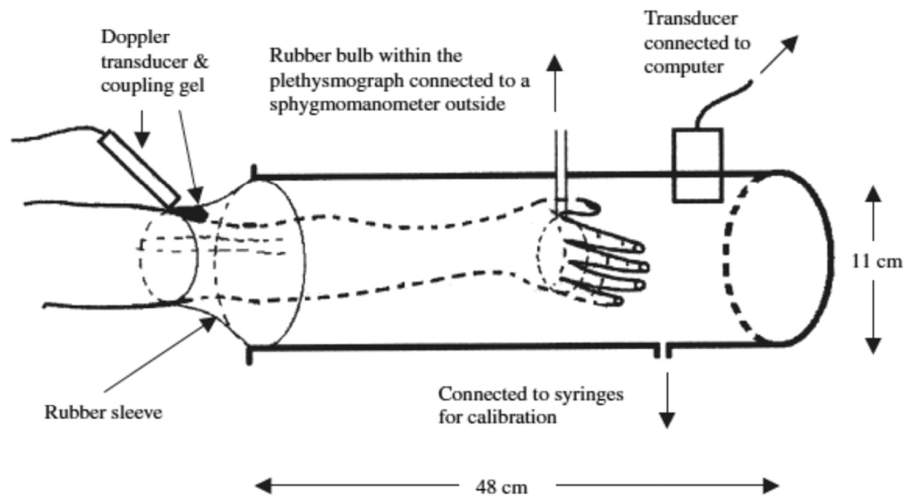


Figure 2.8 Representation of an air plethysmography device. It requires a one-side open cylinder with a rubber sleeve. There is a compartment where the air displacement caused by each cardiac cycle can be measured. Image reproduced from [42]

This method can provide reasonably accurate results, but motion artefact may cause ripples movement affecting the final reading. Furthermore, this method could be burdensome in a low resource setting, or even for surgical applications. It also requires an extra participant to aid with the arm positioning in the chamber and performing the adequate calibration. Also, the portability of this method is quite questionable as it requires many parts to work simultaneously.

2.5.3.2 Strain gauge plethysmography

This method also known as SGP (strain gauge plethysmography), and is a non-invasive method to quantify retrograde outflow in the deep venous system and peripheral arterial disease [7]. It works by applying a strain gauge around the limb being studied. The transducer could be a tube filled in with a conductive material, such as mercury and gallium connected to a source of electricity.

However, alternative methods that do not use clinically banned mercury have been developed using electrical conductive fluids [96]. When the gauge experiences variations of circumference triggered by a change in volume of the rib cage or the pulse in a limb, the resistance of the sensor varies accordingly, thus obtaining an electrical waveform. Increasing the sensitivity for venous filling measurements requires occlusion cuffs, as shown in Figure 2.9.

Principles of Plethysmography and Plethysmographic Methods

This method does not provide reliable quantitative data for venous occlusion, although it does offer qualitative data for the function of the extremity in venous insufficiency [7].



Figure 2.9 Image of a strain gauge plethysmography device [97]. The sensor is attached around the limb under test.

This method presents some advantages when used within a home or low resources setting. First, it is portable since only a single point of measurement is required. Second, it is non-invasive, and requires minimal skills. However, one latent problem is the use of mercury on some sensors; it is a poisonous metal and is not recommended to be used at home. New electrodes can be used [96] instead. Moreover, the instrument merely measures changes of volume in a confined circumference around the sensor. In other words, it does sense changes around a large volume of tissue.

2.5.3.3 Bioelectrical Impedance plethysmography

Bioelectrical impedance plethysmography is yet another method that measures changes in blood volume in different parts of the body, such as the thoracic cavity or limbs [18]. In principle, it senses small changes of bioelectrical impedance due to the increase of blood cells in a volume of tissue. For instance, when the heart's systole increases the blood flow, the volume of a limb rises in accordance with the inflow of blood (swelling) [98]. Consequently, the changes of impedance are correlated to the small variation of volume and flow in a limb.

Some medical applications might necessity the use of pneumatic cuffs in order to analyse venous filling. There are several medical applications for this kind of technique, such as heart stroke volume (SV) measurement, cardiac output (CO), thoracic respiratory volume, oedema and the detection of deep vein thrombosis (DVT) [7]. Studies carried out by Mohapatra [20] and Schraibman [99] revealed a significant linear relationship between bioelectrical impedance plethysmography and strain gauge.

2.5 Methods to measure blood flow and volume

In chapter 3 the principles of operation of this technology are described in greater detail. In summation, this method requires the application of a small amount of current into the body at a specific frequency and amplitude, usually between 1 kHz to 500 kHz [100] and below 5 mA. The body's bioelectrical impedance is a relation between the electrical potential and the electrical current applied. Commonly, a set of four electrodes is placed atop the surface of the skin where a pair converts the electrical conductivity into ionic conductivity to sense the voltage drop. An increase in the amount of blood within a section of body drops its total impedance. Therefore, there is a direct correlation between the population of red blood cells and the measurement of impedance [101].

The blood flow rate can be estimated from the impedance plethysmography signal. Indeed, impedance may be regarded as a measurement of both volume and flow; a change of volume must be attributed to a flow [98]. Some studies incorporate venous occlusion plethysmography as a method to estimate the flow rate [20–22], whereas other techniques focus on the analysis of the plethysmographic signal without integrating occlusion [23–26].

Nyboer et al. [102] proposed the reigning equation (see equation 4.22) from which, the blood flow is estimated. The author opined that the blood flow is proportional to the change of impedance in relation to the distance between the potential electrodes and basal impedance of the tissue. The section 3.8 describes the equation required to convert impedance into the blood flow in greater detail.

Calculating blood flow from the impedance signal is applicable in home or low resources settings as well. Being non-invasive, it only requires four electrodes for measurement, which is one of its main advantages. Additionally, the device uses low-energy in that the current required to read impedance is below 5 mA which can be obtained from a battery operated instrument. Furthermore, the tissue's volume being monitored is more substantial as compared to other techniques, given that the boundary of this measurement is limited by the position of potential electrodes. In fact, the body measurements can be attained as described in free-fat measurements undertaken by Kyle et al. [100].

IPG is less affected by temperature [18]; furthermore, it provides more data than single point measurements to better assess venous blood volume and arterial pulsations [18]. However, this technique does have some shortcomings as well. Like all the methods, it is also sensitive to motion. Secondly, electric current is required for undertaking a measurement, which makes it unsuitable for a certain category of population. Finally, there is an electrode-skin impedance error in the absence of a full contact.

2.5.4 Comparison of the different methods

The previous sections described the general merits and shortcomings of the multiple methods available to measure changes in blood volume or flow. These are just a list of the most common methods in a clinical or research environment.

In general, optical methods provide relevant information about haemodynamics of the vasculature in the body. In fact, PPG is a common method to measure blood oxygenation in the clinical setting present in practically every monitoring device. New technologies based in optics methods are being developed which may allow in the future blood flow quantification, tissue perfusion (i.e. NIRS) and vasculature imaging (LSCI).

However, the most common drawback of the optical methods is the low penetration of the light in the body. This issue presents significant challenges as it is not possible to monitor deep tissue and main vessels blood flow. Another common issue is the uncertainty of the volume of tissue monitored, although surface perfusion may provide details of blood in the vasculature, it cannot provide too much detail of the perfusion of large volumes of muscle tissue.

On the other hand, measuring plethysmography in cylindrical volumes of tissue around limbs present valuable physiological data. It provides details about the total volume of arterial and venous blood coming in and out of an extremity. However, it lacks the level of detail provided on single vessel measurement and superficial vasculatures like those described in section 2.5.1 and 2.5.2. One of the advantages of combining VOP with any of the methods described previously is that it allows estimating blood flow by occluding the upper section of the arm. It also provides an overview of the general health of the vasculature in a greater volume of tissue. Nevertheless, not all patients can have their upper arm obstructed; for this reason, it is recommended to seek ways to monitor venous blood changes without a cuff.

Bioelectrical impedance plethysmography seems to provide an even more in-depth analysis of the tissue compared to the other plethysmography methods since electrical current propagates through all tissue. Hence, it can provide details about the general health of tissue as well as the arterial flow coming into the limb. The capability of having two sources of information may provide double validation of any prognosis. In the following chapter section 3.8, more details about the principle and origin of the impedance plethysmography signal will be cover.

The table 2.3 shows the comparison of the different methods presented here. For a better overview of each method, this table summarises the medical application, the advantages and disadvantages of each technique previously described.

Table 2.3 Comparison of the different methods to measure bioelectrical impedance

Method	Application	Advantages	Disadvantages
Photoplethysmography	<ul style="list-style-type: none"> • Measurement of blood volume • Indirect blood flow quantification using NIRS • Quantification of oxygen saturation in blood 	<ul style="list-style-type: none"> • Non-invasive method • Highly portable • Easy to use, no need of clinical expertise • Widely adopted by the medical community 	<ul style="list-style-type: none"> • Low light penetration for red and infra-red light • Light scattering in tissue makes it impossible to estimate light penetration in skin • Unable to determine the volume of tissue being measured • Measurement diverges with skin dark pigmentation
Laser doppler flowmetry	<ul style="list-style-type: none"> • Measurement of red blood cells velocity • Quantification of vascular bed blood flow • Assessment of micro-circulatory blood flow 	<ul style="list-style-type: none"> • Non-invasive method • Portable • Single sensor on the surface of the skin 	<ul style="list-style-type: none"> • Blood flow quantification based on empirical calibration with other instruments • Information provided is valuable for research but not for medical purposes • Low light penetration, total volume of tissue being measured 0.1 mm
Laser speckle contrast imaging	<ul style="list-style-type: none"> • Monitoring of cerebral blood flow • Micro-circulatory assessment • Dentistry • Wound assessment 	<ul style="list-style-type: none"> • Produces images of vessels perfusion • Colour map of the image provides easy interpretation • No contact device • It can be portable, if processing unit is replaced by a mobile device • Higher surface area covered 	<ul style="list-style-type: none"> • Low light penetration, image is a representation of the surface vasculature • No quantification of blood flow • No information of blood flow of large and deep vessels • Still under development

Continued on next page ...

Table 2.3 – continued from previous page

Method	Application	Advantages	Disadvantages
Air/water plethysmography	<ul style="list-style-type: none"> • Measurement of blood volume in whole extremity • Blood flow quantification using VOP • Evaluation of vascular response 	<ul style="list-style-type: none"> • Non-invasive method • High sensitivity • Allow to measure large volumes of tissue 	<ul style="list-style-type: none"> • It is cumbersome, it requires a chamber filled with air/water • It requires expertise to place all the instruments required • More than one instrument needed to take measurements • Motion affects readings greatly
Strain gauge plethysmography	<ul style="list-style-type: none"> • Quantification of retrograde outflow in the deep venous system • Assessment of peripheral arterial disease • Combined with VOP weighs venous filling 	<ul style="list-style-type: none"> • Non-invasive method • It is portable as only once sensor is required • Easy to use, no clinical training required 	<ul style="list-style-type: none"> • Some sensors use banned mercury • Measures plethysmography in a confined circumference around the sensor location • It does not measures large volumes of tissue
Bioelectrical impedance plethysmography	<ul style="list-style-type: none"> • Monitoring of blood volume in thoracic cavity or limbs • Measurement of heart stroke volume • Quantification of cardiac output • Thoracic respiratory volume • Blood flow estimation • Oedema and detection of deep vein thrombosis (DVT) 	<ul style="list-style-type: none"> • Non-invasive technique. Commonly, two or four electrodes are required • Easy to use, adhesive electrodes can be attached to predefined points in the body • Low energy required, it can be portable • Not affected by temperature or skin pigmentation • It measures large volumes of tissue. Boundary limited by sensing electrodes 	<ul style="list-style-type: none"> • Signal sensitive to motion • Electric current not suitable for whole population (i.e. patients with pacemakers" • Requires measurement of limb section to correct measurement quantification • Requires skin preparation, sweat or alien substances on skin may interfere the readings

2.6 Conclusion

This chapter presented the concept of circulatory system plethysmography and how can be measured with different instruments. The measurement of blood volume or flow getting in an out from tissue ensures the adequate interchange of nutrients and by-products. It is clear that any disease that limits the supply of either arterial or venous blood may lead to the development of ischaemia or hypoxia. The diseases that cause this circulatory problem usually are assessed clinically by qualitative methods, therefore methods that allow the early detection of circulatory blockage are desirable. This section provided a an explanation of the rationale behind monitoring blood volume and flow in a home or low clinical setting. Subsequently, different instruments were elaborated upon, along with the potential to quantify blood flow. In addition, the Doppler Ultrasound method was described along with the various optical instruments. The venous occlusion plethysmography is a useful tool for quantifying blood rate but it is not suitable for whole population. Three different apparatuses have the potential of being used at home or low resource setting. However, obtaining the flow rate from the bioelectrical impedance plethysmography seems to be an excellent choice because it is able to assess a larger volume of tissue as compared to other methods.

Bioelectrical impedance plethysmography

One of the primary objectives of this work is to produce a device capable of detecting, measuring, and quantifying changes in the venous and arterial circulation on a continuous basis. As described in the previous chapter, plethysmography is one of the most common methods used to measure these changes. Armed with this information, it becomes possible to quantify changes in blood volume that can be translated into changes of blood volume or even flow rate. Before delving deeper into the design of this device, it is necessary to understand the principles of operation and theories behind this technology.

This chapter describes the underlying principles behind bioelectrical impedance plethysmography in greater detail. But before doing that, the effect of alternate current (AC) will be described to identify the safe limits when applied to the human body. Subsequently, the basics of the electrical impedance in conductors are illustrated, including the manner in which electrical current distributes in volumes. Next, the electrode-skin interface is examined in order comprehend how electric current conduction converts into ionic conduction, including electrodes topologies.

Bioelectrical impedance elaborates on the effect on AC current flow and the potential differential this generates in the human body. In the following sections of this chapter, a scope of the latest bioelectrical impedance technology will be described, including essential components and methods needed to measure it. Thereafter, the clinical application of impedance plethysmography will be covered in greater detail.

3.1 Electrical current in the human body

Injecting electric current into biological tissue requires some safety measurements to guarantee the patients' welfare. Driving current into the human body may cause unpleasant effects such as heating, electrolysis at the electrode-tissue interface or neuromuscular stimulation [98, 103]. Any direct current above 2 Volts potential may cause electrolysis in the skin. The positive charge ions will migrate to the negative electrodes and the negative charge ions to the positive electrode. As a result, the moisture in the interface skin-electrode becomes alkaline causing full-thermal epidermis damage because of electrolysis of water, oxidation of saline, reduction of hydrogen ions and oxidation (corrosion) of the electrode metal [104].

Neuromuscular stimulation is the most dangerous adverse effect because it controls blood circulation and respiration. At any cost, this effect should be avoided by controlling the current's amplitude, waveform and frequency. The levels of current sensation vary from person-to-person, sex and even electrode geometry. Brown et al. [105] have established a threshold current whereby sensation increases when the frequency rises, the figure 3.1 displays the relation between the threshold current sensation and frequency dependency of the human body. The maximum sensitivity of the nervous system is in the frequency range between 10 Hz to 1 kHz. At frequencies above 1 kHz sensitivity is considerably reduced and is entirely imperceptible above 100 kHz. In fact, the heat effect at these frequencies is so high that electro-surgical devices use it. Square waves should be avoided because they combine the DC and AC effect in one signal. In this case, special consideration should be taken in pulse duration as this increases the DC value of the signal [98].

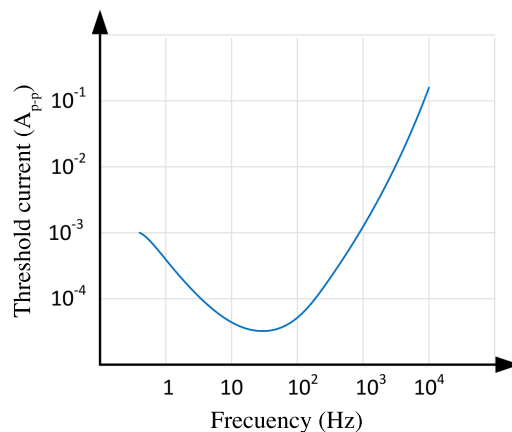


Figure 3.1 Threshold current sensation vs. frequency. Adapted from [105]

The table 3.1 illustrates the tolerance of the human body to different levels of electric current. These effects are mostly predicated on current rather than frequency. When frequen-

3.1 Electrical current in the human body

cies scale beyond 100 kHz especially on the radio-frequency (RF) range (400 kHz to 3 MHz) the heating effect of the tissue tends to be more common. As seen below, in order to avoid discomfort among patients, currents below 5 mA must be used in a bioelectrical impedance device.

Table 3.1 Effect of electric current in the human body at different levels, which may induce ventricular fibrillation. Including levels of tolerance. Table adapted from information from Brown et al. [105]

Current Level	Effect
< 1 mA	<ul style="list-style-type: none"> • Usually not perceptible
1 mA	<ul style="list-style-type: none"> • Threshold of current perception • Tingling sensation
5 mA	<ul style="list-style-type: none"> • Sensory nerve stimulation • Shock sensation
6 mA to 25 mA (Women)	<ul style="list-style-type: none"> • Painful electric shock • Lack of muscular control
9 mA to 30 mA (Men)	<ul style="list-style-type: none"> • Difficult to let go - freezing current range • High muscle contraction
50 mA to 150 mA	<ul style="list-style-type: none"> • Extreme pain • Possible respiratory arrest • Possible ventricular fibrillation • Severe muscular contraction • Possibly death
1 A to 4.3 A	<ul style="list-style-type: none"> • Heart's electric coordination compromised • Muscular contraction and nerve damage • Death likely
10 A	<ul style="list-style-type: none"> • Cardiac arrest • Severe burns • Highly probability of death

Recommendations, guidelines and norms for patient safety are contained in international standards compiled by the International Electrotechnical Commission (IEC). The standard applicable to medical equipments or equipments to be used for humans is referenced as IEC 60601, or IEC 601 [106]. Some of these recommendations regarding safety are expressed as follows: first, the commission considers any frequency below 0.1 Hz as direct current in order to avoid ulcers created by electrode-skin interface; this type of current should be limited to $10 \mu\text{A}_{\text{RMS}}$. Moreover, for frequencies up to 1 kHz, it is recommended to limit the frequency of current at $100 \mu\text{A}_{\text{RMS}}$. Secondly, avoiding nerve stimulation is paramount

for patient safety; at frequencies above 1 kHz, muscular stimulation becomes very difficult. Therefore, it is recommended to use frequencies higher than this value. Thirdly, one important recommendation of the standard is that the maximum amount of current flowing through skin contact must be limited to $500 \mu\text{A}_{\text{RMS}}$ with a single fault equipment. Lastly, as explained before, in the RF range tissue that could be heated, tissue burns can be avoided by limiting the density and duration of current; for instance, it is recommended to use densities of less than 1 mA mm^{-2} [105]. As a final recommendation, the commission has established that regardless of waveform and frequency, no leakage current shall exceed $10 \text{ mA}_{\text{RMS}}$ in normal condition or in single fault condition [106].

3.2 Electrical impedance principle

From the electrical point standpoint, impedance is defined as the opposition that a medium presents to either an alternating current (AC) or voltage (see figure 3.2) [107]. Impedance is equal to the complex ratio between electrical voltage and current. This mathematical fraction produces a complex number which is known as symbol Z (see equation 3.2). This comprises of a resistance (also known as conductance) and/or reactance value, which is commonly represented by the letters R and X respectively. Hence, the impedance measurement can be expressed as a relation of the output magnitude and the phase difference between real and imaginary parts, as shown in equation 3.1; it can be plotted in the complex plane as shown in figure 3.3.

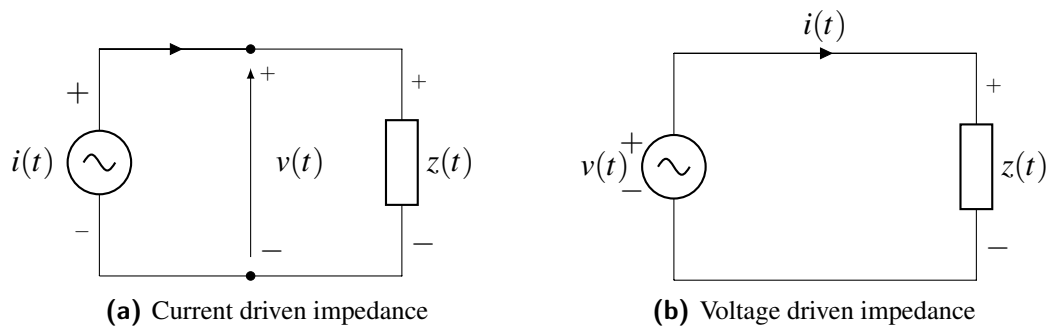


Figure 3.2 Schematic representation of electrical impedance. The three elements that are required are the voltage $v(t)$, the alternating current $i(t)$ and the opposition to the current ($z(t)$). The impedance can be driven by either current or voltage. Image adapted from [107].

$$Z = |Z| \angle \phi \quad (3.1)$$

3.2 Electrical impedance principle

There are different ways to represent impedance. However, bioelectrical impedance can be described in the form of either resistance (R) or reactance (X). Notably, in this complex number, the resistive part signifies the real actual part of the measurement, whereas the reactance constitutes an imaginary one. Therefore, the impedance magnitude can be written as a function in these two values, as illustrated in the equation 3.2.

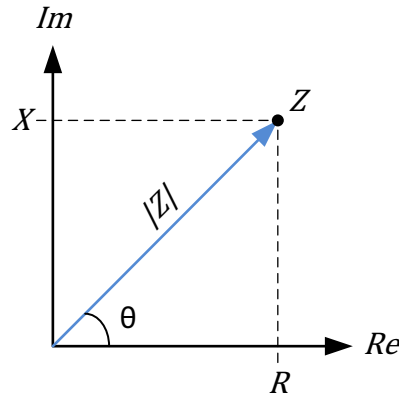


Figure 3.3 Plot of the impedance in the complex plane.

$$Z = Z' + jZ'' = R + jX = |Z|e^{j\theta} \quad (3.2)$$

$$|Z| = \sqrt{ZZ^*} = \sqrt{R^2 + X^2} \quad (3.3)$$

$$\theta = \tan^{-1} \frac{X}{R} \quad (3.4)$$

$$R = |Z|\cos(\theta) \quad (3.5)$$

$$X = |Z|\sin(\theta) \quad (3.6)$$

As seen above, when the angle difference of the impedance is 0° , the load is completely resistive. In contrast, when the phase difference is 90° the load is purely reactive. On the basis of the previous equations, it is possible to represent impedance in the complex plane, as illustrated in figure 3.3.

Another way to express and analyse impedance is using sinusoidals. For instance, when a sinusoidal steady-state waveform injects a current $i(t) = I_A \cos(\omega t)$ into an unknown load, the response is a shifted sinusoidal waveform with a potential equivalent of $v(t) = V_B \cos(\omega t + \phi)$. Figure 3.4 illustrates the representation of both waveforms. Hence, the impedance can be denoted as the ration of these two quantities based on Ohm's law (see equation 3.7).

$$Z = \frac{V}{I} \tag{3.7}$$

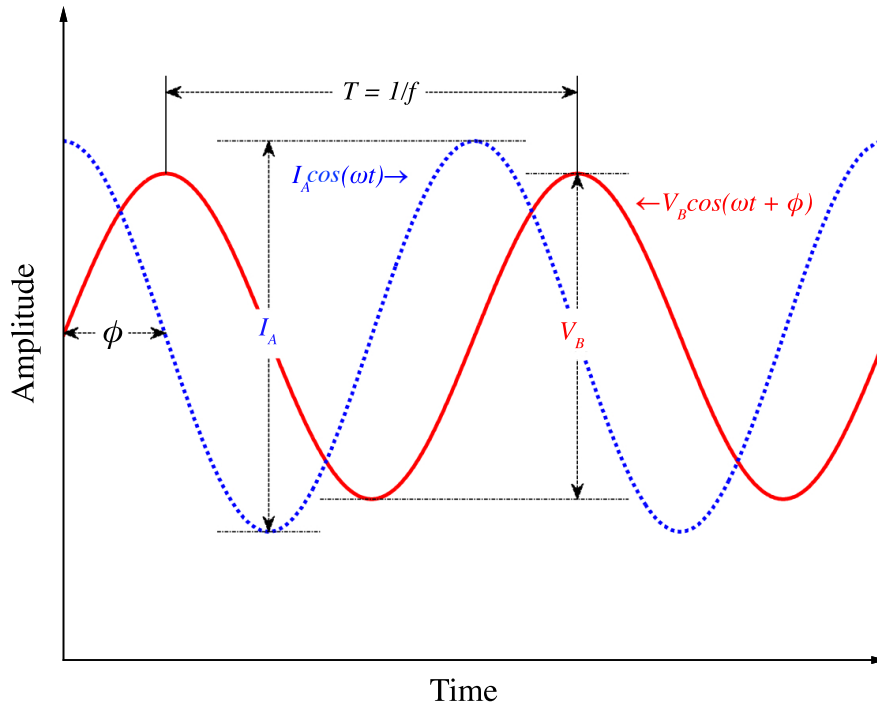


Figure 3.4 Waveform plot of a current ($I_A \cos(\omega t)$) compared to the potential representation ($V_B \cos(\omega t + \phi)$) of an unknown load.

However, performing mathematical operations with trigonometry identities could be quite tedious. Therefore, equivalent methods are used in order to analyse impedance in an electric circuit. Using Euler’s formula allows us to express trigonometric functions in order of e . The equation 3.8 illustrates the relation between both entities.

$$e^{j\omega t} = \cos(\omega t) + j\sin(\omega t) \tag{3.8}$$

Therefore, voltage and current can be rewritten in the form of complex exponential thanks to Euler’s equation.

$$v(t) = V_B \cos(\omega t + \phi) = V_B (e^{j(\omega t + \phi)}) \tag{3.9}$$

$$i(t) = I_A \cos(\omega t) = I_A (e^{j\omega t}) \tag{3.10}$$

3.3 Current distribution in conductors (Geselowitz theorem)

Using Ohm equation 3.7 makes it possible to calculate the resultant impedance of the waveforms. Therefore, the expression using complex exponentials would be equal to:

$$Z = \frac{v(t)}{i(t)} = \frac{V_B(e^{j(\omega t + \phi)})}{I_A(e^{j\omega t})} = \frac{V_B}{I_A} e^{j\phi} \quad (3.11)$$

Based on Euler's equation, it is possible to deduce the real and imaginary parts of the complex exponential of equation 3.11.

$$Z = \frac{V_B}{I_A} e^{j\phi} = \frac{V_B}{I_A} (\cos(\phi) + j\sin(\phi)) \quad (3.12)$$

Using the principle of superposition, it becomes possible to assume that the real and imaginary components of impedance are signified by the following formulae that are equivalents to the ones obtained with phasor analysis equations 3.5 and 3.6.

$$Z' = R = \frac{v(t)}{i(t)} = \frac{V_B}{I_A} \cos(\phi) \quad (3.13)$$

$$Z'' = X = \frac{v(t)}{i(t)} = \frac{V_B}{I_A} \sin(\phi) \quad (3.14)$$

In conclusion, it is possible to obtain real and imaginary values of impedance if the maximum amplitude of the voltage (V_B) and current (I_A) are known, in addition to their difference in phase (ϕ).

3.3 Current distribution in conductors (Geselowitz theorem)

Geselowitz [108] studied the change in conductivity within a constant geometry. In short, his analysis entailed the application of lead field theory into electrical impedance. Simplifying the origin of the equation, the total impedance of the entire volume is equivalent to the sum of all the small impedances within each small volume dV [98].

The analysis of this equation begins from the study of the four-electrode measurement and the change in conductivity of the internal region of a volume conductor [103]. Figure 3.5 posits that a volume conductor is electrically linear and surrounded by an insulator ξ . If the

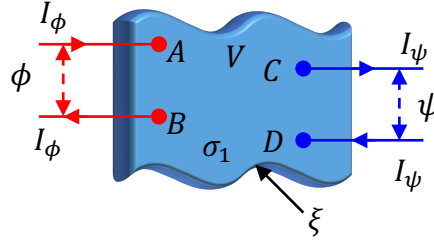


Figure 3.5 Volume conductor V of conductivity σ_1 . A:B represent current injection electrodes and C:D are sensing electrodes. Image adapted from [98]

internal conductivity changes from σ_1 to σ_2 (equivalent to $\sigma_1 + \Delta\sigma$) then the potential field of the current injection will change from ϕ to ϕ' (equal to $\phi + \Delta\phi$) although the potential field ψ will remain unchanged. Then, the field equation will be as follows:

$$\int_{\Omega} \sigma \cdot (\phi - \phi') \cdot \nabla \psi d\bar{S} = \int_V (\sigma_1 - \sigma_2) \cdot (\nabla \phi' \bullet \nabla \psi) \cdot dV \quad (3.15)$$

By replacing the terms with the equivalents, the equation can be rewritten in accordance to the next equation.

$$-\Delta\phi_{CD} \cdot (-I_{\psi}) = - \int_V \Delta\sigma \cdot [\nabla(\phi + \Delta\phi) \bullet \nabla \psi] \cdot dV \quad (3.16)$$

The impedance change can be deducted by dividing the function by the currents involved I_{phi} and I_{ψ} . As a result, the Geselowitz equation is equivalent to:

$$\Delta Z = \frac{\Delta\phi_{CD}}{I_{\phi}} = - \int_V \Delta\sigma(x, y, z) \cdot \left[\frac{\nabla(\phi + \Delta\phi)}{I_{\phi}} \bullet \frac{\nabla \psi}{I_{\psi}} \right] \cdot dV \quad (3.17)$$

The previous equation is the key to calculating the change in impedance in a volume within defined boundaries. However, this only applies to homogeneous and isotropic volume conductors. The equation can be simplified if it is assumed that a unit of current passes through and the volume conductor can be denoted by a number of discrete elements of uniform conductivity within a three dimensional space (x, y, z) . As a result, the equation can be simplified as follows:

$$\Delta Z = -\Delta\sigma \cdot \int_V \nabla(\phi + \Delta\phi) \bullet \nabla\psi \cdot dV = -\Delta\sigma \cdot S \quad (3.18)$$

where S denotes the sensitivity matrix in three dimensions; it is independent of conductance. Calculating this variable requires a series of assumptions, such as the initial conductivity distribution being uniform [109]. This document is not centred on the mathematical analysis of the sensitivity S , but deducing those impedance changes are directly related to the change of geometry within this segment. Several studies provide credence to the fact that sensitivity varies in accordance to the electrodes position and geometry, as researched by Bertemes [103].

3.4 Electrode-skin interface

Electrodes play a crucial role in a bioelectrical impedance system. Indeed, the nuances of electrode geometry, distance and material may influence the final readings from a biological standpoint. Consequently, the impedance of the electrodes should be significantly lower than the ones from the subject under test. For this, highly conductive materials are used in the manufacturing of electrodes like platinum (*Pt*), gold (*Au*) or stainless steel. Furthermore, other independent variables such as temperature, ionic tissue contents and protein adhesion may also influence the changes of electrode impedance [98, 110]. In terms of electrode geometry, Ohm's law (equation 3.19) explains, for instance, how changing the length of the electrode affects its resistance (R).

$$R = \rho \frac{L}{A} \quad (3.19)$$

In the previous equation, ρ denotes the electrical resistivity of the material, A refers to the area of the electrode, and L signifies the longitude or thickness. The resistance (R) reduces when the area (A) of the electrode increases. However, the total resistance (R) is directly proportional to the length of the electrodes.

A physical effect takes place when electrical current passes through the electrode-skin interface. First, only ion conduction takes place in the human body; therefore, at the electrode, an exchange of charges convert electrical current into a transport of ions. Second, an electrochemical reaction known as electrolysis follows at the electrode-tissue boundary. This effect creates a "double layer capacitance (DLC)" which, as its name indicates, adds

Bioelectrical impedance plethysmography

a capacitive effect to the boundary creating an unwanted DC charge [111]. Consequently, applying an AC waveform inverts the electrode polarity during each cycle, thereby minimising this capacitive effect. However, this is also a frequency dependent development which is more noticeable at low frequencies [103].

Figure 3.6 shows the equivalent circuit model of the electrode-tissue interface. This model characterises by the half-cell potential of the dual-layer, portrayed as a battery (E_{hc}), the impedance and polarisation of the electrode-electrolyte interface represented by a charge transfer resistance (R_{CT}) in parallel with the interface's impedance (Z_{CPE}). This circuit is incongruity with the tissue impedance (Z_t) which is equivalent to an RC network [111, 112] (see figure 3.9). Some authors have defined the interface's impedance as either a constant phase or angle impedance or constant phase element (Z_{CPE}) [113–115]. In short, the Z_{CPE} is a correction factor on the empirical electric model of the electrode. This term has been added to fit the experimental data of the electrode's RC response, which deforms and broads the Nyquist diagram when a frequency sweep is applied. This element behaves as an imperfect capacitor; hence, it is frequency-dependent.

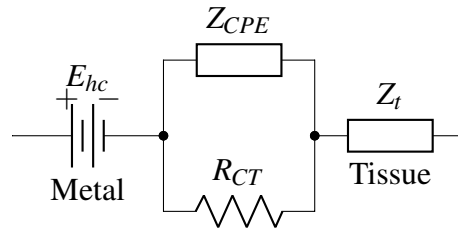


Figure 3.6 Equivalent circuit of the electrode-tissue interface (Adapted from Franks [113])

The value of Z_{CPE} can be calculated from the following empirical equation 3.20 given by McAdams [116, 117].

$$Z_{CPA} = K(j\omega)^{-\beta} \quad (3.20)$$

where K denotes a measure of the magnitude of Z_{CPE} , β represents a constant ($0 \leq \beta \leq 1$) signifying inhomogeneities in the surface (typically 0.8 for a number of biomedical electrode systems) and $\omega = 2\pi f$. When $\beta = 1$, Z_{CPE} is equivalent to a purely capacitive impedance element [113, 115–117].

Electrodes are also a source of error when taking measurements. Some blunders can even distort the original signal; for instance, thermal or Johnson-Nyquist noise. This type of noise is entirely inherent to the electrode and is predicated on external variables such as

temperature and bandwidth of the measurement [116]. Another source of errors caused by electrode can be derived from their position in the body, lack of surface contact, or mismatch in materials and geometries. Therefore, in order to improve and maximise the area of contact, some electrodes necessitate conductive gel. In this matter, according to Caicedo et al. [118], using commercially available electrodes for electrocardiogram (ECG) purposes demonstrated to provide good impedimetric readings, as opposed to specially designed electrodes.

In regards to re-positioning electrodes, an experiment using ECG electrodes was conducted to determine whether removing one or four electrodes and putting them back in the same position could cause errors in readings. It was found that putting electrodes away and then getting them back into the same position for an extended period caused minimum changes in impedance readings. But, the sensitivity to impedance changes depended on the position and area of the voltage-detecting electrodes with respect to those of the current injection electrodes [119].

Using the right amount and position of electrodes in the body may minimise errors in the readings. For this, various electrode topologies are used to take impedance measurements. Some of these options include two-electrode (bipolar), three-electrode (tripolar) and four-electrode setting (tetrapolar). A bipolar or tripolar configuration adds the electrodes complex impedance in series with the tissue. This unknown electrode impedance results in a significant error that is added to the total measurement. If the impedance of the electrodes were greater than the one of the skin, this might completely conceal the actual value of the tissue impedance. Thus, a bipolar configuration is not the best option for bioelectrical impedance measurements.

In the present work, a tetrapolar electrode configuration was used during the experiments. The following section analyses the equivalent circuit of four electrodes measurement showing its effectiveness on diminishing the electrode's impact on the total impedance measurement.

3.4.1 Analysis of tetrapolar electrode configuration

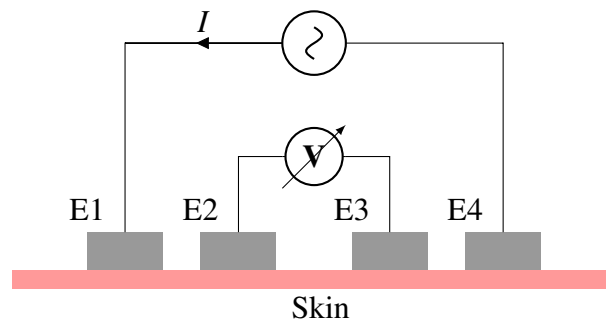
The tetrapolar configuration is the most common method to measure bioelectrical impedance in human limbs [19, 21, 22, 120]. Some of the advantages of this approach are that in theory, it cancels out the added electrode impedance. However, it must comply with the following: first, the input impedance of the measuring instrument should be infinite, or as per the best estimate, the impedance should be higher than the one from the body. Second, the electrode's contact area with the skin surface should flat and even.

Currently, it is difficult to meet these requirements, but it is possible to get close to them. Measuring impedance using state of the art of integrated circuits (IC) is likely to achieve high

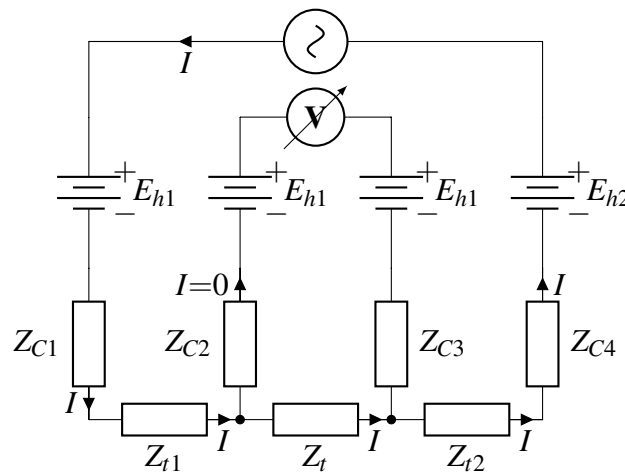
Bioelectrical impedance plethysmography

input impedance, in the order of $G\Omega$ [121]. When compared with hundreds of ohms of the soft tissue in humans [122, 123], the error minimises dramatically. Additionally, the contact area can be improved if the electrodes contain an electrolytic solution. Using this type of gel moisturises the skin reducing its impedance and improving ionic conduction [123, 124].

The figure 3.7 illustrates the common electrode topology and the equivalent circuit. Usually, the outer pair drives current into the body, and external ones measure the potential generated (see figure 3.7a). The figure 3.7b shows the simplified equivalent circuit and the current path. From there, the following analysis will be performed to estimate the impedance contribution of electrode Z_{C2} and Z_{C3} .



(a) Tetrapolar electrode position for most of bioelectrical impedance measurements. The outermost electrodes (E1 and E4) are connected to the AC source. Similarly, the potential electrodes are connected to the inner electrodes (E2 - E3).



(b) Simplified model of the tetrapolar electrodes model. Z_C denotes the impedance of these electrodes. Z_t refers to the impedance of the body at each end of these electrodes. In an ideal setting, the voltmeter has an infinite input impedance; therefore, no current flows through the electrodes Z_{C2} and Z_{C3} .

Figure 3.7 Tetrapolar electrodes position in a measurement over the skin with the equivalent circuit.

In accordance to the figure, the applied sinusoidal current is equal to $I(t) = Ie^{j\omega t}$. Following the current path, the equivalent potential drop around the tissue (Z_t) will be given by the equation 3.21.

$$V(t) = Z_t I e^{j\omega t} \quad (3.21)$$

$$V(t) = V_t e^{j(\omega t + \theta)} \quad (3.22)$$

Due to the high impedance of the measurement device, the current flowing through Z_{C2} and Z_{C3} would be close zero. Then, the measured potential will be equivalent to the one taken from the body segment (Z_t). Therefore, the total impedance (Z_m) measured by the instrument can be calculated using equation 3.23.

$$Z_m(t) = \frac{Z(t)}{I(t)} = \frac{V_t e^{j(\omega t + \theta)}}{I e^{j\omega t}} \quad (3.23)$$

$$Z_m(t) = Z_t e^{j\theta} \quad (3.24)$$

Finally, the measured impedance Z_m is equivalent to the one complex impedance from the body segment $Z_t e^{j\theta}$, thus reducing the incidence of the potential electrodes.

At the moment of taking measurements for localised bioelectrical impedance using tetrapolar configuration, Bertemes et al. [103] demonstrated that the distribution of the electrodes impacts the sensitivity of the system along with the geometry of the cells contained within the tissue. According to the author of the experiments, the separation of injection and detection electrode pairs affects the existing depth of penetration. In other words, the bigger the separation between the pair of electrodes, the deeper the AC signal is likely to go.

3.5 Bioelectrical impedance

Before describing the manner in which impedance plethysmography operates, it would be more prudent to understand how the principle of bioelectrical impedance is defined. Firstly, the term electrical impedance spectroscopy (EIS) refers to the study of the absorption of energy in accordance to the frequency of electromagnetic (EM) waves. When measurements are performed in a biological sample, this method could be referred to as either electrical bioimpedance or bioelectrical impedance [110]. The term to be used in the context of this document will be bioelectrical impedance. The interaction with tissue occurs in the frequency

Bioelectrical impedance plethysmography

range from 100 Hz to 10 MHz [103]. In this thesis, the frequencies of interest are focused in the lower range of the spectrum. Indeed, plethysmography devices are known to commonly operate in the radio wave frequency of the electromagnetic spectrum.

The human body comprises of four basic tissues known as epithelium, muscle, connective tissue and nervous tissue. Epithelium covers the whole surface of the body. Muscles are in charge of the movement, whereas connective tissues impart protection to organs. Nervous tissue provides the internal transmission line for the electrical impulses coming from the brain. Cells that create these tissues play a fundamental role with regard to ionic conduction when an analogue current (AC) is applied to the body [111]. Hence, impedance readings vary based on the parameters of these cells and their protein content. It is especially important to understand the geometry and characteristics of the red blood cells, which transport O_2 around the body.

In the human body, there are more RBCs than any other cells, and they entail particular resistive properties. Its disk shape can be ideally represented as a spherical particle with membranes around the surface, as represented by Figure 3.8. Live cells can be represented as multilayer cells where its internal cytoplasm has a specific permittivity (ϵ_{cp}) and conductivity (σ_{cp}). Likewise, these characteristics are similar to the one surrounding the cell known as extracellular fluid (ϵ_m and σ_m). However, the membrane suffers from a very low permittivity (ϵ_{MBR}) and conductivity (σ_{MBR}) which behaves as a dielectric. In contrast, in the case of dead cells the membrane becomes loose and does not provide resistance to electric current [111].

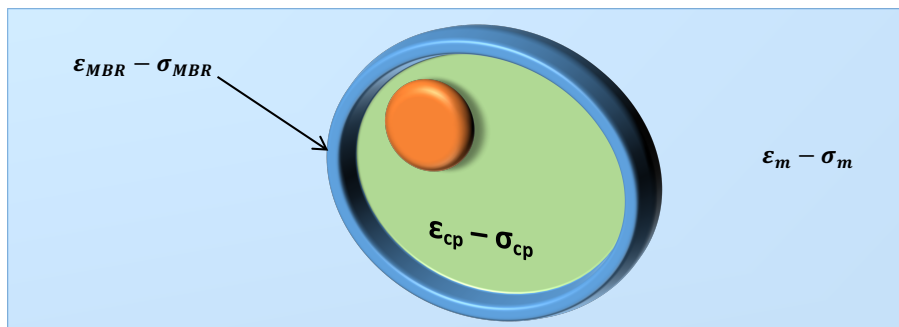


Figure 3.8 Representation of a cell with its electric characteristics. Internal cytoplasm characteristic permittivity ϵ_{cp} and conductivity σ_{cp} . Extracellular fluid permittivity ϵ_m and conductivity σ_m). Membrane permittivity described as (ϵ_{MBR}) and conductivity (σ_{MBR}). Adapted from [98]

A cell can change its internal cytoplasm using two different means, either changing the permeability of their bilayer lipid membrane (BLM) or through the use of ionic channels or pumps. The BLM is about 7 nm thick. Altering its permeability allows lipids and water molecules to pass through [110]. The interface between the extracellular space, the cell

3.5 Bioelectrical impedance

membrane and intracellular space ($\sigma_m \rightarrow \sigma_{MBR} \leftarrow \sigma_{cp}$) behave as a capacitor since membrane is a dielectric between two conductors, denoted as C_m in figure 3.9a.

In contrast, parallel to BLM, the ionic channels and pumps enhance the functionality of membranes. Ionic channels or "channel proteins" allow for the transport and exchange of certain types of ions such as Na^+ , K^+ , Chloride (Cl^-) and Calcium (Ca^{2+}) between the inside and outside part of the cell [111]. Ion pumps are caused by sensitivity of the membrane to a voltage and are responsible for the membrane's non-linear properties as a response to low voltage. This pump causes cell polarisation, enabling the flow of ion charges in the body. Electrically, these channels act as a resistor (R_m).

According to previous analysis, the cell can be simplified in an equivalent electric circuit model, as shown in Figure 3.9. This model indicates that if AC is pumped into the extracellular medium, there are two possible paths for the current to go through. One way is around the cell - represented by the resistive characteristic of the extracellular medium (R_e). Under the second route, current flows through the cell. It is possible that AC flows initially either over the BLM, which is represented as a capacitance (C_m), or across ionic channels (R_m). Upon reaching the cell, current travels via the intracellular medium (R_i) that is mostly resistive. Finally, the electrical current exits from the cell through the membrane, which again lies in the same C_m and R_m .

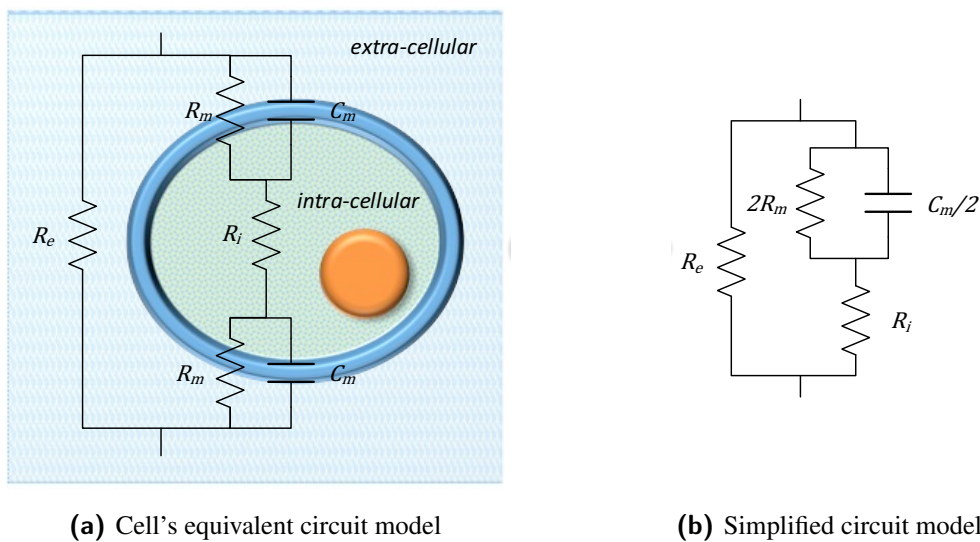


Figure 3.9 Electrical model of the cell and its simplified version. R_e is the resistivity of the extracellular medium, R_i is the resistivity of the intracellular medium and R_m and C_m are the resistivity and capacitance of the membrane. Image adapted from [98]

Bioelectrical impedance plethysmography

Since C_m and R_m share the same values when the current enters and exits the cell, this can be simplified in the electric model as the two resistors in series ($2R_m$) and two capacitances are parallel to each other ($C_m/2$) as indicated by figure 3.9b.

When an EM field is applied on the tissue, cells respond based on the frequency applied, highlighting three distinctive areas in the spectrum, as described by Schwan et al. [125, 126]. Figure 3.10 displays the dielectric response against frequency, which reveals valuable information about the functional and structural properties of the cell [111]. According to the graph, there are three denominating areas α , β and γ dispersion. Firstly, α dispersion (from 10 Hz to a few kHz) is generally associated with frequency dependent properties of the cells' membrane. Secondly, β dispersion (10 kHz to several MHz) is related to the dielectric property of the cell membrane as well as the interaction between the internal and external mediums. Finally, γ dispersion (> 10 GHz) is attributed to the dielectric relaxation of bulk dispersing media, the Debye dispersion in water (17 GHz), and the presence of small molecules.

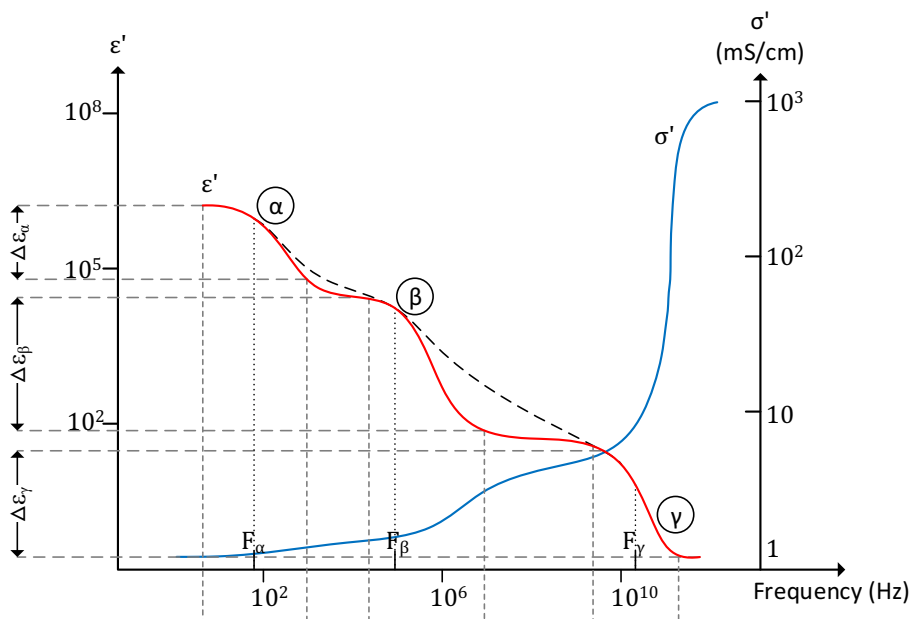


Figure 3.10 Representation of a cell with its dielectric characteristics. Internal cytoplasm characteristic permittivity ϵ_{cp} and conductivity σ_{cp} . Extracellular fluid permittivity ϵ_m and conductivity σ_m . Membrane permittivity described as (ϵ_{MBR}) and conductivity (σ_{MBR}). Adapted from [98, 111]

In addition, the β dispersion region provides supplementary information about the cell. Lvovich [111] divides this area into three subregions in accordance to the interaction of the electrical current with the cell. The β_1 relaxation is caused by the capacitive membrane C_m , occurring in the low kHz range. When the frequency increases between kHz and low MHz

range, the internal cytoplasm of the cell produces a β_3 dispersion owing to a change from resistive to capacitive conduction. However, this capacitive component is often disregarded, thereby simplifying the model into a resistive element R_i . Ultimately, β_2 occurs in the range of low MHz when the electrical charge movement through the cell shifts into a capacitive conduction.

This research document is centred on the β dispersion region between 100 Hz to 1 MHz. The designed impedance plethysmography device presented in chapter 4 operates in a wide selection of frequencies of up to 200 kHz.

The ideal electrical model of the cell is shown in figure 3.9 is a very close approximation that facilitates the prediction of bioelectrical impedance behaviour for dilute cell suspension. However, the tissue is more complex than this particular simplified model because it is comprised of additional elements that must be added to the analysis. For instance, tissues like muscle exhibits extreme anisotropy (conductivity is not the same when measured in different directions) [111, 127, 128]. In addition, different resistivity values have been obtained when measuring bioelectrical impedance during the cardiac cycle longitudinally and transversely [129]. Another instance of how impedance changes in the context of tissues properties can be seen in the performed by Casas et al. [130]. This study showed the differences between normal and ischaemic tissue of a pig's myocardium muscle. Impedance clearly presented a different impedimetric response when a frequency sweep was done between 10 Hz to 1 MHz.

3.5.1 Mathematical representation of electrical impedance

Electrical impedance can yield a different response based on the frequency. In a bioelectrical impedance analysis (BIA), the impedimetric response needs to be represented as a function of the frequencies used along with the magnitude and phase obtained. Different mathematical models have been studied based on the basic and ideal framework, as shown in figure 3.9b. However, this model does not entirely encapsulate the effect of the membrane at high frequencies. Debye came up with the following equation that took the suspension of free poles into consideration [103].

$$\epsilon_r^* = \epsilon_{HF} + \frac{\epsilon_{LF} - \epsilon_{HF}}{1 + j\omega\tau} \quad (3.25)$$

In this equation, ϵ_r^* signifies the complex relative permeability, ϵ_{LF} and ϵ_{HF} represents the permeability at low and high frequency, respectively and τ denotes the relaxation time constant. Meanwhile $j\omega = 2\pi$ refers to the angular frequency in radians. However, it was not

Bioelectrical impedance plethysmography

until 1941 when Cole brothers took into account, dispersion by factoring the Debye equation that an additional parameter called α resulted in the equation 3.26. This mathematical formula is widely used to obtain the approximate value of impedance during the course of taking biomedical measurements [131].

$$\epsilon_r^* = \epsilon_{HF} + \frac{\epsilon_{LF} - \epsilon_{HF}}{(1 + j\omega\tau)^{1-\alpha}} \quad (3.26)$$

The parameter α is limited for values between 0 and 1. When its value is equal to zero, the Cole-Cole equation will yield the Debye equation (3.25) as a solution for polar dielectrics. Consequently, from this mathematical statement, it is possible to obtain data representation known as the Cole-Cole plot. It is a two-dimensional graph where the plot of ϵ'' or the imaginary part of the equation lies in the y -axis vs ϵ' in the x -axis, which forms the real part of the solution.

The representation of data using Cole-Cole representation allows to see changes in frequency for different tissues. This information is valid when spectroscopy studies are being performed. Regarding the most suitable frequency to measure impedance plethysmography, whole body bioelectrical impedance analysis has shown that limbs contributed significantly to the impedance at frequencies 0.5 kHz, 50 kHz and 100 kHz [132]. Therefore, any AC with this frequency spectrum is suitable for an impedance plethysmography instrument.

3.6 State of the art of commercial bioelectrical impedance devices

Measuring impedance plethysmography requires of devices tuned in within the impedance range of the section of the body being studied. Bioelectrical impedance is the technology used to estimate changes of volume in the body using electrical current, the name of the technique is impedance plethysmography (iPG). This kind of technology still keeps the same principles when was first implemented in the 1950s [102] described deeply in the following section. However, the modern development of this method has been centred in the miniaturisation of the electronics, reduction of measurement errors and the development of signal processing algorithms.

There are not many commercial products certified for the measurement of impedance plethysmography. In fact, to the knowledge of the author, only one device is commercially being used for iPG measurements. Three kinds of methods can record impedance plethysmog-

3.6 State of the art of commercial bioelectrical impedance devices

raphy: specially purposed circuits, impedance cardiography and impedance plethysmography devices. Table 3.2 summarises the different commercially available devices including features and applications.

Designing custom bioelectrical impedance devices allow flexibility to work with different signal parameters, like waveforms, frequencies and amplitudes. Additionally, it is possible to apply new algorithms to the raw signal. Off the shelf devices may require the use of the equipment in alternative ways; for instance, some studies used impedance cardiography devices to record plethysmography waveforms from limbs [102]. However, technically, it is still acceptable to use this kind of devices as the technical characteristics are similar to the ones used in impedance plethysmography (see table 3.2). The following are examples of the state of the art of devices capable of taking impedance plethysmography signals.

Nowadays, there are efforts to incorporate this technology as part of wearable devices. For instance, Samsung Electronics has released a hand-wrist size wearable device called *simband* [133]. This is a device designed as a research and development platform. In their product announcement, Samsung uses electrical impedance in order to measure the galvanic impedance response (GSR) and Bio-Impedance (Bio-Z). This sensor performs heart rate measurement by measuring the pulse wave of blood flow in the artery around the wrist. The device acquires different physiological signals but interestingly their architecture is open to develop algorithms that process these waveforms.

In the medical field, a significant number of devices use bioelectrical impedance for different medical applications, such as impedance cardiography (ICG) devices. They have been developed to measure different properties of the heart such as stroke volume (SV), cardiac output (CO) and systemic vascular resistance (SVR) [134]. Nevertheless, apart from its main application, this kind of instrument has also been used to measure plethysmography in limbs aiming other medical application such as detection proximal vein thrombosis (PVT) [135] or the levels of ischaemia during orthopaedic surgery [136].

Another company that has successfully created an FDA approved medical device using bioelectrical impedance in the market is Cheetah Medical [137] from Israel. This company based out of Boston (US) has developed a medical device called Cheetah NICOM which gauges haemodynamics non-invasively using as many as four electrodes configuration. The device is used in different hospital areas such as critical care, haemodialysis, emergency department and operating theatres.

Finally, German company Medis (Medizinische Messtechnik GmbH) [138] is a spin-off company from Institute of Biomedical Engineering of the Technical University Ilmenau. They manufacture medical equipment for the purpose of cardiovascular diagnosis, including

Table 3.2 Commercial devices for measuring bioelectrical impedance plethysmography

Devices	Manufacturer	Features	Application
Simband [133]	Samsung Electronics	<ul style="list-style-type: none"> • Four electrode measurements in the wrist • Current frequency: 40 KHz • Current amplitude: 200 μA • Current shape: Square • ADC Resolution: 12 bits • Sampling frequency: 1024 Hz 	<ul style="list-style-type: none"> • Research purposes, design of algorithms • Measurement of galvanic skin response (GSR) • Heart rate measurement • Measurement of pulse wave of blood flow in wrist artery
Cheetah NICOM [139]	Cheetah Medical	<ul style="list-style-type: none"> • Four electrodes measurement in the thorax • Current frequency: 40 KHz • Signal amplitude: 600 mW • Current shape: Sine • Cheetah's proprietary algorithms interpret the signal to provide stroke volume 	<ul style="list-style-type: none"> • Measurement of cardiac output • Stroke Volume Index (SVI) • Cardiac Index (CI) • Total Peripheral Resistance Index (TPRI), which is a measure of vascular tone
VasoScreen 5000 [138]	Medis	<ul style="list-style-type: none"> • Four electrodes measurement in the legs, arms and head • Current frequency: 85 KHz • Signal amplitude: 1 mA • Current shape: Sine 	<ul style="list-style-type: none"> • Pulse wave analysis in legs, arms and head • Diagnose of arteriosclerotic changes • Detection of stenoses • Diagnose of occlusions • Combination of PPG and cuff occlusion for VOP assessment

3.7 Basic components of a bioelectrical impedance device

impedance cardiograph and impedance plethysmography devices. Furthermore, their devices are combined with other methods such as PPG and ECG to obtain a better assessment of the haemodynamics in the body.

3.7 Basic components of a bioelectrical impedance device

Evidently, there are several medical instruments that incorporate either bioelectrical impedance technology. Nonetheless, regardless of the application, most of the instruments follow the block diagram illustrated in figure 3.11 as part of their basic designs.

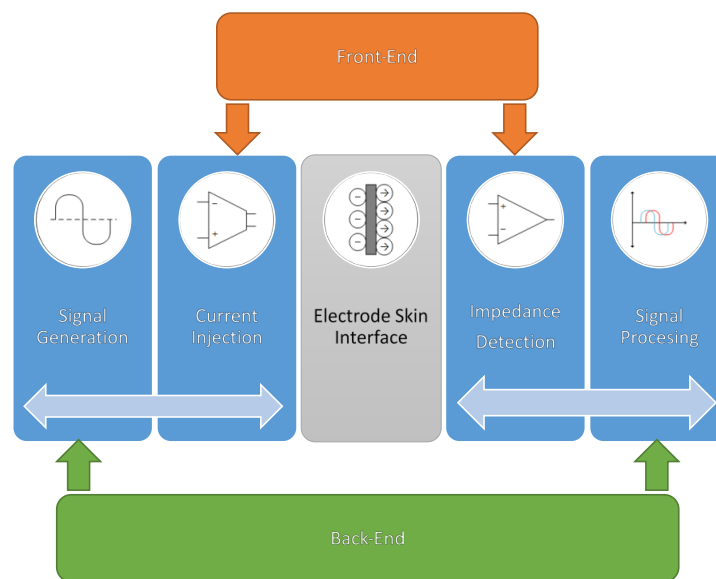


Figure 3.11 A bioelectrical impedance device requires front-end and back-end components in order to detect changes of impedance efficiently.

An impedance system can be categorised into three different blocks: the first one known as back-end commonly comprises of signal generation and a digital signal processing system which analyses the sensed signal. Next is the front-end block comprised of all the circuitry before establishing contact with the skin, such as current injection and signal detection electronics. Ultimately, skin electrode interface behaving as an electronic circuit has been described in section 3.4.

Meanwhile the back-end block is divided into two different sections. First signal generation circuits depend on either extremely precise oscillators or Digital Signal Synthesizers (DDS) to generate accurate signal waves in a wide bandwidth with highly accurate amplitudes. The frequency exactness of these electronic circuits could scale up to 0.1 % [140]. Different kind of waveforms may be applied, but a sinusoidal wave is the most common one.

Bioelectrical impedance plethysmography

Signal processing circuits lie at the other end of the spectrum, and are used to evaluate a signal's amplitude and phase sensed by the front-end block. Notably, powerful processors or microprocessors are used to analyse and digitise the signals identified. Moreover, modern devices are also aided by either Digital Signal Processors (DSP) or high-speed analogue to digital converters (ADC) that are capable of oversampling the detected signals. This level of precision in high-speed processors and chips makes them highly specialised and expensive.

Likewise, the front-end is divided into two different sections: current injection and signal detection circuits. The current injection circuit, as indicated by its name, transmits the signal coming from the wave generator into the electrodes; some characteristics of these circuits are high bandwidth, accuracy and linearity.

On the other hand, signal detection circuits receive the signal after having passed through the sample under test. As opposed to specialised digital circuitry used on the back-end, the front-end mostly relies on highly precise analogue systems. These circuits can be implemented with discrete components or custom chips. However, discrete components may evince a limited response when there is a requirement of bandwidths in the order of megahertz [141–143].

In an ideal system, the output impedance of the current injection circuit is expected to be linear within its full bandwidth. However, at high frequencies, stray capacitances may reduce the output impedance of the current drivers and could produce unwanted oscillations [142]. Some of the factors that cause a change in stray capacitance are the integration between electrode impedance, cable capacitances, the capacitance between neighbouring electrode leads, capacitances between the signal ground of the device and earth, and lead positioning [141, 143]. figure 3.12 shows the stray capacitance (C_s) in parallel with the load (Z_L).

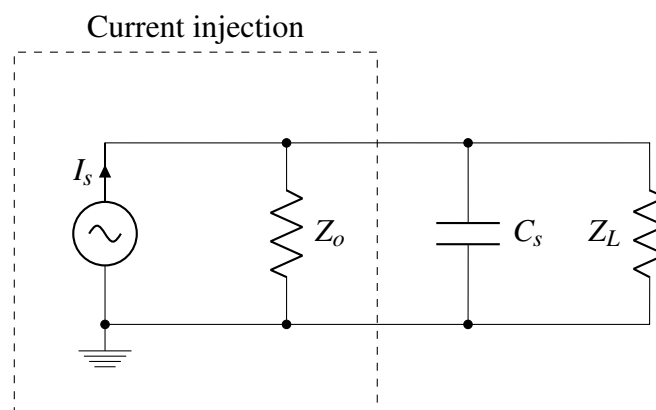


Figure 3.12 Circuit of stray capacitances (C_s) at the output of the current source. These capacitances are in parallel with the load (Z_L), at high frequencies the stray capacitances become more dominant than the load.

3.7 Basic components of a bioelectrical impedance device

Custom microchip design replete with current injection and sensing circuits is a better option because it reduces the influence of some of the stray capacitances. The implementation of a short length of transmission lines, interleaving signal wires with the ground, twizzling of signal paths, less logic and smaller devices reduce intrinsic and extrinsic capacitances of the system [141, 144, 145].

3.7.1 Methods of measuring bioelectrical impedance

Bioelectrical impedance has been used in different ways to get measurements from the human body. A wide range of approaches has been developed using single or multiple frequencies or varying amounts of electrodes. This section describes the most common type of bioelectrical impedance and explains their operation frequency, electrodes location, and data representation. The table 3.3 summarises the different methods to measure bioelectrical impedance including application, advantages and disadvantages.

As the table shows most of the methods focus on whole body measurements. These methods provide an insightful approach to whole body composition analysis, including total body water (TBW), free-fat mass (FFM) and a weighted sum of extracellular water (ECW) and intracellular water (ICW) content resistivities [100]. Nonetheless, the measurements can be significantly affected by the subject's hydration level [146, 147].

On the other hand, localised bioelectrical impedance analysis aims to avoid the incidence of the effects of different variables, such as hydration, fat fraction, geometry boundary conditions, etc. Focusing on well-defined segments of the body enables the minimisation of the effect of these variables. Moreover, when the segment is confined to a small volume, it becomes possible to calculate plethysmography or blood flow. The use of four electrodes assumes great significance for such applications because it creates the boundaries of such a system.

The calculation of bioelectrical impedance also simplifies because it facilitates the application of empirical regression models as per their population [100]. Some cases involve the dimensions of the limb being studied in order to obtain its geometric volume for a more detailed calculation. Some cases where this technique has been successfully applied include the analysis of limb ischaemia [54, 148] breast cancer [149], detection and monitoring of Lymphedema [150] and local abdominal fat mass [151].

Table 3.3 Comparison of the different methods to measure bioelectrical impedance

Method	Application	Advantages	Disadvantages
Single frequency BIA [100, 152]	<ul style="list-style-type: none"> • Whole body impedance analysis • Analysis of full body composition • Quantification of free-fat mass • Measurement of total body water (TBW) 	<ul style="list-style-type: none"> • Easy to use, only four electrodes (contact measurements) • Single frequency measurement (50 KHz) • Low coefficient of variation from 0.3 % to 3.6 % [152] 	<ul style="list-style-type: none"> • Measurements affected by subject's hydration and glycogen levels • Sensors placement • Skin preparation • Variations in manufacturers equations
Multi-frequency BIA [100, 153–155]	<ul style="list-style-type: none"> • Multi-frequency whole body impedance analysis • Similar body analysis as SF-BIA • Assessment of amyotrophic lateral sclerosis (ALS) 	<ul style="list-style-type: none"> • Use more complex mathematical analysis (Cole-cole and Hanai formulas) • Multi-frequency measurements (up top 6 frequencies) • More accurate predicting ECW 	<ul style="list-style-type: none"> • Modelling techniques requires further refinement in some diseases • Poor reproducibility below 5 KHz and above 200 KHz • No clear consensus in which algorithm must be used in calculations • SF-BIA presented better results assessing TBW in critically ill subjects
Bioelectrical impedance spectroscopy (BIS)	<ul style="list-style-type: none"> • Multi-frequency whole body impedance analysis • Cancer tissue analysis [156] • Changes of fluid compartment [157] • Total body analysis TBW-ECW 	<ul style="list-style-type: none"> • Use of Cole-cole and Hanai formulas • More data points than MF-BIA, multiple frequencies • Better results calculating of TBW and ECW 	<ul style="list-style-type: none"> • Requires previous modelling of healthy population • Calibration or different mathematical model required for certain kind of illnesses [158] • Regression method use calculate results

Continued on next page ...

Table 3.3 – continued from previous page

Method	Application	Advantages	Disadvantages
Segmental bioelectrical impedance analysis [100]	<ul style="list-style-type: none"> • Multi-frequency differential body segments impedance analysis • Fluid retention on patients with renal failure • Total body water analysis TBW • Fluid shifts and fluid distribution in some diseases (ascites, renal failure, surgery) 	<ul style="list-style-type: none"> • Noninvasive, simple and inexpensive method for body composition study • Impedance analysis of different body segments (torso, legs and arms) 	<ul style="list-style-type: none"> • Multiple electrodes measurement, more than 4 electrodes required • Lack of standardisation on electrodes position • Not recommended for young adults [159, 160]
Bioelectrical impedance vector analysis [100]	<ul style="list-style-type: none"> • Assessment of fluid body volume 	<ul style="list-style-type: none"> • Four electrodes measurement in the legs, arms and head • Uses real (R) and imaginary (X_c) values • Classification according to body type (Muscular, lean, obese or cachectic) • Tested under different illnesses 	<ul style="list-style-type: none"> • Data output depends on previously healthy population fit • Bad diagnosis could be given if previous population data is not available • Uses estimates, instead of quantified values
Localised bioelectrical impedance analysis [100]	<ul style="list-style-type: none"> • Plethysmographic analysis • Limb ischaemia progression [54, 148] • Breast cancer study [149] • Lymphodema monitoring [150] • Measurement of localised abdominal fat [151] Muscle injury [161] 	<ul style="list-style-type: none"> • Simple to operate and use (4 electrodes) • Hydration or fat does not affect measurement greatly • Electrode boundary limits tissue volume to be analysed • Localise measurement 	<ul style="list-style-type: none"> • Not effective to measure ECW-ICW • Usually single frequency measurement • Lack of standardised electrode placement

3.8 The principle of bioelectrical impedance plethysmography

As previously described in section 2.5.3.3, iPG denotes the measurement of volume changes through the equivalent impedance of a human body part [24]. Indeed, when heart's systole increases the blood flow, the volume of a limb rises due to the inflow of arterial blood (swelling) [98]. Consequently, there are changes of impedance that are correlated to the changes of volume as well as flow in any part of the body. Some of the medical applications of this technology include the measurement of heart stroke volume (SV), cardiac output (CO), thoracic respiratory volume, oedema as well as the detection of deep vein thrombosis (DVT) [7].

The genesis of impedance plethysmography can be traced back to the model that was proposed by Jan Nyboer [102]. The author describes extremities as cylinders, where in an inner cylinder signifies a blood vessel, and surrounding tissue accounts for the outermost part. The whole electrical conductance path results from the sum of the parallel conductance of blood and tissue within a segment. In fact, this theory known as parallel conductor was subsequently confirmed by the experiments performed by Shimazu et al. [162]. There have been some doubts about the extent of the blood's impedance contribution to the total impedance signal. Nonetheless, the in-vitro experiment demonstrated that blood (haematocrit = $26 \pm 4\%$) contributed to 10 % of the impedance signal. In the study, the final result was obtained when comparing the measurements of a saline buffer solution and blood in extensible arteries as well as rigid tubes [163].

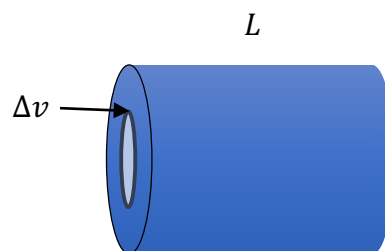


Figure 3.13 Two compartment cylinder model of length L and parallel volume increment of Δv . Image adapted from [98]

In principle, the normal volume (V) of a human forearm contain within a certain length L , the bones, muscle, fat and blood structure around a cross-sectional area (A) (see figure 3.13). When a circulatory cycle takes place, an additional amount of blood enters the limb through the brachial artery to raise total volume of the limb in ΔV . Thus, the new limb's total volume

3.8 The principle of bioelectrical impedance plethysmography

at the peak of this systole will be equivalent to $V + \Delta V$. As a result, shunting impedance Z_b is produced by the following equation [164, 165]:

$$Z_b = \rho_b \frac{L}{\Delta A} \quad (3.27)$$

where ρ_b denotes the blood's resistivity and ΔA refers to the increase of in the cross-sectional area of the limb. However, for this formula to work, some assumptions need to be taken into consideration: the arterial expansion is uniform along the tissue, the blood resistivity (ρ) remains constant, and the flow of current is parallel to the artery [18]. Therefore, the artery volume change can be obtained by using the following formula [164, 165].

$$\Delta V = L \times \Delta A = \rho_b \frac{L^2}{\Delta A} \quad (3.28)$$

During the cardiac cycle, the area of the artery increases from A to $A + \Delta A$. However, the impedance of Z_b is also affected by the additional impedance (ΔZ) that is produced by the increment ΔA , and this Z_b is connected in parallel to Z . Therefore, Nyboer [102] postulated that the practical parallel resistive value of the displaced blood can originate from the parallel relation between the initial base resistance and the new resistance value, signified by the following expression:

$$\Delta Z = (Z_b \parallel Z) - Z = \frac{Z^2}{Z + Z_b} \quad (3.29)$$

where Z is equivalent to the limb's original resistance at diastole and Z_b represents the increase of new total resistance. $Z_b \gg Z$, then Z_b can now be rewritten as:

$$\frac{1}{Z_b} \cong -\frac{\Delta Z}{Z^2} \quad (3.30)$$

Finally, the changes in limb volume in association with the variation of impedance are denoted by the equation 3.31. It must be noted that the negative sign is an indication of direction.

$$\Delta V = -\rho_b \frac{L^2}{Z^2} \Delta Z \quad (3.31)$$

Different equations are derived by complementing Nyboer's work. One of the modifications is the Kubicek et al. method [166–168]. His equation is widely used, especially when taking the measurements of impedance cardiography from the thoracic box and deducting stroke volume of the heart. Another popular work is the contribution of Sramek [169]. The author also modified Kubicek's equation by eliminating the dependence L and ρ_b , and introduced a constant that was obtained using statistical methods named "volume of electrical participating tissue". Alternative calculation methods have been developed using admittance instead of impedance.

In his research and patent work, Yamakoshi [22, 162, 170] uses impedance reciprocal and admittance ($Y = Z^{-1}$) to estimate blood flow using plethysmography which performed better with analogue computers of the time. In his work, the author states that the first gradient of the computation result to time indicates the blood rate in the limb being examined. However, the algorithms used in this study will be confined to the equations proposed by Nyboer.

3.8.1 Alternative applications of impedance plethysmography

The plethysmography waveform is also utilised to quantify the measurements of pulsatile volume, blood flow beat to beat, blood pressure, and pulse wave velocity. In this case, the waveform is equivalent to the AC component of the impedance signal. This signal's contribution to the total quantum of signal is between 0.1 % to 1 % of the total quantum of the signal. Sometimes, it is necessary to implement low noise techniques in order to pick up the hidden signal within the basal impedance.

The most typical application of this waveform is the quantification of blood flow beat to beat. By applying Nyboer's equation to the waveform signal, it is possible to quantify peak-peak blood volume and peak net inflow. For instance, the patent presented by Marks [26] denotes the application of quantifying blood flow in upper extremities by computing the derivatives of the waveform signal producing the claimed results. As another example, the work performed by Porter [23] included taking measurements from lower limbs where an impedance cardiograph was used to obtain the waveform signals and computed using Kubicek's equation [166–168] to validate the signal's potential use in evaluating limb oedema.

3.8 The principle of bioelectrical impedance plethysmography

Another application of this waveform is the continuous evaluation of blood pressure. Blinov [171] demonstrated that pressure could be deducted if the blood flow is known. As explained before, blood flow can be estimated beat-beat by changes into:

$$dV = \rho \frac{L^2}{Z^2} dZ \quad (3.32)$$

Volume rate is denoted by the change of volume in time. Blood flow rate (\dot{Q}) is represented by the following equation:

$$\dot{Q} = \frac{dV}{dt} = -\rho \frac{L^2}{Z^2} \frac{dZ}{dt} \quad (3.33)$$

where W refers to the hydraulic resistance and P signifies the pressure. The hydraulic resistance is a function of the geometry of the artery provided by radius r as well as the viscosity of the blood μ .

$$W = \frac{8l\mu}{\pi r^4} \quad (3.34)$$

By replacing equation W into equation \dot{Q} the pressure for a defined segment can be expressed as:

$$P = -\frac{8L\mu\pi}{\rho} \frac{dZ}{dt} = k \frac{dZ}{dt} \quad (3.35)$$

where k denotes a constant value function of the distance between the electrodes and the physiological constants of the blood at a particular measurement frequency. The sign in equation merely indicates that the changes occurring in the resistance and pressure are opposite. Thus, the sign can be disregarded while performing calculations.

Finally, the waveform obtained from impedance plethysmography can also be applied to evaluate pulse-wave velocity (PWV) in limbs which is an important indicator of deterioration of the cardiovascular system [172, 173]. More in detail, PWV is the time delay between the pulse pressure wave generated by the heart measured at two different points in the body. This can be achieved by placing probes in different sites and recording waveforms simultaneously. It can also be measured independently comparing the time delay against an QRS complex

Bioelectrical impedance plethysmography

of an ECG. As equation 3.36 shows, the PWV is the relation between the distance between of the two measuring points and the time taken by the systolic peak to arrive to the second point.

$$PWV = L/\Delta T \quad (3.36)$$

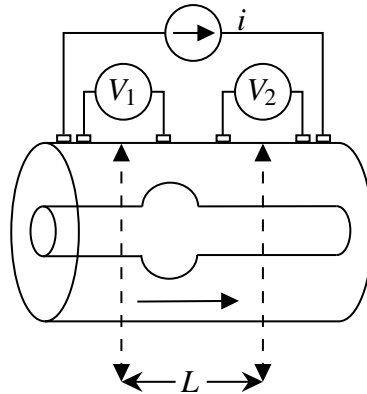
Measuring PWV using bioelectrical impedance can be accomplished by estimating the time difference between both waveforms at the same reference point, which is usually the systolic peak. Figure 3.14 shows an example of how to calculate PWV placing sensors along the path of the pressure waveform and the expected signal outcome. This method requires two or more electrode arrays to measure the differential of electrical potential along a body segment. Importantly, it can be applied to upper and lower limbs. This measurement technology has been successfully demonstrated by researchers like Risacher et al [172] who recorded the measurements using a multi-array electrode system. Some of the recommendations made by the author about the successful application of this method include a strong emphasis on the potential sensitivity to noise of this method [174], the use of high-precision reproducibility by the electrode array, accurate measurement of the distance separating measuring sites, and high sampling frequency to ensure heightened accuracy in the calculation of time intervals. However, there are limitations when recording these signals from a small body where the location and geometry of the electrodes assume prime significance for this application. It is possible to record this signal from an area as small as 1.5 cm by 7 cm which also increases the possibility of portability [173].

3.9 Impedance plethysmography in the forearm

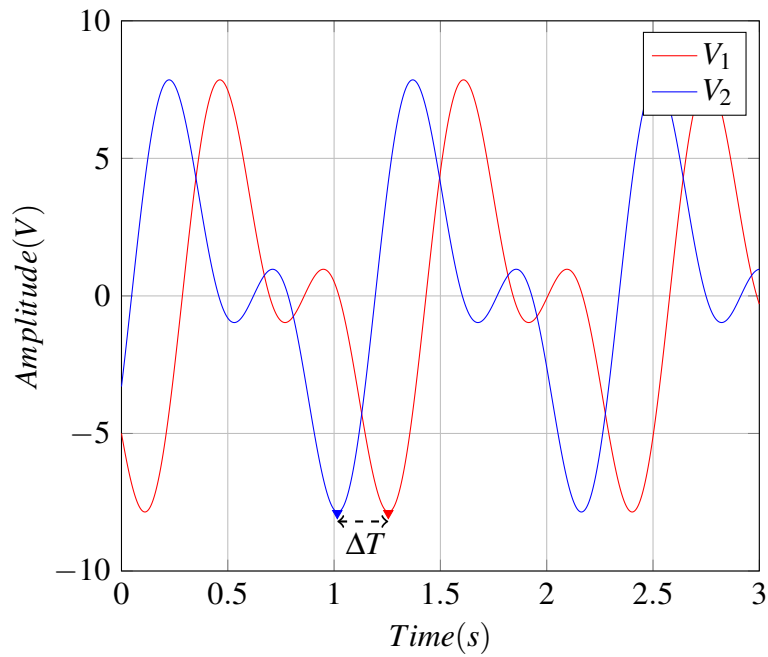
As noted before, impedance plethysmography is capable of measuring the changes of blood in different parts of the body. This section will describe how these changes occur in a limb in greater detail. During this study, localised bioelectrical impedance is found to be the most suitable method to estimate blood flow within a segment of the human body. The cylindrical shape of the forearm is a perfect place to measure impedance plethysmography. This location also provides valuable information about circulatory peripheral illnesses as described in chapter 2.

Depending on the medical application, an impedance plethysmography instrument (iPG) device can provide two types of signals: one dedicated to the basal impedance and the other

3.9 Impedance plethysmography in the forearm



(a) Pulse wave velocity measured using bioelectrical impedance between points V_1 and V_2 . Adapted from [173]



(b) Waveform representation for V_1 and V_2 , the delay between both signals is represented by ΔT

Figure 3.14 Pulse wave velocity between points V_1 and V_2 using bioelectrical impedance. The PWV calculation derives from the distance between the electrodes and the time difference between both signals at selected peaks

Bioelectrical impedance plethysmography

one intended for dynamic component. Both signals can be used to provide important medical information about tissue health and also blood volume. Hence, one significant aim of this study is to design a device that can potentially include an additional sensing channel to carry out differential studies in the future.

There is not much variation in the structure of a bioelectrical impedance device, as seen from figure 3.11 and the impedance plethysmography instrument. The electrodes are the first points of difference observed from a bioelectrical impedance device. Circumferential band electrodes are commonly used to take these measurements, as suggested by some studies [18, 20, 22–24, 175]. However, other studies suggest that there is not much difference when using single point electrodes such as ECG and band electrodes [176–178]. In fact, these studies have demonstrated that spot electrodes improve the signal-to-noise ratio and enhance the quality of the impedance being measured. Infection control is one plausible reason for this. Using disposable ECG electrodes also curtails cross-contamination in a clinical setting.

While bioelectrical impedance measurements can be achieved with only two electrodes, impedance plethysmography measurements commonly use four electrodes configurations. Most of these studies rely on tetrapolar electrodes set-up, which is quite the norm for volume/flow measurements [19, 21, 22, 120]. As shown by figure 3.15 a pair of electrodes placed at the outermost part of the segment is used to inject a high-frequency current. Meanwhile the second pair of electrodes senses the decline in voltage coming from the body segment. These sensing electrodes are arranged between the current electrodes.

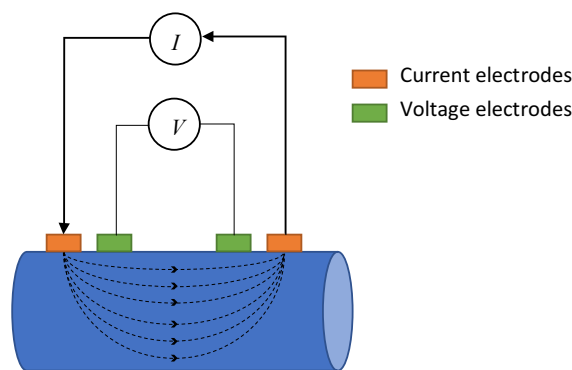


Figure 3.15 Electrodes distribution in tetrapolar configuration. Outermost electrodes (current) inject current into the tissue. Inner electrodes sense the voltage drop caused by the tissue.

Another difference is the frequency used in iPG to measure impedance plethysmography; this usually ranges from 10 kHz to 100 kHz [54, 130, 148, 179]. This level of frequency is large enough to avoid any muscle stimulation that could be hazardous for the patient.

3.9 Impedance plethysmography in the forearm

The electrical currents incorporated by this method are in the range of few micro-amperes (μA) to few milliamperes (mA), confining it within the limits of patient safety, as described in section 3.1. Clearly, the higher the current, the higher the voltage output response, as per Ohm's law ($v = R \times i$); this is because the body segment behaves like a resistor. To ensure patient safety, it is recommended that current is injected instead of voltage because circuits can limit the amount of injected electrical current and provide a better control on the amplitude of the waveform. Overall, the amount of current required to obtain a clean signal depends on the geometry of the volume being tested, the electrodes geometry, and the physiological attributes of the tissue.

The data presented by an impedance device can be exhibited as a real or imaginary part of the impedance. However, it has been demonstrated that operating at these frequencies does not cause a major difference between the real part and the modulus of the measurement. In fact, the imaginary component of the signal is less than 12° [180]. Therefore, the modulus of an impedance plethysmography measure provides sufficient information about the volume change in a limb section [175]. However, this phase might assume significance if higher frequencies are used to isolate a particular tissue or physiological event.

As illustrated by the figure 3.16, it is possible to obtain an impedance plethysmography signal by injecting the required current into the tissue at a specific frequency. One of the most common signals is a sinusoidal waveform at 50 kHz. Once the electrical signals pass into the electrodes, they get transformed into an ionic conduction. The interaction of current with the tissue leads to a decline in voltage that can be detected by the sensing electrodes. From the electrical viewpoint, an amplitude modulated voltage waveform is generated from the tissue. However, this modulation remains synchronous to the heart cycle only represents 0.1 % of the waveform [175]. The impedance modulus is obtained using Ohm's law (equation 3.37). The resultant impedance is known as either basal impedance (BI) or resting baseline impedance (RBI). Moreover, the underlying dynamic signal is known as arterial pulse amplitude (APA).

$$|Z| = \frac{v}{i} \quad (3.37)$$

3.9.1 Blood contribution to impedance

As mentioned before, impedance plethysmography depends on the volume change caused by blood vessels filling up all areas along the cardiac cycle; blood is highly conductive and influences the amplitude of the waveform. However, other particular properties might modify its intrinsic signal. In one of the earliest research works on the conductivity of blood, Sigman

Bioelectrical impedance plethysmography

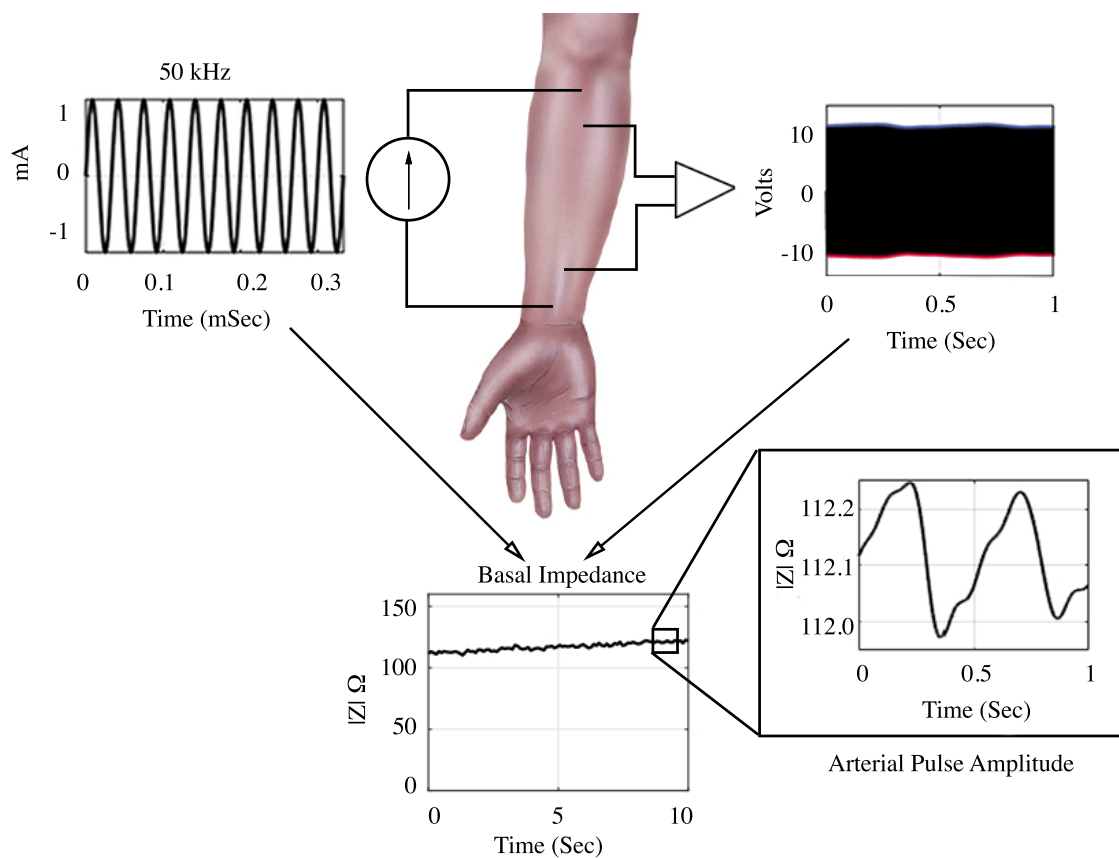


Figure 3.16 An impedance plethysmography waveform can be obtained by applying a constant current and sensing the resultant voltage. The division between the potential and the current provides the impedance module - which is the basal impedance. The arterial pulse amplitude can be seen within the basal impedance.

3.9 Impedance plethysmography in the forearm

et al. [181] demonstrated that blood's resistivity depends on its flow. It was found that when blood velocity decreased from 10 cm s^{-1} to 40 cm s^{-1} its resistivity fell by roughly 7%. Furthermore, it was found that haematocrit and temperature also affect the blood resistivity [182]. However, the temperature remains nearly constant in an in-vivo setting. Blood can be simplified as a suspension of particles (erythrocytes or RBC) using a high resistivity floating within a conductive medium (plasma). The remaining blood cells do not represent a significant component of the change of impedance owing to its small size in comparison with the erythrocytes. In fact, the Sigman effect is absent in either plasma or electrolytes [183].

Blood has also been proven to be electrically anisotropic due to the orientation of the RBC's [184]. Moreover, geometry and orientation also end up affecting the reading of resistivity, which means that direction of measurement also affects the readings.

3.9.2 Impedance plethysmography waveforms

The impedance plethysmography provides important information about the venous and arterial circulatory properties within a particular bodily segment. The impedance waveform comprises of a constant impedance value (basal impedance) and a dynamic component within it (arterial pulse amplitude). However, it is possible to obtain details about peripheral venous circulation when occluding a limb proximally. This kind of method is known as venous occlusion plethysmography (VOP).

Figure 3.17 shows the three different components of an impedance plethysmography waveform. The signal consists of the following components: basal impedance or resting baseline impedance (RBI), venous volumes changes and arterial pulses.

3.9.2.1 Basal impedance

Also known as the resistive baseline impedance, this is the most significant data obtained from an impedance plethysmography device (see figure 3.17). The main contributors to this impedance include muscles, blood and bones. The resistivity of muscles is about $200 \Omega \text{ cm}$ to $300 \Omega \text{ cm}$, whereas the resistivity of bone and fat is greater than $2000 \Omega \text{ cm}$ and the blood resistivity is about $150 \Omega \text{ cm}$ [185]. Therefore, this combination of impedances can be expressed as a parallel model of resistances wherein muscle and blood are the main contributors of the RBI. The range of this impedance value is from 10Ω to 100Ω .

It has been demonstrated that it is possible to gather information about the development of ischaemic tissue by studying the changes of baseline during a time. Some studies have shown that the impedance value increases during ischaemic events in the bandwidth of 1 kHz

Bioelectrical impedance plethysmography

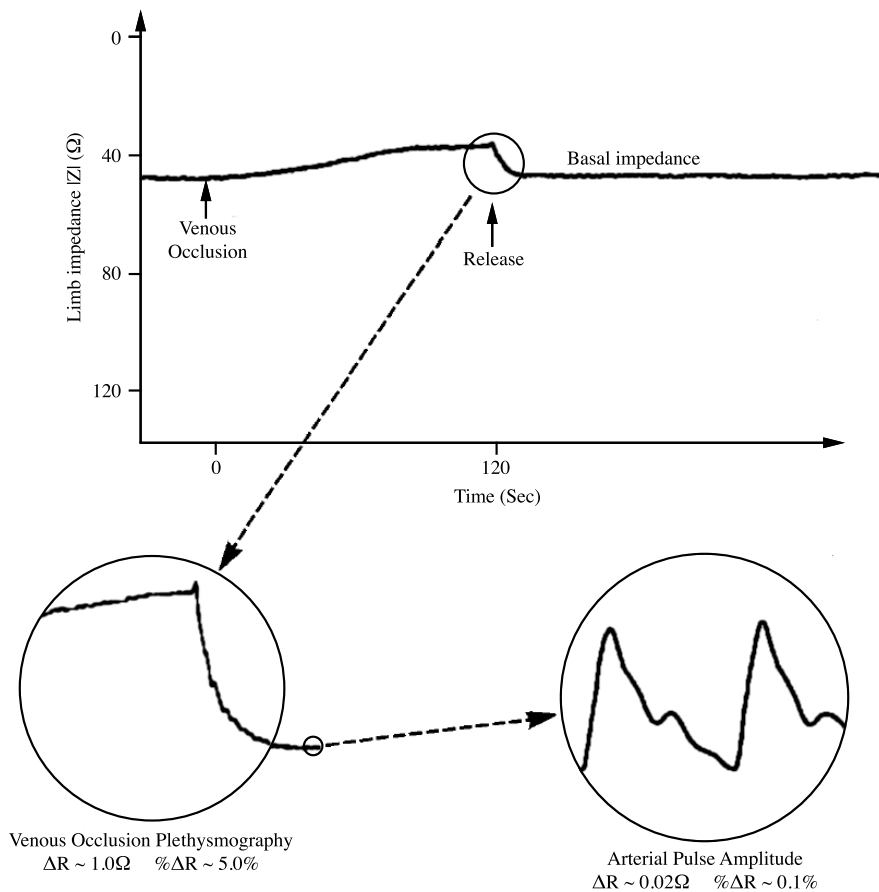


Figure 3.17 An impedance plethysmography device can produce three signals: 1) the basal impedance or resting baseline resistance; 2) by using a blocking venous return at (40 mmHg to 50 mmHg) to extract the venous occlusion plethysmography wave; and 3) within the basal impedance is located the arterial pulse amplitude which changes with the heart beat. Adapted from [175]

3.9 Impedance plethysmography in the forearm

to 100 kHz within different kinds of tissue [54, 130, 148, 179] which is within the frequency measurement of iPG.

3.9.2.2 Venous occlusion plethysmography

The second signal obtained from the baseline signal provides information about the venous volume changes. Variations in venous volume tone occur naturally during respiration, which causes a modulation of the signal during the respiratory cycle between 0.2 Hz to 0.3 Hz. However, by occluding the venous return, it is possible to produce larger volume variations represented as a greater displacement of the basal impedance of nearly 1Ω or 5 % from the mean value.

The most common method to evaluate venous volume is known as venous occlusion plethysmography, which is quite common in the assessment of peripheral vascular diseases such as deep venous thrombosis. Impedance plethysmography VOP (see figure 3.17) provides similar results as other well-established methods such as strain gauge[99] and air/water displacement techniques [186]. This method requires occluding the limb's proximal section using a cuff with a pressure above the venous pressure staying usually about 40 mmHg. The retention of the blood increases the volume of the limb with each heart cycle. The accumulation of blood in the measured segment increases its conductivity and reduces the total resistivity. A deviation from up to 10 % from the basal impedance can be achieved depending on the occlusive pressure, arterial inflow, venous tone, central venous pressure (CVP), and the capacity of the venous vascular bed.

3.9.2.3 Arterial pulse amplitude

The third signal component of an impedance plethysmography is the arterial pulsations, which are waveforms synchronous with the heart cycle (1 Hz to 2 Hz). This signal is just a fraction of the total impedance; it is just 0.1 % of the total impedance signal - approximately 0.02Ω in the limbs of healthy young adults. Obtaining this signal can be challenging since its values are in close proximity to noise levels. Therefore, the signal should be isolated by using sharp filters and averaging some pulses. Changes in the waveform shape are attributed to different reasons such as tissue volume, arterial inflow, arterial vessel compliance, proximal occlusion, peripheral resistance as well as electrodes topology, geometry and location. Changes in the signal amplitude are an indicator of arterial problems. For instance, arteriosclerosis reduces the arteries elasticity with age. Hence the arterial pulse amplitude reduces in magnitude.

3.10 Conclusion

Electrical impedance is the response that any conductive medium presents to an alternating current or voltage. It is frequency dependent and can be described as resistive (R) or reactive (X), which is determined by the resultant signal being in phase with the source or not. When applied to the human body, it is known as bioelectrical impedance, which is a non-invasive method that allows for the analysis of change in the human body using harmless and imperceptible AC. The current applied on any part of the body should be within the limits of patient safety.

Electrical impedance applied to humans can examine the health of tissue as well as changes in blood volume. The measurements produced by this method are attributed to the ions transport in tissue when a set of electrodes converts electrical current into ionic conduction. Bioelectrical impedance measurements can perform both whole body measurements and local body segments. It can be applied using either single or multiple frequencies, or to perform analysis over a wide range of the spectrum.

Bioelectrical impedance plethysmography measures blood-related changes in the human body. It is commonly used in a tetrapolar configuration where a pair of electrodes injects current and a second set measures the voltage drop. Instruments utilising this technology produce two types of data: *basal impedance* is the whole impedance contribution of bones, muscle, fatty tissue, skin and blood. Under normal conditions, this signal tends to be unchangeable. However, within it lies another small signal that contains information about the arterial pulsations, known as *arterial pulse amplitude (APA)*.

Method and protocols

This is the method and protocol chapter. It consists of two sections, one describes the design of the bioelectrical impedance plethysmography device and the second the protocol used to collect data during the experimental procedure.

The first section shows the work performed to design and implement the iPG device. In short, the instrument measures the magnitude of the impedance in the forearm using a tetrapolar configuration at 50 KHz. Complementary information of the schematics and scripts can be found in the appendix section. The second section describes the protocol of the experimental procedure along with the calculations performed in order to quantify the measurements obtained during the test. This study entailed the participation of eight healthy volunteers, where 4 different instruments were attached to their left limb, including the one iPG device presented here. The protocol consisted of 30 mins of measurements, while three different mechanical occlusions were applied to the participant.

4.1 Design of a bioelectrical impedance plethysmography device

As mentioned in the background section, there are multiple applications where impedance plethysmography can be applied. Thus far though, this has only been achieved by devices that can only provide either basal impedance (DC), waveform (AC) or single channel application. This part of the work describes the design of the device that can be used to encompass any of the previous applications in a single apparatus.

Designing an impedance device necessitates functional knowledge about the electrical characteristics of the load under test. Nonetheless, meeting patient safety is a good starting

Method and protocols

point for the recommendations. This implies that the amount of current to be driven by the device should be imperceptible within the limits of the safety standards. To that end, one of the first recommendations is to be able to operate by batteries as a class B device in order to ensure that electrical currents are floating in the patient and guarantee that current will flow through the segment to be studied. The level of current sensation is predicated on factors including gender and is also predicated on the electrode geometry. However, Brown et al. [105] have established a threshold current that is frequency dependent where 5 mA signifies the limit for sensory nerve stimulation and shock sensation. The device designed can deliver as many as four levels of current using a dip-switch (1 mA, 2 mA, 3 mA and 4 mA). For the purpose of this document, the current was fixed at 4 mA which provided excellent sensitivity for the system.

With regard to the electrical current waveform delivered by the device, a programmable wave generator was included in the design which delivers a sinusoidal waveform at frequencies between 20 Hz to 200 kHz, but for the purpose of this study the frequency was locked at 50 kHz was used during the experimental procedure.

4.1.1 Electrodes topology and location

As described in the section 3.4.1, bioelectrical impedance plethysmography measurements can be attained with four electrodes. The device implemented for this study used this kind of interface. A tetrapolar configuration requires four contact points; a pair of electrodes injects current, whereas another couple sense the voltage. Using tetrapolar arrangement minimises the decline in voltage during the measurements because the impedance of potential sensing amplifier is bigger than the interface electrode-skin. This means that electrical current would not flow between the electrodes and voltage amplifier.

Positioning the electrodes close to the main vessel improves the response of this system since there is more conductive material where the free ions can flow through. Figure 4.1 illustrates the position of the electrodes to take measurements from the device. According to the arm anatomy, the radial artery is an ideal site to use one of the current electrodes. The other one was placed close to the brachial artery around the cubital fossa region where this vessel is in closer proximity to the surface. The sensing electrodes were placed towards the right hand side on the elbow, which is the nearest point to the brachial artery connected to the radial artery thus forming the ideal loop to detect the changes in impedance ΔZ .

4.1 Design of a bioelectrical impedance plethysmography device

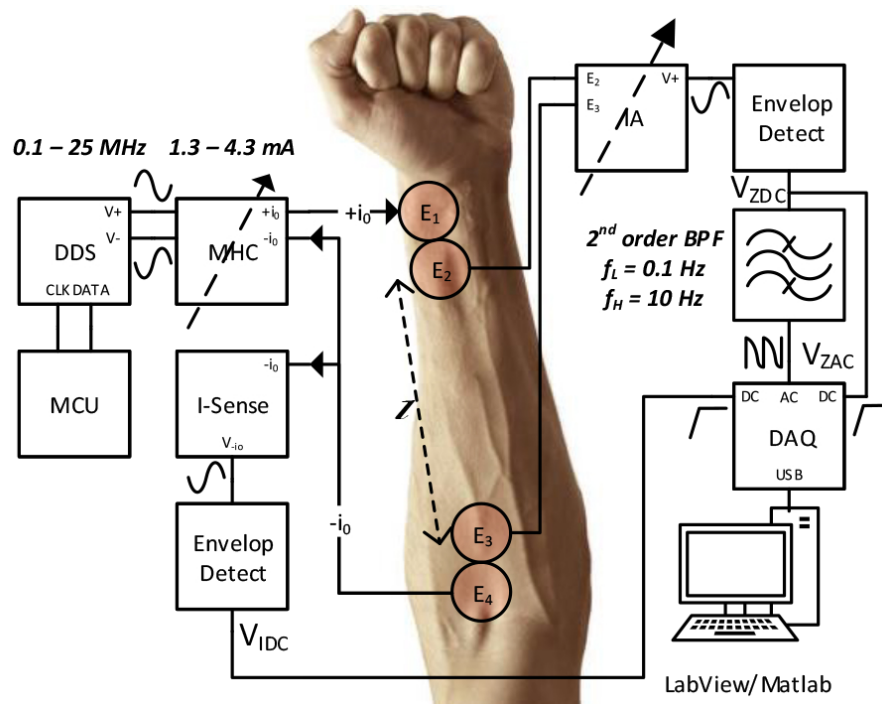


Figure 4.1 General concept of the designed bioelectrical impedance device. It also includes the position of the electrodes in the forearm.

4.1.2 Bioelectrical impedance device modules

A modular approach was used when designing the bioelectrical impedance device. Every print circuit board (PCB) module was implemented in Altium Designer with a size of 50 mm x 50 mm. Using this technique helped isolating any errors without manufacturing an entirely new system. It also allows the experimentation of different circuits to get the most suitable solution in order to obtain the most acceptable waveforms. During its development, different methods were tested to drive current, generate waveform or measure impedance. Towards the end, this solution was seen to present the best results. The optional modules will not be included in this thesis since they were excluded from the studies presented here.

Figure 4.1 illustrates the block diagram of the instrument. Operating the device requires: four ECG electrode, a battery bank, a DAQ card and a PC with LabView [32] installed. In general, some of the characteristics of this instrument are: differential sine wave generation through a DDS controlled by an Arduino Uno MCU [187] operating at 50 kHz. Four different levels of differential current can be supplied 1.33 mA, 2.16 mA, 3.60 mA and 4.36 mA. Current sensing level on electrode E_4 and forearm's potential measurement through electrodes E_2 and E_3 . The impedance quantification value comes from the measurement

Method and protocols

of the current and voltage peaks. The arithmetic operation takes place on the PC after the signals have been digitised.

Following the design structure presented in section 3.7, the proposed system can be subdivided into two sections: 1) front-end, which is the part of the device that interacts directly with the limb under test; and 2) back-end, which performs the wave generation, signal conditioning, computational calculation, and data representation. The figure 4.2 displays the general schematic of this proposed device. The features and characteristics of each module will be illustrated as follows. The full schematics and part of the code used to control the DDS can be found in the Appendix section.

4.1.2.1 Power supply module

Implementing an effective design requires good power supplies that can provide steady voltage output and sufficient current required by the circuitry. Due to the need for applying floating currents, a power supply was designed to operate using batteries by minimising ground loops and increasing patient safety. The selection of this method of supplying power lessens the likelihood of electric shocks and attaining dangerous voltage levels. For these reasons, a couple of batteries A512/2 S (Sonnenschein) were used to power all the circuits. These cells provide 2 Ah of capacity per bank. Some of the unique features needed for power supply includes the ability to provide a dual voltage (± 12 V) and (5 V) for analogue and digital components respectively. Appendix B shows the schematic of the module designed.

In summary, the table 4.1 illustrates the characteristics and IC's used in the power supply module. This includes level voltages, output current per channel and the specific function of each voltage level.

Table 4.1 Components of the Power Supply and its functions

Voltage supply	Current supply	IC	Function
+12 V	1.5 A	LM317	Power supply for single and dual Op-Amps, In-Amps and as power supply for +5 V
-12 V	1.5 A	LM337	Negative power supply for single and dual Op-Amps and In-Amps
5 V	100 mA	AP117E50G	Power supply for digital components working at TTL level

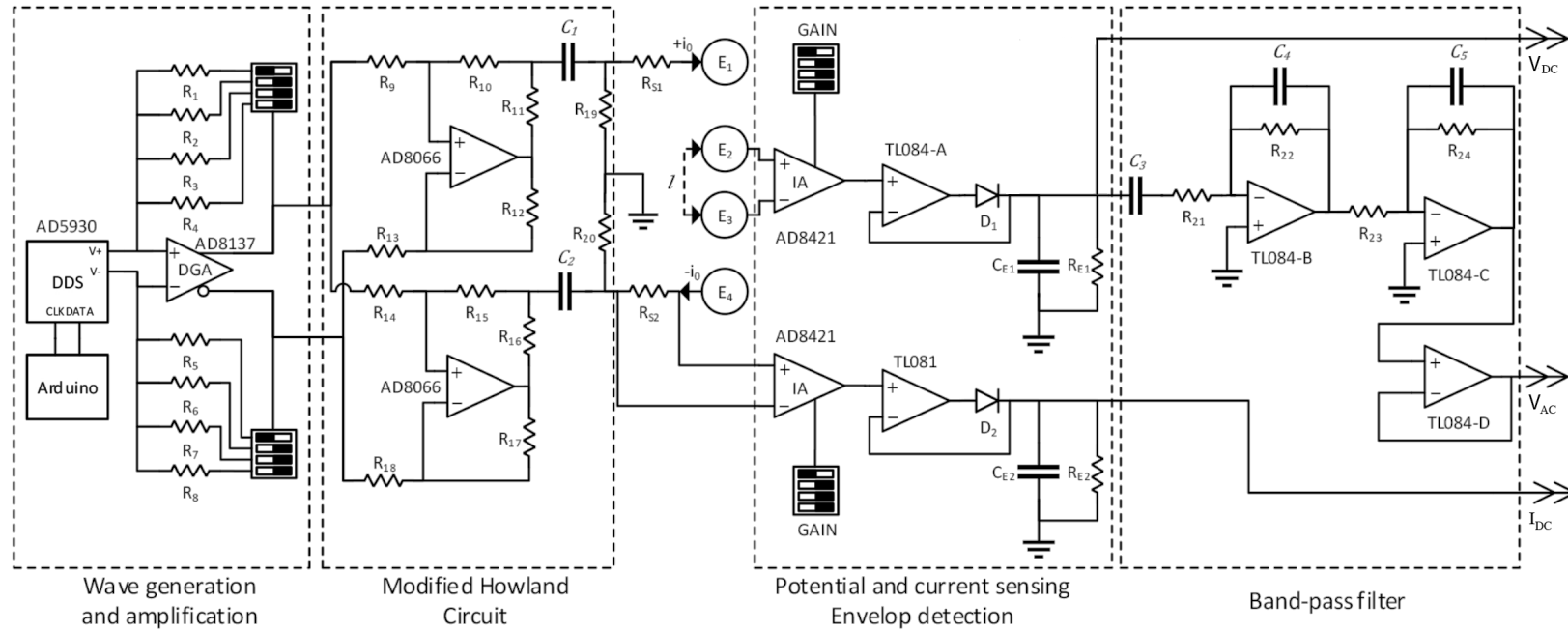


Figure 4.2 Block diagram of the bioelectrical impedance plethysmography device

4.1.2.2 Direct digital synthesis (DDS) module

Following the block diagram from left to right illustrated in the figure 4.2, the first part shows the wave generator. This section of the circuit produces the sinusoidal wave required to take the impedance measurements. This waveform needs to be low in distortion and noise. This signal was created using a programmable direct digital synthesis (DDS) integrated circuit (IC) that can produce sine waves from 10 Hz to 25 MHz. The IC used here is the AD5930 [140]. In summation, a DDS creates a wave in accordance to a table of digital words in memory fed to a DAC that then produces the analogue equivalent. This IC requires a set of instruction to be able to operate.

A microcontroller ATMEL (Arduino) controls the DDS sending commands via serial peripheral interface bus (SPI) transmission interface. By making use of an instruction set by the manufacturer, it is possible to set the oscillation frequency of the sine wave and start/stop the signal generation. The appendix C shows the code used to communicate with the PC and send commands to the DDS. The waveform generated by the DDS is differential, implying that there are two sine waves outputs in a counter-phase (0° and 180°). The DDS provides a current output of 3 mA which is transformed to an electrical voltage using a $200\ \Omega$ resistor at the output of the IC, setting the output at approximately 600 mV. A set of capacitors also filters high-frequency noises. The connection between the microcontroller and other boards is made possible using ribbon cables.

4.1.2.3 Differential amplifier gain module

The following stage consists of a differential voltage amplifier which, as its name suggests, amplifies the sinusoidal waveform coming from the DDS. The gain of this amplifier can be modified using a set of resistors at each side of the amplifier. It can also be adjusted to 16 different combinations of gain using resistors of 1 k Ω , 2 k Ω , 3 k Ω and 4.99 k Ω . Moreover, the gain can be adjusted from 0.49 to 4.99 fold the original input. As a result, the DDS' output voltage changes in accordance to the gain determined in the differential amplifier.

Owing to the fact that the DDS provides a DC coupled sine waveform and high-frequency noises, the input of the DGA incorporates a band-pass filter, formed by a DC blocking capacitor along with a low pass filter set to 1 MHz. The output of this differential amplifier also includes another set of passive band-pass filters to eliminate any residual noise. The figure B.7 in the appendix B shows the schematic.

4.1 Design of a bioelectrical impedance plethysmography device

4.1.2.4 Modified Howland Amplifier module

This is a very popular circuit method used in bioimpedance analysis (BIA) measurements [188], tissue characterization [103, 142], electrical impedance tomography (EIT) and diagnosis of breast cancer [149, 189]. It can be constructed using a single operational amplifier (Op-Amp) as well as a handful of resistors [190]. Subsequently, a transconductance amplifier is used to convert the voltage coming out from the differential amplifier into an electrical current. Selected current will be passing through the patient. The chosen configuration is a modified Howland circuit (MHC) set to 1 mS of gain. The Figure 4.3 illustrates the MHC configuration that offers wide bandwidth operation and low power consumption.

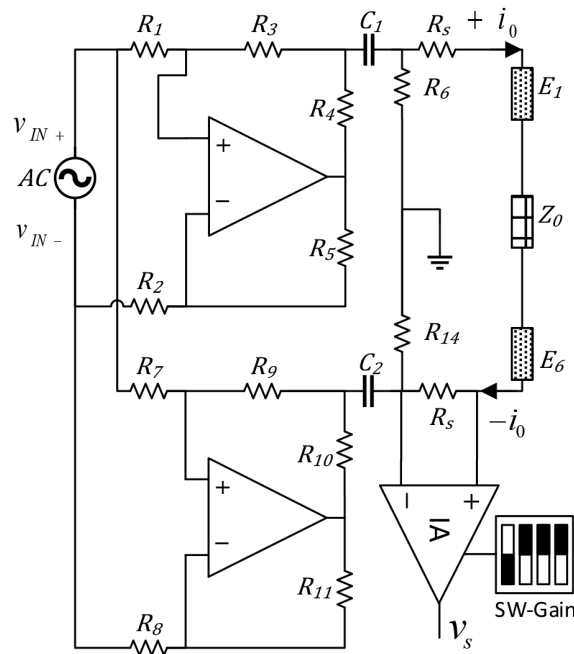


Figure 4.3 Modified Howland circuit schematic

The MHC design requires low tolerance resistors to minimise potential errors caused to the system. As a result, the resistors of 1 k Ω and 100 k Ω with a tolerance of 0.1 % were used in the final implementation. Figure 4.3 shows the implemented schematic of the differential MHC, only the top Op-Amp is analysed to prove that the equivalence was met, the one on the bottom follows the same equations but with an inverted output. The circuit's resistors from the equation are equivalent to the followings: $R_{2A} = R_1$, $R_{2B} = R_2$, $R_1 = R_3 + R_4$, $R_3 = R_5$ and $R_4 = R_6$. Thus, the equation can be re-written as follows:

Method and protocols

$$\frac{R_1 + R_2}{R_3 + R_4} = \frac{R_6}{R_5} \quad (4.1)$$

where $R_1 = R_4 = R_5 = R_6 = 100K\Omega$ and $R_2 = R_3 = 1K\Omega$. Finally, the resistor equivalence is calculated as shown by equation 4.1.

The transconductance of this circuit was calculated from equations 4.1. After the same resistors equivalence that were previously described, the positive transconductance (G_m^+) and negative transconductance (G_m^-) were calculated as described by the following arithmetical operations:

$$G_m^+ = \frac{i_{out}}{v_{in+}} = \frac{100K\Omega + 1K\Omega}{101K\Omega \times 1K\Omega} = \frac{101K\Omega}{101M\Omega} = 1 \times 10^{-3}S \quad (4.2)$$

$$G_m^- = -\frac{i_{out}}{v_{in-}} = \frac{100K\Omega + 1K\Omega}{101K\Omega \times 1K\Omega} = \frac{101K\Omega}{101M\Omega} = -1 \times 10^{-3}S \quad (4.3)$$

As can be seen from 4.2 and 4.3, the transconductance in both feedbacks is equivalent to 1 mS. The negative sign in G_m^- is caused by a phase shift of 180° . Due to the fact that top and bottom Op-Amps shown in figure 4.3 has the same design, the total transconductance of the circuit in differential mode is equal to 1 mS. In other words, for every volt generated at the input (pins input- and input+) the output produces 1 mA of electric current. By interfacing the previous DGA module with this one, it becomes possible to produce sixteen different levels of current. Nonetheless, for the purpose of setting the instrument, only one switch should be activated at a time to provide fixed currents of 1.33 mA, 2.16 mA, 3.60 mA and 4.36 mA.

The design also includes a high-pass filter at the output of the circuit. These RC networks act as DC decoupling and ground clamping because floating loads can witness DC offset coming from the signal, which might cause an error in the current. However, these capacitors also have an effect on the bandwidth of the circuit. The resistor, which could be the potential output impedance of the MHC, was chosen to be as high as possible (1 M Ω).

$$f_c = \frac{1}{2\pi RC} = \frac{1}{2\pi 1M\Omega 1\mu F} = 0.159\text{Hz} \quad (4.4)$$

4.1 Design of a bioelectrical impedance plethysmography device

4.1.2.5 Current and voltage sensing module

As shown in figure 4.3, at the output of the transconductance, amplifier resistors R_s of $10\ \Omega$ were placed at each side of the differential output. These small resistors sense the electrical current passing through the unknown load. Using Ohm's law $v = R \times i$, it is possible to convert this current into a proportional voltage value. However, by combining a small flowing current around mA with a tiny resistor value, the voltage obtained is in the order of mV . Consequently, this resultant voltage is too close to the noise level, and hence cannot be detected by any analogue to digital converter. Therefore, using a high input impedance amplifier is important to avoid current leakage through the current sensing IC and improve the signal to noise ratio.

An instrumentation amplifier with high input impedance and adjustable gain was used to convert the flowing current into an equivalent potential. Figure 4.4 shows how the differential signal was taken from resistor R_s which converts current i_0 into equivalent voltage V_s .

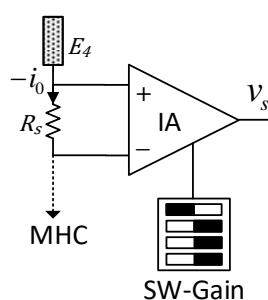


Figure 4.4 Current sensing circuit schematic

Likewise, this same circuit was used to detect the voltage produced by the limb segment. When the biological sample is excited with an electrical current, it leads to the emergence of a potential, as described in section 3.2. To that end, the electrodes E_2 and E_3 (see figure 4.1) provided the connection towards the input pins of the In-Amp AD8421 [121]. The robust input impedance of this IC and typical input bias current of $1\ nA$ guarantees minimal voltage drop from the interface electrode-skin. Therefore, the maximum error introduced by this voltage drop is close to $0.0001\ \%$ per mA which flows through the body segment. The gain of the In-Amp can be modified using its gain pins, increasing the dynamic range of the sensing circuit. Consequently, a dip-switch 4 SPST was used to provide as many as 16 different combinations of amplification that could be adapted as per the nature of the signal. The final schematic can be appreciated in the appendix B figure B.13.

Method and protocols

A sensing module was manufactured by combining the current sense and two channels of potential. Channel one was used to detect the voltage produced by the limb segment, whereas the second channel will be used for future studies carried out on differential impedance measurements. The only difference between the current and potential circuits is the selection of gain resistors that were allocated in accordance to the range of the signals to be detected. The output signal produced by this module is then passed through a peak and envelope detection circuit as described in the next section.

4.1.2.6 Envelope detection and AC extraction circuit module

This module has two functions: the first one detects the peak value of the current and voltage sensing circuit, whereas the other one extracts the plethysmography waveform contained within the baseline impedance. Hence, three output signals are produced by this module. The first signal is a DC voltage equivalent to the amplitude of the voltage detected by the current sense path denominated I_{DC} . The second output channel is a DC signal equal to the potential detected on the limb segment denoted by V_{DC} . The third one is an AC signal that represents the dynamic plethysmography signal or arterial pulse amplitude called V_{AC}

The envelope or peak detection is achieved using a "super diode" or "perfect diode" circuit, which is the combination of an active diode configuration and a hold circuit. In short, the Op-Amp complements the diode's voltage drop when the signal crosses zero. The negative feedback resulting from the output of the diode towards the negative pin of the Op-Amp mitigates the diode's voltage drop. Resultantly, the output signal at the cathode's diode is essentially a half-wave rectified waveform crossing by zero. The figure 4.5 shows a model of this circuit.

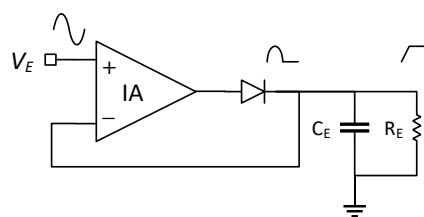


Figure 4.5 Envelope detection circuit schematic

The signal obtained by the super diode circuit is passed on to a hold circuit denoted by C_E and R_E in the figure 4.5. This RC configuration keeps its charge for a period of the signal produced by the wave generator, as described in section 4.1.2.2. The frequency

for measuring impedance plethysmography was selected at 50 kHz which implies that the distance peak-to-peak is 20 μ sec. The time constant (τ) of the RC network can be calculated by the following equation:

$$\tau = RC = 1\mu F \times 120K\Omega = 0.12Sec \quad (4.5)$$

The holding time of the RC network at $5 \times \tau$ is 0.6 sec, which implies that this RC combination can detect the peak of a signal with a frequency as low as 1.66 Hz. Consequently, this circuit produces a DC voltage signal equivalent to the peak value of the input signal. This makes it possible to generate the signals of channels I_{DC} and V_{DC} (see figure 4.2) which are the voltage representations of the current driven by this device and the voltage provided by the unknown load. Therefore, basal impedance is estimated by dividing the potential over the current values. This calculation was performed during the post-processing stage in Matlab [33] after digitisation.

The APA waveform can be extracted by isolating and amplifying the dynamic component within the basal impedance. Therefore, the unbuffered signal from channel V_{DC} channel gets passed through a band-pass filters with low-frequency cut at 10.26 mHz with a roll-off of 20 dB/decade as well as a high-frequency cut at 10.26 Hz with a roll-off of 40 dB/decade. Appendix B figure B.16 explains the design of the circuit and filters used..

Finally, the envelope detection module was manufactured in accordance to these design considerations. The output channels from this PCB are the ports which are known as I_{DC} or peak current value; V_{DC} or peak impedance potential and V_{AC} or arterial pulses.

4.2 Experimental Procedure

This section of the chapter describes the protocol of the experimental procedure along with the calculations performed in order to quantify the measurements obtained during the test. This experimental procedure and protocol gained the approval of the City University London Research Ethics Committee. Examination authorised under reference "SREC 15-16 01 E 29 09 201" of the 11th of November 2015.

This study entailed the participation of eight healthy volunteers; six of these participants were males the remaining ones were females aged between 23 to 37 years-old (mean 28.77). Prior to their recruitment, the participants received the documentation which explained the entire procedure to them. Upon their approval, the party returned the consent form

Method and protocols

signed in order to schedule the study. The experiments took place at the Research Centre for Biomedical Engineering of City, University of London. Upon arrival, the participants acclimatised for 10 min wherein the room temperature was 22 ± 2 °C. During this period, the experimental procedure was clearly explained to the attendant. After filling paperwork and completing the acclimatisation process, the instruments described in table 4.2 were used to acquire the physiological signals used for the present study.

Table 4.2 Instruments used during the study and measurements taken

Instrument	Device	Method	Measurement
ECG	Cardioline® Delta 60 plus [191]	Sense of electrical charges in heart	4 electrodes electrocardiogram
PPG	Zen PPG	Optical	Measurement of changes of volume in vascular bed using a light source at 680 nm
LDF	Moor VMS-LDF2 [192]	Optical	Measurement flow in capillary bed (Cell level) using a laser light at a wavelength of 785 nm
Doppler Ultrasound	Huntleigh MD2 [71]	Electromagnetic	Measurement of flow speed with a sensor head of 8 MHz
iPG	Bespoken	Electrical	Measurement of changes of volume in a segment using tetra-polar electrode configuration

4.2.1 Instruments set-up

This section describes all the steps taken to attached the instruments on the participants. Figure 4.6 illustrates the entire experiment set-up is, including sensors positioning from the different methods. First, all the participants sat in a comfortable chair. Their left arm rested on a soft cushion atop a table placed next to a chair that was adjusted to collaborator's height. Subsequently, blood pressure was taken using an automated instrument by recording diastolic and systolic values for each one. Then, each participant positioned ECG electrodes on themselves to form an Einthoven triangle. According to the device's instructions, electrodes need to be placed on each shoulder and ankle. Leads were secured to the electrodes in order to verify that ECG signal was clean. The apparatus includes an output port that exports the waveform for further processing.

As the next step, the PPG probe from the zen device was placed on the index finger. This instrument was designed by the biomedical research group of City University. This equipment

4.2 Experimental Procedure

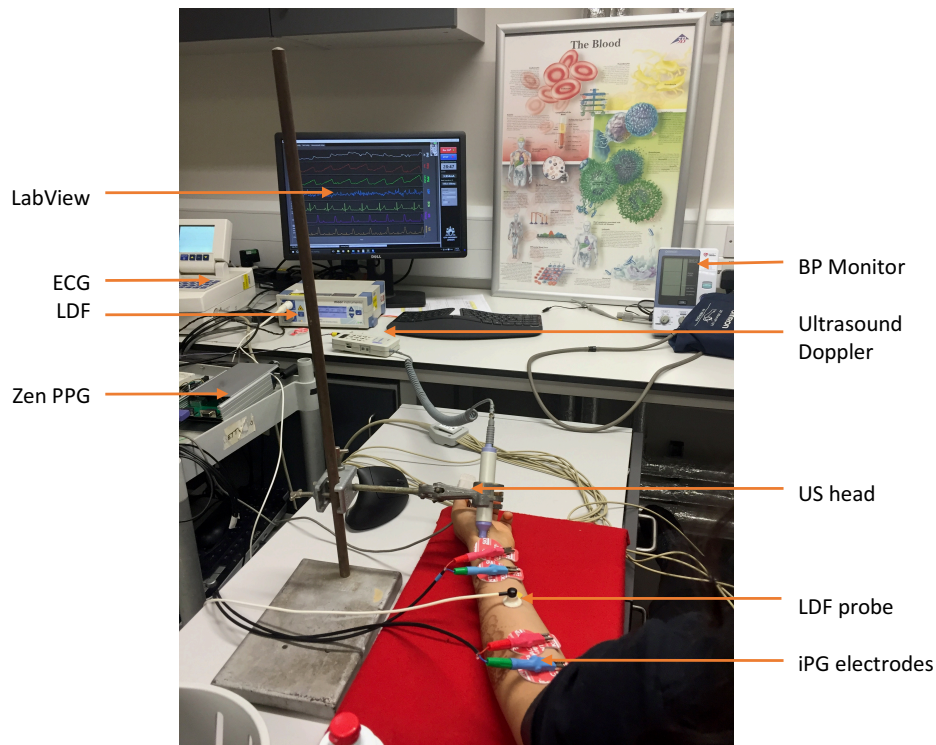


Figure 4.6 Instruments position in the forearm during the experiment procedure

has two available channels, but the experiment required just one port. Each channel provides two outputs containing AC and DC components of the photoplethysmographic waveform.

Next, the laser Doppler Flowmetry probe [192] was attached on the forearm's mid-section. This device detects moving red blood cells within a vessel below the vascular bed in the skin. In addition, this device has an external analogue port where the acquired signal can be exported for post-processing.

The Doppler ultrasound probe was then placed as close as possible to the radial artery. When the probe is placed closed to the main vessel, the speed of blood flow produces a unique audible signal. However, calculating blood flow from this signal requires a set of distinct skills by placing the probe at a fixed angle and maintaining closeness to the artery for a good measurement. Therefore, the probe head of the instrument needs to be placed at a fixed angle. Hence, the instrument's head was secured using a laboratory stand and clamp that was pointing at the party's radial artery on the wrist. The appliance also features an external port for additional off-line processing.

Finally, the impedance plethysmography electrodes were placed on the forearm's skin. To do so, ECG electrodes were used since they provide a good contact point, which is

Method and protocols

essential to carry out the experiment successfully. The electrodes were placed as show in figure 4.1. The diameter of the circumference around these electrodes was recorded along with its distance separation, as well as the distance from heart to shoulder, upper arm length, and shoulder to index finger. These physical measurements facilitate the calculation of the volume of the forearm’s segment that is to be measured.

4.2.2 Physiological measurements

The physiological measurements of the participants were taken at the beginning of the study collecting data such age, sex and arm to heart length. The table 4.3 summarises the information provided by all the participants. The ages of participants ranged between 23 year – old to 37 year – old (mean 29.12 ± 4.94).

Table 4.3 Participants’ age, sex and forearm measurements

	Age	Sex	Dimensions [cm]		
			Arm length	Shoulder to heart	Total length
Participant 1	26	Male	80	26	106
Participant 2	23	Female	66	24	90
Participant 3	27	Female	74	24	98
Participant 4	37	Male	68	24	92
Participant 5	29	Female	62	24	86
Participant 6	36	Male	70	24	94
Participant 7	29	Male	73	23	96
Participant 8	26	Male	69	23	92

In addition to these measurements, the distance between impedance potential electrodes (E_2 and E_3) and the arm circumference was simultaneously recorded using a measuring tape. This data makes it possible to estimate the forearm’s segment total volume by gauging the total distance between the potential electrodes (l), and the circumference of each electrode’s location (C_1 and C_2). Table 4.4 illustrates the dimensions of the participant’s forearm between the sensing electrodes and the segment’s volume as calculated from Equation 4.6.

$$V_e = \frac{l \times (C_1^2 + C_1 \times C_2 + C_2^2)}{(12 \times \pi)} \quad [\text{cm}^3] \quad (4.6)$$

4.2 Experimental Procedure

where V_e denotes the segment's volume, l represents the length between the potential electrodes, and C_1 and C_2 are the circumference measurement at elbow and wrist electrodes, respectively.

Using a measuring tape to accommodate these dimensions may induce some errors in the data. For instance, applying excessive pressure on the arm, when taking the measurements, may provide a lower circumference value. However, this also allows estimating the initial volume of the forearm segment which signifies the original volume of the conductive portion.

Table 4.4 Participants' forearm dimensions and initial total volume

	L [cm]	C ₁ [cm]	C ₂ [cm]	V _e [cm ³]
Participant 1	14.8	17.5	27.5	606.05
Participant 2	11.0	15.0	20.0	269.90
Participant 3	13.0	19.0	26.5	540.27
Participant 4	10.0	17.5	25.0	363.07
Participant 5	10.0	17.5	23.5	336.81
Participant 6	11.0	18.5	27.0	458.32
Participant 7	13.5	15.0	23.0	393.55
Participant 8	11.5	17.0	23.5	378.49

4.2.3 Experimental protocol

One of the key endeavours of this experiment is to look into iPG waveform alterations in case of an obstruction in the blood flow towards the forearm. Restricting blood circulation in this area is possible by applying a mechanical blockage on the upper left arm using a standard inflatable blood pressure instrument. The device necessitates being pumped manually using an inflation bulb. A gauge in the instrument indicates the cuff's pressure level.

The protocol entailed the recording of three different types of blood flow occlusion. The first kind restricts blood flow return by blocking the venous circulation. This method is extensively used to assess peripheral circulatory problems using a Venous Occlusion (VO) Plethysmography technique as described by Wilkinson et al. [15]. This obstruction can be produced by inflating the cuff usually just below the diastolic pressure between 10 mmHg to 20 mmHg. Therefore, blocking the upper arm obstructs blood flow within the median cubital and basilic veins without obstructing the brachial artery's arterial inflow. Overall, the target pressure of the study was 20 mmHg for each participant under their diastolic pressure recorded at the start of the session.

Method and protocols

A partial arterial occlusion (PAO) was the second class of blood flow limitation. This kind of blockage lowers the amount of arterial blood coming into the forearm but also impedes venous blood return. Studies have demonstrated that constricting an artery lowers the arterial flow towards the periphery [193]. This can be obtained by applying a mechanical compression on the upper arm between diastolic and systolic pressures, thereby intensifying the wall pressure of the brachial artery. The midpoint of the partaker's blood pressure was calculated using the following equation.

$$P_m = \frac{P_d + P_s}{2} \quad [\text{mmHg}] \quad (4.7)$$

where P_d is diastolic pressure and P_s is systolic pressure.

The last kind of occlusion needed is total occlusion (TO), which can be achieved by obstructing blood flow above systolic pressure. Also known as "Suprasystolic" or "stop-flow", it can provide valuable tonometric information [194]. In this experiment, blood flow was blocked by inflating the cuff 20 mmHg above participant's recorded systolic value. This method of occlusion completely restricts the inflow and outflow of venous and arterial blood. Hence, no change of volume is expected to take all along this part of the test.

4.2.3.1 Blood flow occlusion protocol

In order to estimate the blood pressure point to achieve venous and arterial occlusion on each participant, the normal blood pressure of each of them needed recording. For this, the blood pressure of each participant was taken using an automated blood pressure instrument brand Omron IntelliSense (Omron Healthcare). The mean systolic and diastolic pressures of all the partakers of this investigation were 116.25 ± 13.66 mmHg and 72.75 ± 7.23 mmHg respectively. The venous occlusion level was targeted at 20 mmHg below systolic pressure the total mean was 55 ± 8.01 mmHg, the partial arterial pressure was calculated using the equation 4.7, the average was about 94.63 ± 10.21 mmHg and total occlusion was around 136.25 ± 13.67 mmHg. Table 4.5 details the blood pressures recorded per participant and the pressures used during the experimental procedure.

The whole protocol required a total of 30 min to record all the signals from the instruments presented in table 4.2. At the commencement, 5 min of data were collected during baseline blood pressure. Then, immediately the cuff was inflated rapidly to 20 mmHg below the diastolic pressure, thus producing venous occlusion along with an increment in the total

4.2 Experimental Procedure

Table 4.5 Participants' initial blood pressure and levels for venous, partial arterial and total occlusion

	Blood pressure [mmHg]	Occlusion 1 (VO) [mmHg]	Occlusion 2 (PAO) [mmHg]	Occlusion 3 (TO) [mmHg]
Participant 1	124/78	50	101	144
Participant 2	105/65	50	85	125
Participant 3	120/78	60	99	140
Participant 4	120/72	60	96	140
Participant 5	100/60	40	80	120
Participant 6	143/82	60	113	163
Participant 7	107/73	65	90	127
Participant 8	111/74	55	93	131

volume of the forearm due to blood pooling effect. This level of blockage was held for 3 min followed by swiftly deflating the cuff.

The next step required producing the partial arterial occlusion using similar time spans as the ones that were used during venous occlusion. As described previously in the literature, reperfusion following an occlusion does not affect blood pressure, heart rate or blood flow [195]. Hence, 5 min provides sufficient time to restore the blood flow to normal limits. It is for this reason that the cuff's air valve was left open to bleed all the air inside. Subsequently, the cuff was quickly inflated again until reaching the pressures shown in column *Occlusion 2* of table 4.5. The cuff's pressure was maintained at this level for 3 min followed by a quick release of pressure.

Last, a similar method was applied for total blood occlusion. Yet again, 5 min of baseline waveforms were taken followed by a fleeting cuff inflation to 20 mmHg above the diastolic pressure. This compression was kept for 3 min. At this point, maintaining this tourniquet effect can become painful after a couple of minutes. As a result, some of the helpers ended up re-accommodating producing motion artefacts in the data. Finally, the last 5 min of baseline waveforms were recorded in order to study the recovering effect.

Figure 4.7 illustrates the pressure levels applied during the entire experiment. For a better understanding of the different stages of this experiment, each event was identified as a region. Thus, the regions 1, 3, 5 and 7 represent the non-occlusive events or baseline readings. In contrast, regions 2, 4 and 6 are equivalent to VO, PAO and TO events.

Method and protocols

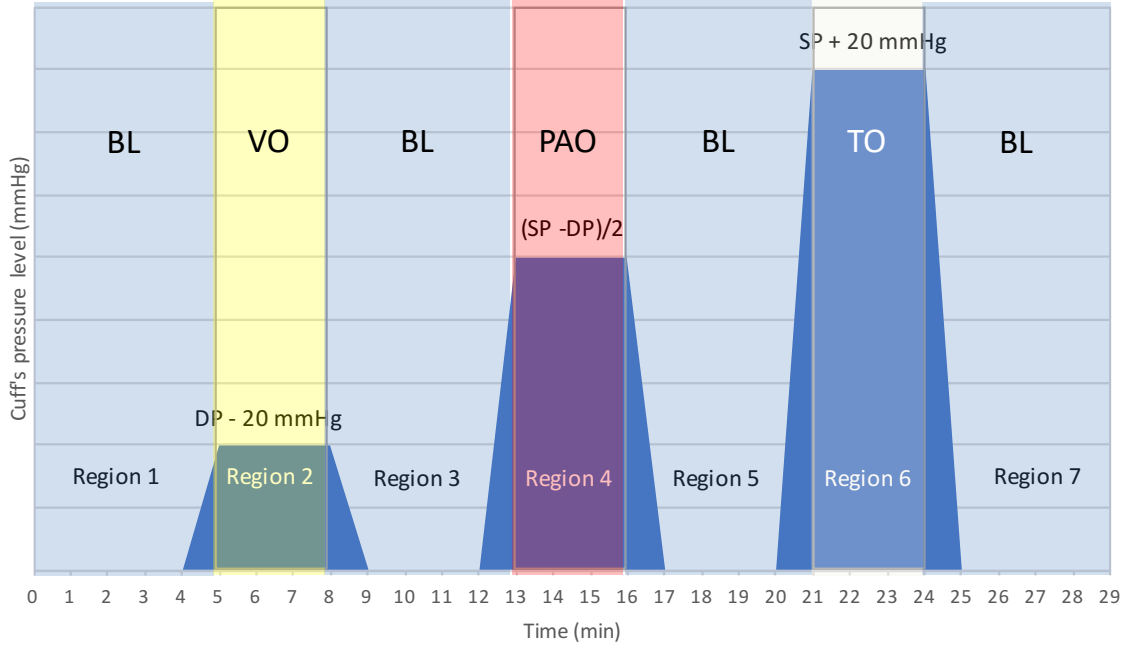


Figure 4.7 Pressure applied to the participant's upper arm during the experiment. The clear areas represent the resting period of 5 min, and the shaded areas denote the pressure applied at the desired level during 3 min. All the regions have been denoted for reference during the analysis.

4.3 Data processing

All instruments used in this experiment provided the external analogue ports for further data processing. These output ports were connected to a DAQ NI-6211 (National Instruments). All signals were sampled at 1 kHz with a reference voltage between 0 V to 10 V for the iPG channel V_{DC} and ± 5 V for the other signals. Therefore, the resolution of DAQ was $152.6 \mu\text{V}$, which was calculated using equation 4.8.

$$Res = \frac{V_{p-p}}{2^n} \quad [\text{V}] \quad (4.8)$$

where V_{p-p} denotes the reference voltage peak to peak with n being number of bits used to sample the signal.

A virtual instrument using LabView [32] was created to display, process and store raw data. In the main tab, the custom virtual instrument was able to display the live waveforms of the iPG, ECG, PPG and Doppler ultrasound instruments. Band-pass filters were applied to the iPG and PPG signals, removing unwanted DC components as well as high frequency

noises. The waveforms from other instruments did not necessitate filtering since the devices served clean signals.

The virtual instrument also included configuration capabilities. Two tabs in the program featured a field for physical measurements, general application settings and other adjustment for the PPG instrument. The participant tab recorded the following measurements: left arm dimensions, blood pressure and file path name. Once this experimental procedure completed, all raw data were stored on a LabVIEW Measurement file format (LVM).

The data imported from the LVM file was decimated to speed up the post-processing time in Matlab [33]. All the waveforms were down sampled to a frequency of 100 Hz. Notably, this data decimation does not impact the waveform data. In fact, according to Nyquist [196] rate, data was over sampled. Physiological signals are between 1 Hz to 3 Hz depending on the heart rate. Thus, 6 Hz would have provided sufficient sampling frequency for the waveforms. Nevertheless, the new sampling frequency accommodates a high resolution of the discrete-time signal which allows the implementation of high order digital filters with sharp cut-off frequencies.

After importing decimated data into Matlab, a custom parsing program converted and saved each waveform into a Matlab file format (.mat). A Graphic User Interface (GUI) Matlab program was created to compare four waveforms time while simultaneously applying filters, finding peaks and windowing different sections of data. A front-end of the application can be seen in figure 4.8. Placing the data into Matlab file format accelerates the loading in memory (of the data) and the waveform presentation within the GUI. Another advantage of such a file conversion is that data processing can be performed online without using extensive computing resources.

4.3.1 Data conversion

The data imported into the GUI represents the volts of the entire physiological measurements. Therefore, this information must be converted into significant values that denote the physical variable. This section describes the mathematical equations and tools used to convert the raw signals effectively in greater detail.

4.3.1.1 Calculation of the basal impedance value

Impedance plethysmography signals must be converted from volts and current values into its standard scale, which is Ohms (Ω). The iPG device has a channel for current sense known as I_{DC} , whose voltage is equivalent to the peak value of the current that is being

Method and protocols

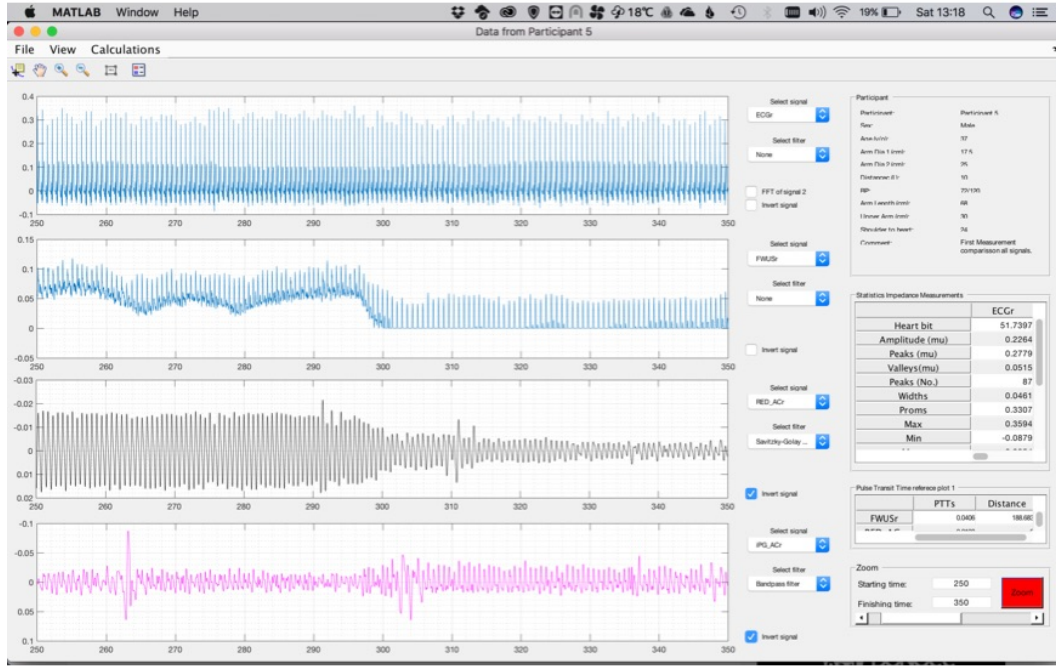


Figure 4.8 Matlab application GUI used to qualify data and post-processing the signals acquired

delivered by the instrument. The effective electrical current in amperes (A) can be calculated by the gain relation of the various stages of the signal path. In accordance to the circuit schematic (see figure 4.3), the electrical current is being sensed by a $10\ \Omega$ resistor (R_s) in the module *Modified Howland Amplifier module* (see section 4.1.2.4). Subsequently, this signal is amplified by an instrumentation amplifier in the *current and voltage sensing module* (see section 4.1.2.5) which gain (G_1) was fixed to 276. Following the signal path, the waveform is fractioned by the super-diode circuit, which acts as a half-wave rectifier in the *envelope detection module* (see section 4.1.2.6). The hold circuit keeps the DC voltage constant at the signal output, which is equivalent to the peak value of the current in volts. Thus, the electrical current in amperes can be calculated using the equation 4.9.

$$I = \frac{V_{IDC} \times 2}{R_x \times G_1} = \frac{V_{IDC} \times 2}{276 \times 10\ \Omega} = \frac{V_{IDC}}{1380\ \Omega} \quad [A] \quad (4.9)$$

The second channel of this iPG device labelled V_{DC} produces a DC voltage tantamount to the impedance of the forearm. Similarly, as the current senses voltage path, the channel passes through a series of circuits that amplifies the original potential being sourced from the

forearm's segment. Therefore, the actual voltage detected by the device can be debunked by the numerous gains involved during the signal path.

First, the unknown load is sensed by the potential electrodes (E_2 and E_3 in figure 4.1) directly connected to the *voltage sense module* (see section 4.1.2.5). The instrumentation amplifier (AD8421) of this module was configured to a gain 35.65. In the *envelope detection module* (see section 4.1.2.6), the signal was rectified using the super-diode circuit and halving the signal amplitude. As a result, the voltage can be deducted by using equation 4.10.

$$V_z = \frac{V_{ZDC} \times 2}{35.65} \quad [\text{V}] \quad (4.10)$$

where V_{ZDC} denotes the DC voltage coming from the port V_{DC} .

Finally, the impedance value can be computed by converting the voltage into impedance using Ohm's law [197]. This can be accomplished by replacing equation 4.9 and 4.10 into 4.11. The GUI programmed in Matlab automatically carries out this impedance conversion when the signal gets loaded in the GUI. This mathematical operation is undertaken by a point-to-point division between the two signals after subtracting their gains from their raw values.

$$Z = \frac{v}{i} = \frac{V_z}{I} \quad [\Omega] \quad (4.11)$$

4.3.1.2 Calculation of the Arterial Pulse Amplitude value

The third channel is the APA signal designated as V_{AC} . This waveform is an amplified version of the dynamic signal within V_{DC} . During the course of analysing the signal's path, it can be seen that the two circuits work on the waveform in tandem. First, it is the circuit from where this signal originates which is the same voltage as seen in port V_{DC} , implying that the gain described in the previous section also has an impact on the signal V_{AC} . The second circuit which affects the signal is the band-pass filter within the *envelope detection module* (see section 4.1.2.6). As can be appreciated in the appendix B figure B.16, this filter entails a fixed gain of 142.42 and eliminates any kind of DC and high-frequency noise components. Subsequently, the voltage of the plethysmography wave can be found by combining both gains using the equation 4.12.

Method and protocols

$$V_{APA} = \frac{V_{ZAC} \times 2}{142.42 \times 35.65} = \frac{V_{ZAC}}{2538.66} \quad [\text{V}] \quad (4.12)$$

where V_{ZAC} denotes the raw AC voltage coming from the port V_{AC} .

Likewise, the dynamic signal's impedance value (V_{AC}) can be calculated using Ohm's law [197] by replacing the APA voltage from equation 4.12 as well as current from equation 4.9. In Matlab, this impedance value is calculated as soon as the signal gets selected by applying this mathematical formula.

$$Z_{iPG} = \frac{v}{i} = \frac{V_{APA}}{I} \quad [\Omega] \quad (4.13)$$

4.3.1.3 Converting ultrasound to flow

The instrument used in this study was a Huntleigh model MD2 with sensor type VP8. The frequency of the transmitter is 8 MHz which makes it ideal for blood flow estimation. The principle of this device pertains to the frequency of a source to its velocity relative to a sensor [69]. Put simply, if an electromagnetic wave gets transmitted at a fixed frequency and is reflected by a moving body, the frequency of the received signal will be shifted [71].

The device can detect moving blood cells inside a vessel. When a cell passes through the electromagnetic beam, a frequency shift occurs that is proportional to the blood flow velocity. Nevertheless, this Doppler shift is also affected by the angle of the head of the probe along with the direction of the flow [69].

Since the average velocities found in the human body lies within the hearable frequency range, the device reproduces this as an audible sound with the help of a speaker. The apparatus has an output channel that produces the equivalent analogue signal for further processing. According to the service manual of this instrument, a 3.5 V signal equals to a 8 kHz shift signal at the output [71]. Keeping this voltage as a reference, the shift frequency can be calculated using the equation 4.14.

$$f_D = \frac{V_{DU} \times 8\text{KHz}}{3.5\text{V}} \quad [\text{Hz}] \quad (4.14)$$

where V_{DU} represents the analogue output voltage of this instrument.

4.3 Data processing

As per the Doppler equation described in 4.15, the velocity of a blood cell derived from its frequency shift can be found. However, there is a correction angle (θ) between the ultrasound beam and the direction of blood flow. Fixing the angle to a set value ensures that all the measurements have the same correction index. As a result, the head of this instrument was positioned at a 45° angle to the radial artery on the wrist.

$$v = \frac{f_D \times C}{2f_0 \times \cos(\theta)} \quad [\text{m s}^{-1}] \quad (4.15)$$

where f_D represents the Doppler frequency, C denotes the speed of sound assumed to be 1540 m s^{-1} , f_0 refers to the oscillation frequency of the Doppler instrument. In this case, 8 MHz and θ the angle between the ultrasound sensor and the target vessel, which is at 45° .

The position of this angle was locked using a laboratory stand and a clamp. The angle was fixed to 45° using a goniometer. Nevertheless, this is one of the shortcomings of this method. The angle can be estimated based on the position of the sensor's case, but not to the surface of sensor crystal. There is an incident error that cannot be quantified easily. However, for this study, the angle was established to be at 45° .

The velocity can be converted into the blood flow if the vessel's cross section area vessel is known, as shown by equation 4.16. Not being precisely aware of this area is another drawback of this method during the course of calculating blood flow accurately. Evaluating the real cross section area of a vessel requires imaging techniques such as Doppler Ultrasonography.

$$\dot{Q} = v \times A \quad [\text{m}^3 \text{ s}^{-1}] \quad (4.16)$$

where \dot{Q} represents flow, v is the velocity of the blood cell and A denotes the cross-sectional area of the radial artery.

However, blood flow can be estimated by using the average cross-sectional area of radial arteries within the general population. A study found that males have a slightly larger radial arteries diameter as compared to females ($2.3 \pm 0.39 \text{ mm}$ and $2.11 \pm 0.29 \text{ mm}$ respectively) [198]. These dimensions were used to calculate the blood flow in the current experiment. This information can be converted into a more conventional scale of a litre per minute by multiplying it by 60 s and converting m^3 into litres.

$$\dot{Q} = v \times A \times 60 \times 1000 \quad [\text{m}^3 \text{s}^{-1}] \quad (4.17)$$

Another drawback of this method is that it needs to be positioned as close as possible to the vessel. Highly skilled technicians can identify the difference in sounds between arteries and veins. For this experiment, the position of the sensor was on the wrist are where the radial artery is closer to the skin. The position of the instrument's head was selected in accordance to the loudest sound when measuring this area. The GUI programmed in Matlab allows the conversion of UD waveform into blood flow straight from the front panel using the equations described here.

4.3.1.4 Converting LDF

The Laser Doppler Flowmetry device utilised in this study was the Moor VMS-LDF instrument [192]. LDF is a non-invasive optical method used to estimate the blood perfusion within the microcirculatory bed under the skin. This device uses the same Doppler principle which is described in section 2.5.1. However, instead of sound, the source is a beam of light. Similarly, when a red blood cell scatters a light of beam, it ends up producing a frequency shift [6].

LDF produces a blood perfusion signal comparable to the RBC perfusion, also known as flux. The units of this measurement include Blood Perfusion Unit (BPU), an arbitrary unit scale. BPU denotes the product of the mean number of moving blood cells into the small volume under probe as well as the average velocity of moving blood cells.

This instrument provides an output port that allows for the export of this waveform. This connector provides a signal between 0 V to 5 V which varies in accordance to the flux signal. The configuration menu allows the medication of output scale. It provides three steps at the peak limit of 1000 BPU, 500 BPU and 100 BPU output for 5 V. The measurements taken in this study were below 100 BPU. Hence, equation 4.18 converts the output voltage into BPU's.

$$BPU = \frac{V_{BPU} \times 100}{5V} \quad (4.18)$$

Using this equation, the data in the Matlab GUI can be displayed using the correct notation. This formula is applied to the data as soon as it gets imported into the software.

4.3.1.5 Volume and flow calculation beat by beat from iPG signal

Impedance plethysmography also allows for the calculation of the change in volume as well as the blood flow from every heartbeat [21, 30, 175, 199]. Achieving this calculation is possible if there is high-quality plethysmography waveform. For this reason, the impedance device includes an analogue port called V_{AC} . As described previously in chapter 4.1, this port extracts the plethysmography waveform from the basal impedance channel V_{DC} . As a matter of fact, due to the filtering as well as amplification stages of the circuit, the signal has been amplified more than 2.500 times, thereby providing additional details of the signal's features and increasing its resolution after the digitisation.

The APA waveform as shown in figure 4.9 signifies a classic example of a plethysmography wave starting from point $L1$ and finishing in $L2$. Notably, this signal is inverted in impedance because an increase of blood indicates a surge in conductivity. As a result, there is a reduction in impedance of the segment being measured.

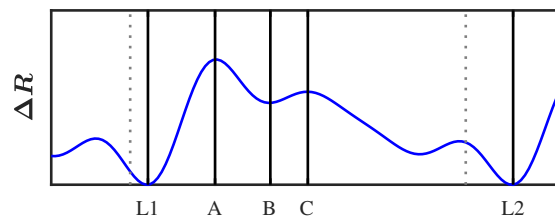


Figure 4.9 APA waveform representation.

The APA signal shows five specific reference points required to calculate volume and blood flow. During the systolic process, two planes are evident in the plethysmography wave. The first one is the upslope of the signal (L_1) during the isovolumetric contraction of the heart. This point marks the beginning of the plethysmography signal. Next, owing to blood ejection from the heart, the aortic outflow raises the pressure within the circulatory system. Therefore, an increase in blood flow is noticeable, which is pronounced as the maximum amplitude in the plethysmography signal denoted as A in figure 4.9.

During the heart cycle's diastolic development, the next observable reference point in the plethysmography wave is the dicrotic notch. This waveform appears after a decline in pressure within the circulatory system. In the APA wave shown in figure 4.9, two points can be seen within this region. The dicrotic notch is located precisely at the landmark B followed by a tiny peak C which marks the post-dicrotic notch segment or diastolic pulse.

Method and protocols

Finally, the cycle gets completed with the last dip in the APA waveform identified as $L2$. It also marks the beginning of the next volumetric cycle. In the wake of these landmarks in the waveform, it is possible to calculate blood flow from the following set of equations adapted from [29]. First, the average basal impedance (R_B) during the course of a pulse cycle can be calculated by averaging the resistance values at points $L1$ and $L2$. The mathematical operation used in Matlab GUI to calculate this basal impedance between cycles was equation 4.19.

$$R_B = \frac{R_{L1} + R_{L2}}{2} \quad [\Omega] \quad (4.19)$$

Subsequently, the extrapolation of the reference points from the APA pulse given by the Nyboer back-projection [29] must be conducted. This value is equivalent to dR/dt in other blood flow equation; instead, two reference points are used. The equation 4.20 exhibits the mathematical operation used to calculate this value.

$$EXHT = (R_B - R_{L1}) + \frac{(t_B - t_{L1})(R_A - R_B)}{t_B - t_A} \quad [\Omega] \quad (4.20)$$

Another key physiological measurement used to calculate blood flow is the heart rate that can be obtained directly from the APA waveform. The HR is equivalent to the difference of time in a cycle multiplied by 60 s. Using equation 4.21 the heart rate in beats per minute (bpm) can be estimated as follows.

$$HR = \frac{60}{(t_{L2} - t_{L1})} \quad [\text{bpm}] \quad (4.21)$$

The segmental blood flow beat to beat can be calculated using the Nyboer's equation 4.22. Equation 4.23 illustrates the equivalent mathematical operation in function of the heart rate that is obtained from equation 4.21 as well as the extrapolated APA pulse amplitude denoted by equation 4.20. Due to the fact that the HR has been included in this equation, the units of this formula are ml/min.

$$\frac{\Delta V}{\Delta t} = \rho \frac{l^2}{R_B^2} \times \frac{\Delta R}{\Delta t} \quad (4.22)$$

$$BF = HR \times EXHT \times \rho \frac{l^2}{R_B^2} \quad [\text{ml/min}] \quad (4.23)$$

where BF represents the blood flow expressed in ml/min, ρ is the specific resistivity of blood $150 \Omega \text{cm}^{-1}$ [102, 199], and l denotes the distance between sensing electrodes ($E2 - E3$).

Blood flow can be observed in different forms. For instance, it can be represented as either flow per total volume of tissue between the potential electrodes or as a fraction of that volume, since clinical use is usually represented as 100 ml of tissue. The equation 4.24 calculates the blood flow per total tissue volume.

$$BFVE = \frac{BF}{V_e} \times 1000 \text{ ml} \quad [\text{ml/min l}] \quad (4.24)$$

where $BFVE$ denotes the blood flow per litre of volume ml/min l, BF represents the blood flow found in 4.23, V_e is the forearm's segment volume in cm^3 from equation 4.6 and 1000 ml is the scaling factor that converts the volume into litre.

The other option is to denote the rate of blood flow in the standardized form per 100 ml of volume of tissue, also known as Perfusion Index (PI). As a result, the blood flow must be segmented to 100 ml of tissue. The total volume can be derived from equation 4.6. Thus, the PI can be calculated using the equation 4.25.

$$BF_{100ml} = \frac{BF}{V_e} \times 100 \text{ ml} \quad [\text{ml/min 100ml}] \quad (4.25)$$

To reiterate, all these flow equations were implemented in Matlab to calculate the blood flow rate during venous occlusion and beat-to-beat.

4.4 Conclusion

This section described the hardware design of an impedance plethysmography device which senses the current delivered as well as the potential generated by an unknown load in the forearm, A shows the final circuit assembly used for the experiments presented in this thesis. The design of this device was replete with patient safety features by delivering an

Method and protocols

imperceptible electrical current. The electrical characteristics of the bioelectrical impedance device included a wave generator (using a DDS) capable of producing a sine waveform of 50 kHz delivering four different levels of current between 1.33 mA, 2.16 mA, 3.60 mA and 4.36 mA (using a Modified Howland Circuit). The measurement of impedance was made possible by measuring the delivered current and the potential measured. The sensing circuits were implemented using high input impedance instrumentation amplifiers to guarantee high noise rejection.

One of the unique features of this instrument is the capability to produce not just the total impedance of a targeted segment of the limb, but also the arterial pulses amplitude. The two signals have been used separately to either measure volume changes using venous occlusion plethysmography [20–22] or estimate blood flow beat by beat [23–26]. However, the author was of the view that additional information should be obtained when combining both measurements. Therefore, it was imperative to design a device capable of providing both signals in real time, similar to the ones presented in the literature which primarily focused on one of the waveforms. Thus, The designed impedance plethysmography device incorporated 3 output channels. The first channel named I_{DC} , provided the peak value of the electrical current being driven into the patient. Thus, it is possible to sense the impedance readings more accurately since the delivered current is constantly measured for real time processing. One of the channels labelled as V_{DC} provides readings of the peak voltage obtained from the patient. The other channel called V_{AC} displays the AC component of the impedimetric signal lying within the impedance measurements.

An experiment was set up to measure the changes of impedance that can be converted into blood flow when an occlusion occurs. The entire experiment aims to collect data when three different kinds of occlusion occur: venous occlusion, partial arterial occlusion and total occlusion. The protocol was designed to take 5 min of resting data followed by 3 min of readings at the time of each flow restriction. The data derived from the instruments is in volts V which does not represent a physiological measurement. Therefore, all these equations that were required to convert the data were explained in significant detail. The data sourced from the impedance device was also examined in greater detail in order to better understand and use two methods of measuring blood flow.

In the end, the entire data along with the mathematical operations were input into Matlab where a custom GUI was programmed. From this interface, it is possible to qualify and quantify the data. In addition, filters were applied and a statistical analysis was undertaken. This work adequately complements the design of iPG device, which combines the equations, filters and algorithms presented in this chapter to produce equivalent physiological readings.

Investigation of changes of the basal impedance signal

This chapter shows the results of the changes in basal impedance during the whole experimental procedure. The results presented in this chapter elaborate on the different elements that could potentially impact the baseline impedance during the course of a measurement. The different regions from the study were taken under consideration to analyse the distinct changes during resting and occlusive periods. First, it was analysed the variation of baseline impedance during the resting periods (regions 1, 3, 5 and 7). The data showed that the median impedance changed around -0.6384% from the original baseline region 1.

The second part of the chapter includes an in-depth analysis of the change of impedance during each of the occlusive periods (regions 2, 4 and 6). The results are shown in three modalities: one describing the change of the measured impedance baseline, the second presenting the change of impedance compared to the initial baseline and the third as the change of impedance in time (dZ/dt) per every ten heartbeats. In general, the data showed a decrease in baseline impedance during the occlusive periods due to the pooling effect of blood. The difference in slope between venous and partial arterial occlusion provided the initial clue in how to differentiate between these two occlusive events.

5.1 Basal impedance measurements during baseline

The basal impedance of the participants forearm was recorded from the port denominated Z_{DC} of the designed device. In general, the iPG device detected the forearm's segment impedance quite remarkably. Furthermore, the obtained values fell within the reported resistive value

Investigation of changes of the basal impedance signal

in the tens Ohms as per the estimation given in the literature [122, 123, 200]. However, there are different artefacts that can alter the basal impedance during a measurement, such as motion or respiration movement [201–204]. This section will analyse the extent of change in the basal impedance between the measurements.

All participants were asked to stay still for the entire duration of the test. However, in practical terms, this is not entirely possible as staying still in the same position for a prolonged period of time can be quite tiresome. Inflating the cuff to a pressure above diastolic level may also cause discomfort to the participants, like tingling sensation or even pain. Thus, moving the limb to restore blood flow is a normal response of the body. The first 2 min of the baseline impedance readings may be affected by the rearrangement of the participant's position, particularly after the upper arm's occlusion. Moreover, the restriction in blood flow also induced a physiological response which needed some time to revert to the baseline value. Hence, the baseline data after 2 min is used for this analysis, thereby allowing some time for recovery.

The data used for this analysis was compiled by extracting the lower envelope of the raw basal impedance. The command envelope in Matlab [33] allows the isolation of the desired signal baseline signal omitting the APA pulses. Figure 5.1 displays the waveform extracted with the respective mean value for each region per participant. The region 1 is applicable to the time when the initial reference was recorded; in total, 5 min were recorded but the last 3 min of data was extracted right before the occlusion between 120 s to 300 s. This basal impedance is the reference to the other readings as it was unaffected by occlusion of any kind. The other sections of data correspond to region 3, which denotes the recovery after venous occlusion. The information extracted belongs to the time slot between 600 s to 780 s. In a similar manner, the region 5 after partial arterial occlusion retrieves the last 3 min of data between 1080 s to 1260 s. Finally, there is data after total occlusion in the region 7 between 1560 s to 1740 s.

The first observation from this figure is the presence of oscillations in the baseline signal. This signal was present in all participants with subtle frequency variations between each region. The frequency was calculated by extracting the period of the signal as the difference between its peaks. On average, the frequency of the oscillation was 0.0685 ± 0.0027 Hz. At this point, it is not possible to establish whether this is a common noise from the instrument or a physiological response. In the literature, there is lack of sufficient information about impedance plethysmographic oscillations at this frequency band. However, a study that used laser Doppler flowmetry found that the physiological measurements into this frequency spec-

5.1 Basal impedance measurements during baseline

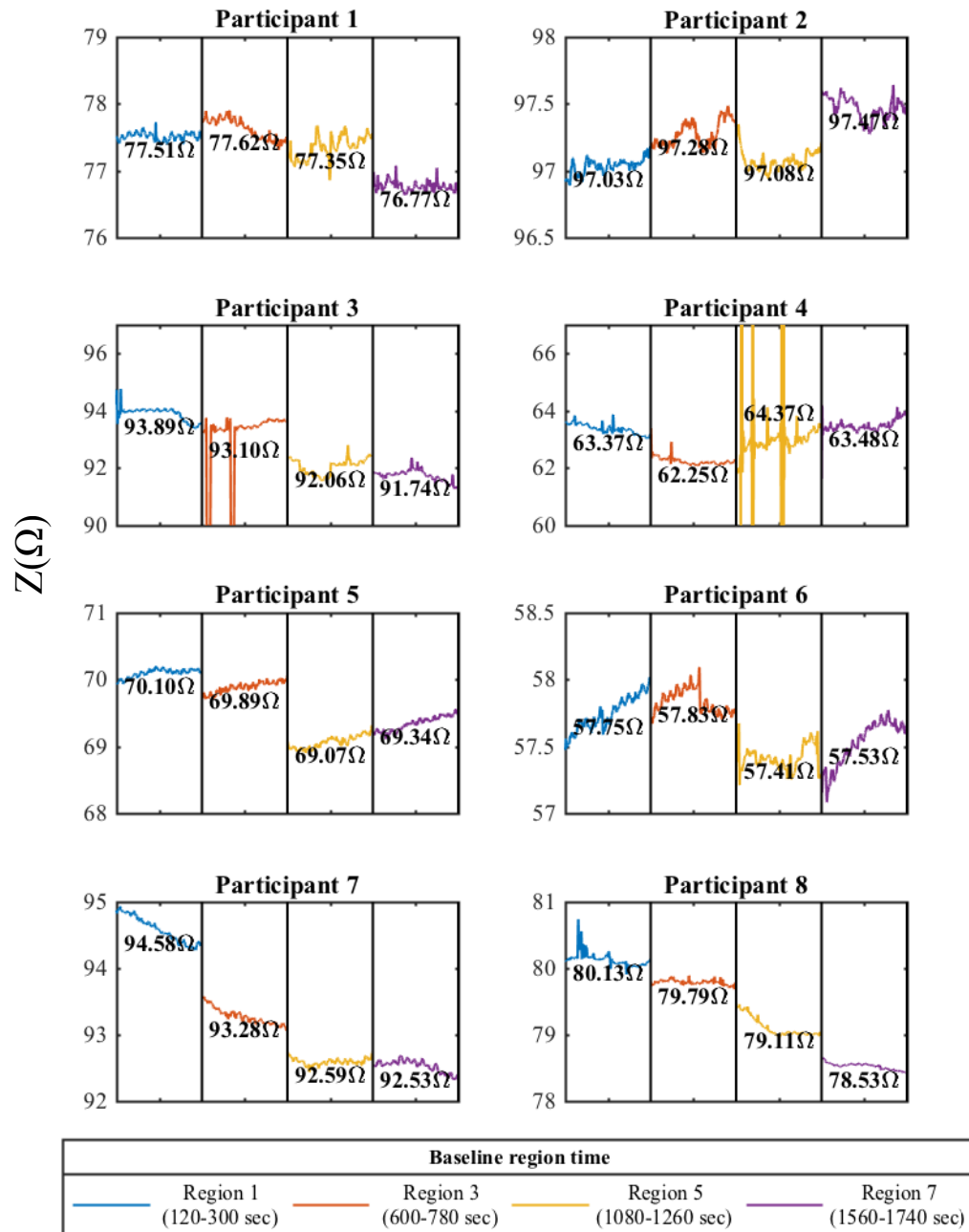


Figure 5.1 Basal impedance of all the participants during the entire study. The data has been divided into regions. The regions (1, 3, 5 and 7) in white colour represent baseline measurements.

Investigation of changes of the basal impedance signal

trum may pertain to the sympathetic activity (0.02 Hz to 0.06 Hz) [205]. Further investigation needs to be undertaken in order to discover the roof of this signal.

It is evident that the motion artefact did make some alterations into the measurements. Participants 3 and 4 clearly displayed deviation from their mean values in region 2 and region 4, respectively. As a matter of fact, the figure had to be clipped off to adequately fit the waveform information. On the other hand, it became difficult to detect changes on partaker 1, but region 3 displayed significant variations when compared with other regions. Hence, this qualitative analysis confirms the quantitative results shown in figure 5.2.

Additionally, it is also clear that there are variations on the baseline impedance between different regions. Furthermore, there is an absence of a clear trend on either the increase or decrease of basal impedance, with the exception of participants 7 and 8 where there a decrease on impedance is observed. Big gaps ($< 0.8 \Omega$) between regions can be noticed on participant 5 and participant 7, respectively.

From the quantitative standpoint, the figure 5.2 illustrates the statistical values of the median basal impedance during the regions 1, 3, 5 and 7. The mean resistive baseline impedance of all the participants was $78.62 \pm 14.61 \Omega$. It must be noted that the impedance was entirely independent of their gender.

Again, the analysis confirms that motion artefact triggered the outliers of the readings. As noticed from the box plot figure, participants 1, 3 and particularly 4 presented the deviated points during the study. Additionally, participants 3, 4 and 8 exhibited the biggest distribution between interquartile values higher than 1Ω (mean $1.41 \pm 0.39 \Omega$). The remaining participants showed a distribution within first and third interquartile of about $0.57 \pm 0.27 \Omega$.

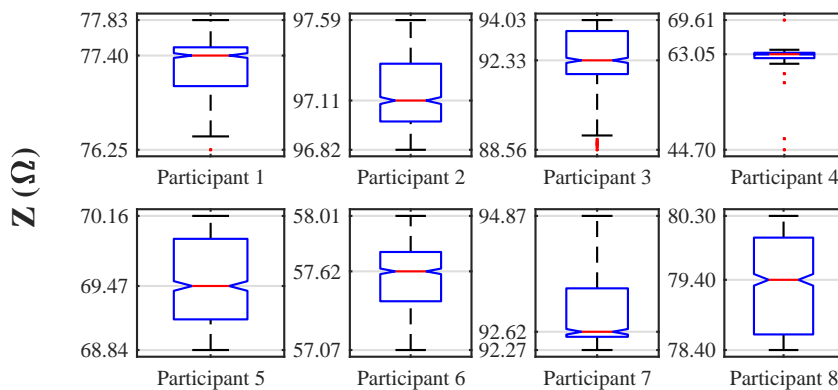


Figure 5.2 Mean basal impedance box plot of all the participants during the last 3 min of the baseline regions 1, 3, 5 and 7.

5.1.1 Deviation of the basal impedance from baseline

The basal impedance signal contains noises that may deviate from the signal (from the baseline). This section will quantify the error as compared to the basal impedance at the beginning of the experiment. Numerous factors could affect a bioelectrical impedance reading. One of this is the change of impedance on the electrode-skin interface. As described in section 3.4, when there is a change in the geometry or the area of contact of the electrode, it gets converted into variations in the total impedance. Also, air pockets that could potentially form between the two elements could contribute to substantial changes in impedance. Another contributing factor is the motion artefact. In this case, the movement of the skin and muscles creates different current paths. As a result, the basal impedance deviates from the baseline.

In an in-vivo setting, it is difficult to keep a participant completely motionless for the entire duration of the experiment. During each baseline, the upper arm's occlusion caused the participants to move and re-accommodate. Eventually, there was a change of impedance that will be analysed; it could be caused by that movement or perhaps a physiological response.

The figure 5.3 shows the deviation in percentage from the baseline in region 1. Thus, the median impedance was the starting point in this region. The data was calculated by extracting the envelope of the impedance waveform. In the figure, each point denotes the median value of the resistance and the whiskers the range of data. It was the oscillatory component described in the previous section that triggered the major variations the resistance. The baseline impedance tended to decrease in majority of the participants, except number 2.

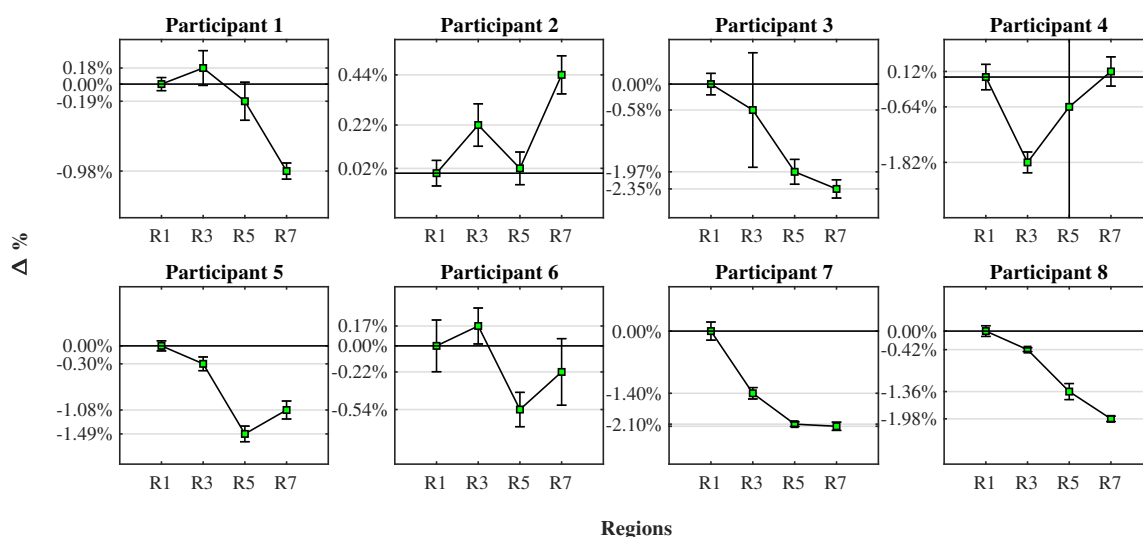


Figure 5.3 Deviation of the basal impedance for all the participants compared to region 1. Each plot shows how much the impedance increase or decrease against the reference value for regions 3, 5 and 7.

Investigation of changes of the basal impedance signal

The effect of the motion artefact can be observed on the large whiskers of some of the participants. For example, participants 3 and 4 demonstrated the bigger ones in region 3 and 5, respectively. Indeed, the data from participant 4 was clipped as the whiskers showed a huge variation of up to 200 %. It is also important to note that only a few signals were able to return to baseline. For instance, the waveforms that experienced a variation below 0.25 % included regions 3 and 4 of participant 1, participant 2 in region 5, participant 4 in region 7 and participant 6 in regions 3 and 7. The rest experienced changes of roughly -2.353% to 0.441% from the baseline region 1.

The table 5.1 illustrates the range and mean of changes of impedance for all the participants. The average impedance of the entire study was -0.6384% with a range of about 1.5264% . Certainly, participants 1, 2 and 7 illustrated the least impedance change with less than 0.25% , whereas the second one increased and others decreased. A change occurring between 0.25% to 1% was experienced by participants 4, 5 and 8. Finally, participants 3 and 7 recorded the biggest change of impedance of over 1% .

Table 5.1 Mean and range of the impedance change for each participant.

	range ($\Delta\%$)	mean ($\Delta\%$)
Participant 1	1.157 %	-0.247%
Participant 2	0.441 %	0.170 %
Participant 3	2.353 %	-1.226%
Participant 4	1.939 %	-0.584%
Participant 5	1.489 %	-0.719%
Participant 6	0.707 %	-0.148%
Participant 7	2.147 %	-1.412%
Participant 8	1.979 %	-0.940%

5.1.2 Confidence interval of the basal impedance baseline

Identifying when the basal impedance is outside normal levels requires a statistical analysis. By using the entire percentage deviation ($\Delta\%$) from the initial baselines as the data range, it was calculated as the normal probability density function (PDF). Using the Matlab command *normfit* the normal distribution was computed from the $\Delta\%$. The calculation returned a $\mu = -0.6384$ and a $\sigma = 0.8518$. Then the probability density function (PDF) of the standard normal distribution was calculated using the command *normpdf* with the parameters previously found. By plotting the probability distribution function, it can be seen how the probability was distributed. Then by using the σ that was obtained from the data, a new

5.2 Change of basal impedance during occlusions

PDF was calculated which centred at $\mu = 0$. Therefore, the PDF produces a similar data distribution where the confidence band (95 %) was calculated at $\pm 1.96 \times \sigma$.

Figure 5.4 shows the PDF obtained from the data and the new one calculated. The yellow plot shows the confidence area from the baseline. Therefore, the confidence band is located between $\Delta\% = \pm 1.66\%$. In other words, all changes of impedance within this confidence band can be considered to be statistically important and is located within normal limits.

By comparing the results shown from the PDF, most participants were found to be within that range. Nevertheless, some partaker's regions do not lie within this confidence band. These include regions 5 and 7 in participants 3 and 7, region 3 of participant 4 and region 7 of participant 8.

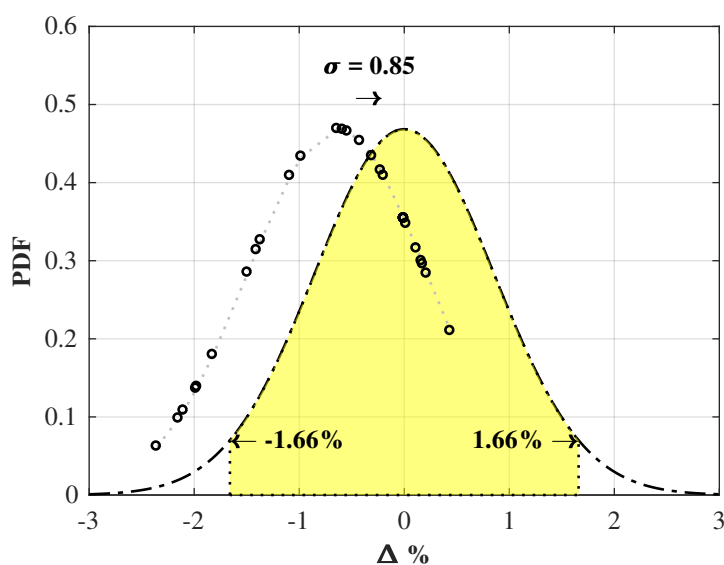


Figure 5.4 Confidence interval of the baseline impedance. The yellow area shows the PDF when $\mu = 0$. The dotted points shows the PDF with the normal points calculated ($\mu = -0.6384$ and a $\sigma = 0.8518$). The confidence band is located between $\Delta\% = \pm 1.66\%$. In other words, all changes of impedance within this confidence band can be considered to be statistically important and is located within normal limits.

5.2 Change of basal impedance during occlusions

From the experimental procedure, the data from the occlusive regions were extracted in accordance to the type of blood restriction applied, as depicted in figure 4.7. The data were separated in this section into the readings from venous occlusion (VO), partial arterial

Investigation of changes of the basal impedance signal

occlusion (PAO) and total blockage. The following is the data analysis performed to the signal. Again, the arterial pulses were eliminated from the signal. Only, the lower envelope of this impedance signal was used to perform this investigation.

The dataset for this study was subdivided in the following manner: two minutes of baseline data followed by the occlusive period and two minutes of return to baseline after releasing the cuff's pressure. This is the analysis of the results obtained.

5.2.1 Basal impedance shift during venous occlusion

As expected, the basal impedance declined while performing venous occlusion in each participant. As confirmed by figure 5.5, all the partakers witnessed a decline in their basal impedance in region 2 of the experiment. The boxplot illustrates that three regions that were part of this study. The data of the region 1 (*R1*) were the last 2 min of the initial baseline (180 s to 300 s). Thereafter, it is the venous occlusion in region 2 (*R2*) during 3 min at the pressure levels described by the column *occlusion 1* in table 4.5. This makes it clear that the median resistance value decreased. While analysing this candle-stick, it can be surmised that bigger the distribution of the upper and lower quartile, the greater the resistance decline as registered by most other participants, with the exception of participant 6 whose impedance measurement settled quickly. After releasing the cuff's air, the median impedance in region 3 was expected to return to a value close to the initial baseline. However, partakers 3 and 4 were unable to recover completely. While their resistance values improved for a few seconds, they continued to reduce below the lower whisker of region 2. Meanwhile participants 1 rose over the initial baseline median. Participant 3 was the only one who showed a return to baseline.

Figure 5.6 illustrates that the deviation of impedance in terms of the changes in percentage of impedance ($\Delta Z\%$) from the median baseline in region 1. The shaded area represents the venous occlusion between 300 s to 400 s. These dots are the points of foot of the signal equivalent to (R_B). This signal was smoothed using the command *smooth* in Matlab which assigns a lower weight to outliers within the regression [33]. This method assigns zero weight to data outside of the six mean absolute deviations. By doing so, it eliminates most of the rapid variations of impedance triggered by motion artefact.

The figure clearly reveals a linear trend during venous occlusion for majority of the subjects. Nonetheless, the resistance of participant reduced immediately upon occlusion, but the participant moved his arm a minute later to reverse the trend. Subsequently, the impedance continued to decline again. Furthermore, participant 6 also showed a similar response when the individual moved his arm, but the resistance settled instead of reversing the

5.2 Change of basal impedance during occlusions

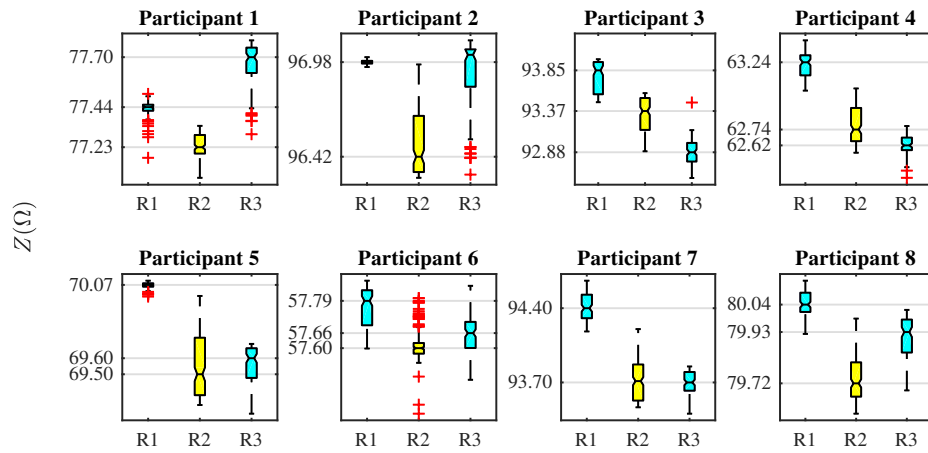


Figure 5.5 Box plot showing the statistical change of impedance in Ω during venous occlusion. The cyan boxplot represents the baseline before (Region 1) and after (Region 3) the occlusion. The yellow marker is the impedance during venous occlusion (Region 2).

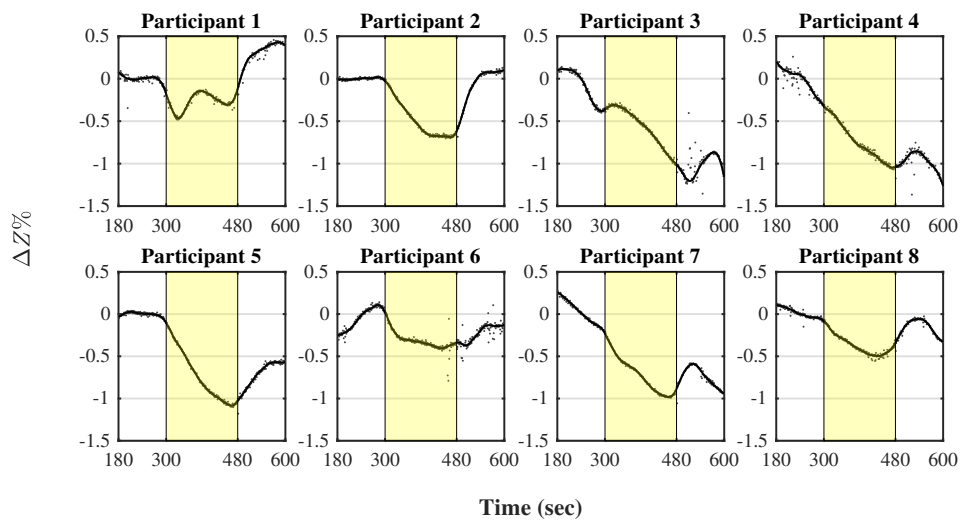


Figure 5.6 Percentile change of impedance during venous occlusion. The reference baseline is the average baseline impedance during the last 2 min before the venous occlusion.

Investigation of changes of the basal impedance signal

trend in this case. Interestingly, participant 2 showed a saturation point after a few seconds, which was specific for this subject.

The table 5.2 summarises the changes of impedance caused during the venous occlusion. The average median of the resistance decline from the baseline value stood at roughly $-0.546 \pm 0.076 \%$, where participants 4, 5 and 7 recorded the biggest losses of impedance ($>0.5 \%$). The column *Change* on the same table shows the impedance difference from the point of initial occlusion to the minimum point of the smooth curve, which was calculated using equation 5.1. During the venous occlusion the whole slope was seen to record a variation of $0.658 \pm 0.230 \%$.

$$\Delta Z\%_T = \Delta Z\%_{300sec} - \Delta Z\%_{min} \quad (5.1)$$

Table 5.2 Statistical analysis of the percentile change of impedance during venous occlusion. The data denotes the median percentile change of impedance per participant, the maximum and minimum value of the occlusion, and the difference between these two peak values.

	Median [$\Delta Z\%$]	Max [$\Delta Z\%$]	Min [$\Delta Z\%$]	Change [$\Delta Z\%$]
Participant 1	-0.26 ± 0.09	-0.20	-0.47	0.26
Participant 2	-0.58 ± 0.21	-0.03	-0.69	0.66
Participant 3	-0.51 ± 0.22	-0.35	-1.00	0.66
Participant 4	-0.79 ± 0.22	-0.32	-1.06	0.74
Participant 5	-0.82 ± 0.30	-0.11	-1.09	0.98
Participant 6	-0.33 ± 0.09	0.03	-0.41	0.43
Participant 7	-0.72 ± 0.22	-0.22	-0.98	0.77
Participant 8	-0.40 ± 0.11	-0.09	-0.50	0.41

It is tempting to observe the immediate change of impedance as soon as the venous occlusion occurs. The capability of impedance plethysmography device of detecting venous occlusion in all participants is remarkable and almost instantaneous. As soon as the blockage occurs, the impedance reduces for some time. If motion does not bring about changes in the trend, some of them could reach the saturation point, as seen in the case of participant 2. However, it is also apparent that other signals reached a point of saturation, signalling a decline of impedance in an exponential trend than linear.

This effect can be summarised in figure 5.7. The plot describes the change of impedance in time (dZ/dt) against some data points (beats) during the venous occlusion. Accordingly, 10 data points of R_B synchronised with the heart cycle were clustered computing dZ/dt .

5.2 Change of basal impedance during occlusions

This differential value is equivalent to the velocity of the change in basal impedance per second (Ωs^{-1}). In general, the average impedance all along the occlusion was observed at -0.0026 ± 0.0018 beats.

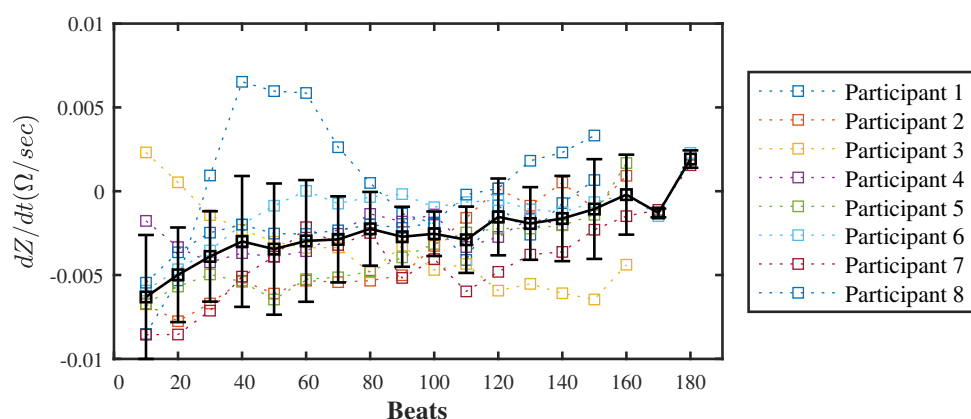


Figure 5.7 Speed of change of impedance in time (dZ/dt) per every 10 heartbeats during venous occlusion. The colour lines represent the data per each participant. The dark bold line is the mean of all the measurements.

Based on the figure, it can be surmised that during the first 10 beats, there is a higher drop of impedance as compared to the last data points. Indeed, the rate of change of resistance during the first 10 beats was on average $-0.0063 \pm 0.0037 \Omega/s$. After 90 beats, the result of this derivation was more than halved to an average of $-0.0027 \pm 0.0018 \Omega/s$. At 160 beats, the ratio was reduced to merely $-0.0002 \pm 0.0024 \Omega/s$. The final data points (180 beats) exhibited a reversion of the trend ($0.0019 \pm 0.0005 \Omega/s$). However, this is because only a few participants were able to achieve that amount of heart beats. Moreover, at this point, some data were already returning to the baseline because the cuff could have been released a few seconds earlier.

5.2.2 Basal impedance change during partial arterial occlusion

The same analysis performed on the VO was applied to the partial arterial occlusion. A partial restriction of arterial blood flow is achieved by mechanically occluding the upper arm between diastolic and systolic pressures. The load levels used to create these occlusions are detailed on the column *occlusion 2* in the table 4.5. Similar time lapses were incorporated to analyse the data, the last 2 min of the region 3 (660 s to 780 s), the entire partial arterial

Investigation of changes of the basal impedance signal

blockage in region 4, 3 min between 780 s to 960 s, followed by 2 min of return to the baseline after releasing the pressure of the cuff in region 5 (960 s to 1080 s).

Occluding the blood flow at this pressure level induced a sense of discomfort among participants; some of them felt numbness in their arms during the experiment. Therefore, some partakers moved their arms like participant 1. In the case of others, the duration of occlusion had to be shortened as was done in the case of participant 4 where the occlusion occurred subsequently (840 s to 960 s) because ECG sensors had to be relocated and participant 8 who asked to terminate the blockage a minute earlier (780 s to 900 s).

During this kind of occlusion, there is no venous return. In addition, the inflow is slightly restricted as well. Indeed, the occlusion constricts the brachial artery where only a small amount of blood passes through the obstruction. Moreover, the blood flow becomes turbulent after the cuff's constriction. Due to the venous occlusion, the arm is expected to increase its volume as blood pools within the forearm to reduce the basal impedance.

Figure 5.8 confirms the reduction of the basal impedance all along the partial arterial occlusion. When compared to VO, the box-plot shows a higher upper and lower quartile distribution for majority of the participants in region 4, owing to a continued decline in basal impedance during that occlusive action. However, partaker 4 depicted a significant number of outliers primarily caused by motion artefact. Only a few participants were able to get back close to baseline resistance, such as participants 2 and 7. Interestingly, some members showed a swift recovery in region 5. For instance, the large data distribution across participants 1, 2, 4, 6, 7 and 8 suggests a quick trend to return to the baseline. However, it generally seems that a longer recovery time is required in order to return to an impedance value close to the baseline after partial arterial occlusion.

Through a qualitative analysis of the change of impedance by percentage from baseline region 3, figure 5.9 shows a linear trend during the cuff's pressure exerted in region 4. It can be seen that the impedance decline is more pronounced than the one recorded from venous occlusion (see figure 5.6). In participant 1, the motion artefact becomes more evident, the step drop of basal impedance immediately before releasing the cuff's pressure is a reflection of his forearm's muscular movement. In this case, it is evident that the arm movement augmented the change of impedance throughout the occlusion. While other participants also experienced motion artefact, the change of impedance was within a few heart beats. For example, participant 2 only showed a data point off the smooth line. However, in participants 3 and 4, the amount of data points off the soft signal was significantly higher. In summation, majority of the participants described a straight drop of impedance, particularly linear in participants 2 and 5.

5.2 Change of basal impedance during occlusions

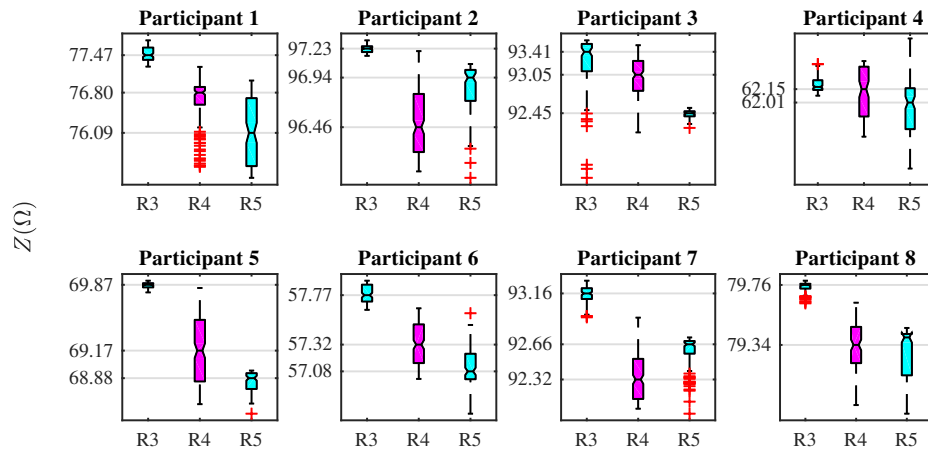


Figure 5.8 Box plot of the statistical change of impedance in Ω during partial arterial occlusion. The cyan marker represents the baseline before (Region 3) and after (Region 5) the occlusion. The magenta marker is the impedance during partial arterial occlusion (Region 4).

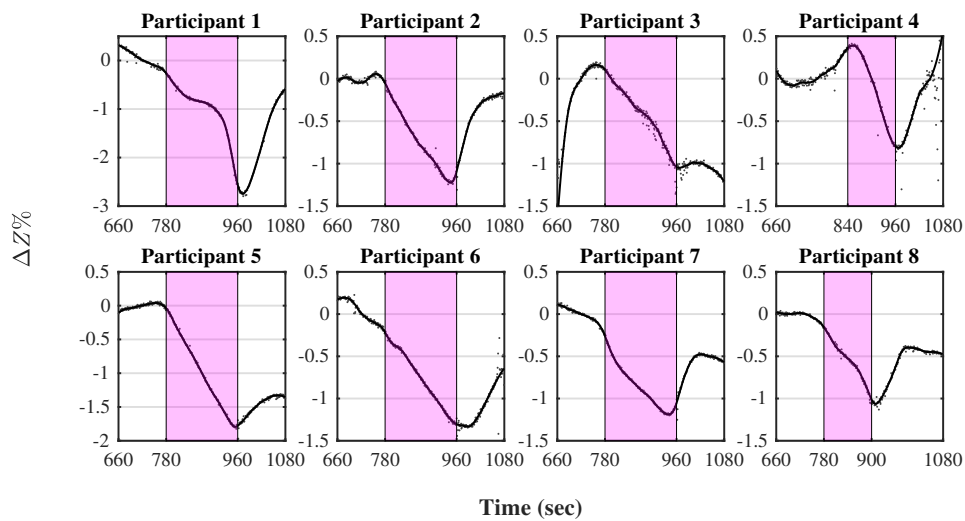


Figure 5.9 Percentile change of impedance during partial arterial occlusion using as reference average baseline impedance during the last 2 min before the occlusion.

Investigation of changes of the basal impedance signal

After releasing the cuff's pressure, it is apparent that most of the signals change their slope. The only member that did not reflect this change was participant 3. This impedance correction is indicative of a restoration of blood circulation and a decline in the forearm's volume. Moreover, a lack of apparent settling impedance value can be observed, barring participants 7 and 8. In general, this change in trend also confirms that the body might require a longer time to recover after the partial arterial occlusion.

Table 5.3 reports the variations in percentage from the baseline impedance in region 3 in greater depth. The median impedance decline from the baseline was approximately $-0.783 \pm 0.324 \%$. However, participant 4 exhibited a lower median value since the initial impedance value stood above the baseline average at 0.34% . Evidently, there is a greater reduction of impedance or an increase in the forearm's volume as opposed to VO. The median change of impedance from the maximum to the minimum value was nearly $1.133 \pm 0.482 \%$ which is about double when compared with venous occlusion. A physiological response might have caused this increase in volume. The blood pooling could not have caused this volume increase given that the arterial blood flow was restricted, which lowered the amount of blood to enter the forearm segment.

Table 5.3 Statistical analysis of the percentile change of impedance during partial arterial occlusion. The data represents the median percentile change of impedance per participant, the maximum and minimum value during the occlusion and the difference between these two peak values.

	Median [$\Delta Z\%$]	Max [$\Delta Z\%$]	Min [$\Delta Z\%$]	Change [$\Delta Z\%$]
Participant 1	-0.85 ± 0.50	-0.28	-2.56	2.29
Participant 2	-0.80 ± 0.35	-0.05	-1.23	1.18
Participant 3	-0.38 ± 0.32	0.10	-1.04	1.14
Participant 4	-0.03 ± 0.41	0.34	-0.78	1.13
Participant 5	-1.01 ± 0.54	-0.04	-1.80	1.76
Participant 6	-0.77 ± 0.33	-0.21	-1.30	1.09
Participant 7	-0.90 ± 0.26	-0.25	-1.19	0.93
Participant 8	-0.53 ± 0.22	-0.15	-1.01	0.85

The calculation of the velocity of the change of impedance (dZ/dt) displayed a similar exponential response as was seen in VO. Figure 5.10 shows the calculation of these points across all participants. The plot indicates that the first 10 beats of changes on a ratio average of $-0.0074 \pm 0.0037 \Omega/s$ was the largest acceleration. Subsequently, between 20 and 110 beats, the velocity stabilised to $-0.0053 \pm 0.0007 \Omega/s$. After this apparent settling, a new increase was witnessed in the differentiation. However, it seems to have been aided by the motion artefact seen on participant 1 for a few beats.

5.2 Change of basal impedance during occlusions

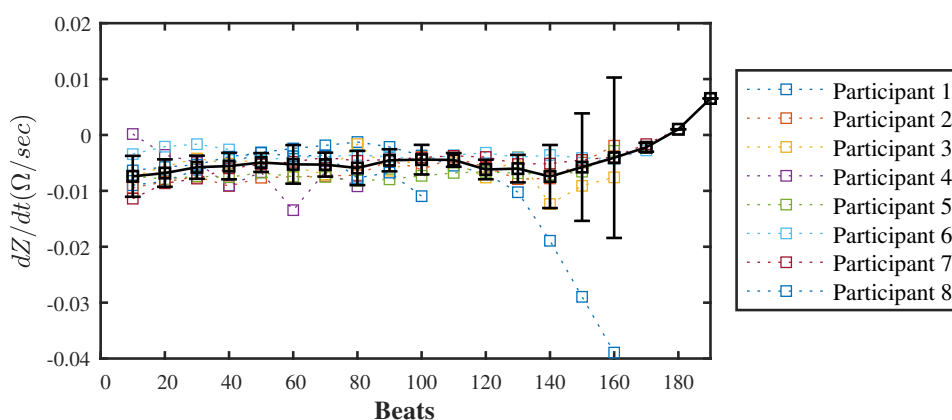


Figure 5.10 Speed of change of impedance in time per every 10 heartbeats during partial arterial occlusion. The colour lines represent the data per each participant. The dark bold line is the mean of all the measurements.

5.2.3 Basal impedance variation during total occlusion

In this study the blood supply towards the forearm was completely blocked by inflating the cuff above systolic pressure, around 20 mmHg above this point. The column *occlusion* 3 in the table 4.5 illustrates the pressure level applied for the research. The data regions involved in this part of the investigation were regions 5, 6 and 7. As was the case with previous occlusions analysis, the last 2 minutes of the data sourced from region 5 were used as impedance baseline (between 1140 s to 1260 s). The cuff was then inflated to accomplish complete blood flow obstruction; the occlusion was maintained for 3 min between 1260 s to 1440 s. Finally, the cuff's air was released immediately, and the readings were taken for further 2 min.

This test caused plenty of discomfort to most participants. Numbness and an unwillingness to move their limb was commonly seen in all the participants. Hence, they ended up moving their arms on a voluntary basis. Due to the absence of blood flow or pooling during this aspect of the experiment, small impedance variations were expected. Additionally, the mean restive value would be equivalent to the impedance of the tissue's components within the segment in addition to the impedance of the residual blood within the forearm. However, when a change of resistivity takes place, this is mostly caused by the participant's re-accommodation as opposed to a physiological variable.

Figure 5.11 shows how the impedance changes during the total occlusion. Initially, it can be seen that there was an absence of consensus on the signal trend all along the occlusion,

Investigation of changes of the basal impedance signal

as seen in the previous tests. Some of the participants reflected a small reduction in their median impedance, such as study members 1, 4, 5, 6 and 8. Meanwhile the rest experienced a slight increase. In addition, the trend of signal during the occlusion is ambiguous; different signals have different data distribution points. For instance, participants 1 and 7 displayed a large data distribution, indicating a constant change of their median impedance. In contrast, the rest exhibited a data distribution centred in the median, illustrating a little impedance variation during the occlusion. Only participant 5 exhibited a significant number of outliers, denoting swift changes at one point of the measurement. In general, there is no linear trend, as reported by the other kinds of occlusions.

After releasing the cuff's pressure, no definite trend was observed in the direction of the impedance. As figure 5.12 shows, some participants displayed an increase of resistivity. However, participants 4 and 5 exhibited exaggerated changes in impedance. While the nature of this rare variation remains unclear, it could be attributed to the limb movement after the occlusion. Moreover, there was no swift change of impedance as was experienced in other types of occlusions. This is congruent with the fact that no blood rushed in or out of the forearm.

By analysing the variation of impedance during the occlusion as compared to the baseline (region 5), the magnitude and direction of the resistivity change can be seen. Evidently, participant 1 displayed the biggest and continuous impedance decrease, which is unusual for this type of occlusion. Another unexpected resistivity response was shown by participant 7 where his impedance increased, albeit slightly.

The table 5.4 illustrates the impedance changes during the occlusion in detail. The median impedance during total occlusion was $-0.135 \pm 0.441 \%$ which is fairly close to zero. However, the sign of column *median* indicates that five out of eight exhibited a negative trend in the impedance direction to indicate resistivity loss. In fact, most of the measurements were below 0.5%; only participants 1 and 5 exhibited higher changes of impedance. By calculating the $\Delta\%$ from the maximum and minimum changes (column *Change*), it can be surmised that only participant 1 showed a change greater than 1%, between 0.5% to 1%, participants 3 and 6 displayed this data range, whereas the rest were below 0.5%. In general, the changes described by total occlusion were found to be significantly lower than the other occlusions, indicating a minimum increase of volume. For instance, partakers 2 and 5 median impedance signified a clear illustration of this. Some impedance changes were presented in some measurements which can be associated with a muscular activity.

Figure 5.13 illustrates the analysis of velocity rate (dZ/dt) which is altered by the basal impedance. Evidently, the basal impedance of participant 1 decreased swiftly when compared

5.2 Change of basal impedance during occlusions

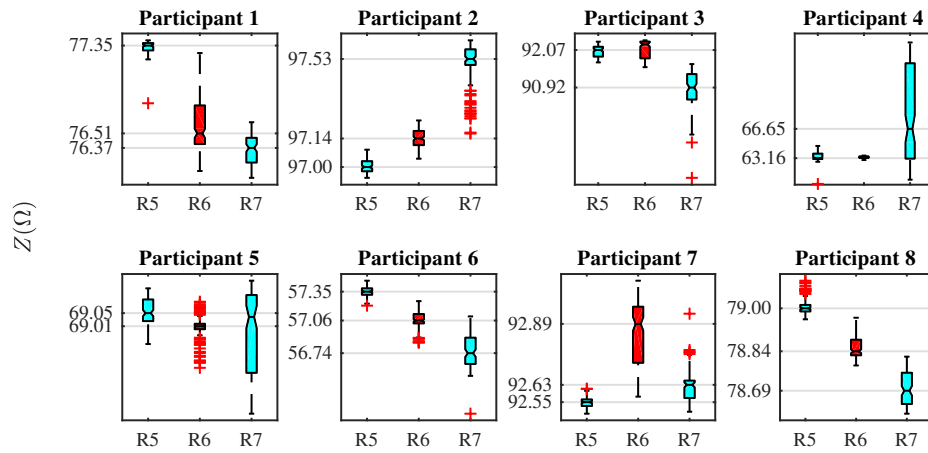


Figure 5.11 Box plot of statistical change of impedance in Ω during total occlusion. The cyan marker represents the baseline before (Region 5) and after (Region 7) the occlusion. The red marker denotes the impedance during total occlusion (Region 6).

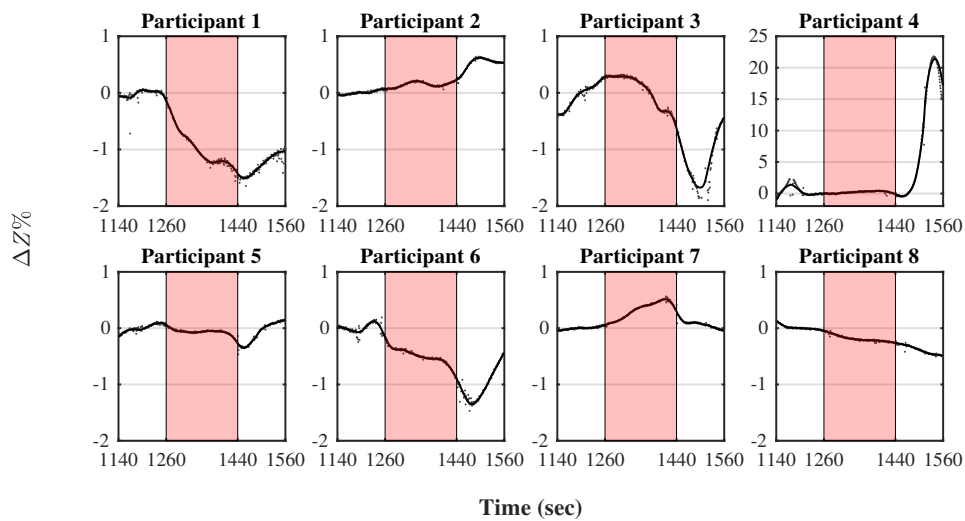


Figure 5.12 Percentile change of impedance, using as reference average baseline impedance all along the last 2 min before the total occlusion.

Investigation of changes of the basal impedance signal

Table 5.4 Statistical analysis of the percentile change of impedance during total occlusion. The data signifies the median percentile change of impedance per participant, the maximum and minimum value during the occlusion, and the difference between these two peak values.

	Median [$\Delta Z\%$]	Max [$\Delta Z\%$]	Min [$\Delta Z\%$]	Change [$\Delta Z\%$]
Participant 1	-1.09 ± 0.33	-0.14	-1.38	1.24
Participant 2	0.14 ± 0.04	0.07	0.07	0.00
Participant 3	0.18 ± 0.28	0.30	-0.50	0.81
Participant 4	0.21 ± 0.16	0.05	-0.14	0.19
Participant 5	-0.06 ± 0.05	0.05	-0.23	0.28
Participant 6	-0.51 ± 0.14	-0.15	-0.89	0.75
Participant 7	-0.36 ± 0.15	0.05	0.05	0.00
Participant 8	-0.21 ± 0.06	-0.05	-0.27	0.22

to the rest. Moreover, participant 3 witnessed a rapid impedance drop between 80 beats to 140 beats. In general, the average velocity for the total occlusion procedure stood at around $-0.00061 \pm 0.00170 \Omega/s$ which is considerably small when compared with occlusions. However, at the beginning of this occlusion, a modest increase was seen in the velocity; the average for the first 10 beats stood at around $-0.0027 \pm 0.0052 \Omega/s$. Subsequently, it stabilised close to the median value of the entire measurements until 140 beats. Nonetheless, between 140 beats to 180 beats, an increase was seen in the velocity due to the contribution of negative trends before releasing the occlusion.

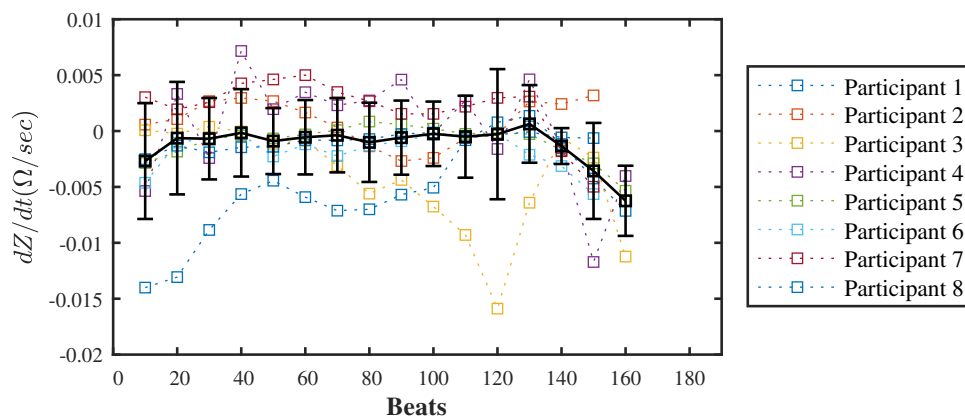


Figure 5.13 Speed of change of impedance over time per every 10 heartbeats during the total occlusion. The colour lines denote the data per each participant. The dark bold line represents the mean of all the measurements.

5.3 Conclusion

There are different bodily tissues that contribute to the impedimetric signal, such as fat, muscle, blood and bone. Most of these organs or tissues entail intrinsic impedances. The device took measurements within the expected ranges of a human forearm. However, motion artefact or the interface electrode-skin, may have contributed to the change in resistance value of the measurement. The baseline basal impedance varied from the median measurement in average -0.6384% with a maximum deviation of -2.353% . After a statistical analysis of these variances was undertaken, it was found that any values within $\pm 1.66\%$ lie within statistical normal values.

From detection of circulatory problems point of view, it is evident that the basal impedance changed linearly when an occlusion took place in the forearm. By occluding the venous return and not bringing about changes in the arterial flow, blood can enter into the limb but cannot depart from it. As a result, the volume of the forearm increased constantly when the occlusion occurred. Hence, this capacity gain can be quantified by the impedimetric method as a variation of the basal impedance median value. With an increase in blood cell population, the conductivity of the forearm section also increased in terms of value. Therefore, the resistivity declined proportionally.

During the occlusive events, the iPG device detected changes of impedance magnitude caused due to the pooling effect attributed to the constriction of the upper arm. Clearly, the basal impedance reduced during both partial and venous occlusion. Interestingly, the impedance changed at a different ratio when venous and partial arterial occlusion was applied. The impedance during the VO varied in a $0.658 \pm 0.230\%$. On the other hand, all along PAO, the impedance was seen to change in $1.13 \pm 0.482\%$. This greater slope might be indicative of a higher increase of blood volume. However, this could be incorrect as restricting the brachial artery lowers the flow towards the arm's distal section [206]. According to the data, an arterial occlusion might be denoted in a swift decline of impedance, whereas in a venous occlusion, the impedance might reduce at a slower pace. In contrast, the impedance did not change as dramatically during total occlusion when compared to the other episodes. The impedance went in different directions without establishing any common trend. This effect might have been caused by forearm accommodation as opposed to a physiological response. On average, the ratio change was well below the other occlusions around $0.250 \pm 0.446\%$.

Analysing the acceleration of blood during the occlusions, it was found that after the upper arm occlusion that occurred during the first 10 heartbeats, the impedance changed at a faster pace when compared to the rest involved in this study. During these heartbeats, the

Investigation of changes of the basal impedance signal

change of impedance stood at around $-0.0063 \pm 0.0037 \Omega/s$ for venous occlusion; quite closely, partial arterial occlusion was about $-0.0074 \pm 0.0037 \Omega/s$, whereas total occlusion was $-0.0027 \pm 0.0052 \Omega/s$. This acceleration indicates a physiological response of the veins to allow additional blood supply in the forearm. Some studies [94, 207] suggest that an increase in blood flow may be attributed to a syncopal response as a regulatory response of the human body. Nonetheless, there is a need to conduct further research to corroborate these assumptions.

All along the total occlusion (Region 6) no clear decline or increase of basal impedance was observed that was common to all the participants. In general, the change of impedance stood at about $-0.135 \pm 0.441 \%$. A reason for this value close to zero was that neither arterial nor venous blood was able to flow through the limb, which meant that no change in volume was seen. In the end, this value was seen as the real basal impedance where all the tissues were measured with their blood content. The information provided here is an indicator of the development of ischaemia. A study has demonstrated that when total occlusion occurs, cells starvation ensues, paving the way for the development of ischaemia [179] which could be detected as a drop in the basal impedance.

Research of the shape changes of the arterial pulses during proximal occlusions

The arterial pulses amplitude (APA) signifies a dynamic component of the impedance plethysmography signal. Importantly, it is located within the basal impedance that accounts for around 0.1 % of the total impedimetric value [175]. It can be fairly challenging to acquire these signals since noise levels can be higher than the actual signal, which makes it difficult to isolate this waveform. However, such data collection imparts valuable information concerning the haemodynamics per heartbeat. The shape of the waveform has been demonstrated to be a major indicator of haemodynamic problems within the peripheral circulation [29]. This chapter will analyse the waveforms with an aim to differentiate morphological changes between signals in normal state and the ones that occur during venous, partial arterial and total occlusion, respectively.

As it has been demonstrated in the previous chapter, the impedance plethysmographic baseline shifts during each occlusion at different rates. However, it is also important to examine the changes occurring in the APA pulses. This information offer clues as to whether an occlusion may occur in the arterial or venous circulation. As illustrated in the design section 4.1.2.6, the iPG device features an output port denominated Z_{AC} that provides a high-resolution view of these arterial pulses waveform. Additional post-processing was needed to conditioning the signal. In this regard, tighter filters were applied in order to remove low and high frequency components within the signal. In addition the lower envelope component was removed and levelled to zero.

The APA waveform produced by this device is inverted, as represented by various other plethysmography methods like photoplethysmography. During the systolic cycle, there is an

expansion of blood vessels, which allows for more blood volume. As a result, the impedance declines proportionally to the quantum of blood due to the fact that the forearm's segment is more electrically conductive. Meanwhile during the diastolic cycle, blood vessels end up emptying, causing a decline in the quantity of blood contained within the arm segment. Consequently, the impedance goes up.

The analysis of plethysmographic wave was carried out by averaging the detected waveforms using specialised algorithms in order to identify an APA signal. In short, two different shapes of APA signal materialise during venous and arterial occlusion, which may allow discerning between these two events. First, venous occlusion has shown an increase in the three points measured (systolic peak, dicrotic notch and diastolic peak). Conversely, partial arterial occlusion has displayed a decrease of the diastolic pulse amplitude in relation to the dicrotic notch. As a result, a novel index ratio that combines the data from baseline and APA is proposed to help to differentiate between these two kind of occlusions when certain conditions are met. The following section discusses the changes within a wave shape from a non-occlusion state to an occluded one.

6.1 Reference points and algorithm for the arterial pulse amplitude analysis

The isolated APA waveforms from the iPG device reproduce the change in volume per heart beat within the sensing electrodes placed in the forearm. Filling the vessels with blood leads to small changes in resistivity that tend to vary with the circulatory cycle, describing different peaks during the course of a heart cycle.

Commonly, an APA wave consists of several identifiable peaks and valleys. Figure 6.1 illustrates a typical impedance plethysmography pulse from the arm synchronous with a heartbeat. The table 6.1 summarises the noticeable markers of these pulse waveforms when compared to an ECG and used in this analysis to identify morphological changes.

An APA wave needs to be identified as a valid one in order to be included in the computational analysis. As a result, the programmed algorithm begins with the identification of the commencement and end of a pulse by locating the upslope point $L1$ and $L2$ in the waveform. Upon the identification of these spots, the systolic peak A can be placed within this time frame. The point B is expected to be a valley with an amplitude lower than the previous peak. Subsequently, the algorithm looks at the following change of slope - the diastolic peak C . If any of these conditions could not be met, the algorithm searches through

6.1 Reference points and algorithm for the arterial pulse amplitude analysis

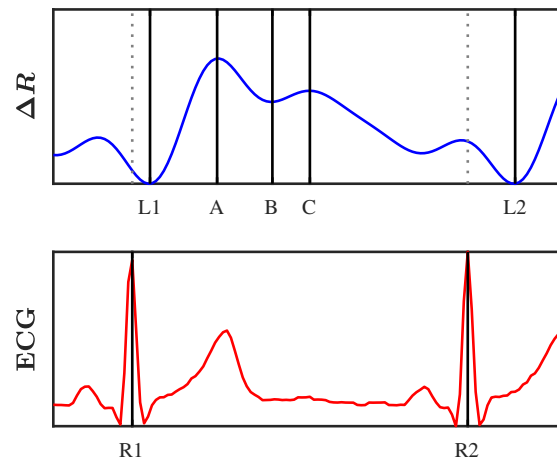


Figure 6.1 Peaks and valleys of an iPG waveform (ΔR) compared to ECG waveform.

Table 6.1 Markers on the APA waveform

Marker	Description
R1	Peak of the ECG QRS complex before an APA pulse.
L1	Start of the systolic upslope of the APA signal. Point where rapid change of impedance occurs.
A	Systolic point. Maximum peak of the APA signal.
B	Dicrotic notch on the APA wave.
C	Maximum pulse after the dicrotic notch, named diastolic pulse
R2	Peak of the ECG QRS complex after the APA pulse.
L2	Starting point of the next APA wave.

Research of the shape changes of the arterial pulses during proximal occlusions

the APA wave from the subsequent lower data point, seeking a matching wave pattern again. In case a pattern is found ($L1 > A < B > slopechange(C) > L2$), this is considered as a viable wave. In the absence of a match, the pulse is marked as missing. In order to minimise waves with abnormal amplitudes caused due to noise, the algorithm then calculates the mean peak at A of the last 20 valid APA waves. If this value is found to be greater than 25% ($A > A * 1.25$) the wave is discarded.

The table 6.2 compiles the amount of APA waves recognised by the algorithm. The column *detected waves* describes the pulses that adhere to the profile of an iPG plethysmography wave. Meanwhile the third column highlights the total pulses that did not match the anticipated guide; subsequently, the algorithm attempted to fix them by identifying the pattern within the next slope. Consequently, the fixed column shows the total amount of identified pulses, whereas the last column shows the ones discarded.

Generally speaking, the quality of APA pulses validated by the iPG device and verified by the algorithm were on average $57.86 \pm 16.37\%$. Participants 3, 4 and 8 showed the highest number of pulses with errors (above 50%). However, by incorporating the fixing method, the number of valid peaks improved to a total of $84.94 \pm 7.64\%$.

Table 6.2 Total amount of iPG waves detected by the algorithm. Starting from the detection of valleys followed by the detection of systolic peak, diastolic notch point and diastolic peak. It also includes the waves reconstructed by the software

	Total valleys	Detected waves	Waves with errors	Fixed waves	Discarded waves
Participant 1	1604	840 (52.37 %)	764 (47.63 %)	491 (30.61 %)	273 (17.02 %)
Participant 2	1689	1159 (68.62 %)	530 (31.38 %)	409 (24.22 %)	121 (7.16 %)
Participant 3	1651	699 (42.34 %)	952 (57.66 %)	695 (42.10 %)	257 (15.57 %)
Participant 4	1625	645 (39.69 %)	980 (60.31 %)	562 (34.58 %)	418 (25.72 %)
Participant 5	1664	1199 (72.06 %)	465 (27.94 %)	345 (20.73 %)	120 (7.21 %)
Participant 6	1745	936 (53.64 %)	809 (46.36 %)	471 (26.99 %)	338 (19.37 %)
Participant 7	1907	1654 (86.73 %)	253 (13.27 %)	146 (7.66 %)	107 (5.61 %)
Participant 8	1651	784 (47.49 %)	867 (52.51 %)	491 (29.74 %)	376 (22.77 %)

The algorithm compiled the location of all the valid spots A , B and C . The data showed points of inflection when an occlusion occurs in the arm. The following analysis centres on the changes of impedance amplitude all along the different regions of this experiment, as well as the change of area of the waveform before and after the diastolic notch point (B).

6.2 Changes of the plethysmography waveform during different occlusions

The detection of the APA waveforms makes it possible to independently analyse the change of the shape form. To that end, an average waveform was computed for all these regions during the experiment. The following section details the relevant changes made for each of these points of interest.

6.2.1 Plethysmography waveform change during venous occlusion

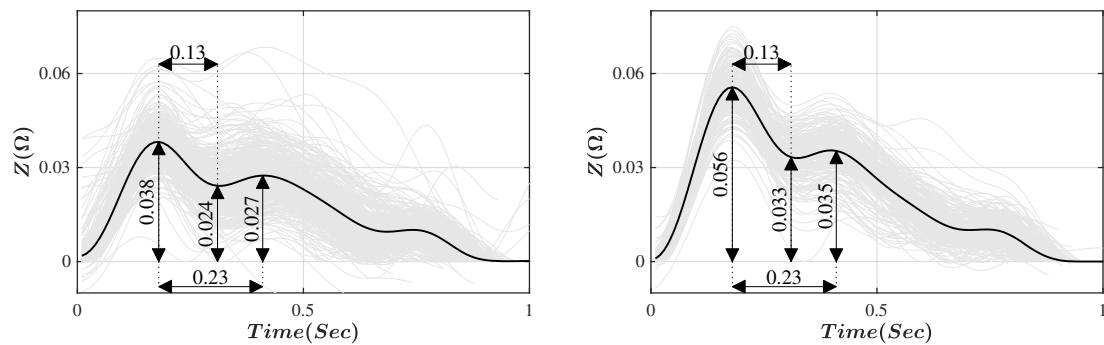
The analysis performed in this section corresponds to the APA waveforms captured during the baseline in region 1 (0 s to 300 s), venous occlusion region 2 (300 s to 480 s) and return to control signal region 3 (480 s to 780 s). The previous section described the method of collecting valid pulses. Consequently, all other valid pulses were grouped and aligned as per region to calculate the average waveform.

Figure 6.2a shows an impedance plethysmography waveform calculated from one of the participants during baseline and venous occlusion, with indicators of their amplitudes located at the points of interest. These markers show the calculation of distance between systolic peak (Point A) to diastolic notch (Point B) and diastolic peak (Point C), along with the amplitude for each of these markers. The distance between (A → B) and (A → C) was later transposed into the occlusion wave in order to identify their values during the VO test. Clearly, from a qualitative viewpoint, a difference can be noticed in the morphology of the waveform that occurred during the occlusion. Indeed, figure 6.3 shows the change in amplitude at these points for every participant as well as the return to baseline after releasing the cuff pressure. A comprehensive analysis of this change (at each point) is detailed in the following manner.

6.2.1.1 Changes in systolic peak (Point A)

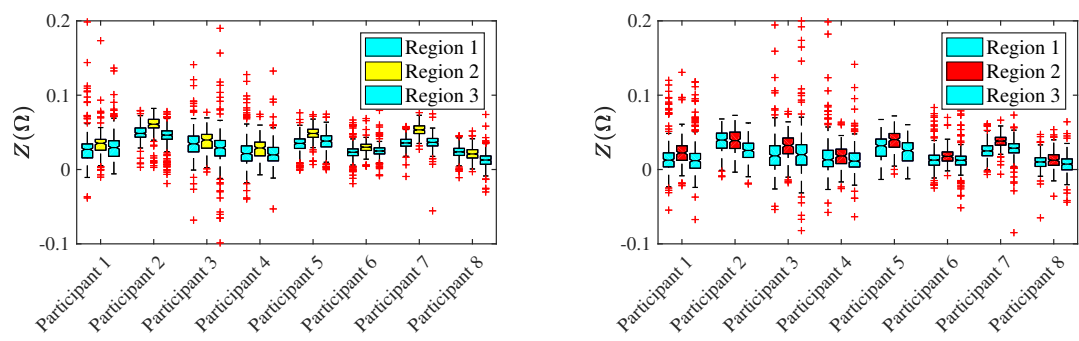
Figure 6.3a shows the statistical variation of the systolic peak magnitude (point A) during the three conditions of the test baseline-occlusion-baseline. After the cuff was inflated below the diastolic pressure, most APA signals showed an increase of the impedance magnitude of this peak. As detailed in table 6.3, 87 % of the participants exhibited an increment in electrical resistance during the venous occlusion of about 31.80 %; the lone exception was participant 8 where his/her impedance dropped in -12.01 %. When the cuff's pressure got released, all participants showed a decline in peak value with an average of -32.21 %, returning to similar baseline values prior to the venous occlusion.

Research of the shape changes of the arterial pulses during proximal occlusions

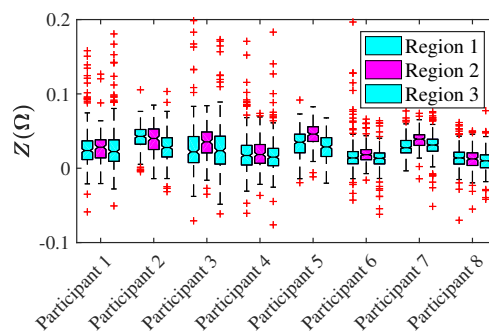


(a) Average APA waveform for baseline region 1 (0 s to 300 s) (b) Average APA waveform during venous occlusion region 2 (300 s to 480 s)

Figure 6.2 Plethysmography waveform of the participant seven between baseline and venous occlusion



(a) Change of amplitude of the waveform at point A. (b) Change of amplitude of the waveform at point B.



(c) Change of amplitude of the waveform at point C.

Figure 6.3 Changes of the impedance peak values during baseline, venous occlusion and return to baseline for points A,B and C.

6.2 Changes of the plethysmography waveform during different occlusions

Table 6.3 Change of amplitude of the waveform at peak A during the transition from baseline (region 1), venous occlusion (region 2) and the return to baseline (region 3). The column change shows the percentile variations between the different regions.

Point A	Baseline [Ω]	Occlusion [Ω]	Baseline [Ω]	Change	
	(Region 1)	(Region 2 - VO)	(Region 3)	R1-R2	R2-R3
Participant 1	0.0270 \pm 0.0233	0.0353 \pm 0.0191	0.0295 \pm 0.0305	30.49 %	-21.41 %
Participant 2	0.0485 \pm 0.0102	0.0609 \pm 0.0140	0.0462 \pm 0.0449	25.50 %	-30.24 %
Participant 3	0.0345 \pm 0.0351	0.0397 \pm 0.0144	0.0292 \pm 0.0294	14.96 %	-30.55 %
Participant 4	0.0214 \pm 0.0303	0.0289 \pm 0.0139	0.0197 \pm 0.0222	35.17 %	-43.11 %
Participant 5	0.0352 \pm 0.0112	0.0485 \pm 0.0098	0.0382 \pm 0.0376	37.99 %	-29.20 %
Participant 6	0.0232 \pm 0.0105	0.0300 \pm 0.0124	0.0249 \pm 0.0251	29.16 %	-21.77 %
Participant 7	0.0357 \pm 0.0080	0.0534 \pm 0.0081	0.0365 \pm 0.0365	49.33 %	-47.17 %
Participant 8	0.0238 \pm 0.0094	0.0209 \pm 0.0091	0.0128 \pm 0.0127	-12.01 %	-34.27 %

6.2.1.2 Changes in dicrotic notch peak (Point B)

It can be seen that dicrotic notch (point B) is situated between the systolic (point A) and diastolic peaks (point C), as illustrated in figure 6.1. Similarly, in congruity with the changes experienced by the systolic peak during this part of the experiment, point B also ended up increasing in its magnitude. Subsequently, when the cuff's pressure got released, the amplitude at this location returned to a level that was fairly close to the baseline. The table 6.4 shows that most of the participants (87.5 %) exhibited an increase in magnitude of their dicrotic notch point. Among those who experienced this increment, the impedance changed roughly 47.73 % as compared to region 1, with the exception of partaker two whose impedance decreased -2.06 %. In contrast, after releasing the upper arms blockage, all participants experienced a decline in their point B magnitude of about -51.68 %.

Table 6.4 Change of amplitude of the waveform at peak B during the transition from baseline (region 1), venous occlusion (region 2) and the return to baseline (region 3). The column change shows the percentile variations between the different regions.

Point B	Baseline [Ω]	Occlusion [Ω]	Baseline [Ω]	Change	
	(Region 1)	(Region 2 - VO)	(Region 3)	R1-R2	R2-R3
Participant 1	0.0126 \pm 0.0231	0.0223 \pm 0.0195	0.0119 \pm 0.0153	76.94 %	-82.52 %
Participant 2	0.0397 \pm 0.0144	0.0388 \pm 0.0167	0.0257 \pm 0.0252	-2.06 %	-33.19 %
Participant 3	0.0184 \pm 0.0315	0.0323 \pm 0.0181	0.0200 \pm 0.0224	75.98 %	-67.36 %
Participant 4	0.0130 \pm 0.0294	0.0183 \pm 0.0149	0.0113 \pm 0.0138	40.21 %	-53.52 %
Participant 5	0.0319 \pm 0.0158	0.0402 \pm 0.0138	0.0254 \pm 0.0237	25.92 %	-46.26 %
Participant 6	0.0127 \pm 0.0138	0.0177 \pm 0.0161	0.0124 \pm 0.0128	39.75 %	-41.55 %
Participant 7	0.0250 \pm 0.0108	0.0382 \pm 0.0092	0.0287 \pm 0.0276	52.71 %	-37.97 %
Participant 8	0.0102 \pm 0.0111	0.0125 \pm 0.0117	0.0073 \pm 0.0071	22.58 %	-51.08 %

Research of the shape changes of the arterial pulses during proximal occlusions

6.2.1.3 Changes in diastolic peak (Point C)

The last analysed peak corresponds to point C or the diastolic pulse of the waveform. To reiterate, figure 6.3c illustrates that most of these participants (71.4 %) exhibited an increase in magnitude of about 31.92 % as compared to region 1. Only participants 2 and 8 witnessed a decline in their impedance (-7.97%). Table 6.5 illustrates the mean values of impedance at this location within the waveform. In contrast, after releasing the pressure from the upper arm, a decrease was observed in the diastolic peak impedance of all participants, at an average of -32.33% . As a result, the diastolic peak returned to values that were similar to the baseline, barring the ones that experienced a diminished resistance during the occlusion.

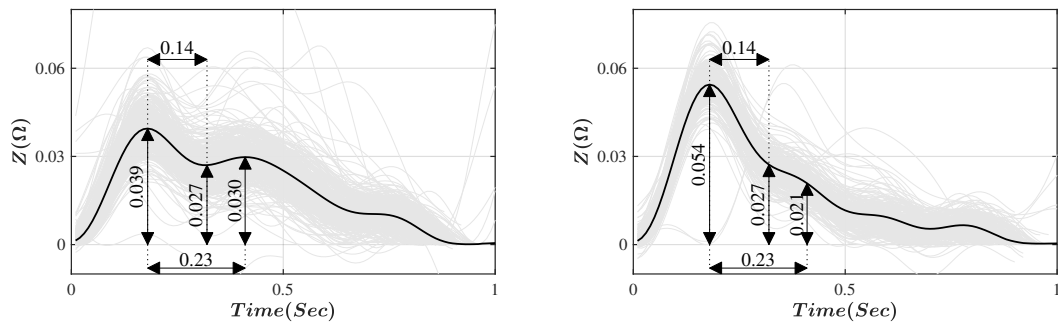
Table 6.5 Change of amplitude of the waveform at peak C during the transition from baseline (region 1), venous occlusion (region 2) and the return to baseline (region 3). The column change shows the percentile variations between the different regions.

Point C	Baseline [Ω]	Occlusion [Ω]	Baseline [Ω]	Change	
	(Region 1)	(Region 2 - VO)	(Region 3)	R1-R2	R2-R3
Participant 1	0.0238 ± 0.0281	0.0283 ± 0.0260	0.0224 ± 0.0286	18.81 %	-24.75 %
Participant 2	0.0429 ± 0.0150	0.0401 ± 0.0191	0.0279 ± 0.0278	-6.48 %	-28.45 %
Participant 3	0.0221 ± 0.0397	0.0355 ± 0.0219	0.0236 ± 0.0310	60.85 %	-53.94 %
Participant 4	0.0171 ± 0.0380	0.0184 ± 0.0174	0.0149 ± 0.0178	7.42 %	-20.30 %
Participant 5	0.0350 ± 0.0175	0.0459 ± 0.0151	0.0287 ± 0.0279	31.16 %	-49.18 %
Participant 6	0.0138 ± 0.0212	0.0182 ± 0.0251	0.0133 ± 0.0151	31.53 %	-35.22 %
Participant 7	0.0276 ± 0.0127	0.0391 ± 0.0111	0.0312 ± 0.0309	41.77 %	-28.58 %
Participant 8	0.0138 ± 0.0140	0.0125 ± 0.0163	0.0100 ± 0.0096	-9.47 %	-18.24 %

6.2.2 Plethysmography waveform change during partial arterial occlusion

During the partial occlusion of the brachial artery, the majority of the participants exhibited a change in shape of their waveforms. An analysis of this section resembles the baseline time outlined in region 3 (480 s to 780 s), three minutes of the partial venous occlusion in region 4 (780 s to 960 s) and a return to baseline region 5 (960 s to 1260 s). Next, the cuff was inflated to the pressure presented in column *Occlusion 2* in Table 4.5, laying between diastolic and systolic pressures. Figure 6.4 illustrates the average waveform of all signals that were aligned at baseline and during the arm's occlusion for one of these participants. Evidently, there is a surge in the systolic peak (point A), and a reduction in the diastolic peak at point C. Figure 6.5 also highlights the impedance change in all participants during the three regions. The following sections will describe the changes made in each of the spots in greater detail.

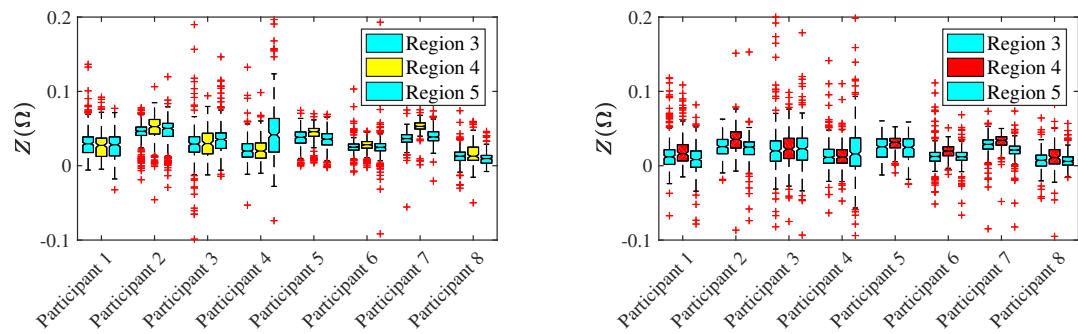
6.2 Changes of the plethysmography waveform during different occlusions



(a) Average baseline plethysmography waveform before partial arterial occlusion region 3 (480 s to 780 s)

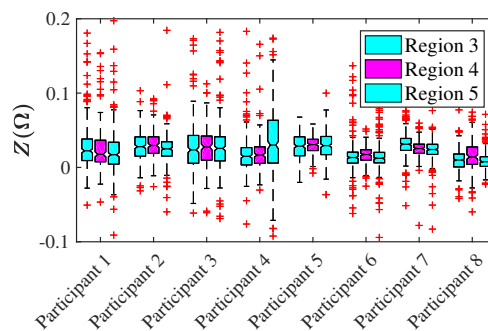
(b) Average plethysmography waveform during partial arterial occlusion region 4 (780 s to 960 s)

Figure 6.4 Plethysmography waveform of the participant seven between baseline and partial arterial occlusion



(a) Change of amplitude of the waveform at point A.

(b) Change of amplitude of the waveform at point B.



(c) Change of amplitude of the waveform at point C.

Figure 6.5 Changes of the impedance peak values during baseline, partial arterial occlusion and return to baseline for points A,B and C.

Research of the shape changes of the arterial pulses during proximal occlusions

6.2.2.1 Changes in systolic peak (Point A)

Figure 6.5a illustrates the change in amplitude for each participant. In addition, table 6.6 summarises the average impedances along with the variations in each region. Through this occlusive experiment, seven participants (87.5 %) showed an increase in electrical resistivity at point A of about 13.52 %. However, some of them exhibited a small surge in their peaks between 0.29 % to 2.24 %. In general, the increase at this point can be observed. After the deflation of the cuff, most participants (62.5 %) exhibited a decline in peak on an average of –21.86 %. In contrast, participants 1, 3 and 4 registered an increase in impedance reading, the latter being an outlier with a hike in his magnitude of 110.69 %.

Table 6.6 Change of amplitude of the waveform at peak A during the transition from baseline (region 3), partial arterial occlusion (region 4) and the return to baseline (region 5). The column change shows the percentile variations between the different regions.

Point A	Baseline [Ω]	Occlusion [Ω]	Baseline [Ω]	Change	
	(Region 3)	(Region 4 - PAO)	(Region 5)	R3-R4	R4-R5
Participant 1	0.0295 ± 0.0194	0.0274 ± 0.0190	0.0282 ± 0.0265	-7.03 %	2.59 %
Participant 2	0.0462 ± 0.0140	0.0526 ± 0.0197	0.0503 ± 0.0461	13.78 %	-5.11 %
Participant 3	0.0292 ± 0.0379	0.0298 ± 0.0185	0.0354 ± 0.0356	2.24 %	19.02 %
Participant 4	0.0197 ± 0.0242	0.0198 ± 0.0152	0.0416 ± 0.0453	0.29 %	110.69 %
Participant 5	0.0382 ± 0.0133	0.0458 ± 0.0115	0.0357 ± 0.0351	19.81 %	-26.55 %
Participant 6	0.0249 ± 0.0096	0.0282 ± 0.0081	0.0247 ± 0.0251	13.21 %	-14.09 %
Participant 7	0.0365 ± 0.0097	0.0529 ± 0.0092	0.0388 ± 0.0394	44.90 %	-38.73 %
Participant 8	0.0128 ± 0.0104	0.0128 ± 0.0160	0.0096 ± 0.0098	0.38 %	-24.86 %

6.2.2.2 Changes in dicrotic notch peak (Point B)

In the dicrotic notch position (point B), the increase of magnitude is more apparent than it is in the systolic peak. In fact, all participants experienced an increase in their respective impedance values at this point. Figure 6.5b encapsulates these changes in all the regions before and after the occlusion. Table 6.5b details the participants' median impedances along with the ratio of change in each region.

In general, the average increase at the dicrotic notch stood at about 29.91 % as soon as the occlusion was applied. When the pressure to restrict the blood flow was taken away, six out of eight members witnessed decline in electrical resistivity towards the baseline. On average, it was seen to reduce by –51.72 %. Here again, participants 3 and 4 were exceptions to this reduction; their impedance increased by 37.37 % and 3.25 %, respectively.

6.2 Changes of the plethysmography waveform during different occlusions

Table 6.7 Change of amplitude of the waveform at peak *B* during the transition from baseline (region 3), partial arterial occlusion (region 4) and the return to baseline (region 5). The column change shows the percentile variations between the different regions.

Point B	Baseline [Ω]	Occlusion [Ω]	Baseline [Ω]	Change	
	(Region 3)	(Region 4 - PAO)	(Region 5)	R3-R4	R4-R5
Participant 1	0.0119 \pm 0.0232	0.0162 \pm 0.0220	0.0083 \pm 0.0087	36.07 %	-66.02 %
Participant 2	0.0257 \pm 0.0142	0.0354 \pm 0.0212	0.0251 \pm 0.0231	38.02 %	-40.44 %
Participant 3	0.0200 \pm 0.0536	0.0222 \pm 0.0247	0.0229 \pm 0.0244	11.33 %	3.25 %
Participant 4	0.0113 \pm 0.0256	0.0116 \pm 0.0177	0.0158 \pm 0.0143	2.64 %	37.37 %
Participant 5	0.0254 \pm 0.0155	0.0314 \pm 0.0107	0.0248 \pm 0.0237	23.55 %	-26.29 %
Participant 6	0.0124 \pm 0.0150	0.0197 \pm 0.0096	0.0121 \pm 0.0141	58.95 %	-61.59 %
Participant 7	0.0287 \pm 0.0128	0.0340 \pm 0.0104	0.0211 \pm 0.0205	18.34 %	-44.99 %
Participant 8	0.0073 \pm 0.0118	0.0110 \pm 0.0196	0.0058 \pm 0.0069	50.41 %	-71.01 %

6.2.2.3 Changes in diastolic peak (Point C)

Changes in the diastolic peak also presented a similar (increasing) trend as evidenced in points A and B. However, these changes were not as pronounced as the ones witnessed in the diastolic notch. Figure 6.5c and Table 6.8 summarise the total obtained values. In total, 75 % of the participants illustrated an increase of impedance between region 3 and 4. It went up with a median of 18.74 %. Participant 8 witnessed a change that was significantly higher than the mean (44.11 %). Meanwhile study members 1 and 7 exhibited a decline electrical resistivity in -19.91 % on average.

On the opposite side of the spectrum, upon the release of pressure, (87.5 %) of the participants experienced a decline in their impedance, including those whose impedance was seen to increase during the occlusion. On average, it reduced by -19.77 % in total. Participant 4 exhibited a surge in the ratio of change prior to and after the blockage, thereby significantly exceeding the median of all measurements. Moreover, this specific study member outperformed the average ratio after the occlusion (90.32 %). As evidenced by other measuring points, it confirms the fact that the data obtained from this participant were not related to physiological origin, but motion or randomness.

This point of the data is a clear differentiator between venous and arterial occlusion. It seems that the diastolic pulse dims during arterial occlusion. Still, it is not clear if the drop of this peak is due to compliance or derived from the blood flow restriction. One could assume that vessel compliance might play a role in the waveform change, but so far, the data shows that it is only present in this place of the data, which makes it unique compared to the other observed points.

Research of the shape changes of the arterial pulses during proximal occlusions

Table 6.8 Change of amplitude of the waveform at peak C during the transition from baseline (region 3), partial arterial occlusion (region 4) and the return to baseline (region 5). The column change shows the percentile variations between the different regions.

Point C	Baseline [Ω]	Occlusion [Ω]	Baseline [Ω]	Change	
	(Region 3)	(Region 4 - PAO)	(Region 5)	R3-R4	R4-R5
Participant 1	0.0224 ± 0.0323	0.0176 ± 0.0307	0.0171 ± 0.0206	-21.35 %	-2.21 %
Participant 2	0.0279 ± 0.0196	0.0295 ± 0.0272	0.0250 ± 0.0252	5.96 %	-16.45 %
Participant 3	0.0236 ± 0.0826	0.0275 ± 0.0284	0.0256 ± 0.0283	16.56 %	-7.98 %
Participant 4	0.0149 ± 0.0327	0.0166 ± 0.0229	0.0301 ± 0.0306	11.22 %	90.32 %
Participant 5	0.0287 ± 0.0171	0.0308 ± 0.0119	0.0293 ± 0.0287	7.32 %	-5.03 %
Participant 6	0.0133 ± 0.0252	0.0174 ± 0.0111	0.0123 ± 0.0176	30.32 %	-37.72 %
Participant 7	0.0312 ± 0.0189	0.0254 ± 0.0124	0.0241 ± 0.0232	-18.48 %	-4.27 %
Participant 8	0.0100 ± 0.0139	0.0141 ± 0.0224	0.0076 ± 0.0087	41.11 %	-64.75 %

6.2.3 Plethysmography waveform variation during total occlusion

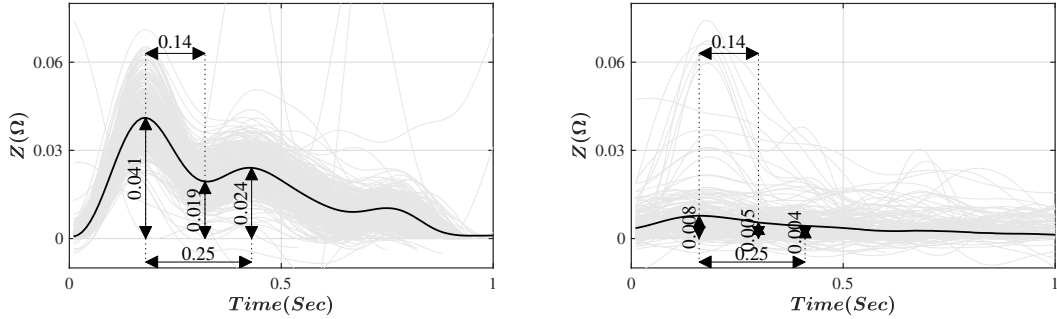
It was observed that performing a total occlusion completely blocks both the inflow and outflow of blood below the arm's cuff. This implies that there is no change of volume within the arm's segment. As a result, it can be surmised that impedance plethysmography must not present the changes in magnitude.

Figure 6.6 shows the APA waveform during the baseline in region 5 (960 s to 1260 s) and the total occlusion in region 6 (1260 s to 1440 s) of the seventh participant. As clearly illustrated by the figure 6.7, the amplitudes of most participants reduced during the occlusion. However, participant 4 experienced different behaviours across all these points. The member's standard deviation also suggests a problem with his plethysmography signal during this test.

In general, point A decreased by -66.15% on average at its peak value occlusion. Upon the release of pressure, impedance recovered its value in 75.98% . A similar event occurred at point B; peak signals reduced by a median of -63.29% during blockage and recovered on average by 74.02% . Similarly, point C decreased (on average) by -50.27% and rose by 58.71% following the occlusion.

The previous section showed that the baseline impedance during this type of occlusion did not change in a clear trend. However, from the analysis of the APA waveform, it can be concluded that the total absence of peaks in the signal is equivalent to no flow in the forearm. At this point, it becomes essential to observe the changes in basal impedance for more extended periods, as a high increase in impedance may suggest the development of hypoxia or even ischaemia.

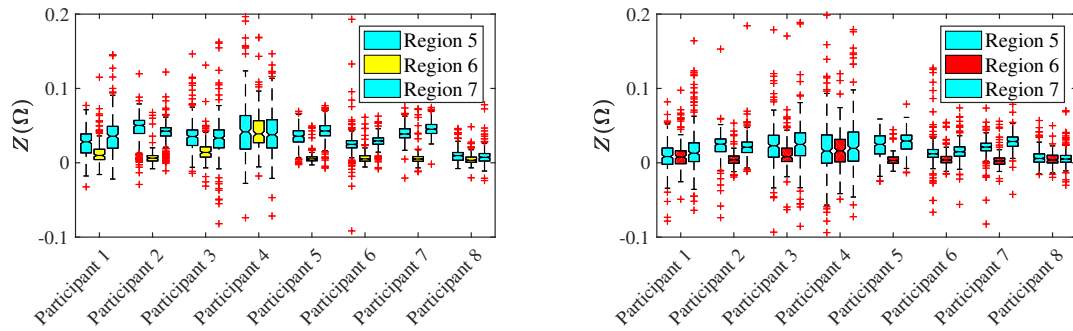
6.2 Changes of the plethysmography waveform during different occlusions



(a) Average plethysmography waveform during venous occlusion region 5 (960 s to 1260 s)

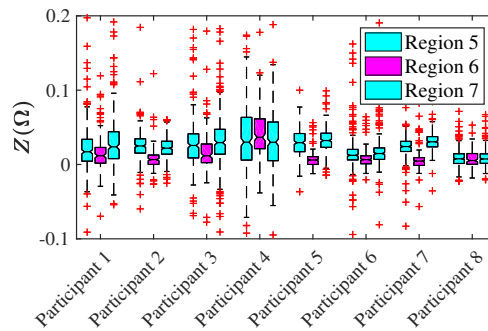
(b) Average plethysmography waveform during venous occlusion region 6 (1260 s to 1440 s)

Figure 6.6 Plethysmography waveform of the participant seven between baseline and total occlusion



(a) Change of amplitude of the waveform at point A.

(b) Change of amplitude of the waveform at point B.



(c) Change of amplitude of the waveform at point C.

Figure 6.7 Changes of the impedance peak values during baseline, total occlusion and return to baseline for points A,B and C.

6.3 Novel evaluation of blood obstructions using iPG baseline over APA waveforms

The information provided by the designed iPG device comprises of basal impedance and arterial pulses amplitude. These two variables have been studied separately as an effective source of information for circulatory problems. However, still more studies are required to find methods that allow to discern between arterial and venous circulatory problems. To the authors knowledge, the results presented in the this sections are the first to combine the readings from baseline impedance and the morphological change of the APA waveform into a qualitative indicator.

The chapter 5 demonstrated that during a circulatory occlusion, the baseline impedance decreases slightly. Although the basal impedance drop rate is one of the first indicators of occlusion, still the variation between both kind of blockages is quite close. The literature has studied extensively the changes of baseline impedance during the venous occlusion plethysmography manoeuvre and the continuous monitoring tissue health [102, 21, 22, 120]. Additionally, simulations using COMSOL models have corroborated the change of impedance of a vessel in normal condition, stenosis, blockage and swelling. The study presented by Shash et al. [208] suggested that using a frequency of 50 kHz is high enough to penetrate tissue at high depth. Additionally, it demonstrated that the total impedance changes at different rates according to the kind of flow restriction simulated. This results agree with the one demonstrated in this study where the basal impedance varied according to the levels of occlusion applied. From this information can be concluded that using the baseline impedance is the first source of information for detecting anomalies in the circulatory path but double-checking with additional data may help to corroborate diagnosis.

The use of the APA signal to investigate changes in the circulatory path has been used from the qualitative point of view. Studies have used the amplitude pulses as a method of quantifying blood flow in different parts of the body. The literature have demonstrated to be quite effective to measure changes of volume, oedema and the detection of deep vein thrombosis (DVT) [134]. However, this kind of measurements use amplitude of the pulses to compute these physiological variables. Regarding to the analysis of the morphology of the waveform, an attempt to analyse the waveform has been performed by Montgomery et al. [29]. However, the analysis of the waveform was used to assess the progression of Lymphedema during arterial and venous cycles of the iPGb waveform. Their work flagged

6.3 Novel evaluation of blood obstructions using iPG baseline over APA waveforms

out changes in the waveform morphology and changes in the dicrotic notch when compared to the opposite healthy arm.

Another example of decomposing the iPG can be seen in the work of Klum et al. [209]. In this report, the author uses the iPG waveform as method to extract the respiratory rate. In there, the study decomposes the waveform in different points and amplitude of the systolic and diastolic peak. These two studies validate the use of waveform decomposition to study physiological changes in the body.

The findings presented here demonstrated that morphological changes occur to the arterial pulses during blood flow restriction. Two different shapes of APA signal materialise during venous and arterial occlusion, which may allow discerning between these two events. First, venous occlusion has shown an increase in the three points measured (systolic peak, dicrotic notch and diastolic peak). Conversely, partial arterial occlusion has displayed a decrease of the diastolic pulse index in relation to the dicrotic notch.

However, it could be quite challenging to make decisions by considering only one parameter of the impedimetric signal. For this reason, a method that combines both sources of data could provide an immediate indicator of a possible occlusion. Therefore, a ratio index between the APA waveform and the basal impedance is proposed to differentiate between venous and arterial circulatory problems. To do so, it is imperative to identify the three points of the plethysmographic waveform: systolic peak, dicrotic notch, and diastolic pulse. For this reason, the section 6.1 described the algorithm required to break down the impedimetric signal into the baseline value and these three points.

The following steps briefly describe the process to calculate the index ratio. Due to the noise in the signal, further processing takes place which conditions the waveform. First, all the baseline points of the raw impedance signal need extraction; this can be achieved by identifying the point $L1$ (figure 6.1). This value is equivalent to the impedance baseline (Z_{BAS}). All these points in the signal also represent the lower envelope of the impedimetric signal. The second step requires extracting the APA waveform. For this, the baseline impedance is deducted from the raw signal leaving just the APA waveform. In this study, the APA waveform was extracted electronically using the port V_{AC} of the designed device. This APA signal also contains high-frequency noise. Therefore, the waveform is filtered, removing these unwanted components. The next step consists of zeroing the waveform. So, the points $L1$ and $L2$ are synchronised with the heart rate and levelled to zero. All the waveform points are moved accordingly to the new reference point.

The final stage consists of identifying the three markers of the APA signal (Points A, B and C). Waveforms that comply with the expected plethysmography shape ($L1 > A < B >$

Research of the shape changes of the arterial pulses during proximal occlusions

slope change ($C > L2$) are detected and data points collected. In a constant heart rate, the location of these points can be predicted by averaging the previous time between points. Hence, the algorithm takes the previous twenty heartbeats to predict roughly the position of the current peak or valley. Moreover, to make sure that the algorithm is detecting the right spot, the program also analyses the change of slope. Therefore, if a change of slope occurs in the expected time-frame, this can be disclosed as a valid APA waveform.

With this information, a relation between baseline impedance and the amplitude value of every point can be used to magnify the change of position of the systolic peak (point A - $\Delta Z(A)$), dicrotic notch (point B - $\Delta Z(B)$) and diastolic pulse (point C - $\Delta Z(C)$). Hence, the proposed ratio consists of the relationship between the impedance amplitude at each of these points over the baseline point (Z_{BAS}). The introduced index ($i_{Z(x)}$) can be calculated using the following equation.

$$i_{Z(A)} = \frac{\Delta Z(A)}{Z_{BAS}} \quad i_{Z(B)} = \frac{\Delta Z(B)}{Z_{BAS}} \quad i_{Z(C)} = \frac{\Delta Z(C)}{Z_{BAS}} \quad (6.1)$$

The index ratio is dimensionless with three indicators referencing each point of the impedance plethysmography waveform. The method was applied to the study participants data, and the results were outlined in figure 6.8. The data was separated into three waveforms representing the index at point A (blue line —), point B (orange line —) and point C (yellow line —). The strong continuous line in the graph represents the mean value of the point in every region.

The index ratio value highlights some of the events registered in this study. Analysing the data for the systolic point (point A), straight away can be noticed an increment of the index during venous and arterial occlusion in most of the participants. Compare to the previous baseline value; the value swelled in most participants. An elevated index value at this point might suggest a circulatory problem. This information could be useful in post-surgery recovery, where blood cloths need tracking after a procedure or for home patients that require constant PVD monitoring.

The dicrotic notch (point B) and the diastolic pulse (point C) seem to change as a matching pair for the majority of the baseline signals (regions 1, 3 and 5). In general, the dicrotic notch appears to be slightly lower than the diastolic pulse under normal conditions. However, during venous occlusion, the index value seems to swap for these two points. This seems to be caused by the nearly absence of the diastolic pulse during this part of the test.

Nevertheless, something remarkable happens all along with partial arterial occlusion. The index value swapped position for some of the participants. Before the arterial occlusion, the location of the markers follows suit as a standard baseline ($i_{Z(A)} > i_{Z(C)} > i_{Z(B)}$). However,

6.3 Novel evaluation of blood obstructions using iPG baseline over APA waveforms

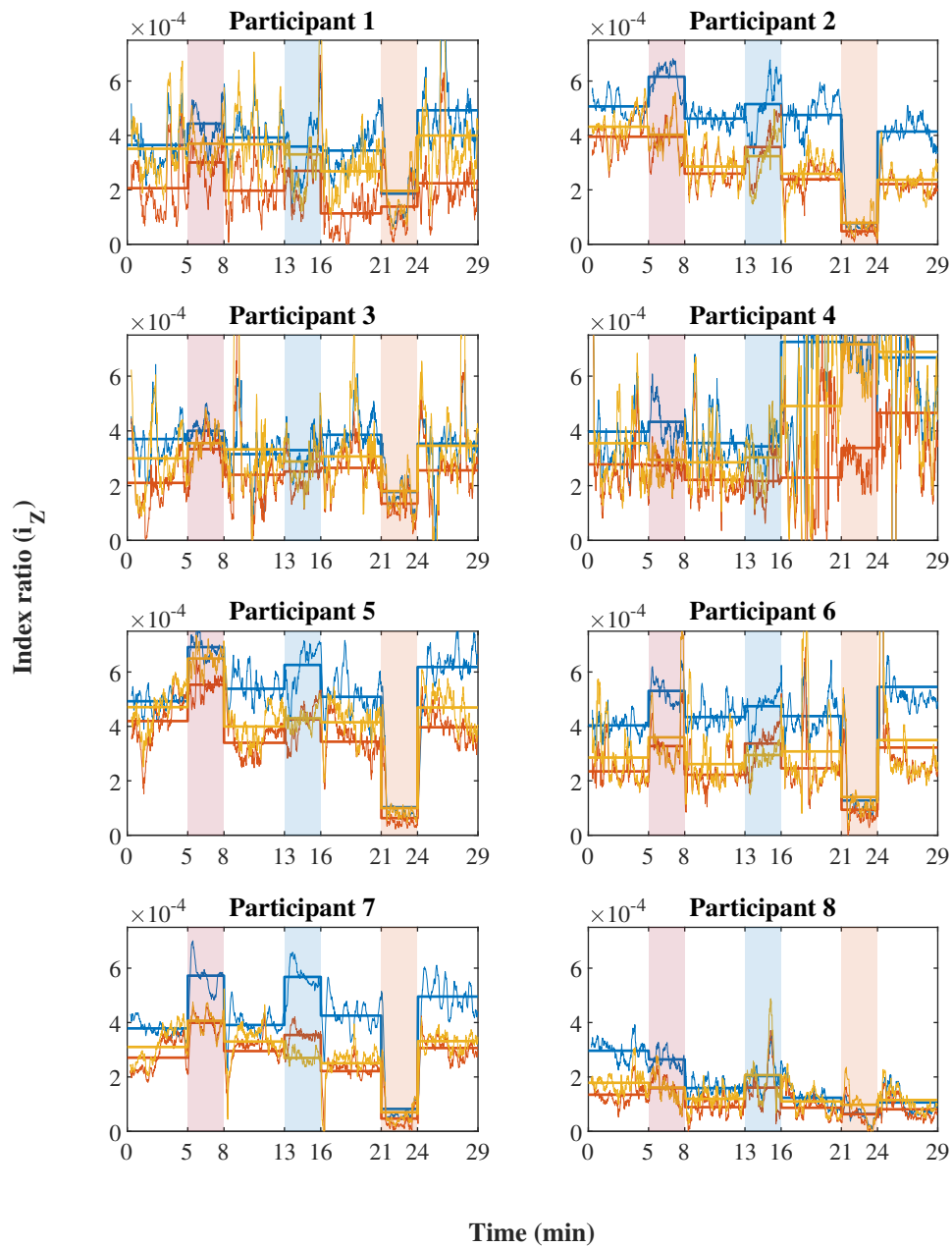


Figure 6.8 Representation of the calculated the index ratio between the APA waveform over the basal impedance during the whole experiment. The blue line represents the index ratio at the systolic peak (*Point A* — $i_{z(A)}$), the yellow line the dicrotic notch (*Point B* — $i_{z(B)}$) and the red line the diastolic pulse (*Point C* — $i_{z(C)}$). The continuous line en each region is the mean value of the index ratio

Research of the shape changes of the arterial pulses during proximal occlusions

during partial arterial occlusion, there is a change in the position ($i_{Z(A)} > i_{Z(B)} > i_{Z(C)}$). This event is a clear differentiator between the two types of flow restriction. Participant 2, 6 and 7 are the perfect example of the behaviour of the index when these conditions are met. The rest of the participants showed a different behaviour, but these readings were affected by motion artefact and other issues described in this document.

6.3.1 Analysis of the novel index ratio between the three different levels of occlusion

The index ratio (i_Z) required an extensive signal analysis to extract the relevant data. However, according to the data recorded the waveform varied at the dicrotic notch and diastolic pulse is the most critical differentiator to distinguish between venous and arterial occlusion. This detail is an initial clue of the potential of impedance haemodynamic analysis on the detection of circulatory problems. Figure 6.9 and table 6.9 show the mean index ratio value for each participant during the initial baseline data, venous, partial arterial and total occlusion. In the figure, markers have been added to facilitate interpretation. In there, the blue bar represents the index ratio at the systolic peak (point A ■), the dicrotic notch index with the orange bar (point B ▲), and the diastolic pulse with the yellow bar (point C ●).

In general, from this point of view, it is possible to identify the general enlargement of the waveform during venous occlusion, which it is also confirmed in table 6.9. Most of the participants presented an increase of index in nearly all the points. Nonetheless, participant 8 showed a different trend possibly associated with discomfort in the course of the test. Furthermore, participant 4 also displayed adverse trend for point B and C, possibly related to external factors as his/her signals were noisy after this part of the study.

In terms of partial arterial occlusion, most of the participants experienced an increase of the systolic index and a shortening or inversion in the index ratio between point B and C. The data in table 6.9 shows that participants 2, 6 and 7 showed the ideal response for the system. Once again, participants 1, 4 and 8 depicted adverse results related to the events previously mentioned and motion artefact. Performing partial arterial occlusion can be painful and required most of the participants to re-accommodate during the data collection causing extra data noise. In total occlusion the data is more conclusive as almost everyone experienced a decrease in the index ratio in values below baseline signal. The only exception was again participant 4 for the same motives described.

6.3 Novel evaluation of blood obstructions using iPG baseline over APA waveforms

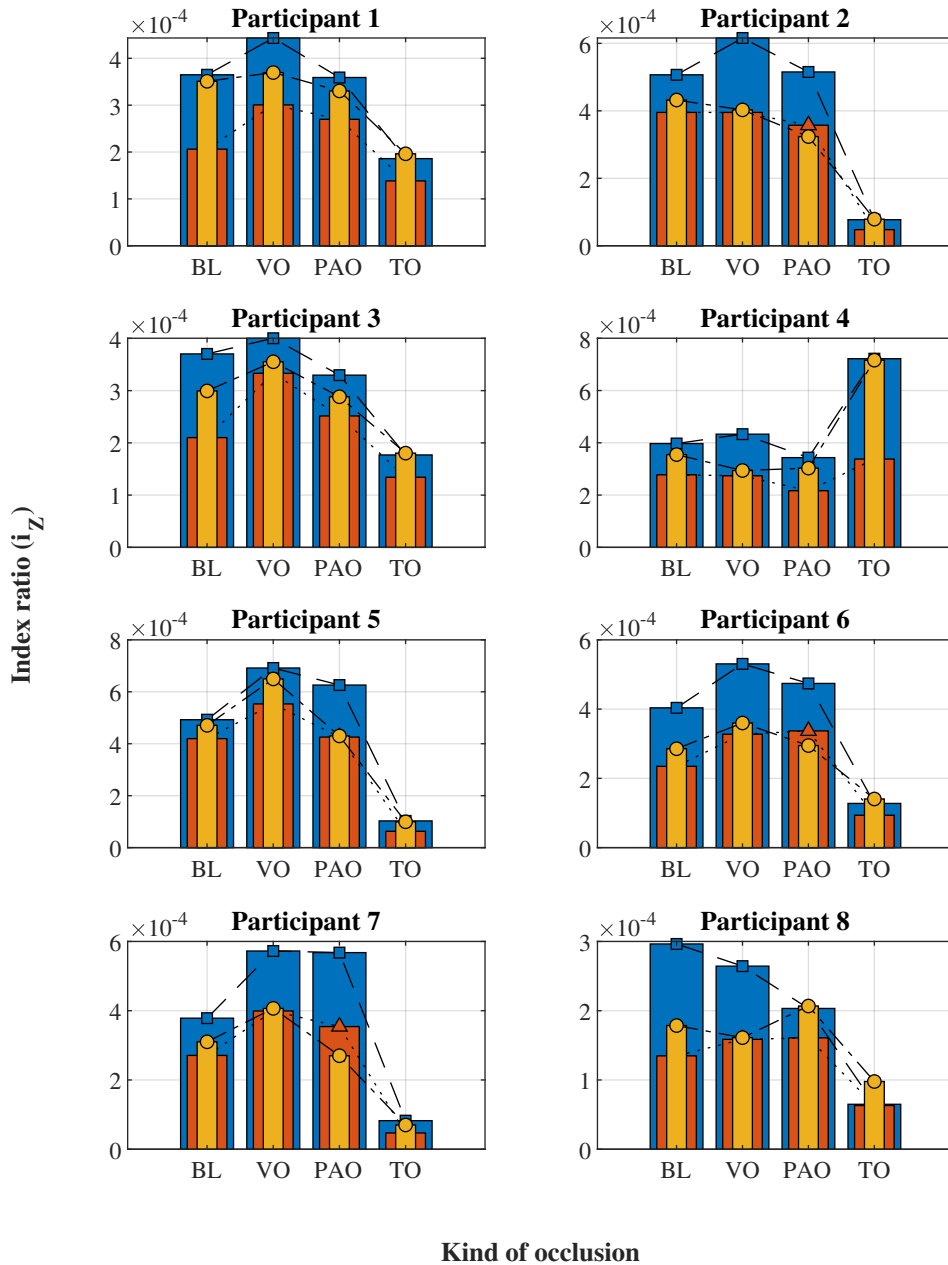


Figure 6.9 Bar graph of the index ratio i_z for every point during baseline (BL - region 1), venous occlusion (VO - region 2), partial arterial occlusion (PAO - region 4) and total occlusion (TO - region 6). In the figure the blue bar represents the index ratio at the systolic peak (point A ■), the dicrotic notch index with the orange bar (point B ▲), and the diastolic pulse with the yellow bar (point C ●).

Table 6.9 Index ratio i_z for every point of interest during baseline (BL - region 1), venous occlusion (VO - region 2), partial arterial occlusion (PAO - region 4) and total occlusion (TO - region 6). This is the data used to create the figure 6.9, the colours used in the headers match the ones in the figure. The index value was calculated using the equation 6.1 for each point. In venous occlusion, the bold numbers represent the indexes which increased in value compared to baseline. The values in partial arterial occlusion that are bold and italic are the ones where the dicrotic notch is higher than the diastolic pulse.

Study member	Baseline ($i_z * 10^{-4}$)			Venous occlusion ($i_z * 10^{-4}$)			Partial arterial occlusion ($i_z * 10^{-4}$)			Total occlusion ($i_z * 10^{-4}$)		
	Point A	Point B	Point C	Point A	Point B	Point C	Point A	Point B	Point C	Point A	Point B	Point C
Participant 1	3.65	2.06	3.51	4.43	3.01	3.70	3.59	2.70	3.30	1.86	1.38	1.96
Participant 2	5.07	3.95	4.32	6.16	3.95	4.03	5.15	3.57	3.24	0.77	0.48	0.79
Participant 3	3.70	2.10	2.99	4.00	3.33	3.55	3.30	2.52	2.88	1.77	1.34	1.80
Participant 4	3.97	2.78	3.55	4.33	2.74	2.94	3.43	2.17	3.03	7.22	3.38	7.16
Participant 5	4.93	4.20	4.71	6.92	5.53	6.50	6.26	4.26	4.30	1.03	0.63	1.00
Participant 6	4.04	2.35	2.86	5.31	3.28	3.60	4.74	3.37	2.95	1.28	0.94	1.41
Participant 7	3.79	2.71	3.10	5.72	3.99	4.07	5.68	3.54	2.70	0.83	0.47	0.70
Participant 8	2.96	1.35	1.79	2.64	1.59	1.61	2.03	1.61	2.07	0.65	0.63	0.98

6.4 Conclusions

The iPG signals provided additional information about blood distribution during the occlusive events. The oscillations of the APA signal are attributed to the expansion of arteries and veins during the heart cycle, thereby creating small changes in the impedance. While this tiny waveform is contained within the basal impedance, it is merely a fraction of it.

The designed impedance device in its entirety, including hardware and software algorithms, was able to identify the plethysmography waveforms by localising distinctive landmarks such as the systolic peak, dicrotic notch and diastolic pulse. Obtaining this level of detail was vital because it provided more details about the changes occurring in different segments of the impedance plethysmography waveform. From this premise, it could recognise the changes in shape during each types of occlusions performed during the test. It is evident that at the time of each occlusive event, the amplitude of systolic and diastolic peaks manifested a particular response in accordance to the type of blood flow restriction. Notably, the waveform shape might be unique to this kind of set-up, and it is possible that altering the electrodes distance or using different frequencies may impact the impedance waveform.

Meanwhile changes were observed in the size of the systolic peak (point A), dicrotic notch valley (point B) and diastolic peak (point C) when an occlusion took place. The increase in size might be attributed to a physiological response during the occlusion where the volume capacity of veins increased to accommodate the pooled blood. An example of this is evident in figure 6.3 which described the differences between region 1, 2 and 3. According to the figure, there was an increase in the size of all reference points in majority of the participants during the occlusion, which was followed by a return to the baseline. However, the observations made in the partial occlusion for regions 3, 4 and 5 suggested that while the systolic peak did increase in size, the dicrotic notch and diastolic peak declined in amplitude when compared to the venous occlusion and baseline waveform. The difference in waveform is an accurate indicator of an obstruction in either a arterial or venous circulation.

The chapter 5 demonstrated that during the occlusions, a different slope was noted during in each kind of occlusion. By combining the information of basal impedance with the APA waveform, it is possible to generate a 3-point ratio index that could be indicative of a potential obstruction within the forearm. This observation suggested that if there is a significant increase in the relation index of the systolic peak, it could be the first prominent indicator of circulatory blockage. On the other hand, an increase in the dicrotic notch and the diastolic pulse indicates that the occlusion might occur in the venous return if the dicrotic notch ratio index is higher than the other following one. While undertaking a comparison,

Research of the shape changes of the arterial pulses during proximal occlusions

the data showed that if there is a surge in systolic peak size, the diastolic pulse index tends to reduce or is at similar amplitude of the dicrotic notch ; it might then be an indicator of an imminent arterial occlusion.

Quantification and correlation of iPG, Doppler Ultrasound, LDF and PPG

This chapter describes the quantification of the raw data obtained from the different instruments inclusive the bespoke iPG device. The data acquired from the aforementioned device and the other methods were quantified and correlated to establish the statistical association between the impedance's APA signal (iPG technique), arterial flow (US method) and micro-circulatory flow (optical methods).

As mentioned in chapter 4, the iPG device recorded the basal and APA impedances. Some of the other signals recorded were: the heart's electrical signals using the ECG. The Doppler Ultrasound used to estimate the arterial blood flow in the wrist's radial artery. The PPG placed on the index finger provided plethysmographic information from the vascular bed close to the fingers' area. Finally, the Laser Doppler Flowmetry attached to the mid-section of the forearm gauged the changes of RBC in the vascular bed around the arm.

The signals provided by the instruments were scaled in volts, hence these needed translation into physiological measurement units. So, the first section of this chapter shows the data converted from voltages to values like flow (m^3/s). The second section describes the correlation between the iPG data and the other measurements. This investigation endeavours to understand the contributing factors to the impedance plethysmography signal. As explained in previous chapters, blood flow can be estimated from the APA; but still, it is not clear the contribution of venous and arterial blood. The extent of blood flow belonging to any blood type remains ambiguous. Besides, it was evident that the main blood vessels contribute to the measurement of blood flow, although microcirculation might also be able to provide additional information under the iPG waveform.

7.1 Quantification of the measurements of the devices

This section describes the measurements of all the devices attached to the partakers. The signals were converted to clinical values, and the changes registered during each occlusion were quantified and analysed. The measurements showed that every instrument showed a particular change in slope or waveform amplitude during each occlusion applied.

7.1.1 Measurements from the ECG device

The ECG signals provided information concerning the electrical activity of the heart during the study. Therefore, extreme changes occurring in the heart rate or shape could not be registered through the test unless there was a bad connection. The data that was gathered also served as a clock reference during the data processing. Figure 7.1 illustrates the typical ECG for one of the participants.

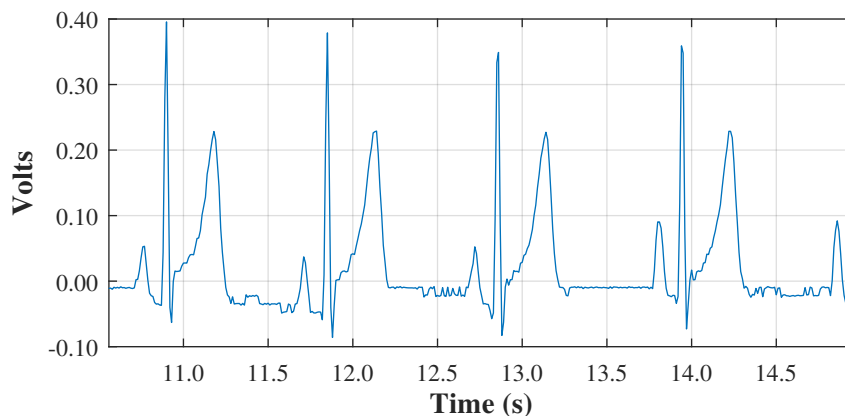


Figure 7.1 ECG measurement from one of the participants. The points can be clearly identified as P, Q, R, S and T. This signal did not change during the entire experiment.

All the detected waveforms were typical and provided sufficient information about the characteristic peaks in an ECG waveform. The points P, Q, R, S and T were visible in all the signals. Nonetheless, participant 1 showed an elevated T-wave, which is presumably attributed to his athletic vocation. He said that he had a ventricular hypertrophy, which implies that one of his ventricles got enlarged.

7.1.2 Blood flow calculation from arterial pulses signal

Thus far, blood flow has been analysed from occlusive methods that incorporated the techniques described in section 2.5.3. However, these procedures necessitate mechanical occlusion to produce an increase in volume within the forearm that is being measured. Nevertheless, this can oftentimes be uncomfortable, particularly when the pressure is applied above the systolic value or when the person is unable to tolerate restricted blood flow.

For such cases, analysing the waveform offers key information about various aspects of blood flow. The rush of blood into the vessel leads to a tiny surge in volume within the limit of potential electrodes, which then can be translated into a quantifiable blood flow. It is imperative to have a device that is sensitive enough to detect these changes providing an accurate estimation of the blood flow (speed). As mentioned in section 3.9.2, the waveform contained within the basal impedance got amplified by the device, thereby attaining a great level of detail.

In fact, different studies have demonstrated that it is indeed possible to calculate blood flow by analysing the APA waveform [21–26]. Here, the change of impedance used to perform this calculation takes place between the foot of the wave and the systolic peak. This ΔZ is used to calculate blood flow by applying Nyboer's equation 3.31.

Figure 7.2 illustrated the flow of blood derived from the amplitude of systolic peak throughout the entire experimental session. Green dots indicate blood flow measurements taken during baseline readings (regions 1, 3, 5 and 6). Meanwhile venous occlusion is shown in blue, partial arterial occlusion in red, and total obstruction in grey. The dark line drawn above the signals corresponds to the smoothing of each measurement event using *robust loess* method of the *smooth* command in Matlab. Overseeing the amplitude transition in every region will help explain how the flow changes with each occlusive event. The value of the calculated blood flow depicted in the figure excludes the negative sign that denotes the direction of flow relative to the potential electrodes.

As portrayed in this figure, between each transition - in the middle of baseline and occlusion - some participants clearly described the marked shifts in the calculated flow. In most participants, when the venous occlusion occurred, the changes between baseline and venous occlusion created a blood surge that was followed by a tendency for the flow to stabilise. Notably, the increment of blood flow in participant 2 occurred prior to the venous occlusion because the obstruction probably commenced before 300 s and the pressure exerted on the arm was rather slow. Meanwhile there are other instances where the flow change took place at such a quick pace that an entirely blank space can be seen to connect both

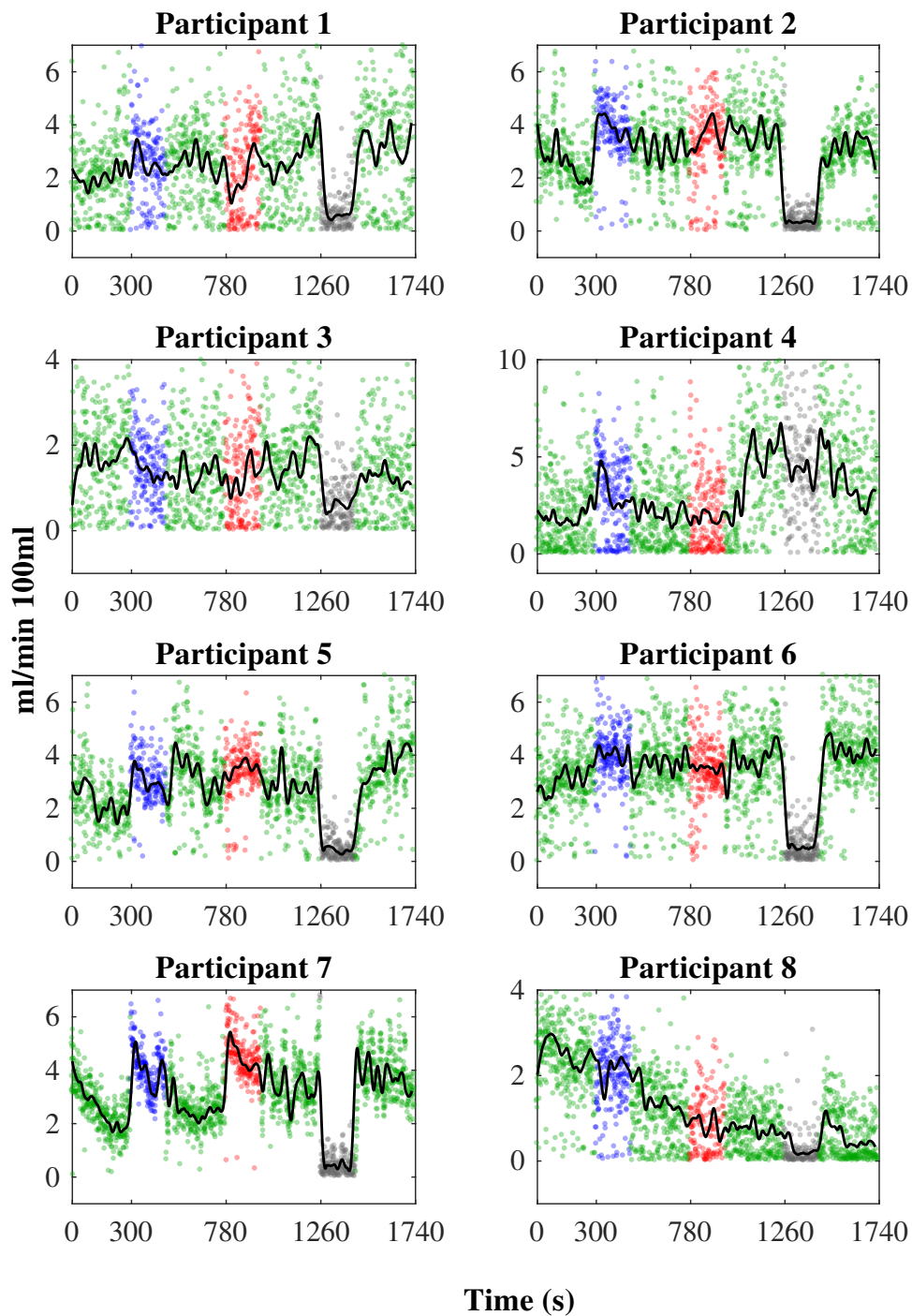


Figure 7.2 Blood flow calculated from the impedance plethysmography for all the participants during the whole experiment. Each dot signifies the peak value of the waveform that has been converted into flow (ml/ min 100ml). The green dotted area denotes the baselines measurements (regions 1,3,5 and 7). The region 2 (venous occlusion) is represented by the blue dots; arterial occlusions (region 4) are in red and total occlusions (region 6) are in grey.

7.1 Quantification of the measurements of the devices

events, as was seen in participants 5 and 7. This scenario, in contrast to participant 2, was more probable since the cuff was inflated at a faster pace, which led to a sudden change in flow, as opposed to a gradual one. However, it could also be correlated with a physiological bodily response such as vasodilation response, where one reacts faster than others. Finally, participant 8 was an exception to this rule and experienced a decline in the calculated flow, which was followed by a period of stabilisation. A flow surge was not identifiable in this participant.

Between venous occlusion and the return to baseline in region 3, the cuff was swiftly deflated so as to restore blood flow to the normal level. However, the calculated data suggests that no extreme changes were observed in the blood flow between these two sections immediately after the release of blockage. As noted before, most participants, except partakers 5 and 7, did not experience significant changes between these two sections, indicating a slight change in blood flow. This can be attributed to a hyperaemic effect where as soon as the pressure is released off the cuff, the blood in the vessels of the forearm rushes out to the upper part of the arm. Subsequently, the blood flow tended to stabilise towards an average value.

Similarly, as seen between regions 1 and 2, the change between baseline (region 3) and partial arterial occlusion (region 4 - red colour) generated alterations in the calculated blood flow. Some participants, such as partakers 6 and 7, experienced a rapid surge in blood flow after the occlusion followed by a settlement in the blood velocity, where the latter becomes more prominent. Meanwhile others such as participants 1, 2, 3 and 5 showed a Gaussian bell-shaped flow during the occlusion. Evidently, their flow did not set in a mean value. The only ones that enacted a different behaviour were participants 4 and 8, who did not experience a significant change. However, the continuous change of amplitude in participant 8 became prominent at this point, which is in contrast to the remaining participants.

The change occurring between partial arterial occlusion (red dotted section) and baseline entailed a similar effect as the one described for releasing the pressure of venous blockage. Most participants had a decreased blood flow, immediately upon the release of cuff's pressure, possibly due to a hyperaemic effect. At this point, participant 4 began exhibiting random blood flow readings.

Total occlusion (grey dots) evinced an expected response in nearly all the members. When the blood flow was completely stopped, its calculated value was expected to be zero. In this case, the device could successfully detect these changes. Participant 4 was the lone exception who again displayed random results. There were strong indications that there could be something wrong with his measurements. Upon the release of tourniquet, the blood

Quantification and correlation of iPG, Doppler Ultrasound, LDF and PPG

flow returned in an exponential form and was then set to an average value. In this case, the hyperaemic effect became more visible. Importantly, participant 8 witnessed a decline in blood flow towards the midpoint of the test. This event concurs with the partaker's expression of not feeling too well by the end of the test. It can be speculated as pure coincidence, or it could be that the device was indeed able to detect these physiological changes within him.

It is likely that there is a blood surge when an occlusion occurs from the impedance computation. Thereafter, the blood flow tends to stabilise at an average value. After the release of blockage, it seems that in certain cases, the flow tends to decrease; in other instances, no apparent change is found. The following sections will extrapolate on the findings of the change in median blood flow during each occlusive event.

7.1.2.1 Blood flow quantification and analysis during occlusion

The following is the analysis of the quantified blood flow rate during the three occlusive stages. The table 7.1 sums up the results obtained by the measurement flow in the scale ml/min 100ml. To reiterate, the results do not signify an absolute value, dropping the negative sign as this is indicative of the direction of the flow relative to the electrodes.

Table 7.1 Median blood flow calculation in ml/min 100ml from the iPG APA waveform

	Region 1	Region 2	Region 3	Region 4	Region 5	Region 6	Region 7
	(ml/min 100ml)						
Participant 1	2.046	2.688	2.710	2.251	2.977	0.564	3.466
Participant 2	2.516	3.766	3.119	3.484	3.537	0.284	2.922
Participant 3	1.794	1.416	1.325	1.299	1.647	0.567	1.277
Participant 4	1.811	3.296	1.748	1.665	4.832	4.350	3.786
Participant 5	2.033	3.024	3.110	3.454	2.841	0.342	3.500
Participant 6	3.054	4.019	3.566	3.417	3.866	0.448	4.103
Participant 7	2.555	3.993	2.483	4.441	3.389	0.343	3.689
Participant 8	2.461	2.068	1.207	0.882	0.693	0.098	0.399

The mean blood flow in region 1 was about 2.283 ± 0.437 ml/min 100ml. When the venous occlusion occurred by inflating the cuff below the diastolic value, the average blood flow calculated in region 2 stood at 3.034 ± 0.938 ml/min 100ml, reflecting an increase of blood flow of approximately 33%. This rise could be attributed to a physiological response. It appears as if a vasodilation process allowed for the retention of extra blood in the venous circulation. However, study members 3 and 8 were outliers depicting a decrease in blood flow during this transition. After releasing the cuff's tension in region 3, the data portrayed a decrease in blood flow. Six out of eight of the participants witnessed a reduced flow rate

7.1 Quantification of the measurements of the devices

during this section of the experiment. The average blood flow for region 3 stood at nearly 2.409 ± 0.885 ml/min 100ml, equivalent to a 5.5 % difference with the initial baseline at region 1.

The change of blood flow between the baseline (region 3) and partial arterial occlusion (region 4) was not as apparent as the venous one. It can be seen that three out of eight participants did show an increase in their blood flow, whereas the others witnessed a slight decline. During the partial arterial occlusion, the average blood flow of all the participants increased from baseline in about 8.4 % to approximately 2.612 ± 1.266 ml/min 100ml. When the upper arm pressure was released in region 5, most of the participants were expected to experience a decline in their flow rate. However, this was not the case. At this stage, the average blood flow stood at 2.973 ± 1.293 ml/min 100ml, equivalent to an increment of 23 % from the baseline region 3. Three study members recorded a drop in their rate (5, 7 and 8) with an average of -0.618 ± 0.431 ml/min 100ml. The remaining members meanwhile showed a surge in their data of nearly 0.948 ± 1.263 ml/min 100ml. At this stage, it is not possible to draw a clear conclusion as to whether an arterial occlusion would indeed result in an increase or decrease of blood flow from the impedance measurement.

During the total occlusion, the APA amplitude was merely a fraction of the baseline waveform. Therefore, the ΔZ obtained to calculate the blood flow is a small number, which results in a low or null calculation. In this aspect of the analysis, most of the study members showed a decline in blood circulation rate close to zero. Table 7.1 makes it clear that nearly all participants posted a significant decline in their blood flow calculation when the brachial arterial constriction was applied in region 6, lowering the flow rate to nearly 0.3953 ± 0.1412 ml/min 100ml. Normally, one would expect the reading to show zero as no blood flow passed through the forearm. However, this could be due to an error of equipment measurement induced by noise which was picked up by the device. After the withdrawal of tourniquet, the blood flow recovered exponentially, portraying a fast return to the baseline accompanied by an overshoot peak and followed by the settlement towards a midpoint, as indicated by figure 7.2. This shape is typical of a hyperaemia where the return of blood flow produces such an overshoot response, owing to the rapid filling of the vessels. The mean blood flow in region 7 stood at about 2.892 ± 1.332 ml/min 100ml, which is very close to the original baseline region 5. At this stage, the sensitivity for the calculation of small changes in blood flow requires improvement because it detected flow values in other participants when there was an absence of plethysmography signal. However, it is quite remarkable that the instrument detected changes in trend.

7.1.3 Blood flow estimation from Doppler ultrasound instrument

As part of the procedure, a Doppler ultrasound was used to estimate blood flow using the radial artery in the wrist as a reference. The raw data produced by this instrument was in the form of volts, which was subsequently converted into more meaningful data using the equations 4.15 and 4.17 which convert this information into units litres per minute ($l \text{ min}^{-1}$). As described in these equations, the angle was fixed at 45° using a laboratory support and a clamp. The cross-sectional area for calculating the blood flow was the median value of [198]. The head of this ultrasound device was placed as close to the artery as described in the user manual, using a conductive gel as an interface between the skin and the device. When taking the last participant measurements, the Doppler ultrasound instrument had an electrical problem. Hence, it was not possible to collect the data from participant 8. The data presented in figure 7.3 and table 7.2 comprise of the results of the first seven participants.

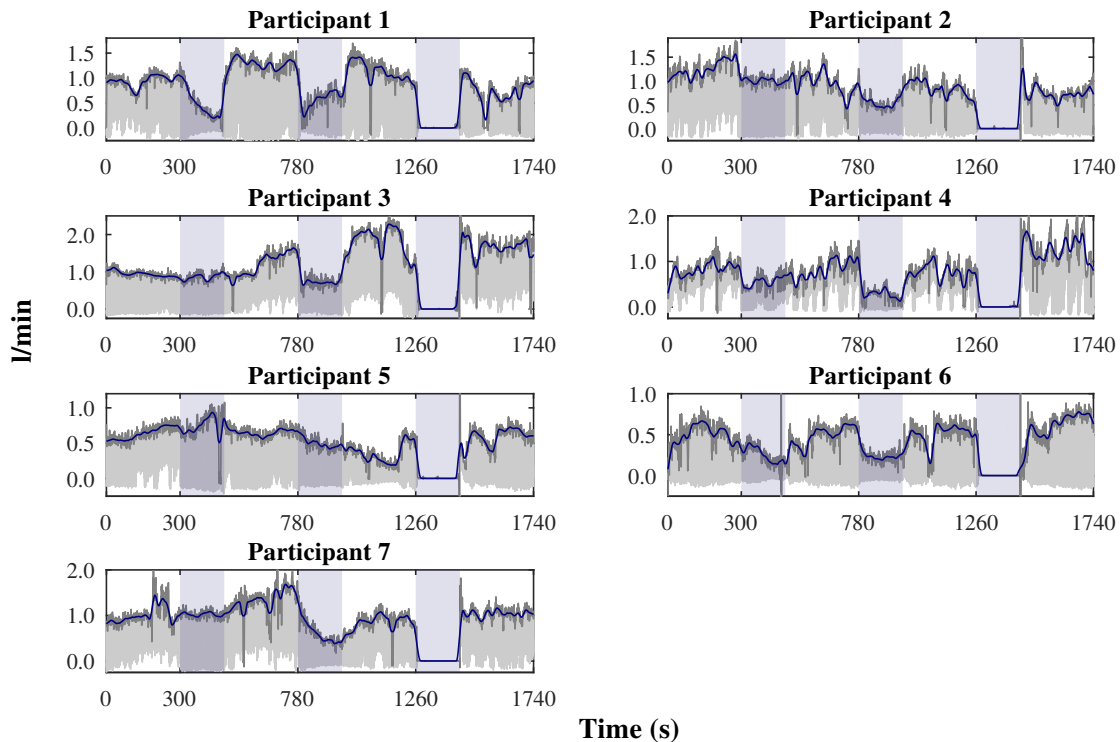


Figure 7.3 Blood flow calculated from the Doppler ultrasound measurements for all the participants during this experiment. The greyed out areas are indicative of the raw sign of the DU waveform whereas the dark blue lines represent the envelope calculated from the peak values. The data was converted into blood flow with units (l/min).

7.1.3.1 Blood flow estimation from Doppler Ultrasound instrument

Figure 7.3 shows the peak values of the Doppler ultrasound that were converted into the arterial flow rate. The shaded areas signify the occlusive events during the study. The measurements depict the blood flow of the radial artery and the changes occurring during each occlusive event. During venous occlusion, no significant change in arterial flow rate was expected since the brachial artery was not occluded higher than the diastolic pressure. On the other hand, a partial arterial occlusion between the diastolic and systolic pressure curbs the inflow of blood flow towards the radial artery. Finally, at the moment of occluding the brachial artery above the systolic pressure, null blood flow is likely to be displayed.

A qualitative analysis of DU data shows that various participants showed an alteration in their calculated median arterial flow during the venous occlusion in region 2. Whereas others experienced a rapid variation within the first few seconds, others took some time to show a resting point. Participant 1 evidenced an exponential flow rate drop during this aspect of the test. Further, participants 2 and 4 displayed a swift decline within the first few seconds followed by a settling at a mid-point. However, the remaining participants did not show a significant change in flow rate during this transition. Nevertheless, the quantified data showed in 7.2 demonstrated that during the transition between baseline regions 1 and 2, five out of seven participants witnessed a reduction in their median blood flow, being Participant 1 the most obvious among them with a drop of 52.41 % of the blood speed. The other ones who exhibited a slight decline were partakers 2,3,4 and 6 whose their blood flow was about 25.80 ± 18.50 %. On the other hand, participants 5 and 7 showed a slight surge in their calculated blood flow in 10.16 % and 6.25 %, respectively. Upon the release of the cuff's pressure, most participants showed a recovery within the detected blood flow. Only participants 2 and 5 exhibited a minimal decline.

During the partial arterial occlusion, the arterial blood flow changed unmistakably in all the participants. In this case, it is evident that the narrowing of the brachial artery curbed blood flow in the arm's arterial circulation, altering the flow rate speed that was detected by the DU. As shown by the figure, most participants exhibited a swift change of blood flow as soon as the constriction was applied, with the exception of participant 5. Generally speaking, the reduction of blood flow in the radial artery stood at around 48.79 ± 11.91 %. As soon as the flow was restored, majority of the participants witnessed a surge in their blood flow caused by a rush of blood within the arterial circulation passing through a quick inflow for a few seconds. However, participant 5 showed a different response which might have been caused by the misalignment of the sensor head.

Quantification and correlation of iPG, Doppler Ultrasound, LDF and PPG

Table 7.2 Mean blood flow calculated from the Doppler Ultrasound waveform during all the regions of the experiment.

	Region 1	Region 2	Region 3	Region 4	Region 5	Region 6	Region 7
				(l/min)			
Participant 1	0.954	0.430	1.285	0.618	1.049	0.003	0.719
Participant 2	1.211	1.014	0.967	0.546	0.843	0.002	0.712
Participant 3	0.928	0.860	1.307	0.716	1.940	0.002	1.675
Participant 4	0.826	0.581	0.764	0.297	0.754	0.002	1.245
Participant 5	0.643	0.708	0.655	0.483	0.348	0.003	0.606
Participant 6	0.495	0.248	0.499	0.230	0.542	0.002	0.641
Participant 7	0.962	1.022	1.320	0.535	0.876	0.002	1.040

Finally, the tourniquet effect can be noticed in the composition of the signal all along the total occlusion with a sharp decline as soon as the occlusion took place. As expected, no arterial flow was recorded; the minimum values might signify the artefacts in the signals. After releasing the tourniquet, all participants experienced a surge in their flow rate to values of normality.

7.1.4 Measurements from Laser Doppler Flowmetry

The LDF device provided raw data in Volts which was subsequently converted into BPU units. This conversion was made possible by applying equation 4.18 to the collected data. As explained in section 4.3.1.4, it resulted in an arbitrary unit, which denotes the movement of blood cell beneath the skin's micro-circulatory bed. This unit called BPU refers to the product of the mean number of moving blood cells into the small volume under the probe and the average velocity of moving red blood cells in the forearm. Converting the raw data to BPU unit could be done using the equation 4.18.

Figure 7.4 shows the peaks of the LDF waveform signal in BPU. The grey points are the measurements' raw data. The purple line in this figure represents the smoothed signal averaged per heartbeat. The boxed areas describe the data portions where these occlusions occurred. This plot shows that evidently, the movement of blood cells is affected when an occlusion occurs. Indeed, there is a diminution of the magnitude of signal during each flow restriction. During the course of experiment, the LDF signal was very susceptible to noises; this explains the rationale behind massive peaks witnessed during some of the measurements. In particular, participants 1 and 3 showed a significant number of high peaks. From the qualitative viewpoint, the strong impact on some parts of the data is evident, such as in participants 1 and 4.

7.1 Quantification of the measurements of the devices

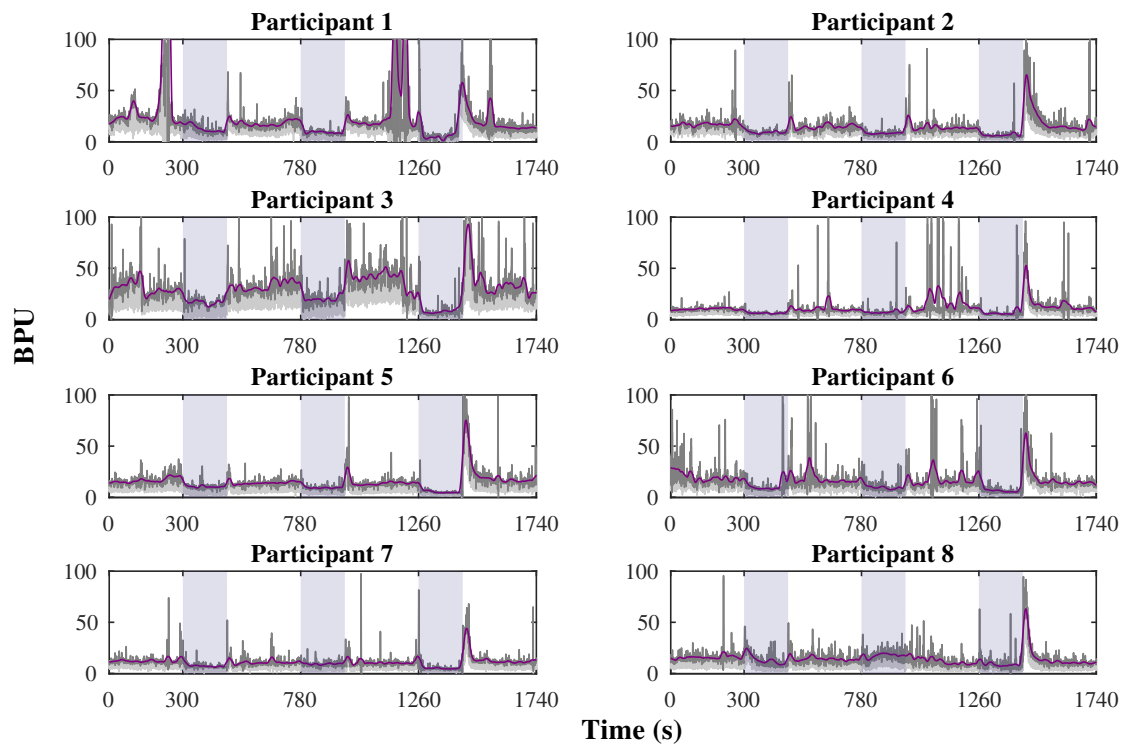


Figure 7.4 Results of the Laser Doppler Flowmetry measurement for all the participants after being converted to BPU. The values presented in purple are equivalent to envelope signal of the peak points.

Nevertheless, a trend is noticeable in all the participants. During the occlusions, a drop in the red blood cell movement was noticed. It seems that the blockage of venous return in regions 3 and 5 slowed down the movement of RBC in the capillaries. Additionally, during total occlusion, the amplitude reaches its lower values. After the restoration of blood flow, the RBC movement depicted a Gaussian bell shape peak throughout most participants. This hyperaemic effect shows an acceleration of blood cells following the blockage event. While this acceleration is evident in every occlusion, it varies in magnitude with each occlusion. The BPU magnitude is clearly larger on in all participants following the total occlusion. In comparison, two other occlusions created a smaller Gaussian shape as a response where the one that ensued after the partial arterial appears to be slightly bigger. Nevertheless, participant 8 seems to be an exception to this rule. The BPU measurements increased only slightly during the transition from region 3 to 4. Also, in contrast to the other participant's waveforms in the transition from partial arterial occlusion to the baseline in region 5, his mean BPU dropped. The results obtained from this participant could also explain some of the adverse readings that were captured by the iPG signals.

Quantification and correlation of iPG, Doppler Ultrasound, LDF and PPG

Lastly, during total occlusion, all the mean BPUs of the participants reduced significantly. At a subsequent stage when the tourniquet was released, the rush of blood flow is evident in the hyperaemic effect registered by the instrument, which was also detected by other instruments. Table 7.3 reviews the values of the mean BPU data. These results are in absolute harmony with the figure that was previously analysed.

Table 7.3 Media perfusion index (flux) calculated from the LDF data for all the regions during the experiment.

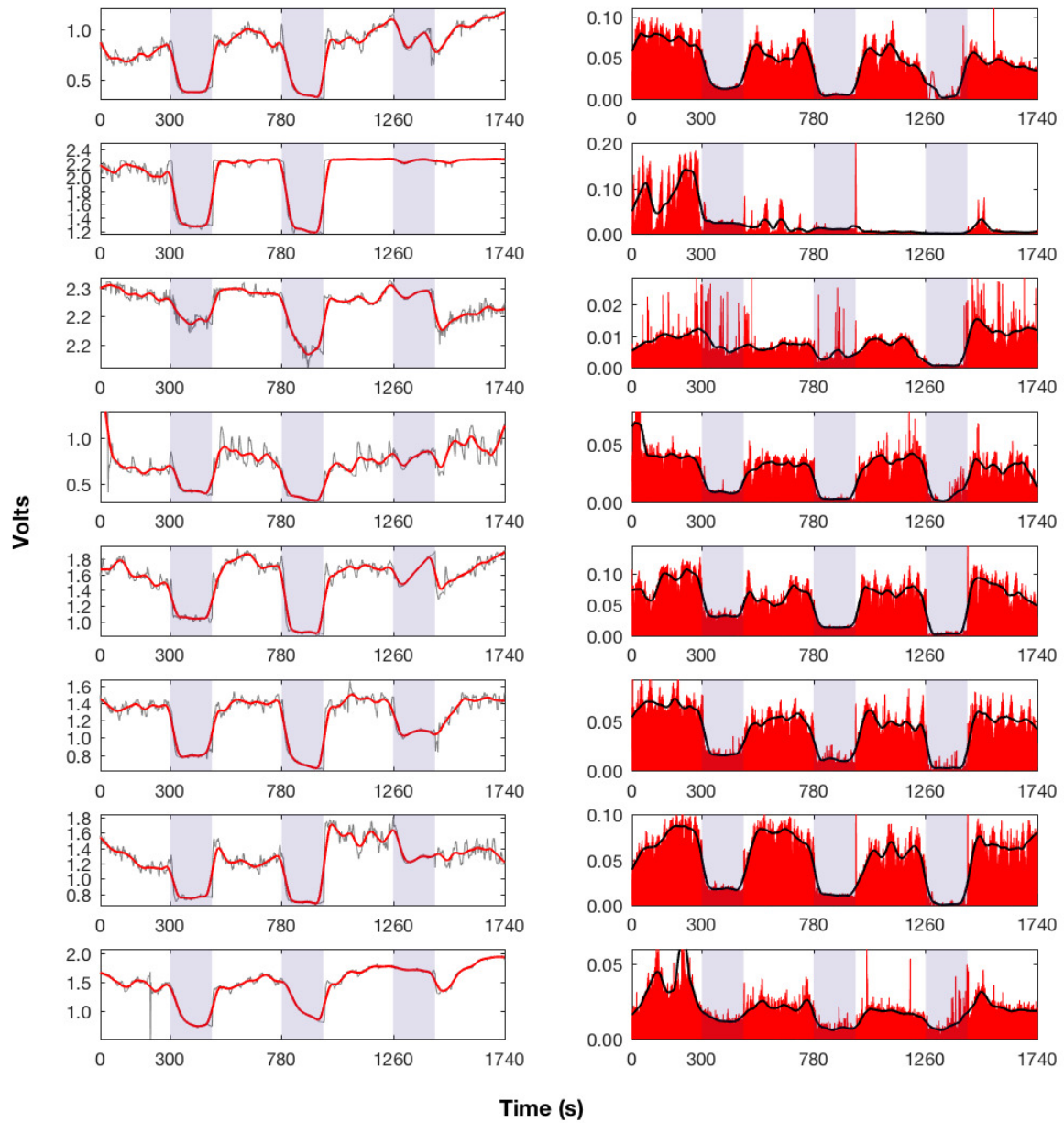
	Region 1	Region 2	Region 3	Region 4 (BPU)	Region 5	Region 6	Region 7
Participant 1	23.65	11.59	17.20	9.20	19.81	5.16	14.60
Participant 2	16.88	9.10	14.44	8.19	13.17	6.07	14.83
Participant 3	29.46	17.43	32.86	19.76	41.80	7.83	33.87
Participant 4	9.81	6.14	9.53	6.99	14.11	5.94	12.19
Participant 5	15.56	10.35	13.85	9.28	14.02	4.73	18.03
Participant 6	18.66	8.80	16.03	9.56	15.06	6.60	14.56
Participant 7	11.96	7.25	10.37	9.51	10.24	5.08	11.91
Participant 8	15.54	12.40	13.85	17.93	12.29	8.40	10.97

7.1.5 Measurements from the PPG Red-light signal

The photoplethysmographic device provided key information about the change of volume within the vascular bed underneath the skin. It is capable of detecting venous or arterial blood change in accordance to the light wavelength [210]. The finger probe used throughout the experiment comprised of red and infrared sensors. Nevertheless, the red-light information was collected because it was more sensitive to the changes made in the venous blood. The device employed in this experiment has an output port that provides the unprocessed raw photoplethysmography waveform. Similarly, as is evident in the iPG signal, the PPG comprises of DC and AC components. The DC portion of this signal is equivalent to the blood volume noted under the light beam. Moreover, it contains data about the respiratory rate in addition to other physiological information, which is not necessary for this experimental setting. On the contrary, the magnitude of AC component changes synchronously with the cardiac cycle and blood volume under the capillaries.

The raw signal displayed in figure 7.5 reveals the DC (left side) and the AC (right side) components of all the participants. Additionally, within the plot, the shaded regions are indicative of each occlusive event during the experiment. The DC component of the signal was obtained by decoding the bottom values that envelope the raw PPG waveform. In other words, these are points on the foot of the waveform. In addition, the AC component of

7.1 Quantification of the measurements of the devices



(a) DC component of the PPG waveform for each of the participants
 (b) AC component of the PPG waveform for each of the participants

Figure 7.5 PPG measurements using the red spectrum. The plots show the DC and AC components of the waveform. The shaded areas represent the occlusion events during the venous occlusion (region 2), partial arterial occlusion (region 4) and total occlusion (region 6))

Quantification and correlation of iPG, Doppler Ultrasound, LDF and PPG

this signal was obtained by subtracting the low envelope of the raw data. Furthermore, the resultant waveform was inverted to permit only the dynamic element of the signal. Lastly, the peaks detected from the plethysmography waveform were redrawn in black, thus highlighting the peak values during all the occlusive events.

7.1.5.1 Changes in the DC component of the signal

After analysing the DC signal, it can be seen from the figure that all participants showed a definite decline in their DC components during venous occlusion (region 2) and partial arterial occlusion (region 4). It illustrates that the DC value reduced dramatically in most participants following the occlusive event. Nevertheless, some participants displayed an exponential drop in their recordings, as shown in participants 3 and 8 during both occlusive events.

The visible changes of the DC value is confirmed when analysing the mean values of the DC data presented in Table 7.4. From there on, the calculated average baseline prior to the occlusions were 1.44 ± 0.55 V for Region 1 and 1.51 ± 0.54 V for Region 3. In contrast, the DC components dropped about 0.435 ± 0.210 mV and 0.528 ± 0.247 mV during the occlusive transitions for region 2 and region 4, respectively. When comparing the DC values between both events, it can be seen that difference between the two is not significant - only 4.47%. Nevertheless, during total occlusion, the signals were erratic with no definite shape or direction. Some participants did exhibit a slight decline, but others did not display significant changes. In general, the DC data provided valuable information during the venous and partial arterial occlusion, but no conclusive results could be observed when the blood flow stopped altogether.

Table 7.4 Mean peak value of the PPG DC signal for all the participants in all the regions.

	Region 1	Region 2	Region 3	Region 4	Region 5	Region 6	Region 7
				(V)			
Participant 1	0.75	0.44	0.91	0.43	0.94	0.91	1.03
Participant 2	2.09	1.38	2.22	1.33	2.25	2.24	2.24
Participant 3	2.24	2.20	2.24	2.16	2.23	2.24	2.20
Participant 4	0.76	0.46	0.80	0.36	0.72	0.79	0.89
Participant 5	1.60	1.07	1.73	0.93	1.66	1.64	1.64
Participant 6	1.36	0.84	1.38	0.76	1.41	1.08	1.35
Participant 7	1.26	0.79	1.25	0.75	1.56	1.32	1.34
Participant 8	1.48	0.88	1.48	1.07	1.64	1.71	1.70

7.1 Quantification of the measurements of the devices

7.1.5.2 Changes in the AC component of the signal

The AC component also produced a notable swing of magnitude during each blockage event. When compared to the DC, the AC signal not only changed its amplitude all along the venous and partial arterial occlusion, but also during the total occlusion, where it reached its minimum magnitude which is consistent with the fact that no change of volume is evident at that precise instant. Reviewing the AC signals qualitatively, participants 2, 3 and 5 exhibited low-quality waveforms since amplitudes were quite close to noise levels (amplitude < 10 mV). Participant 2 registered noisy waveforms during region 1 of the study and small magnitudes for the remainder of this experiment. Participant 3 meanwhile exhibited low signal amplitude and over peaks during the entire test, although the changes through each occlusion continue to be visible.

From the numeric point of view, Table 7.5 shows the average values of the amplitude in mV. During all baseline measurements (regions 1, 3, 5 and 7), the mean peak value stood at 436.41 ± 110.81 mV. However, it is evident that the overshooting displayed considerably higher values than the mean.

In general, during venous occlusion, the signal amplitude dropped in all the experiment members in around 422.97 ± 212.17 mV. However, participant 3 was an outlier showing the smallest change (24.50 mV) in comparison to the remaining signals. It seems that the poor-quality signal ended up affecting the entire measurement. After the cuff's pressure was released during the transition from venous occlusion to baseline, participants 2 and 3 witnessed a decline in their mean amplitude. Yet again, their poor signal quality caused them to show conclusive measurements. The rest of the partakers recorded a recovery in their peak signal to a peak of nearly 221.28 ± 211.24 mV.

Table 7.5 Mean peak value of the PPG AC signal for all the participants in all the regions.

	Region 1	Region 2	Region 3	Region 4 (mV)	Region 5	Region 6	Region 7
Participant 1	724.83	180.45	546.76	66.13	490.87	109.85	441.54
Participant 2	926.02	245.24	158.34	110.32	51.30	5.97	92.58
Participant 3	94.21	69.72	68.76	37.19	71.62	10.54	122.67
Participant 4	436.74	92.42	315.26	37.22	354.44	58.08	296.36
Participant 5	873.38	324.60	638.53	155.21	703.81	51.36	751.62
Participant 6	658.05	188.75	501.10	112.57	480.41	38.14	517.01
Participant 7	731.50	190.43	746.34	125.76	547.89	26.92	660.43
Participant 8	360.69	130.06	216.80	74.43	168.52	89.77	217.06

Quantification and correlation of iPG, Doppler Ultrasound, LDF and PPG

During partial arterial occlusion in region 4, this device detected the physiological response. In this case, all participants witnessed a drop in their mean PPG signals amplitude of an average of 309.14 ± 219.43 mV. When comparing the mean values during occlusions in region 2 and 4, the signal amplitude in region 4 was slightly lower than the one in region 2 by close to 87.86 ± 46.91 mV, which is the difference between both circulatory occlusions 49.75 %.

Finally, throughout the total occlusion, all participants exhibited a substantial reduction in their AC amplitudes. This was expected due to the absence of blood flow within the vessels. In entirety, the signals went below 109 mV with an average value of 48.83 ± 36.62 mV. In fact, this confirms that the measurements taken from participants 3 were below this level.

In conclusion, the PPG waveform witnessed changes of DC and AC components during all the occlusions conducted throughout the study. The DC signal successfully detected changes during both venous and partial arterial occlusions. The difference of their mean DC values during these two events was minimal at only 4.47 %. Furthermore, during total occlusion, no noticeable change in DC value of the signal was observed. On the other hand, the AC component effectively distinguished between venous and partial occlusion. The difference between these two regions stood at about 50 %. Moreover, the signal lost most of its magnitude during total occlusion due to inadequate blood flow.

7.2 Correlations of the iPG amplitude wave and Doppler ultrasound, PPG and LDF

In this section, the correlation between iPG and the other techniques will be analysed. An analysis in the frequency domain will be shown, identifying the similarities between measurements and noise levels. The Bland et al. [211] method was used to analyse the correlation of the measurements comparing the normalised data magnitude between modalities.

The endeavour of this investigation is to understand the contributing factors of the potential impedance plethysmography signal. As explained in previous chapters, the change of volume in the forearm section allowed the estimation of blood flow. However, both arterial and venous blood contributes to the information of blood flow that was calculated by the iPG device. The extent of blood flow belonging to any blood type remains ambiguous. Besides, it was evident that the main blood vessels contribute to the measurement of blood flow, although microcirculation might also be able to provide additional information under the iPG waveform.

7.2.1 Analysis of the heartbeat detection in the frequency domain

The signals obtained from each device throughout the experiment are synchronous with the heartbeat. Due to this synchronisation, the systolic peak is also present in the waveform of these instruments in their dynamic component.

Nonetheless, some noises do have a negative impact on the proper detection of systolic peaks carried out during the study. The designed algorithm can detect the shape of the waveform by finding the signal's foot and peaks. Nevertheless, some of its peaks might be missing due to the noise levels.

A Fast Fourier Transform was used to detect the waveforms' main harmonic in a random window data set. The data was selected between 580 s to 780 s for the AC components only, hence the data from Z_{AC} channel. The algorithm was programmed to detect the frequency peak (f_p) from 0.85 Hz to 1.75 Hz. Meanwhile the FFT was limited to detect the frequencies between 0 Hz to 5 Hz owing to the filters applied to the waveforms, as explained in section 4.1.2.6.

From Figure 7.6 the frequency components from all the participants' measurements can be seen. The ECG plots illustrate the frequency response that is typical of such a signal. Some signals presented a high level of high-frequency components such as the ones witnessed in participants 1 and 8. Participant 3 illustrated a high 2 Hz harmonic peak whose power was greater than the first harmonic. This response seems odd, but by examining the waveform in detail, it showed a lower Q wave which might influence the abnormal frequency component presented in the graph.

The iPG device had a mixed frequency response to detect the cardiac heartbeat. As can be seen from the shown plots, some signals exhibit a low-frequency noise which, in some cases, is bigger than the first expected harmonic. For instance, participants 1, 3, 4 and 6 found it difficult to detect the frequency peak related to the cardiac cycle for this particular data set. However, the remainder of partakers registered a frequency peak at a similar heartbeat like the ECG.

PPG frequency components were quite evident in all participants. Some of them showed a high-frequency noise, such as participant 8. However, this signal generally shows low signal to noise ratio in comparison to iPG, which is understandable, as the PPG-AC is significantly bigger than the iPG-AC amplitude.

Lastly, DU exhibited clear FFT components in most participants. Only Participant 1 demonstrated a high noise component in his measurements; the rest showed a response that was similar to the ECG.

Quantification and correlation of iPG, Doppler Ultrasound, LDF and PPG

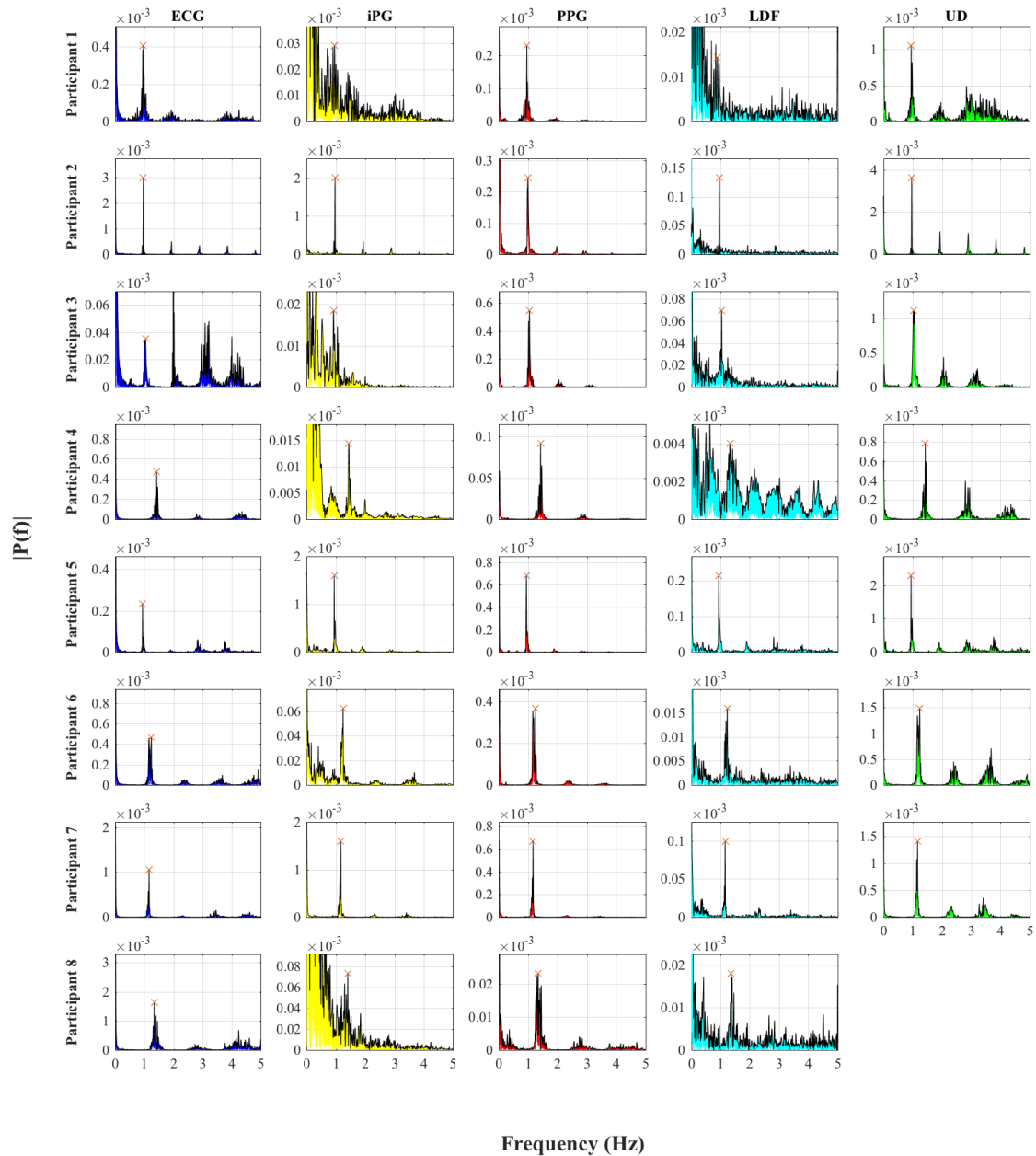


Figure 7.6 Fast Fourier transform for all the measurements in the study. Any DC level was removed previous the FFT. The main harmonic represents the heart frequency. The data range corresponds to the time between 580 s to 780 s for the AC components at the measurements.

7.2 Correlations of the iPG amplitude wave and Doppler ultrasound, PPG and LDF

Table 7.6 demonstrates how close the cardiac frequency is to each instrument. However, the iPG mean harmonic and frequency distribution from participant 8 clearly shows that his data was not clean.

Table 7.6 Cardiac frequency obtained from the Fast Fourier Transform for each of the instruments used during the experiment. This peak corresponds to the one with in the hearth cycle in the study ($0.5 \text{ Hz} < f_p < 1.5 \text{ Hz}$)

	ECG	iPG	PPG	LDF	DU
	$(f_p \text{ [Hz]})$				
Participant 1	0.967	0.952	0.949	0.897	0.949
Participant 2	0.964	0.964	0.989	0.964	0.964
Participant 3	1.041	0.916	1.041	1.038	1.019
Participant 4	1.425	1.437	1.422	1.321	1.425
Participant 5	0.940	0.940	0.937	0.940	0.940
Participant 6	1.239	1.242	1.242	1.233	1.239
Participant 7	1.163	1.163	1.163	1.163	1.163
Participant 8	1.346	1.401	1.337	1.367	N/A

7.2.2 Correlation between iPG and Doppler ultrasound

The Chapter 6 showed how the waveforms obtained during the course of this experiment changed in amplitude at each occlusive event. By observing the equation 4.15 from the Doppler ultrasound section, it can be surmised that the velocity (v) is directly proportional to the Doppler frequency (f_D). The remaining terms can be assumed as constant. Subsequently, the same rule holds true when this velocity is converted into blood flow. Equally, the blood flow calculated from this iPG device with equation 4.23 signifies a function of R_B that is directly proportional to the impedance waveform's amplitude at the point $L1$ (see figure 6.1) as illustrated by equation 4.19. In other words, the magnitude of both these measurements alters in accordance to the blood flow.

However, the Doppler ultrasound is solely focused on arterial flow over the blood vessel under observation. Instead, iPG records the changes in flow of both arterial and venous circulation in the volume segment under test. Notably, both devices measure blood flow, albeit in a different manner. The Doppler ultrasound requires precision when placing the instrument's head on the patient's skin. The best signal is obtained when the device is kept exactly over the blood vessel. Hence, the clarity is predicated on the operator's skills to maintain a constant angle and always over the artery. During the course of the experiment, this procedure was replicated using laboratory instruments, keeping angle and skin contact constant. However, using this set-up does not counter rest the participant's arm movement,

Quantification and correlation of iPG, Doppler Ultrasound, LDF and PPG

which causes a misalignment of the sensor. Consequently, the amplitude of this ultrasound signal is not as steady as one might expect.

As was observed in section 7.2.1 the AC components of the iPG device are not clean of noise among all partakers. In fact, participant 2, 5, 6 and 7 showed the best signals to work with. For this reason, the waveforms from these partakers were used when performing the correlation between both instruments.

Figure 7.7 shows the correlation between iPG and DU. The data range corresponds to the entire duration of the experiment and includes the changes of blood flow caused by the occlusions. In the plot, this data was discriminated with a different marker point and colour in accordance to every event during the test. It can be noted that odd regions are baselines, and even regions are blockages. The data was normalised and referenced to the highest peak of the total data set. Each systolic peak detected from the iPG waveform was used to find the corresponding Doppler ultrasound systolic peak around the same segment of time. Subsequently, the iPG and DU data sets were smoothed by calculating the mean value of every 20 peaks detected within a non-cumulative average.

The method for analysing the correlation of both measurements was proposed by Bland et al. [211]. It allows for the comparison of a traditional technique with a new method. Hence, it is ideal to compare the measurements between DU and the designed device. This technique is mostly used to compare similar unit measurements. For this reason, the data were normalised. Therefore, the comparison will be made on the change of magnitude undertaken between both modalities.

On the left side of the plot, the result of the linear regression between both waveforms can be seen. At a certain degree, the data trend is off the line of equity (dotted line), implying that there is no perfect agreement between the two methods concerning their amplitudes. As a matter of fact, this graph shows the linear correlation between both signals with a coefficient correlation of $r^2 = 0.35$ to confirm a link between both signals. However, there is an absence of perfect alignment of the reference signal's (DU) variability alongside the y-axes.

Analysing region by region illustrates how the data points were distributed along the correlation graph. For instance, there seems to be a good data distribution in both axes throughout regions 1 and 2. It is evident that both waveforms amplitudes spread quite uniformly. Region 1 appears to be closer to the line of equity than region 2 when venous occlusion took place. Apparently, the magnitude of DU signal did not change when compared to the iPG's ones. Undeniably, the impedance plethysmography device detected changes that could not be noticed by DU, which is in agreement as the venous occlusion does not alter the arterial flow.

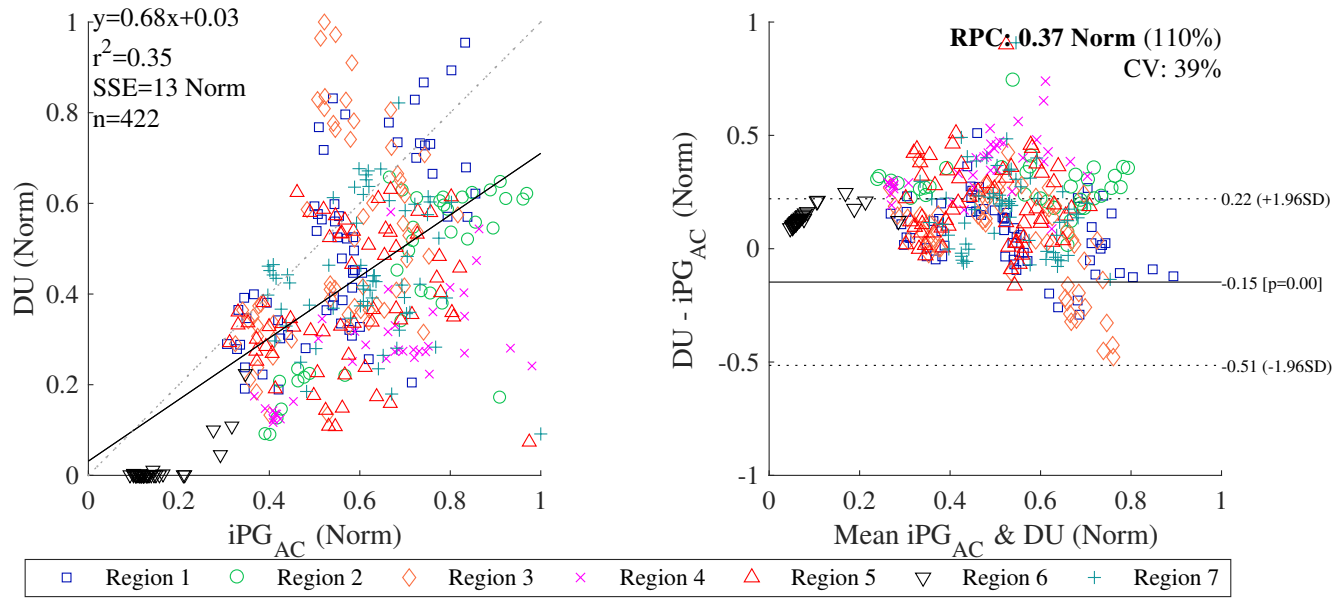


Figure 7.7 Bland and Altman [211] plot of the relation between Doppler ultrasound and iPG. Data set corresponds to participants 2, 5, 6 and 7. The data has been normalised comparing the amplitude of both measurements. The different regions have been plotted with various colours and symbols to differentiate every event. The dotted line represents the perfect agreement; the dark line is the linear regression.

Quantification and correlation of iPG, Doppler Ultrasound, LDF and PPG

However, region 3 shows a bigger distribution of data points (than iPG) adjacent to y-axes. It is possible that the participants' movements caused this significant variation of the DU amplitude. By reviewing the envelope of signal illustrated in figure 7.3 it can be seen that Participant 7 showed the largest waveform amplitudes; this can also be confirmed in the mean blood flow computed on the same region. In fact, the linear regression improves to $r^2 = 0.45$ when the data was run without this participant.

Region 4 demonstrates a similar behaviour as region 2; there is a good amount of data distribution, but the iPG amplitude changes more than the DU. Notably, there is a greater concentration of data points in the lower region of both axes. However, this is expected as there is a reduction of arterial blood during this event. The higher data points towards the iPG axes pertain to the blood flow rush towards the beginning of the occlusion on participant 7, which is illustrated in 7.2.

Region 5 shows a higher distribution of the data adjacent to the iPG axes. On the other hand, some data points on the lower part of the DU axes impact the linear regression in this region. During total occlusion occurring in region 6, the DU device witnesses a better response. Here, a significant number of the Doppler's ultrasound data points are set to zero, whereas the data from iPG is mostly distributed among 0 and 0.2. Finally, region 7 exhibits a good distribution that is adjacent to the line of equity, which is in congruity with some of the other baseline behaviours.

The plot on the right side of figure 7.7 shows the precision between the estimated limits of agreement of the experiment. On the y-axes, the mean difference between the two measurements and the points of its standard deviation is plotted. The differences have normally been distributed in a Gaussian space. Hence, 95 % confidence interval of the difference should be located between $\pm 1.96SD$. This graph shows a high number of points out of $+1.96SD$. However, it can be seen that values from regions 2 and 4 are outside of the agreement region. This confirms that when an occlusion occurs, there is a different response between iPG and DU.

7.2.3 Correlation between iPG and PPG

The correlation between iPG and PPG was also investigated when looking for amplitude similarities between both signals during the occlusive events. In a similar manner, the method used in the previous chapter was used here as well in order to analyse the change of magnitude between both AC waveforms. The two signals represent the changes of volume within a part of the body, PPG in the finger and iPG in the forearm. Although the PPG reflects blood movement within the blood vessels beneath the skin in a not so well-defined volume [39],

7.2 Correlations of the iPG amplitude wave and Doppler ultrasound, PPG and LDF

iPG provides crucial information about the change of volume by the blood vessels being filled with blood but limited by the sensing electrodes.

However, the PPG method used in this study was very simplistic when compared to more sophisticated methods that may be able to detect the changes in venous and arterial flow using other wavelengths, sensor placement, or data interpretations. The correlational study of this section looks to decipher the changes in amplitude among AC components of both signals. As detailed in previous chapters, both signals illustrated changes within their DC components for the time that they were occluded. However, the AC component of both signals changed oppositely. While there was a magnitude increment in the iPG waveform all along the occlusions (see figure 7.2), the PPG waveform (see figure 7.5) witnessed a decline in amplitude during these events.

As shown in figure 7.2 participant 2 displayed abnormal AC amplitudes during the time of this experiment. Also, detailed in the previous section, participants 2, 5, 6 and 7 showed a better AC response. It is for this reason that the data of participant 2 was excluded from the correlation between these two waveforms. The data sets were smoothed by calculating the mean value of every 20 peaks in a non-moving average.

The Bland et al. [211] statistical analysis was also implemented in this study. Figure 7.8 shows the correlation between iPG and PPG magnitudes. The chart on the left shows the absence of a perfect correlation during the study, which was expected because the signal's amplitude goes in opposite directions all along the venous and arterial occlusions. Notably, the graph shows a poor linear correlation between both signals with an $r^2 = 0.07$.

Most of the baseline data points (regions 1,3,5 and 7) are closer to the line of equity. In fact, if the venous and arterial occlusive events were removed, there would be a significant improvement in the correlation between both measurements ($r^2 = 0.40$). By analysing the results of this graph, it can be confirmed that the iPG magnitude changed significantly while PPG's amplitude reduced during the course of venous and arterial occlusions. It is also verified that the PPG amplitude all along the arterial blockage is lower than venous occlusion, as illustrated by the data points in the figure. On the other hand, there was a similar response to both signals at the time of total occlusion, and the absence of blood flow translated into small amplitude values. The PPG data points were closer to zero in comparison to the iPG magnitudes that were closer to 0.1.

The BA (Bland and Altman) plot on the left side of figure 7.8 illustrates greater precision at the time of these baseline readings. Most of the data points are within the 95 % confidence interval ($\pm 1.96SD$), while the measurements taken during occlusion were mostly outliers.

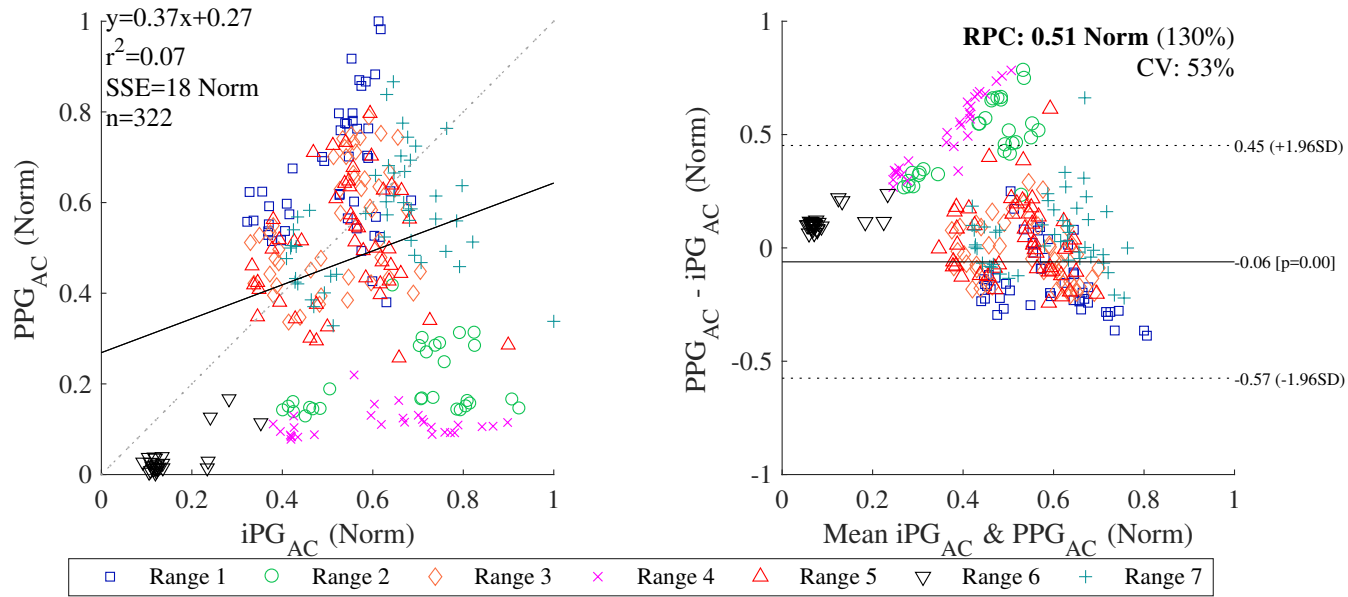


Figure 7.8 Bland and Altman [211] plot of the relation between PPG and iPG. Data set corresponds to participants 5, 6 and 7. The data was normalised comparing the amplitude of both measurements. The different regions have been plotted with various colours and symbols to differentiate every event. The dotted line represents the perfect agreement, and the dark line is the linear regression.

7.2.4 Correlation between iPG and LDF

The signal from the LDF device provides information about the flow movement of red blood cells within the microvascular network under the skin. However, a weak correlation between measurements is not surprising because data errors in this instrument have been widely documented, especially at low blood flow [212]. Another shortcoming of this technique is that it is unclear whether the measurements belong to a venous or arterial blood, although some peaks seem in sync with the cardiac cycle. However, this is expected as the movement of RBCs occurs during the systolic peak.

The position of this LDF sensor head helps understand the blood flow under microvascular bed beneath the forearm. In there, it is possible to monitor microvessels like terminal arterioles, metarterioles, capillaries, and venules. As described in section 4.2.1, the sensor was placed on the forearm midpoint between the iPG's sensing electrodes but it is not possible to assert with certainty the kind of blood being monitored, only the movement of RBCs in that section of the skin.

The signal coming from the LDF device is similar to a plethysmography wave, which is formed by the AC component on a DC signal. For the purpose of a correlation analysis of this study, the DC component of this signal had to be removed, which only left the comparison between of normalised AC magnitudes of the LDF and iPG signals. Similarly, as evidenced in the previous analysis, the data was smoothed by taking the average value of 20 data points. Due to the high level of noise of the signal in some participants, the data depicted in this analysis belongs to participants 2, 5, 6 and 7.

Figure 7.9 illustrates the linear regression and BA analysis between both signals. Notably, the data points show a poor correlation among both signals ($r^2 = 0.08$). Most data points are far from the line of equity and mostly spread across the plot x-axis. The data points from this LDF signal are not well scattered around the figure. This imbalance can mostly be noticed in the region 7. One plausible explanation of this effect is that the LDF peak extension is impacted by the hyperaemic effect upon the release of total occlusion, as can be seen in figure 7.4. Nonetheless, if this portion of the data were removed from the plot, there would still be a weak agreement between both signals ($r^2 = 0.08$).

Based on the BA chart, on the left can be observed poor linear correlation between both normalised signals. On the right side of the figure, a poor accuracy is observed when comparing the amplitude of both signals. Practically, all the data points are outside the confidence area ($\pm 1.96SD$). Therefore, it is not possible to establish any relation within the magnitude waveform of these two instruments.

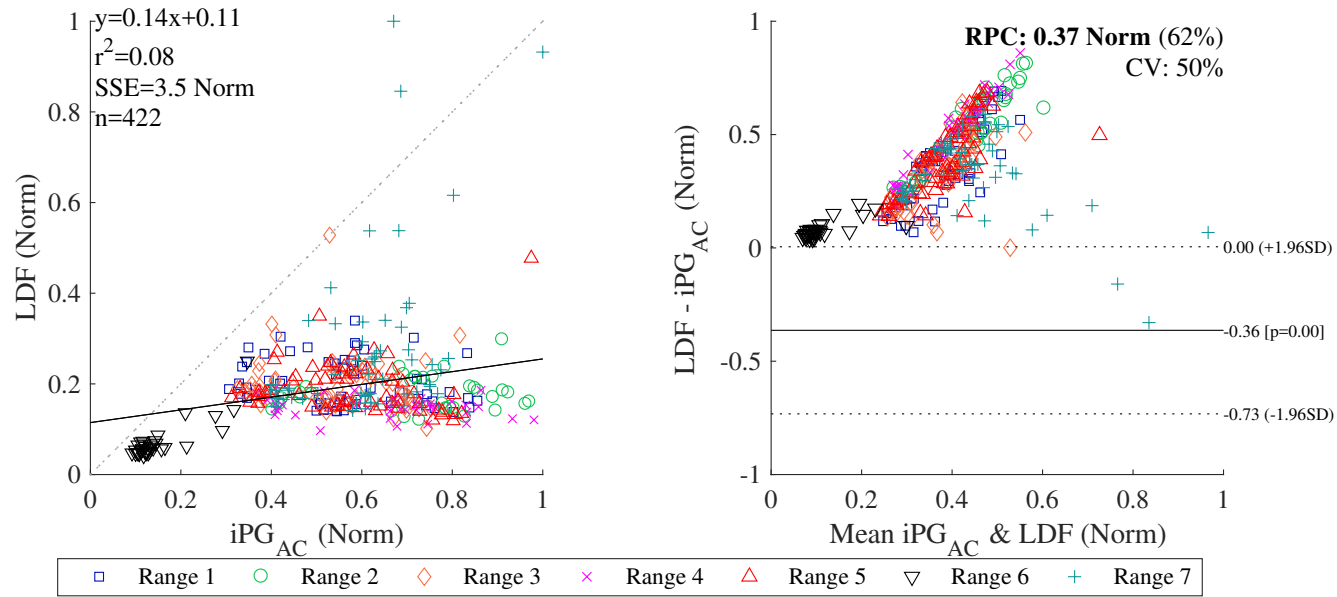


Figure 7.9 Bland and Altman [211] plot of the relation between LDF and iPG. Data set corresponds to participants 2, 5, 6 and 7. The data was normalised when comparing the amplitude of both measurements. The different regions have been plotted with various colours and symbols to differentiate every single event. The dotted line represents the perfect agreement, and the dark line signifies the linear regression.

7.3 Summary of the changes and correlations

The information presented in this chapter showed the changes in the clinical numeric values of the different instruments used in the experiment. As the table 7.7 shows, all the instruments were able to distinguish changes during venous occlusion, partial arterial and total occlusion. This table indicates the percentile change between baseline and the following circulatory occlusion, from the quantified value in clinical units.

Interestingly, the blood flow calculated from the iPG signal showed dramatic changes throughout venous and partial arterial occlusions. For instance, during venous occlusion, the iPG signal showed an increment in the estimated blood flow, which may be related to the pooling effect of blood. Once again, during partial arterial occlusion, the blood flow calculated from the iPG signal also surged but on a smaller scale. Which, it suggests a differentiator between both type of occlusions. In contrast, all the other instruments illustrated a decrease in all their measure units.

It is noticeable the change of values obtained from the other instruments. The Doppler Ultrasound monitoring arterial blood flow perceived some restriction during venous occlusion but effectively detected changes while partial arterial occlusion. The correlation between Doppler and iPG suggests that the latter follows the arterial pulses during normal conditions but the behaviour changes through occlusive periods. The optical methods also distinguished changes in the course of venous and partial arterial occlusion. However, the settling values between both occlusions are quite tight together, making it hard to identify variation values between both occlusions.

One common point between all the instruments is the severe reduction of quantifiable data during total occlusion. The Doppler ultrasound unquestionably showed nearly zero flow, followed by PPG and iPG values. However, the LDF performed a bit poorly as the readings were close to the ones during occlusive periods.

Table 7.7 Summary of the comparison between the changes of blood flow calculated from the iPG data, the arterial flow from the Doppler modality, flux from LDU and volts from the PPG.

Method	Venous Occlusion Region 1-2	Partial arterial occlusion Region 3-4	Total occlusion Region 5-6	Corr
iPG APA	32.84%	8.43%	-70.58%	
DU	-19.21%	-49.61%	-99.75%	$r^2 = 0.35$
LDF	-41.31%	-29.43%	-64.55%	$r^2 = 0.08$
PPG AC	-70.42%	-77.48%	-86.38%	$r^2 = 0.07$

7.4 Conclusion

This chapter described all the instrument's waveform changes during the entire experiment and their correlation with the iPG APA signal. The devices used in the experiment evinced a different signal response following the technology used by each one of them. The data obtained from these devices (except PPG) was converted into meaningful clinical units to decipher the changes occurring in circulatory occlusion.

In general, the impedance APA waveform in units of blood flow showed apparent amplitude changes characteristic of each occlusion. During venous occlusion in region 2, the blood rate increased by nearly 33 % when compared to the previous baseline in region 1. In contrast, during partial arterial occlusion, the calculated flow rate increased 8.4 % (on average) in region 4. While the blood flow was expected to reduce as the normal artery flow got restricted, the impedimetric measurement presented a slight surge in blood flow. In both cases, it appears as if the rise in blood flow might be attributed to a vasodilation response where the forearm veins' cross-sectional area got enlarged, which allowed for blood pooling. The extra blood flowing into the expanded vein may be viewed as a surge in the blood flow rate.

The other methods also detected changes in the arterial and venous circulation. The Doppler Ultrasound instrument perceived arterial flow changes during both partial arterial and total occlusion. The arterial blood rate reduced to nearly 48.79 ± 11.91 % throughout partial arterial occlusion, and practically zero in the course of complete obstruction. However, any miss-aligning between the device's head and the vessel would introduce errors to the measure.

The optical methods yielded data about the venous circulation. The LDF provided details of the blood cells moving into the capillary bed, whereas the PPG in the red spectrum correlated to the venous circulation. The LDF amplitude average signal displayed changes during each occlusion. However, the high level of noise avoided identifying common trends changes in all the participants. Regarding PPG, the DC component of the signal showed no apparent distinction between venous and partial arterial occlusion (4.47 % voltage difference). However, the AC signal showed a clear difference between both type of blockage with an amplitude change of nearly 50 %.

The data correlation between the iPG arterial pulses and other instruments helps us understand the kinds of blood that significantly contribute to the iPG signal. The data from blood flow (per volume of tissue) quantified from the iPG data shown in section 7.1.2 highlighted increments in their respective systolic peaks all along the venous or partial

arterial. Indeed, the systolic pulses during partial arterial occlusion were slightly higher than the ones that occurred during venous occlusion — this information contrasted with the data observed in Doppler Ultrasound measurements. As described in section 7.1.3 the arterial flow was mostly affected when the blockage occurred at a point that was above diastolic pressure. The amplitude of the iPG's systolic pulses was also expected to decrease during disturbances of the arterial flow due to restricted blood flow into the limb, but it actually increased. One explanation could be that the body triggered a vasodilatory response when an occlusion occurred where the veins' cross-section area veins increments to accommodate more blood into the tissue.

The response seen from the iPG signal is unique since other instruments exhibited a reduction in their systolic peaks in a similar proportion. For instance, as shown in 7.1.4 and 7.1.5 both signals witnessed a reduction in their amplitudes during venous and partial arterial occlusion. This same response can be attributed to the measurement of changes in the venous blood, but not in the arterial. In fact, the decline in LDF amplitude suggests a reduction in the velocity of RBC coming into the microcirculation. Additionally, this decline of the PPG amplitude is indicative of a shift in blood volume activated by the venous occlusion. During this experiment, the magnitude of PPG reduced significantly during partial arterial occlusion.

In general, it appears as though the arterial blood is a significant contributor of the iPG's APA signal by not merely detecting the arterial blood coming into the limb, but by also giving an insight into how the tissue responded to a blood occlusion. The acceptable correlation with the Doppler Ultrasound ($r^2 = 0.35$) as shown in section 7.2.2, illustrated that the iPG waveform amplitude did change with the arterial blood. Nevertheless, while reducing the arterial blood, the forearm's iPG waveform reacted differently, causing a spike in the systolic magnitude possibly because of a venous response. When correlating the iPG data with optical methods like PPG (see chapter 7.2.4) and LDF (see chapter 7.2.3), a low correlation was found ($r^2 < 0.08$); this was apparently caused by the different direction that the amplitudes went towards during venous and arterial blood blockage. While the iPG increased, the optical methods decreased. This reaction seems to indicate that the changes occurring in venous blood presented an increase in the iPG amplitude pulses, probably due to an increase in the vessels' diameter during an occlusion.

General conclusion and future work

The primary objective of this thesis was to present a home diagnostic system that would be capable of measuring changes in blood volume - and by extension flow - using bioelectrical impedance. Such a system was realised in 4.1 in the form of a modular device which carried out the required measurements and exhibited the capability of being used safely in a home setting. The device functioned as expected within the stated operational characteristics. Some of its key technological achievements and innovative features are highlighted as follows:

- Some of the studies described in the literature had used impedance devices that were not explicitly designed to measure blood-related alterations in limbs. For instance, some investigations used impedance cardiographers [23, 136, 120, 213], whereas other circuits merely aimed to measure either basal impedance [20, 22, 102, 170, 120] or arterial pulses [20, 21, 24, 25, 120, 214]. In comparison, the instrument presented in this thesis is primarily focused on measuring impedance within the range of the limbs' tissue [185], simultaneously measuring the changes in the basal impedance and arterial pulses.
- Although some studies used either their circuits or IC designs to measure bioelectrical impedance, most of their techniques focused on quadrature demodulation and the average DC value of the signal [215–217]. The method outlined in this thesis incorporates the envelope demodulation with a super diode circuit; this returns the peak value of the detected signals.
- Using envelope technique to measure the current amplitude and voltage from the limbs reduces the need for calibration. This instrument continuously measures the amplitude of the injected current and the voltage sensed from the limb's segment. Thus, the impedance was calculated directly from these two waveforms.

General conclusion and future work

- The iPG data presented in this literature are either basal impedance or arterial pulses. Some instruments extract the arterial pulses from basal impedance, which results in low-quality waveforms [20, 120]. The instrument separates the arterial pulses from the forearm impedance via hardware. Thereafter, both signals are separately displayed which provides the opportunity to analyse changes in both signals at the same time.

The instrument's innovation presented in this thesis not only lies in the hardware design, but also in the analysis of impedance plethysmography waveform. The protocol of this experimental procedure described in section 4.2 impacted the blood flow towards the limb. The instrument was able to effectively detect changes in the basal impedance as well as arterial pulses, which is evidenced in chapters 5 and 6 respectively. More importantly, clear changes could be detected in most participants when performing venous and partial arterial occlusions. According to the author, considering the changes observed during this experimental procedure, the following innovations can be derived:

- Although studies performing occlusive techniques have been carried out, they have largely focused on the quantification of flow rate or volume heightened volume during VOP [20–22]. However, none of these studies provided details on the rate of change during either venous or partial arterial occlusion. In contrast, the analysis presented in 5 showed that the rate of change during partial arterial occurred occurred more swiftly than venous occlusion. This slope change may be one of the first indicators as to when an arterial blockage may occur when it is continuously monitored.
- A study reported changes in the arterial pulses wave morphology during issues surfacing in the lymphatic system [29], but based on the author's understanding, no evidence of analysis was furnished during the mechanical occlusion. As evident in this thesis, it is clear that the morphology of this waveform varies in accordance to the type of occlusion applied to the upper arm. The data demonstrated that during both kinds of occlusions the systolic peak increased considerably. Thus, this might be an indicator of irregular blood flow towards the limb. Moreover, the data revealed that a difference in amplitude at the dicrotic notch as well as after pulse. During partial arterial occlusion, the amplitude of these points was seen to be considerably lower than venous occlusion. In fact, the information demonstrated that during partial arterial occlusion, the post dicrotic amplitude tended to be of a lower magnitude when compared to dicrotic notch. Therefore, this is a clear differentiator between the two kinds of occlusion.
- To the best of the author's knowledge, no other study had previously been able to focus on the methods for early detection of venous and arterial circulatory problems using

iPG. After a quantitative as well as qualitative analysis of the basal impedance and the arterial pulses, measuring the ratio between both signals in order to identify faster alterations in the circulation was considered. It was demonstrated that there was a shift in either basal impedance or APA morphology during each blockage. therefore, by combining these two sets of information, it is possible to detect early changes in the blood circulation.

8.1 Future work

The present work showed an initial prototype to measure iPG within an upper limb along with the potential to detect circulatory problems in a limb. Nonetheless, some improvements in hardware and software would be able to refine the full prototype. The author recommends a comparative study between the device presented in this document and a commercial impedance device. The results from this investigation will allow to validate the performance of the iPG apparatus shown in this study.

Furthermore, clinical experiments are suggested to confirm whether the systemic body response triggers changes in the iPG waveform differentiating between arterial and venous components of the impedance signal. One suggested examination would be cold room studies. In this kind of test, a cold environment may set off a sympathetic stimulation, causing vasoconstriction in the skin, arms and legs [218]. The analysis should centre in the changes of impedance baseline, as well as the three APA points signalled in this document.

Finally, the author considers that performing experiments in a clinical setting would be beneficial to confirm the accuracy of the methodology presented here. Patients with any peripheral vascular disease, arterial occlusive disease or lymphedema would be perfect candidates to analyse their impedimetric waveforms.

8.1.1 Improvements of the iPG device

The device performed well during all the tests. However, there are items of interest that could be implemented in future studies. From the standpoint of design, there is room to miniaturise the instrument. A modular approach was used for this initial prototype. Nonetheless, designing an integrated PCB, which could include the MCU on board along with a DAQ system, would simplify the design considerably. Some challenges may arise for the design of the board. During the PCB manufacturing, it was found that combining digital with analogue

General conclusion and future work

channels increased the crosstalk between signals. Therefore, special care must be undertaken when designing a board of these characteristics.

In addition to this improvement, the device could accommodate a small set of batteries. The instrument included battery packs of 12 V but it would be possible to achieve a better portability if lower power banks were installed. Furthermore, using a small current could be considered as an option to use a smaller battery bank. However, this may also lead to additional challenges. For instance, the impedance magnitude will get closer to the floor noise when using a lower electrical current. Therefore, the noise will cover the signal of interest. Another potential improvement to the design will be analysing the signal phase. As is the case with most bioelectrical impedance devices, the instrument only measured the magnitude of the impedance. However, additional information about volume or flow haemodynamics may be embedded within the phase shift data. Therefore, a channel dedicated to this phase could be an interesting add-on for future research. Nonetheless, there are quite a few challenges to achieve this. First, the phase shift at the frequency which the instrument was implemented at is only 12° [180]. Therefore, the level of noise at that level can pose a serious challenge. Using a higher frequency could be an option, but then that would affect the actual part of the signal.

8.1.2 Waveform analysis under different conditions

The use of additional instruments provided insightful information on the changes in blood volume, arterial flow and microcirculation. However, it could be of high interest to compare the iPG waveforms and NIRS method. The latter can provide critical data about tissue oxygenation, and within the basal impedance, reading yields information about the amount of blood within the tissue. Therefore, the effectiveness of iPG in measuring perfusion changes can be established and compared to an optic method.

The analysis of waveforms has divulged differences when calculating the blood flow during both venous and partial arterial occlusion. The results that have been presented throughout the course of this experiment suggested an increase of blood flow, which can only be explained by a vasodilation caused by a syncopal response. However, performing cold tests are recommended to investigate whether the narrowing of vessels also causes changes in the dirotic notch point. Analysing the waveform in legs could also be of high interest. Some illnesses like diabetic food require constant monitoring of blood delivery towards the feet. The instrument could be adjusted to take the measurements within the impedance level so as to obtain a clear waveform signal. The changes in basal impedance and amplitude waveform could lead to an accurate indicator of poor perfusion in the compromised limbs.

References

- [1] S. Novo, G. Coppola, and G. Milio, "Critical limb ischemia: definition and natural history," *Current Drug Targets-Cardiovascular & Hematological Disorders*, vol. 4, no. 3, pp. 219–225, 2004.
- [2] "Key to a long life? having good blood circulation, new study finds," <http://www.express.co.uk/life-style/health/707497/Key-long-life-having-good-blood-circulation-new-study-finds>, accessed: 2017-10-10.
- [3] T. J. Orchard and D. E. Strandness, "Assessment of peripheral vascular disease in diabetes: Report and recommendations of an international workshop sponsored by the american heart association and the american diabetes association," *Diabetes Care*, vol. 16, no. 8, pp. 1199–1209, 1993.
- [4] A. T. Hirsch, M. H. Criqui, D. Treat-Jacobson, J. G. Regensteiner, M. A. Creager, J. W. Olin, S. H. Krook, D. B. Hunnigake, A. J. Comerota, M. E. Walsh *et al.*, "Peripheral arterial disease detection, awareness, and treatment in primary care," *Jama*, vol. 286, no. 11, pp. 1317–1324, 2001.
- [5] L. Y. Orekhova and A. A. Barmasheva, "Doppler flowmetry as a tool of predictive, preventive and personalised dentistry," *EPMA Journal*, vol. 4, no. 1, p. 21, 2013.
- [6] I. Fredriksson, C. Fors, and J. Johansson, "Laser doppler flowmetry-a theoretical framework," 2007.
- [7] T. V. Holohan, *Plethysmography: Safety, Effectiveness, and Clinical Utility in Diagnosing Vascular Disease*. DIANE Publishing, 1996.
- [8] M. C. Van Beekvelt, W. N. Colier, R. A. Wevers, and B. G. Van Engelen, "Performance of near-infrared spectroscopy in measuring local O_2 consumption and blood flow in skeletal muscle," *Journal of Applied Physiology*, vol. 90, no. 2, pp. 511–519, 2001.
- [9] F. Harel, A. Denault, Q. Ngo, J. Dupuis, and P. Khairy, "Near-infrared spectroscopy to monitor peripheral blood flow perfusion," *Journal of clinical monitoring and computing*, vol. 22, no. 1, pp. 37–43, 2008.

References

- [10] R. A. De Blasi, M. Cope, C. Elwell, F. Safoue, and M. Ferrari, “Noninvasive measurement of human forearm oxygen consumption by near infrared spectroscopy,” *European Journal of Applied Physiology and Occupational Physiology*, vol. 67, no. 1, pp. 20–25, 1993.
- [11] K. Gurley, Y. Shang, and G. Yu, “Noninvasive optical quantification of absolute blood flow, blood oxygenation, and oxygen consumption rate in exercising skeletal muscle,” *Journal of biomedical optics*, vol. 17, no. 7, pp. 0750101–07501010, 2012.
- [12] U. Dirnagl, B. Kaplan, M. Jacewicz, and W. Pulsinelli, “Continuous measurement of cerebral cortical blood flow by laser—doppler flowmetry in a rat stroke model,” *Journal of Cerebral Blood Flow & Metabolism*, vol. 9, no. 5, pp. 589–596, 1989.
- [13] A. Bashkatov, E. Genina, V. Kochubey, and V. Tuchin, “Optical properties of human skin, subcutaneous and mucous tissues in the wavelength range from 400 to 2000 nm,” *Journal of Physics D: Applied Physics*, vol. 38, no. 15, p. 2543, 2005.
- [14] D. Briers, D. D. Duncan, E. Hirst, S. J. Kirkpatrick, M. Larsson, W. Steenbergen, T. Stromberg, and O. B. Thompson, “Laser speckle contrast imaging: theoretical and practical limitations,” *Journal of biomedical optics*, vol. 18, no. 6, pp. 066018–066018, 2013.
- [15] I. B. Wilkinson and D. J. Webb, “Venous occlusion plethysmography in cardiovascular research: methodology and clinical applications,” *British Journal of Clinical Pharmacology*, vol. 52, no. 6, pp. 631–646, 2001.
- [16] W. P. Sy, “Ulnar nerve palsy possibly related to use of automatically cycled blood pressure cuff,” *Anesthesia & Analgesia*, vol. 60, no. 9, pp. 687–688, 1981.
- [17] P. C. Creevy, J. F. Burris, and W. J. Mroczek, “Phlebitis associated with noninvasive 24-hour ambulatory blood pressure monitor,” *JAMA*, vol. 254, no. 17, pp. 2411–2411, 1985.
- [18] T. K. Bera, “Bioelectrical impedance methods for noninvasive health monitoring: a review,” *Journal of medical engineering*, vol. 2014, 2014.
- [19] J. Nyboer, P. Murray, and J. A. Sedensky, “Blood-flow indices in amputee and control limbs by mutual electrical impedance plethysmography,” *American heart journal*, vol. 87, no. 6, pp. 704–710, 1974.
- [20] S. Mohapatra and H. M. Arenson, “The measurement of peripheral blood flow by the electrical impedance technique,” *Journal of medical engineering & technology*, vol. 3, no. 3, pp. 132–137, 1979.
- [21] K. Costeloe and P. Rolfe, “Continuous limb blood flow estimation in the newborn using electrical impedance plethysmography,” *Pediatric research*, vol. 14, no. 9, pp. 1053–1060, 1980.
- [22] K. Yamakoshi, “Limb blood flowmeter,” May 27 1980, uS Patent 4,204,545.

- [23] J. Porter, I. Swain, and P. Shakespeare, "Measurement of limb blood flow by electrical impedance plethysmography." *Annals of The Royal College of Surgeons of England*, vol. 67, no. 3, p. 169, 1985.
- [24] C. Corciova, R. Ciorap, R. Matei, and A. Salceanu, "Peripheral vascular measurement using electrical impedance plethysmography," in *International Conference on Advancements of Medicine and Health Care through Technology*. Springer, 2011, pp. 136–139.
- [25] B. Brown, W. I. Pryce, D. Baumber, and R. Clarke, "Impedance plethysmography: can it measure changes in limb blood flow," *Medical and Biological Engineering and Computing*, vol. 13, no. 5, pp. 674–682, 1975.
- [26] L. A. Marks, "Computer assisted admittance plethysmograph," Oct. 22 1985, uS Patent 4,548,211.
- [27] D. S. Bhargava, A. Singhb, A. K. Uttamb, and A. Ranjanb, "Flow meter using impedance plethysmography technique," *blood*, vol. 4, no. 10, p. 11, 2014.
- [28] H. Töreyn, S. Shah, S. Hersek, O. T. Inan, and J. Hasler, "Proof-of-concept energy-efficient and real-time hemodynamic feature extraction from bioimpedance signals using a mixed-signal field programmable analog array," in *2017 IEEE EMBS International Conference on Biomedical & Health Informatics (BHI)*. IEEE, 2017, pp. 233–236.
- [29] L. D. Montgomery, M. S. Dietrich, J. M. Armer, B. Stewart, and S. H. Ridner, "Segmental blood flow and hemodynamic state of lymphedematous and nonlymphedematous arms," *Lymphatic research and biology*, vol. 9, no. 1, pp. 31–42, 2011.
- [30] J. C. Golden and D. S. Miles, "Assessment of peripheral hemodynamics using impedance plethysmography," *Physical therapy*, vol. 66, no. 10, pp. 1544–1547, 1986.
- [31] E. Mašanauskienė, S. Sadauskas, A. Naudžiūnas, A. Unikauskas, and E. Stankevičius, "Impedance plethysmography as an alternative method for the diagnosis of peripheral arterial disease," *Medicina*, vol. 50, no. 6, pp. 334–339, 2014.
- [32] LabView, *version 12*. Austin, Texas: National Instruments Corporation, 2016.
- [33] MATLAB, *version 9.1.0.441655 (R2010b)*. Natick, Massachusetts: The MathWorks Inc., 2016.
- [34] A. A. Kamshilin and N. B. Margaryants, "Origin of photoplethysmographic waveform at green light," *Physics Procedia*, vol. 86, pp. 72–80, 2017.
- [35] R. Turcott, "Methods and devices for vascular plethysmography via modulation of source intensity," May 4 2004, uS Patent 6,731,967.
- [36] W. Nichols, M. O'Rourke, and C. Vlachopoulos, *McDonald's blood flow in arteries: theoretical, experimental and clinical principles*. CRC press, 2011.

References

- [37] J. E. Hall, *Guyton and Hall Textbook of Medical Physiology*. Saint Louis, UNITED STATES: Elsevier Health Sciences, 2015. [Online]. Available: <http://ebookcentral.proquest.com/lib/kcl/detail.action?docID=2074577>
- [38] K. Sakamoto and H. Kanai, "Electrical characteristics of flowing blood," *IEEE Transactions on Biomedical Engineering*, no. 12, pp. 686–695, 1979.
- [39] M. Elgendi, "On the analysis of fingertip photoplethysmogram signals," *Current cardiology reviews*, vol. 8, no. 1, pp. 14–25, 2012.
- [40] R. C. Sibley III, S. P. Reis, J. J. MacFarlane, M. A. Reddick, S. P. Kalva, and P. D. Sutphin, "Noninvasive physiologic vascular studies: A guide to diagnosing peripheral arterial disease," *RadioGraphics*, vol. 37, no. 1, pp. 346–357, 2016.
- [41] R. Donnelly, D. Hinwood, and N. J. London, "Abc of arterial and venous disease: non-invasive methods of arterial and venous assessment," *BMJ: British Medical Journal*, vol. 320, no. 7236, p. 698, 2000.
- [42] S. S. Chuah, P. I. Woolfson, B. R. Pullan, and P. S. Lewis, "Plethysmography without venous occlusion for measuring forearm blood flow: comparison with venous occlusive method," *Clinical physiology and functional imaging*, vol. 24, no. 5, pp. 296–303, 2004.
- [43] V. C. Scanlon and T. Sanders, *Essentials of anatomy and physiology*. FA Davis, 2014.
- [44] C. Culmsee, C. Zhu, S. Landshamer, B. Becattini, E. Wagner, M. Pellicchia, K. Blomgren, and N. Plesnila, "Apoptosis-inducing factor triggered by poly (adp-ribose) polymerase and bid mediates neuronal cell death after oxygen-glucose deprivation and focal cerebral ischemia," *The Journal of neuroscience*, vol. 25, no. 44, pp. 10 262–10 272, 2005.
- [45] S. Novo, "The patients with intermittent claudication. everyday problems in clinical cardiology," *Excerpta Medica: Amsterdam*, vol. 5, no. 7, 1995.
- [46] E. N. Marieb and K. Hoehn, *Human anatomy & physiology*. Pearson Education, 2007.
- [47] W. B. Kannel and D. McGee, "Diabetes and glucose tolerance as risk factors for cardiovascular disease: the framingham study," *Diabetes care*, vol. 2, no. 2, pp. 120–126, 1979.
- [48] H. U. Janka, E. Standl, and H. Mehnert, "Peripheral vascular disease in diabetes mellitus and its relation to cardiovascular risk factors: screening with the doppler ultrasonic technique," *Diabetes care*, vol. 3, no. 2, pp. 207–213, 1980.
- [49] J. O. Menzoian, W. W. LaMorte, C. C. Paniszyn, K. J. McBride, A. N. Sidawy, F. W. LoGerfo, M. E. Connors, and J. E. Doyle, "Symptomatology and anatomic patterns of peripheral vascular disease: differing impact of smoking and diabetes," *Annals of vascular surgery*, vol. 3, no. 3, pp. 224–228, 1989.

- [50] B. Eliasson, "Cigarette smoking and diabetes," *Progress in cardiovascular diseases*, vol. 45, no. 5, pp. 405–413, 2003.
- [51] J. W. Stephens, G. Ambler, P. Vallance, D. J. Betteridge, S. E. Humphries, and S. J. Hurel, "Cardiovascular risk and diabetes. are the methods of risk prediction satisfactory?" *European Journal of Cardiovascular Prevention & Rehabilitation*, vol. 11, no. 6, pp. 521–528, 2004.
- [52] L. Norgren, W. R. Hiatt, J. A. Dormandy, M. R. Nehler, K. A. Harris, F. G. R. Fowkes, T. I. W. Group *et al.*, "Inter-society consensus for the management of peripheral arterial disease (tasc ii)," *European Journal of Vascular and Endovascular Surgery*, vol. 33, no. 1, pp. S1–S75, 2007.
- [53] M. B. Morgan, T. Crayford, B. Murrin, and S. C. Fraser, "Developing the vascular quality of life questionnaire: a new disease-specific quality of life measure for use in lower limb ischemia," *Journal of vascular surgery*, vol. 33, no. 4, pp. 679–687, 2001.
- [54] L. Songer, "Tissue ischemia monitoring using impedance spectroscopy: Clinical evaluation," Ph.D. dissertation, Worcester Polytechnic Institute, 2001.
- [55] P. Chhabra, N. Gupta, A. Kaushik *et al.*, "Compartment syndrome as a spectrum of purple glove syndrome following intravenous phenytoin administration in a young male: A case report and review of literature," *Neurology India*, vol. 61, no. 4, p. 419, 2013.
- [56] D. R. Lamborn and C. Schranz, "Compartment syndrome as a complication of ileofemoral deep venous thrombosis: a case presentation." *The American journal of emergency medicine*, vol. 32, no. 2, pp. 192–e1, 2014.
- [57] A. Dodd and I. Le, "Foot compartment syndrome: diagnosis and management," *Journal of the American Academy of Orthopaedic Surgeons*, vol. 21, no. 11, pp. 657–664, 2013.
- [58] I. Uçkay, K. Gariani, Z. Pataky, and B. A. Lipsky, "Diabetic foot infections: state-of-the-art," *Diabetes, Obesity and Metabolism*, vol. 16, no. 4, pp. 305–316, 2014.
- [59] K.-S. Cheng, Y.-F. Ko, and T. Wang, "The application of bioimpedance method for foot sole blood perfusion characterization," in *Genetic and Evolutionary Computing (ICGEC), 2012 Sixth International Conference on*. IEEE, 2012, pp. 211–213.
- [60] M. d. C. dos Reis, F. A. Soares, A. F. da Rocha, J. L. Carvalho, and S. S. Rodrigues, "Insole with pressure control and tissue neof ormation induction systems for diabetic foot," in *2010 Annual International Conference of the IEEE Engineering in Medicine and Biology*. IEEE, 2010, pp. 5748–5751.
- [61] E. S. Papazoglou, M. S. Weingarten, L. Zubkov, M. Neidrauer, and K. Pourrezaei, "Assessment of diabetic foot ulcers with diffuse near infrared methodology," in *BioInformatics and BioEngineering, 2008. BIBE 2008. 8th IEEE International Conference on*. IEEE, 2008, pp. 1–5.

References

- [62] N. Yusuf, M. Omar, A. Zakaria, A. Abdullah, L. Kamarudin, A. Shakaff, M. Masnan, N. I. Zakaria, E. Yeap, A. Othman *et al.*, “Diagnosis of bacteria for diabetic foot infection using electronic nose technology,” in *Wireless Sensor (ICWISE), 2013 IEEE Conference on*. IEEE, 2013, pp. 114–118.
- [63] A. M. Noyes and J. Dickey, “The arm is not the leg: pathophysiology, diagnosis, and management of upper extremity deep vein thrombosis,” *RI Med J*, vol. 100, pp. 33–36, 2017.
- [64] A. Sayın, H. Güngör, M. Bilgin, and U. Ertürk, “Paget-von schrötter syndrome: upper extremity deep vein thrombosis after heavy exercise,” *Turk Kardiyol Dern Ars*, vol. 40, no. 4, pp. 354–357, 2012.
- [65] R. L. Hardman, O. Jazaeri, J. Yi, M. Smith, and R. Gupta, “Overview of classification systems in peripheral artery disease,” in *Seminars in interventional radiology*, vol. 31, no. 04. Thieme Medical Publishers, 2014, pp. 378–388.
- [66] T. Winsor, “Influence of arterial disease on the systolic blood pressure gradients of the extremity,” *Am J Med Sci*, vol. 220, pp. 117–126, 1950.
- [67] D. P. Casey, T. B. Curry, and M. J. Joyner, “Measuring muscle blood flow a key link between systemic and regional metabolism,” *Current opinion in clinical nutrition and metabolic care*, vol. 11, no. 5, p. 580, 2008.
- [68] “Summit doppler l300ac lifedop abi doppler system,” <https://tinyurl.com/yc9ajlbt>, accessed: 2017-09-29.
- [69] K. Vowden and P. Vowden, “Hand-held doppler ultrasound: The assessment of lower limb arterial and venous disease,” 2002.
- [70] A. Jayanthi, N. Sujatha, and M. R. Reddy, “Measuring blood flow: techniques and applications-a review,” *International Journal of Recent Research and Applied Studies*, vol. 6, no. 2, 2011.
- [71] *Service Manual - Dopplex[®] Hand Held Dopplers*, Huntleigh Healthcare, 2004, rev. 726374-2.
- [72] R. W. Gill, “Pulsed doppler with b-mode imaging for quantitative blood flow measurement,” *Ultrasound in medicine & biology*, vol. 5, no. 3, pp. 223–225, 1979.
- [73] G. Rådegran, “Limb and skeletal muscle blood flow measurements at rest and during exercise in human subjects,” *Proceedings of the Nutrition Society*, vol. 58, no. 4, pp. 887–898, 1999.
- [74] “Chapter 4, blood flow hemodynamics, cardiac mechanics, and doppler echocardiography,” http://samples.jbpub.com/9780763779351/79351_CH04_BulwerSec.pdf, accessed: 2016-10-10.

- [75] P. Schmitt, M. Kotas, A. Tobermann, A. Haase, and M. Flentje, "Quantitative tissue perfusion measurements in head and neck carcinoma patients before and during radiation therapy with a non-invasive mr imaging spin-labeling technique," *Radiotherapy and oncology*, vol. 67, no. 1, pp. 27–34, 2003.
- [76] D. J. Culbert, "User identification system based on plethysmography," Jun. 6 2017, uS Patent 9,668,676.
- [77] J. L. Higgins and A. Fronek, "Photoplethysmographic evaluation of the relationship between skin reflectance and skin blood volume," *Journal of biomedical engineering*, vol. 8, no. 2, pp. 130–136, 1986.
- [78] J.-M. Kim, K. Arakawa, K. T. Benson, and D. K. Fox, "Pulse oximetry and circulatory kinetics associated with pulse volume amplitude measured by photoelectric plethysmography," *Anesthesia & Analgesia*, vol. 65, no. 12, pp. 1333–1339, 1986.
- [79] J. Allen and A. Murray, "Development of a neural network screening aid for diagnosing lower limb peripheral vascular disease from photoelectric plethysmography pulse waveforms," *Physiological Measurement*, vol. 14, no. 1, p. 13, 1993.
- [80] D. T. Williams, K. G. Harding, and P. Price, "An evaluation of the efficacy of methods used in screening for lower-limb arterial disease in diabetes," *Diabetes care*, vol. 28, no. 9, pp. 2206–2210, 2005.
- [81] M. E. Alnaeb, N. Alobaid, A. M. Seifalian, D. P. Mikhailidis, and G. Hamilton, "Optical techniques in the assessment of peripheral arterial disease," *Current vascular pharmacology*, vol. 5, no. 1, pp. 53–59, 2007.
- [82] R. T. Eberhardt and J. D. Raffetto, "Chronic venous insufficiency," *Circulation*, vol. 111, no. 18, pp. 2398–2409, 2005.
- [83] C. S. Norris, A. Beyrau, and R. W. Barnes, "Quantitative photoplethysmography in chronic venous insufficiency: a new method of noninvasive estimation of ambulatory venous pressure," *Surgery*, vol. 94, no. 5, pp. 758–764, 1983.
- [84] T. Wu, "Ppgi: new development in noninvasive and contactless diagnosis of dermal perfusion using near infrared light," *J. GCPD eV*, vol. 7, no. 1, pp. 17–24, 2003.
- [85] B. A. Fallow, T. Tarumi, and H. Tanaka, "Influence of skin type and wavelength on light wave reflectance," *Journal of clinical monitoring and computing*, vol. 27, no. 3, pp. 313–317, 2013.
- [86] E. Cooke and N. Almond, "Laser doppler flowmetry," *Journal of medical engineering & technology*, vol. 14, no. 5, pp. 177–177, 1990.
- [87] A. K. Dunn, H. Bolay, M. A. Moskowitz, and D. A. Boas, "Dynamic imaging of cerebral blood flow using laser speckle," *Journal of Cerebral Blood Flow & Metabolism*, vol. 21, no. 3, pp. 195–201, 2001.

References

- [88] F. Domoki, D. Zölei, O. Oláh, V. Tóth-Szúki, B. Hopp, F. Bari, and T. Smausz, "Evaluation of laser-speckle contrast image analysis techniques in the cortical microcirculation of piglets," *Microvascular research*, vol. 83, no. 3, pp. 311–317, 2012.
- [89] C. Stoianovici, P. Wilder-Smith, and B. Choi, "Assessment of pulpal vitality using laser speckle imaging," *Lasers in surgery and medicine*, vol. 43, no. 8, pp. 833–837, 2011.
- [90] C. Stewart, R. Frank, K. Forrester, J. Tulip, R. Lindsay, and R. Bray, "A comparison of two laser-based methods for determination of burn scar perfusion: laser doppler versus laser speckle imaging," *Burns*, vol. 31, no. 6, pp. 744–752, 2005.
- [91] T. Son, J. Lee, and B. Jung, "Contrast enhancement of laser speckle contrast image in deep vasculature by reduction of tissue scattering," *Journal of the Optical Society of Korea*, vol. 17, no. 1, pp. 86–90, 2013.
- [92] D. D. Duncan and S. J. Kirkpatrick, "Can laser speckle flowmetry be made a quantitative tool?" *JOSA A*, vol. 25, no. 8, pp. 2088–2094, 2008.
- [93] J. W. Goodman, "Statistical properties of laser speckle patterns," *Laser speckle and related phenomena*, vol. 9, pp. 9–75, 1975.
- [94] M. J. Joyner, N. M. Dietz, and J. T. Shepherd, "From belfast to mayo and beyond: the use and future of plethysmography to study blood flow in human limbs," *Journal of Applied Physiology*, vol. 91, no. 6, pp. 2431–2441, 2001.
- [95] R. Joannides, J. Bellien, and C. Thuillez, "Clinical methods for the evaluation of endothelial function—a focus on resistance arteries," *Fundamental & clinical pharmacology*, vol. 20, no. 3, pp. 311–320, 2006.
- [96] E. P. Flowers, "Strain gauge plethysmograph," Mar. 31 1981, uS Patent 4,258,720.
- [97] D. Ulman. medical electronics iii. [Online]. Available: <http://medical-electronics-iii.blogspot.com/2007/09/>
- [98] O. G. Martinsen and S. Grimnes, *Bioimpedance and bioelectricity basics*. Academic press, 2011.
- [99] I. Schraibman, D. Mott, G. Naylor, and D. Charlesworth, "Comparison of impedance and strain gauge plethysmography in the measurement of blood flow in the lower limb," *British Journal of Surgery*, vol. 62, no. 11, pp. 909–912, 1975.
- [100] U. G. Kyle, I. Bosaeus, A. D. De Lorenzo, P. Deurenberg, M. Elia, J. M. Gómez, B. L. Heitmann, L. Kent-Smith, J.-C. Melchior, M. Pirlich *et al.*, "Bioelectrical impedance analysis—part i: review of principles and methods," *Clinical nutrition*, vol. 23, no. 5, pp. 1226–1243, 2004.
- [101] C. F. Mattern, F. S. Brackett, and B. J. Olson, "Determination of number and size of particles by electrical gating: blood cells," *Journal of applied physiology*, vol. 10, no. 1, pp. 56–70, 1957.

- [102] J. Nyboer, "Electrical impedance plethysmography: A physical and physiological approach to peripheral vascular study," *Circulation*, vol. 2, pp. 811–821, Dec. 1950.
- [103] P. Bertemes Filho, "Tissue characterisation using an impedance spectroscopy probe," Ph.D. dissertation, University of Sheffield, 2002.
- [104] J. A. Orpin, "Unexpected burns under skin electrodes." *Canadian Medical Association Journal*, vol. 127, no. 11, p. 1106, 1982.
- [105] B. H. Brown, R. Smallwood, D. Barber, P. Lawford, and D. Hose, *Medical physics and biomedical engineering*. CRC Press, 1998.
- [106] "International standard, iec 60601-1," http://www.ele.uri.edu/courses/bme484/iec60601-1ed3.0_parts.pdf, accessed: 2017-12-1.
- [107] L. Callegaro, *Electrical impedance: principles, measurement, and applications*. CRC Press, 2012.
- [108] D. B. Geselowitz, "An application of electrocardiographic lead theory to impedance plethysmography," *IEEE Transactions on biomedical Engineering*, no. 1, pp. 38–41, 1971.
- [109] H. Dehghani, D. Barber, and I. Basarab-Horwath, "Incorporating a priori anatomical information into image reconstruction in electrical impedance tomography," *Physiological measurement*, vol. 20, no. 1, p. 87, 1999.
- [110] A. Ivorra, "Bioimpedance monitoring for physicians: an overview," *Centre Nacional de Microelectrònica Biomedical Applications Group*, pp. 1–35, 2003.
- [111] V. F. Lvovich, *Impedance spectroscopy: applications to electrochemical and dielectric phenomena*. John Wiley & Sons, 2012.
- [112] M. R. Neuman, *The Biomedical Engineering Handbook: Second Edition*, J. D. Bronzino, Ed. CRC Press LLC, 2000.
- [113] W. Franks, I. Schenker, P. Schmutz, and A. Hierlemann, "Impedance characterization and modeling of electrodes for biomedical applications," *IEEE Transactions on Biomedical Engineering*, vol. 52, no. 7, pp. 1295–1302, 2005.
- [114] E. Barsoukov and J. R. Macdonald, *Impedance spectroscopy: theory, experiment, and applications*. John Wiley & Sons, 2005.
- [115] E. McAdams, J. Jossinet, R. Subramanian, and R. McCauley, "Characterization of gold electrodes in phosphate buffered saline solution by impedance and noise measurements for biological applications," in *Engineering in Medicine and Biology Society, 2006. EMBS'06. 28th Annual International Conference of the IEEE*. IEEE, 2006, pp. 4594–4597.
- [116] E. McAdams, A. Lacknermeier, J. McLaughlin, D. Macken, and J. Jossinet, "The linear and non-linear electrical properties of the electrode-electrolyte interface," *Biosensors and Bioelectronics*, vol. 10, no. 1-2, pp. 67–74, 1995.

References

- [117] M. E. Orazem and B. Tribollet, *Electrochemical impedance spectroscopy*. John Wiley & Sons, 2017.
- [118] J. Caicedo-Eraso, C. González-Correa, and C. González-Correa, "Use of electrocardiogram (ecg) electrodes for bioelectrical impedance analysis (bia)," in *Journal of Physics: Conference Series*, vol. 407, no. 1. IOP Publishing, 2012, p. 012008.
- [119] A. Lozano, "Electrode errors in bioimpedance measurement systems for long-term applications," in *Biomedical Engineering Conference, 1997., Proceedings of the 1997 Sixteenth Southern*. IEEE, 1997, pp. 3–6.
- [120] Y. Yamamoto, T. Yamamoto, and P. Öberg, "Impedance plethysmography for blood flow measurements in human limbs," *Medical and Biological Engineering and Computing*, vol. 30, no. 5, pp. 518–524, 1992.
- [121] $3\text{ nV}/\sqrt{\text{Hz}}$, *Low Power Instrumentation Amplifier AD8421*, Analog Devices, 2012, rev. O.
- [122] T. Faes, H. Van der Meij, J. De Munck, and R. Heethaar, "The electric resistivity of human tissues (100 hz-10 mhz): a meta-analysis of review studies," *Physiological measurement*, vol. 20, no. 4, p. R1, 1999.
- [123] S. Grimnes, "Impedance measurement of individual skin surface electrodes," *Medical and Biological Engineering and Computing*, vol. 21, no. 6, pp. 750–755, 1983.
- [124] E. McAdams, J. Jossinet, A. Lacknermeier, and F. Risacher, "Factors affecting electrode-gel-skin interface impedance in electrical impedance tomography," *Medical and Biological Engineering and Computing*, vol. 34, no. 6, pp. 397–408, 1996.
- [125] H. P. Schwan, "Electrical properties of tissue and cell suspensions." *Advances in biological and medical physics*, vol. 5, p. 147, 1957.
- [126] H. P. Schwan and H. J. Morowitz, "Electrical properties of the membranes of the pleuropneumonia-like organism a 5969," *Biophysical journal*, vol. 2, no. 5, pp. 395–407, 1962.
- [127] D. Dean, T. Ramanathan, D. Machado, and R. Sundararajan, "Electrical impedance spectroscopy study of biological tissues," *Journal of electrostatics*, vol. 66, no. 3, pp. 165–177, 2008.
- [128] K. R. Foster and H. P. Schwan, "Dielectric properties of tissues," *Handbook of biological effects of electromagnetic fields*, vol. 2, pp. 25–102, 1995.
- [129] P. Steendijk, G. Mur, E. T. Van Der Velde, and J. Baan, "The four-electrode resistivity technique in anisotropic media: theoretical analysis and application on myocardial tissue in vivo," *IEEE Transactions on Biomedical Engineering*, vol. 40, no. 11, pp. 1138–1148, 1993.
- [130] O. Casas, R. Bragos, P. Riu, J. Rosell, M. Tresanchez, M. Warren, A. RODRIGUEZ-SINOVAS, A. Carreno, and J. Cinca, "In vivo and in situ ischemic tissue characterization using electrical impedance spectroscopy," *Annals of the New York Academy of Sciences*, vol. 873, no. 1, pp. 51–58, 1999.

- [131] K. S. Cole and R. H. Cole, "Dispersion and absorption in dielectrics i. alternating current characteristics," *The Journal of chemical physics*, vol. 9, no. 4, pp. 341–351, 1941.
- [132] D. Bracco, D. Thiebaud, R. L. Chioléro, M. Landry, P. Burckhardt, and Y. Schutz, "Segmental body composition assessed by bioelectrical impedance analysis and dexa in humans," *Journal of Applied Physiology*, vol. 81, no. 6, pp. 2580–2587, 1996.
- [133] "Simsense," <https://www.simband.io/documentation/sensor-module-documentation/simsense/simsense-2nd-gen.html>, accessed: 2019-07-10.
- [134] S.-X. Neath, L. Lazio, and D. A. Guss, "Utility of impedance cardiography to improve physician estimation of hemodynamic parameters in the emergency department," *Congestive Heart Failure*, vol. 11, no. 1, pp. 17–20, 2005.
- [135] R. Hull, D. W. Taylor, J. Hirsh, D. L. Sackett, P. Powers, A. Turpie, and I. Walker, "Impedance plethysmography: the relationship between venous filling and sensitivity and specificity for proximal vein thrombosis." *Circulation*, vol. 58, no. 5, pp. 898–902, 1978.
- [136] V. DiStefano, J. Nixon, and R. Stone, "Bioelectrical impedance plethysmography as an investigative tool in orthopaedic surgery. a comparative study of limb exsanguination techniques." *Clinical orthopaedics and related research*, no. 99, pp. 203–206, 1973.
- [137] "Clinical application," <https://www.cheetah-medical.com/clinical-applications/>, accessed: 2016-02-10.
- [138] "Patient monitoring and cardio-vascular diagnosis," <https://medis.company/cms/>, accessed: 2017-10-10.
- [139] B. Levy, S. Marcovitch, E. Shusman, D. Rotenberg, and D. Avidor, "Method and system for monitoring hemodynamics," Jul. 5 2016, uS Patent 9,380,947.
- [140] *Programmable Frequency Sweep and Output Burst Waveform Generator AD5930*, Analog Devices, 2015, rev. C.
- [141] H. Hong, M. Rahal, A. Demosthenous, and R. H. Bayford, "Comparison of a new integrated current source with the modified howland circuit for eit applications," *Physiological measurement*, vol. 30, no. 10, p. 999, 2009.
- [142] A. S. Ross, G. Saulnier, J. Newell, and D. Isaacson, "Current source design for electrical impedance tomography," *Physiological measurement*, vol. 24, no. 2, p. 509, 2003.
- [143] F. Seoane, R. Macias, R. Bragos, and K. Lindcrantz, "Simple voltage-controlled current source for wideband electrical bioimpedance spectroscopy: circuit dependences and limitations," *Measurement science and technology*, vol. 22, no. 11, p. 115801, 2011.

References

- [144] M. Wolf, *Chapter 4 - Sequential Machines*, M. Wolf, Ed. Boston: Morgan Kaufmann, 2017. [Online]. Available: <http://www.sciencedirect.com/science/article/pii/B9780128093818000043>
- [145] T. Darwish and M. Bayoumi, *5 - Trends in Low-Power VLSI Design*, W.-K. CHEN, Ed. Burlington: Academic Press, 2005. [Online]. Available: <http://www.sciencedirect.com/science/article/pii/B9780121709600500220>
- [146] R. Gudivaka, D. Schoeller, R. Kushner, and M. Bolt, "Single- and multifrequency models for bioelectrical impedance analysis of body water compartments," *Journal of Applied Physiology*, vol. 87, no. 3, pp. 1087–1096, 1999.
- [147] D. A. Schoeller, "Bioelectrical impedance analysis what does it measure?" *Annals of the New York Academy of sciences*, vol. 904, no. 1, pp. 159–162, 2000.
- [148] S. Kun and R. A. Peura, "Tissue ischemia detection using impedance spectroscopy," in *Engineering in Medicine and Biology Society, 1994. Engineering Advances: New Opportunities for Biomedical Engineers. Proceedings of the 16th Annual International Conference of the IEEE*, vol. 2. IEEE, 1994, pp. 868–869.
- [149] Y. Zou and Z. Guo, "A review of electrical impedance techniques for breast cancer detection," *Medical engineering & physics*, vol. 25, no. 2, pp. 79–90, 2003.
- [150] F. Vicini, C. Shah, M. Lyden, and P. Whitworth, "Bioelectrical impedance for detecting and monitoring patients for the development of upper limb lymphedema in the clinic," *Clinical breast cancer*, vol. 12, no. 2, pp. 133–137, 2012.
- [151] H. Scharfetter, T. Schlager, R. Stollberger, R. Felsberger, H. Hutten, and H. Hinghofer-Szalkay, "Assessing abdominal fatness with local bioimpedance analysis: basics and experimental findings," *International Journal of obesity*, vol. 25, no. 4, p. 502, 2001.
- [152] C. Beestone, "Bioelectrical impedance analysis (bia)," May 2018. [Online]. Available: <https://www.scienceforsport.com/bioelectrical-impedance-analysis-bia/>
- [153] L. L. Wang, A. J. Spieker, J. Li, and S. B. Rutkove, "Electrical impedance myography for monitoring motor neuron loss in the sod1 g93a amyotrophic lateral sclerosis rat," *Clinical Neurophysiology*, vol. 122, no. 12, pp. 2505–2511, 2011.
- [154] W. Hannan, S. Cowen, C. Plester, K. Fearon, and A. DeBeau, "Comparison of bio-impedance spectroscopy and multi-frequency bio-impedance analysis for the assessment of extracellular and total body water in surgical patients," *Clinical Science*, vol. 89, no. 6, pp. 651–658, 1995.
- [155] R. V. Patel, E. L. Peterson, N. Silverman, and B. J. Zarowitz, "Estimation of total body and extracellular water in post-coronary artery bypass graft surgical patients using single and multiple frequency bioimpedance," *Critical care medicine*, vol. 24, no. 11, pp. 1824–1828, 1996.
- [156] R. J. Halter, A. Schned, J. Heaney, A. Hartov, S. Schutz, and K. D. Paulsen, "Electrical impedance spectroscopy of benign and malignant prostatic tissues," *The Journal of urology*, vol. 179, no. 4, pp. 1580–1586, 2008.

- [157] S. Weyer, L. Rothlingshofer, M. Walter, S. Leonhardt, and R. Bensberg, "Evaluation of bioimpedance spectroscopy for the monitoring of the fluid status in an animal model," in *2012 Ninth International Conference on Wearable and Implantable Body Sensor Networks*. IEEE, 2012, pp. 22–27.
- [158] A. Schwenk, W. Eschner, G. Kremer, and L. Ward, "Assessment of intracellular water by whole body bioelectrical impedance and total body potassium in hiv-positive patients," *Clinical Nutrition*, vol. 19, no. 2, pp. 109–113, 2000.
- [159] J. LaForgia, S. M. Gunn, and R. T. Withers, "Body composition: validity of segmental bioelectrical impedance analysis," *Asia Pacific journal of clinical nutrition*, vol. 17, no. 4, pp. 586–591, 2008.
- [160] S. Leahy, C. O'Neill, R. Sohun, and P. Jakeman, "A comparison of dual energy x-ray absorptiometry and bioelectrical impedance analysis to measure total and segmental body composition in healthy young adults," *European journal of applied physiology*, vol. 112, no. 2, pp. 589–595, 2012.
- [161] V. Francavilla, T. Bongiovanni, F. Genovesi, P. Minafra, and G. Francavilla, "Localized bioelectrical impedance analysis: how useful is it in the follow-up of muscle injury?" *MED SPORT*, vol. 68, pp. 323–34, 2015.
- [162] H. Shimazu, K.-I. Yamakoshi, T. Togawa, M. Fukuoka, and H. Ito, "Evaluation of the parallel conductor theory for measuring human limb blood flow by electrical admittance plethysmography," *IEEE Transactions on Biomedical Engineering*, vol. 29, no. 1, pp. 1–7, Jan. 1982.
- [163] R. Peura, B. Penney, J. Arcuri, F. Anderson Jr, and H. Wheeler, "Influence of erythrocyte velocity on impedance plethysmographic measurements," *Medical and Biological Engineering and Computing*, vol. 16, no. 2, pp. 147–154, 1978.
- [164] D. Swanson and J. Webster, "Origin of the electrical impedance pulse in the limbs," in *Proceedings of the 29th Annual Conference on Engineering in Medicine & Biology*, vol. 18, 1976, p. 324.
- [165] J. Webster, *Medical instrumentation: application and design*. John Wiley & Sons, 2009.
- [166] J. Karnegis, W. Kubicek, R. Mattson, R. Patterson, and D. Witsoe, "Development and evaluation of an impedance cardiac output system." *Aerospace Medicine*, vol. 37, no. 12, pp. 1208–1212, 1966.
- [167] W. Kubicek, R. Patterson, and D. Witsoe, "Impedance cardiography as a noninvasive method of monitoring cardiac function and other parameters of the cardiovascular system," *Annals of the New York Academy of Sciences*, vol. 170, no. 1, pp. 724–732, 1970.
- [168] W. G. Kubicek, E. Kinnen, R. P. Patterson, and D. A. Witsoe, "Impedance plethysmograph," Sep. 25 1979, uS Patent RE30,101.
- [169] B. Sramek, "Bomed's electrical bioimpedance technology for thoracic applications (nccom): Status report, may 1986 update," *Irvine, BoMed Ltd*, vol. 19, no. 2, 1986.

References

- [170] K. Yamakoshi, H. Shimazu, T. Togawa, and H. Ito, "Admittance plethysmography for accurate measurement of human limb blood flow," *American Journal of Physiology-Heart and Circulatory Physiology*, vol. 235, no. 6, pp. H821–H829, 1978.
- [171] A. Blinov and E. Selivanov, "Plethysmographic impedance device for measuring blood pressure," *Measurement techniques*, vol. 40, no. 2, pp. 188–192, 1997.
- [172] F. Risacher, J. Jossinet, E. McAdams, J. McLaughlin, Y. Mann, M. Schmitt, A. Matias, and R. Jarry, "Impedance plethysmography for the evaluation of pulse-wave velocity in limbs," *Medical and Biological Engineering and Computing*, vol. 31, no. 3, pp. 318–322, 1993.
- [173] M.-C. Cho, J.-Y. Kim, and S. Cho, "A bio-impedance measurement system for portable monitoring of heart rate and pulse wave velocity using small body area," in *2009 IEEE International Symposium on Circuits and Systems*. IEEE, 2009, pp. 3106–3109.
- [174] F. Risacher, J. Jossinet, E. McAdams, C. Eynard, J. McLaughlin, and M. Schmitt, "Computation of the pulse wave velocity in limbs from multichannel impedance plethysmography," in *Engineering in Medicine and Biology Society (EMBS), 1992. 14th Annual International Conference of the IEEE*, vol. 5, 1992, pp. 1744–1745.
- [175] F. A. Anderson, "Impedance plethysmography in the diagnosis of arterial and venous disease," *Annals of biomedical engineering*, vol. 12, no. 1, pp. 79–102, 1984.
- [176] M. Qu, Y. Zhang, J. G. Webster, and W. J. Tompkins, "Motion artifact from spot and band electrodes during impedance cardiography," *IEEE Transactions on Biomedical Engineering*, no. 11, pp. 1029–1036, 1986.
- [177] A. Sherwood, S. Royal, R. Turner, and S. Hutcheson, "Comparison of spot and band electrodes for monitoring cardiac performance by impedance cardiography during exercise," in *Engineering in Medicine and Biology Society, 1991. Vol. 13: 1991., Proceedings of the Annual International Conference of the IEEE*. IEEE, 1991, pp. 796–796.
- [178] R. Patterson, L. Wang, and S. Raza, "Impedance cardiography using band and regional electrodes in supine, sitting, and during exercise," *IEEE transactions on biomedical engineering*, vol. 38, no. 5, pp. 393–400, 1991.
- [179] B. Ristic, S. Kun, and R. Peura, "Muscle tissue ischemia monitoring using impedance spectroscopy: analysis of $r_{sub 0}/and/spl tau/$ variations with ischemia," in *Bioengineering Conference, 1997., Proceedings of the IEEE 1997 23rd Northeast*. IEEE, 1997, pp. 7–8.
- [180] M. Jaffrin and C. Vanhoutte, "Quantitative interpretation of arterial impedance plethysmographic signals," *Medical and Biological Engineering and Computing*, vol. 17, no. 1, pp. 2–10, 1979.
- [181] E. Sigman, A. Kolin, L. Katz, and K. Jochim, "Effect of motion on the electrical conductivity of the blood," *American Journal of Physiology–Legacy Content*, vol. 118, no. 4, pp. 708–719, 1937.

- [182] K.-I. Yamakoshi, H. Shimazu, T. Togawa, M. Fukuoka, and H. Ito, "Noninvasive measurement of hematocrit by electrical admittance plethysmography technique," *IEEE Transactions on Biomedical Engineering*, no. 3, pp. 156–161, 1980.
- [183] K. K. Tremper, "Principles of applied biomedical instrumentation," 1990.
- [184] K. R. Visser, "Electric properties of blood and impedance cardiography," Ph.D. dissertation, University of Groningen, 1992.
- [185] C. Gabriel, S. Gabriel, and E. Corthout, "The dielectric properties of biological tissues: I. literature survey," *Physics in medicine and biology*, vol. 41, no. 11, p. 2231, 1996.
- [186] J. Fleming, T. Hames, and J. Smallwood, "Comparison of volume changes in the forearm assessed by impedance and water-displacement plethysmography," *Medical and Biological Engineering and Computing*, vol. 24, no. 4, p. 375, 1986.
- [187] "Arduino uno rev3," <https://store.arduino.cc/arduino-uno-rev3>, accessed: 2017-10-1.
- [188] K. R. Aroom, M. T. Harting, C. S. Cox, R. S. Radharkrishnan, C. Smith, and B. S. Gill, "Bioimpedance analysis: a guide to simple design and implementation," *Journal of Surgical Research*, vol. 153, no. 1, pp. 23–30, 2009.
- [189] G. J. Saulnier, N. Liu, C. Tamma, H. Xia, T.-J. Kao, J. Newell, and D. Isaacson, "An electrical impedance spectroscopy system for breast cancer detection," in *Engineering in Medicine and Biology Society, 2007. EMBS 2007. 29th Annual International Conference of the IEEE*. IEEE, 2007, pp. 4154–4157.
- [190] D. Sheingold, "Impedance & admittance transformations using operational amplifiers," *Lightning Empiricist*, vol. 12, no. 1, pp. 1–8, 1964.
- [191] *Cardioline® Delta 60 Plus Service Manual*, Remco Italia S.p.A, 1996, version/IN/Rel. 1.4.
- [192] *moorVMS-LDF User Manual*, Moor instruments Ltd, 2009, version 2.0
Date:14/01/2009.
- [193] Y. Uchida, N. YOSHIMOTO, S. MURAO, and K. INOUE, "Cyclical reduction in blood flow of partially constricted coronary artery in dogs ii. an arteriographic study," *Japanese circulation journal*, vol. 41, no. 11, pp. 1221–1230, 1977.
- [194] A. Lowe, W. Harrison, E. El-Aklouk, P. Ruygrok, and A. Al-Jumaily, "Non-invasive model-based estimation of aortic pulse pressure using suprasystolic brachial pressure waveforms," *Journal of biomechanics*, vol. 42, no. 13, pp. 2111–2115, 2009.
- [195] R. Kharbanda, U. Mortensen, P. White, S. Kristiansen, M. Schmidt, J. Hoschtitzky, M. Vogel, K. Sorensen, A. Redington, and R. MacAllister, "Transient limb ischemia induces remote ischemic preconditioning in vivo," *Circulation*, vol. 106, no. 23, pp. 2881–2883, 2002.
- [196] H. Nyquist, "Certain topics in telegraph transmission theory," *Transactions of the American Institute of Electrical Engineers*, vol. 47, no. 2, pp. 617–644, 1928.

References

- [197] G. S. Ohm, *Die galvanische Kette, mathematisch bearbeitet*. TH Riemann, 1827.
- [198] T. Ashraf, Z. Panhwar, S. Habib, M. A. Memon, F. Shamsi, and J. Arif, "Size of radial and ulnar artery in local population," *JPMA-Journal of the Pakistan Medical Association*, vol. 60, no. 10, p. 817, 2010.
- [199] S. N. Mohapatra, *Non-invasive cardiovascular monitoring by electrical impedance technique*. Pitman Medical, 1981.
- [200] T. Dai and A. Adler, "In vivo blood characterization from bioimpedance spectroscopy of blood pooling," *IEEE Transactions on Instrumentation and Measurement*, vol. 58, no. 11, pp. 3831–3838, 2009.
- [201] V. K. Pandey and P. C. Pandey, "Cancellation of respiratory artifact in impedance cardiography," in *Engineering in Medicine and Biology Society, 2005. IEEE-EMBS 2005. 27th Annual International Conference of the*. IEEE, 2006, pp. 5503–5506.
- [202] D. Swanson and J. Webster, "Errors in four-electrode impedance plethysmography," *Medical and Biological Engineering and Computing*, vol. 21, no. 6, pp. 674–680, 1983.
- [203] S. Ansari, A. Belle, K. Najarian, and K. Ward, "Impedance plethysmography on the arms: Respiration monitoring," in *Bioinformatics and Biomedicine Workshops (BIBMW), 2010 IEEE International Conference on*. IEEE, 2010, pp. 471–472.
- [204] J. Rosell, K. P. Cohen, and J. G. Webster, "Reduction of motion artifacts using a two-frequency impedance plethysmograph and adaptive filtering," *IEEE transactions on biomedical engineering*, vol. 42, no. 10, pp. 1044–1048, 1995.
- [205] P. Kvandal, S. A. Landsverk, A. Bernjak, A. Stefanovska, H. D. Kvernmo, and K. A. Kirkebøen, "Low-frequency oscillations of the laser doppler perfusion signal in human skin," *Microvascular research*, vol. 72, no. 3, pp. 120–127, 2006.
- [206] K. K. McCully, S. Smith, S. Rajaei, J. S. Leigh, and B. H. Natelson, "Muscle metabolism with blood flow restriction in chronic fatigue syndrome," *Journal of Applied Physiology*, vol. 96, no. 3, pp. 871–878, 2004.
- [207] R. Hainsworth, "Syncope: what is the trigger?" 2003.
- [208] Y. H. Shash, M. A. Eldosoky, and M. T. Elwakad, "Bioimpedance analysis in detecting vascular diseases using blood pooling method," *Journal of medical engineering & technology*, vol. 42, no. 8, pp. 578–587, 2018.
- [209] M. Klum, D. Osterland, A.-G. Pielmus, T. Tigges, and R. Orglmeister, "Peripheral vascular impedance plethysmography for respiratory rate estimation using beat-to-beat features," *Pulse*, vol. 2, p. 5, 2018.
- [210] N. E. Almond, D. P. Jones, and E. D. Cooke, "Noninvasive measurement of the human peripheral circulation: relationship between laser doppler flowmeter and photoplethysmograph signals from the finger," *Angiology*, vol. 39, no. 9, pp. 819–829, 1988.

- [211] J. M. Bland and D. Altman, "Statistical methods for assessing agreement between two methods of clinical measurement," *The lancet*, vol. 327, no. 8476, pp. 307–310, 1986.
- [212] I. Perakash, "Difficulties in laser doppler measurement of skin blood flow under applied external pressure," *Journal of rehabilitation research and development*, vol. 25, no. 3, 1988.
- [213] N. P. Couch, J. M. Van De Water, and J. R. Dmochowski, "Noninvasive measurement of peripheral arterial flow: Impedance cardiograph and ultrasonic doppler flowmeter," *Archives of Surgery*, vol. 102, no. 5, pp. 435–439, 1971.
- [214] J.-J. Wang, W.-C. Hu, T. Kao, C.-P. Liu, S.-K. Lin *et al.*, "Development of forearm impedance plethysmography for the minimally invasive monitoring of cardiac pumping function," *source: Journal of Biomedical Science and Engineering*, vol. 4, 2011.
- [215] A. Yufera, G. Leger, E. Rodriguez-Villegas, J. Muñoz, A. Rueda, A. Ivorra, R. Gomez, N. Noguera, and J. Aguiló, "An integrated circuit for tissue impedance measure," in *Microtechnologies in Medicine & Biology 2nd Annual International IEEE-EMB Special Topic Conference on*. IEEE, 2002, pp. 88–93.
- [216] R. Pallas-Areny and J. G. Webster, "Bioelectric impedance measurements using synchronous sampling," *IEEE transactions on biomedical engineering*, vol. 40, no. 8, pp. 824–829, 1993.
- [217] M. Min, O. Märten, and T. Parve, "Lock-in measurement of bio-impedance variations," *Measurement*, vol. 27, no. 1, pp. 21–28, 2000.
- [218] N. Rintamaki, "Human responses to cold," *Alaska medicine*, vol. 49, no. 2, p. 29, 2007.
- [219] *LMx37 3-Terminal Adjustable Regulators*, Texas Instruments, Jan. 2015, revision L.
- [220] *1A LOW DROPOUT POSITIVE ADJUSTABLE OR FIXED-MODE REGULATOR*, Diodes Incorporated, Oct. 2008, rev. 12.
- [221] *Precision Micropower, Low Dropout Voltage References*, Analog Devices, 2011, rev. L.
- [222] *Low Cost, Low Power, Differential ADC Driver AD8137*, Analog Devices, 2012, rev. E.
- [223] *Very low drop voltage regulator with inhibit function*, ST Microelectronics, May 2017, rev. 31.
- [224] *High Performance, 145 MHz FastFET Op Amps AD8065/AD8066*, Analog Devices, 2016, rev. K.
- [225] *TL08xx JFET-Input Operational Amplifiers*, Texas Instruments, May 2015, rev. I.
- [226] *Small Signal Fast Switching Diodes*, Vishay Semiconductors, Jul. 2017, rev. 1.4.

Appendix A

Final assembly circuit

The figure A.1 shows the final circuit assembly. All these modules were fixed to a board, and the different circuit stages were interconnected using jumper cables. In the same board, a DAQ NI USB-6212 (National Instruments) was mounted to connect the output channels I_{DC} , Z_{DC} and Z_{AC} . Additionally, in order to ensure a cohesive system, the Arduino MCU was also affixed and connected to the DDS module.

As inputs and outputs, the instrument includes data and power ports. The data ports have two USB cables connected to the DAQ box and the Arduino PCB. They work as a digital data bus and system command controller, respectively. The system is powered by the battery bank using the PSU module. For this to happen, a 4-pins cable was designed as interface. The electrodes cables run from the MHC and sensing boards. These cables were designed using alligator clips that got hooked on to the electrodes end.

Final assembly circuit

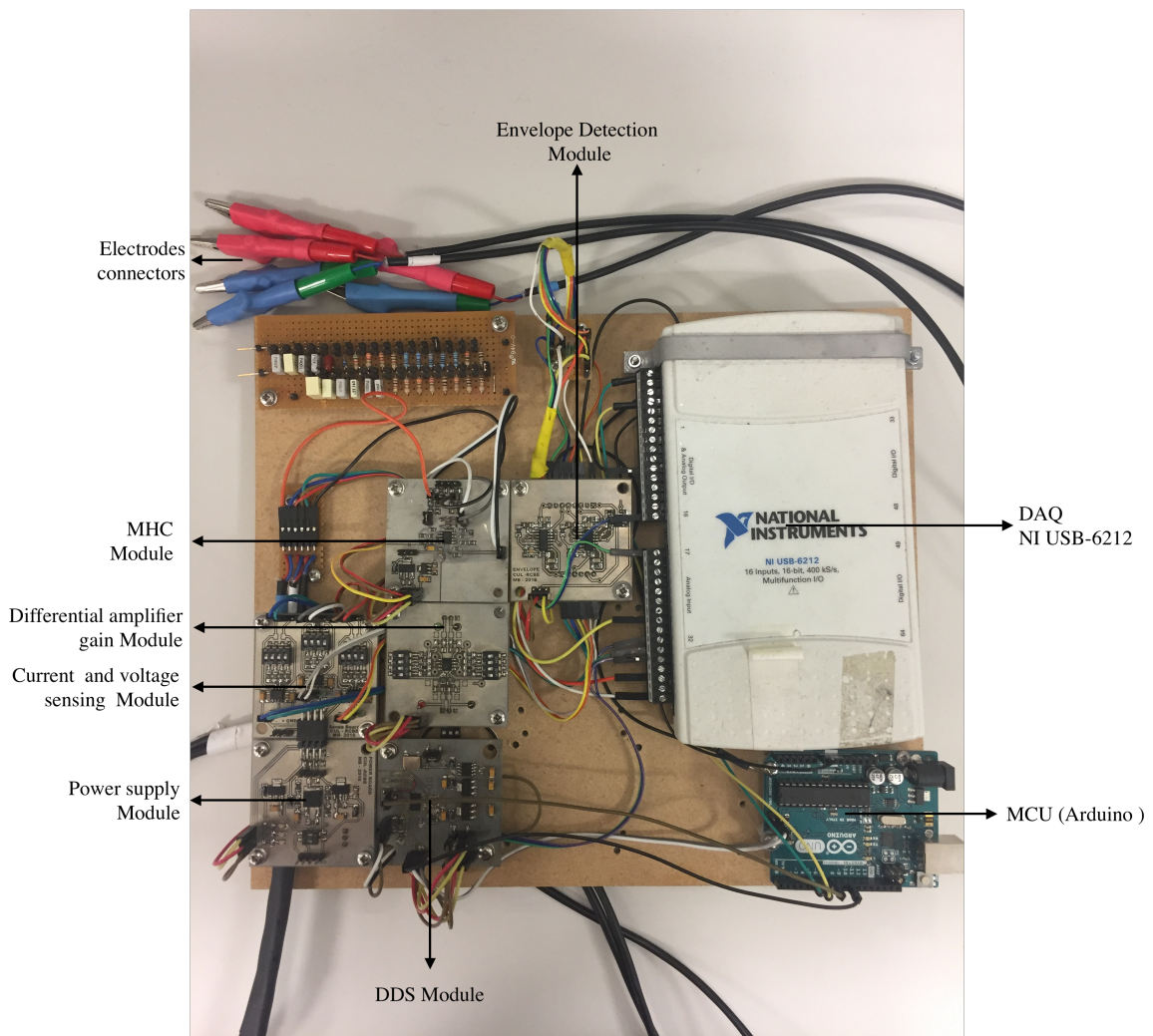


Figure A.1 Assembly of the bioelectrical impedance device showing all the modules, electrodes, DAQ and MCU.

Appendix **B**

Schematics of the iPG instrument

Power supply

The schematic circuits for the power supply designed are mentioned in the appendix B, figure B. Operating the iPG device requires positive (VIN+) and negative (VIN-) supplies that can be provided by any external power. For safety purposes, batteries were the source of choice. The table 4.1 shows the components employed in the implementation, which operates within the desired appropriate range as required by the device. The regulators LM3XX [219] are voltage variable regulators. However, their output was set to ± 12 V for each source using the appropriate selection of resistors. The capacitors which were added to all the regulators were selected in accordance to the manufacturer's recommendation to evade the prospects of any ripple at the output voltage.

In Altium Designer a PCB of 50 mm x 50 mm was produced considering input and ports in addition to indicators and sensors. For instance, the ports included three input voltage pins VIN+, VIN- and ground (GND) coming from the batteries, along with an eight-pin male connector that provides regulated board to the next board. These indicators and sensors included a dip-switch working as power ON/OFF button, a set of three red-LED indicating the power of +12 V, -12 V and 5 V, and a three-pin port connected to the ADC port of the microcontroller which monitors the batteries' capacity. It also includes additional regulated voltage ports in order to feed other external modules.

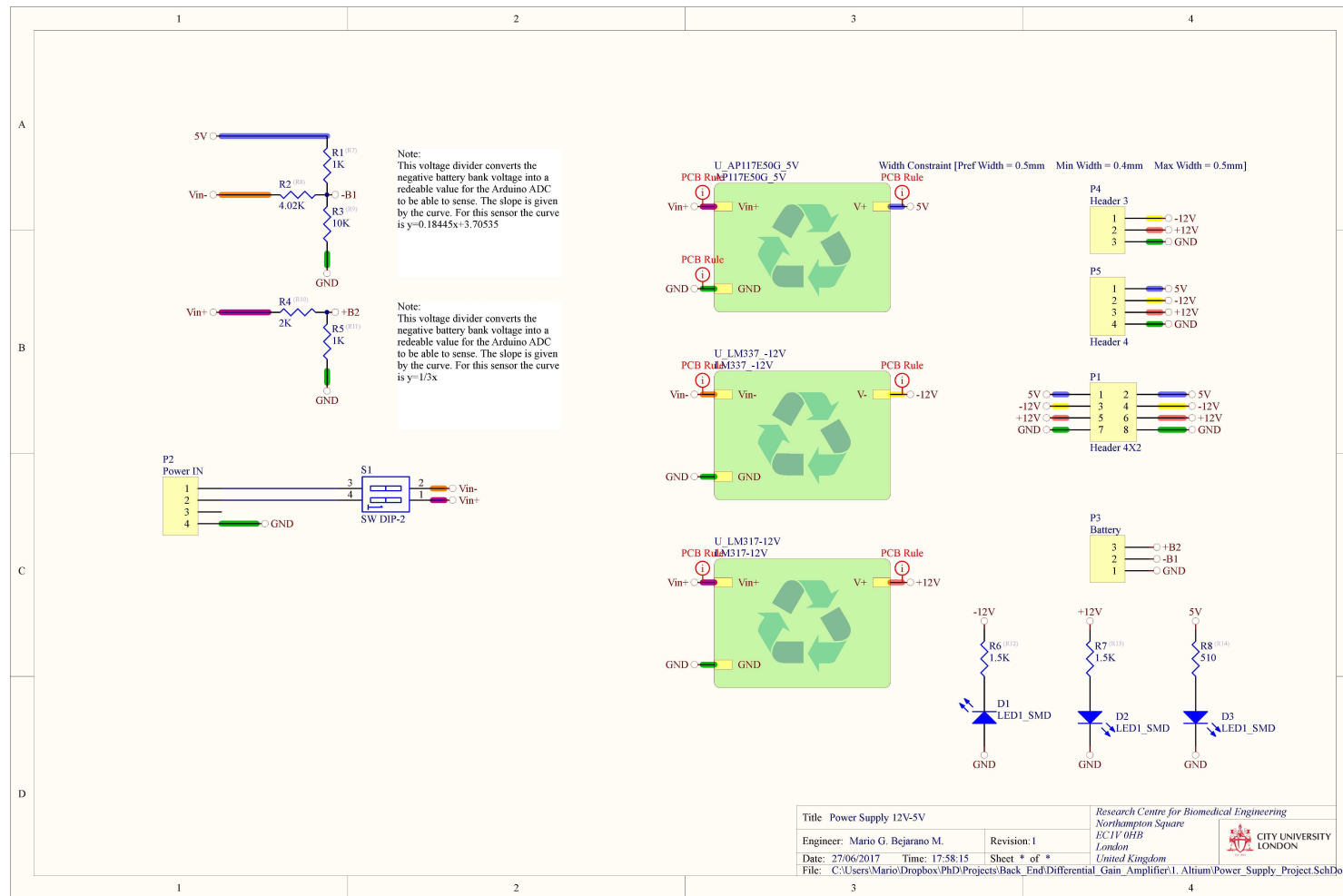


Figure B.1 Top-up view of the power supply. Each box represents the Voltage regulators circuits. The schematic also includes indicators LED, switches and output ports.

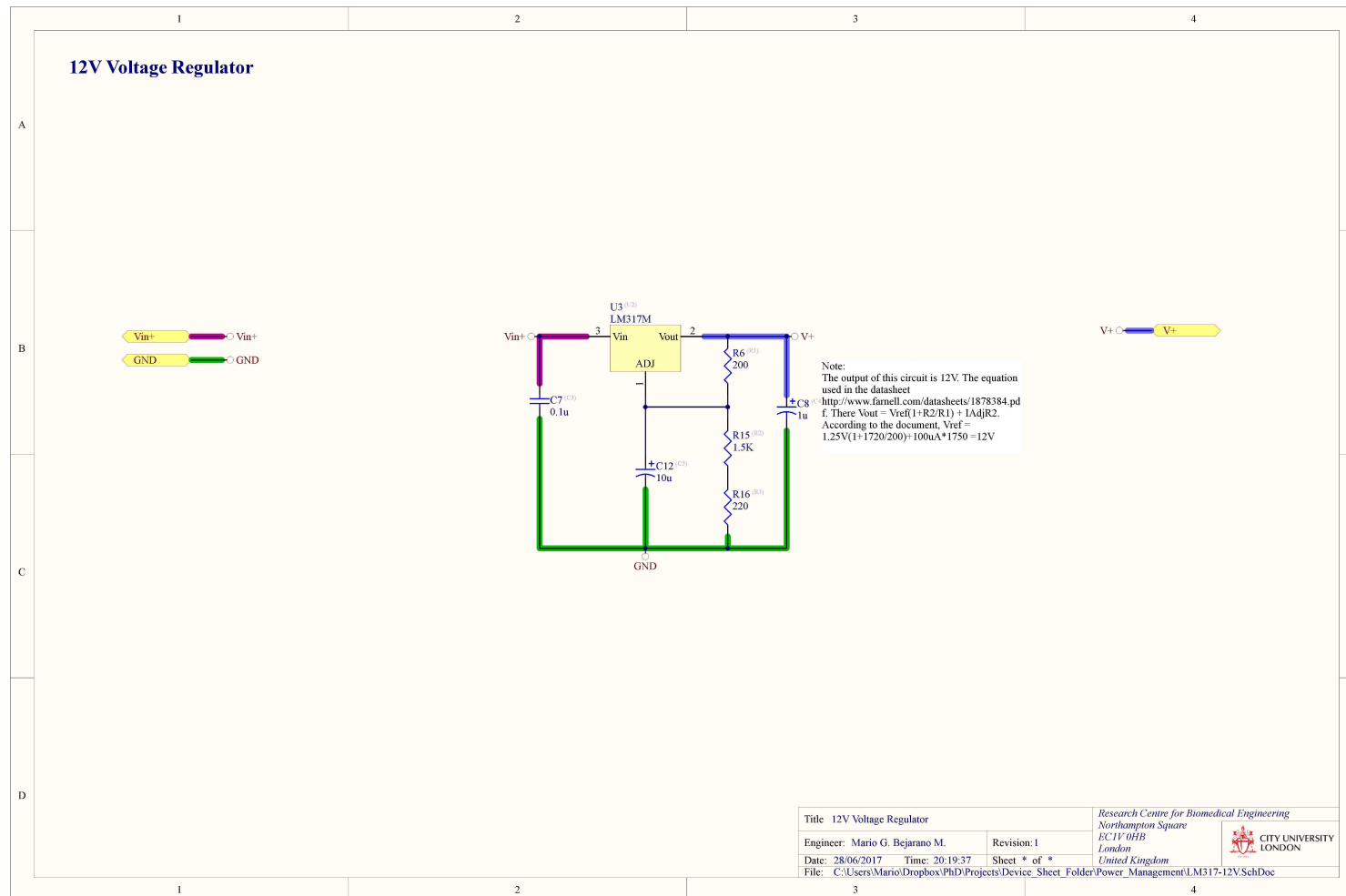


Figure B.2 The schematic shows the configuration of the voltage regulator LM317, the resistors selected set the output voltage at 12 V. The capacitors filter ripples from the batteries.

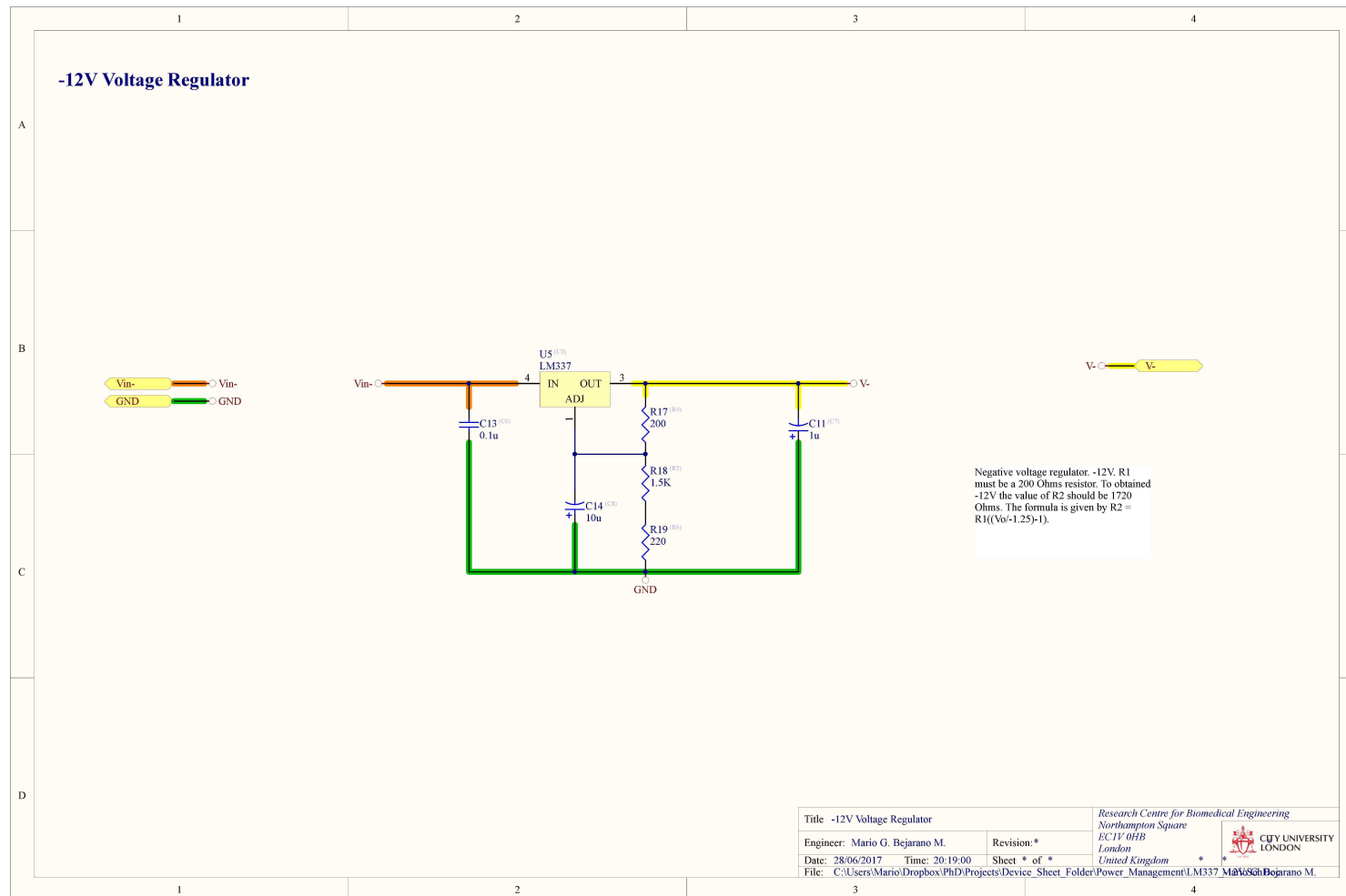


Figure B.3 The schematic shows the configuration of the voltage regulator LM337, the resistors selected set the output voltage at -12 V. The capacitors filter noise peaks.

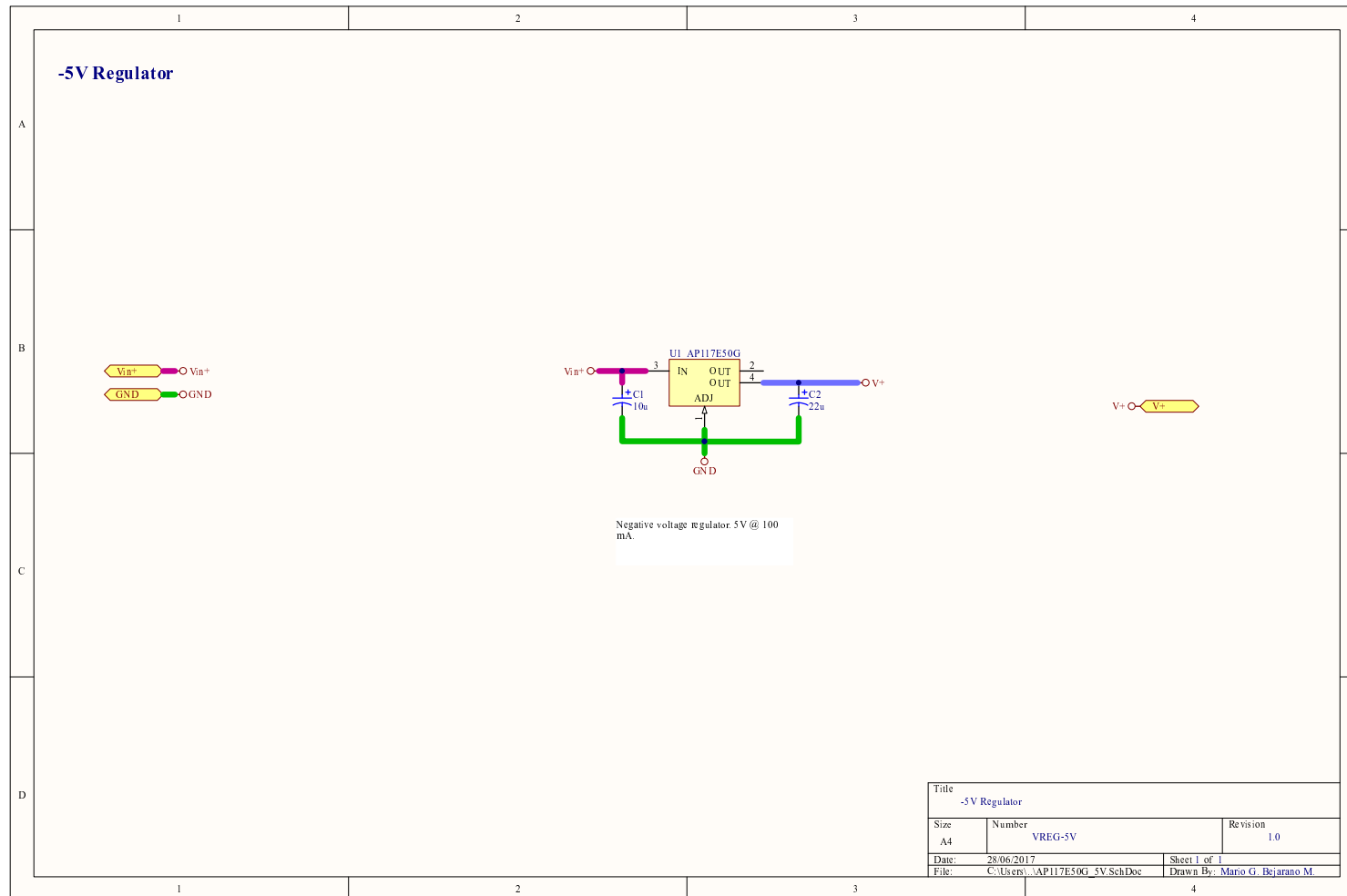


Figure B.4 The schematic shows the configuration of the voltage regulator AL117E50G, the output is fixed to 5 V. The capacitors filter noises from the power bank.

DDS

The figure B.5 shows the schematic used in the design of the wave generator. Owing to the noise that a digital circuit would feed into an analogue system, a separate power supply powers up this module. For this purpose, two voltage regulators (AP117E50G [220]) provide 5 V energy sources for digital and analogue components using two separated ground paths (GND - AGND). In addition, a 3 V reference is needed for the oscillator to operate - which is supplied by the IC REF196 [221]. The DDS requires an external clock in order to work. Therefore, a 50 MHz oscillator provides the desired clock signal.

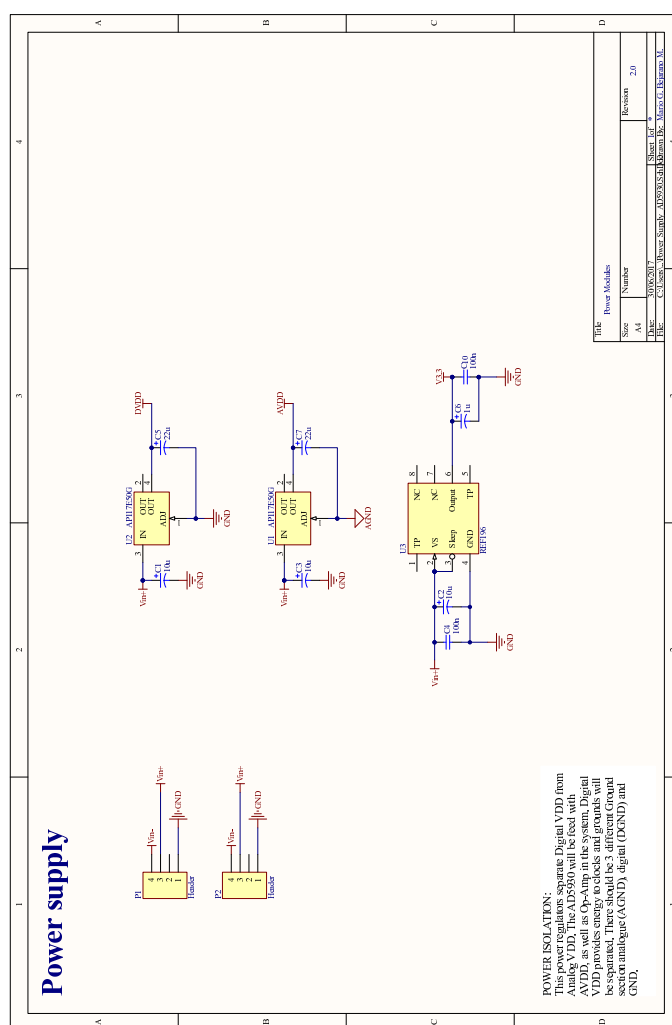


Figure B.5 The power supply circuit provides 3 different voltages 5 V for analogue and digital circuitry, and 3 V for voltage reference. There are three different ground paths for each source.

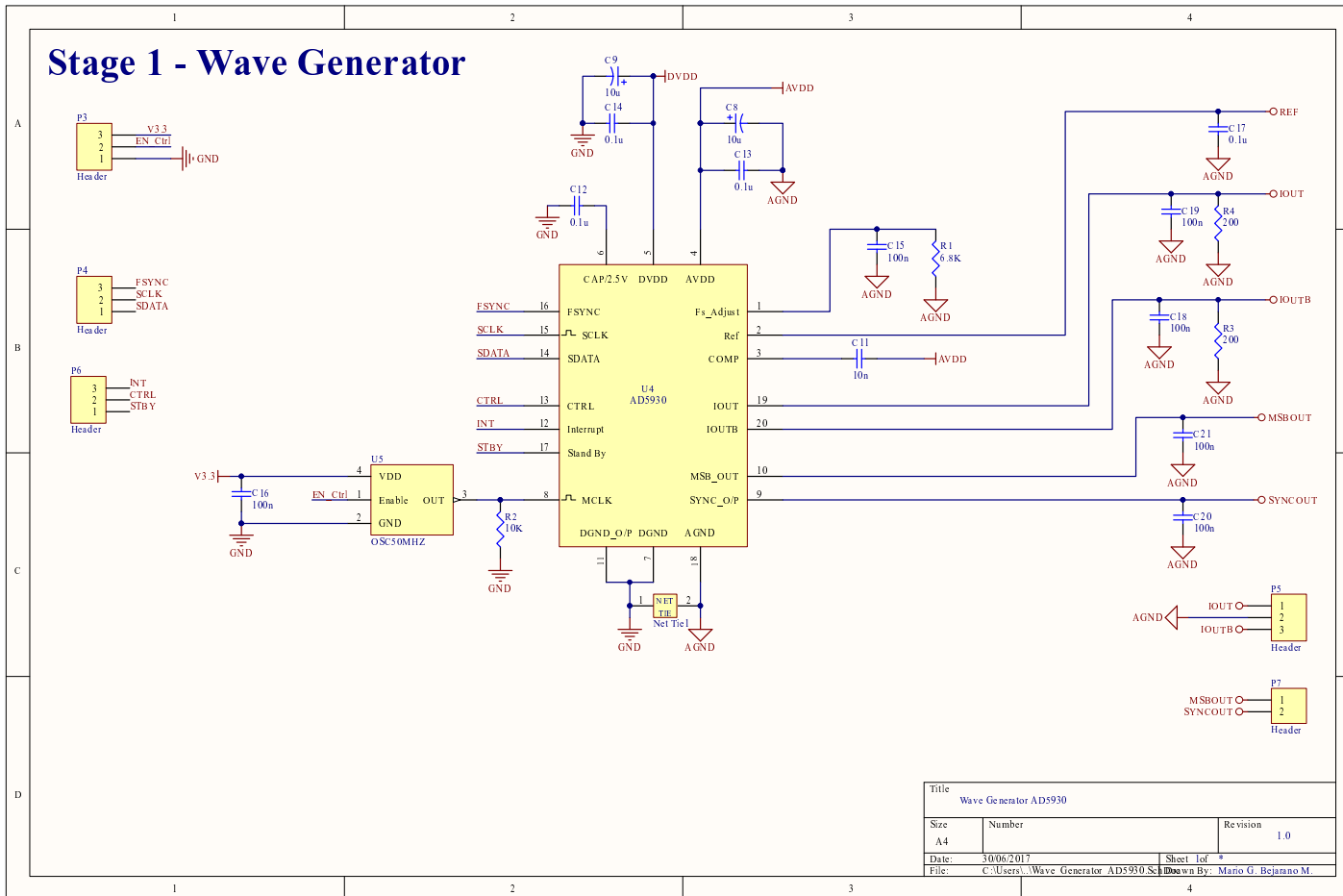


Figure B.6 Schematic of the AD5930, it includes the 50 MHz oscillator and output filters.

Differential gain amplifier

The IC AD8137 [222] was the main component of the DGA. Low tolerance resistors were placed at each channel to achieve a steady gain at the output. Since the DGA needed a separate power supply to operate within the limits of the batteries, a dual power supply of 6 V and -6 V was designed using the IC LF60CDT [223] and LM337 [219], respectively. Since the latter is a variable voltage regulator, a set of resistors was used to adjust the level of regulation to the desired level. The schematic circuits can be found in the appendix B, figures B.8 and B.9

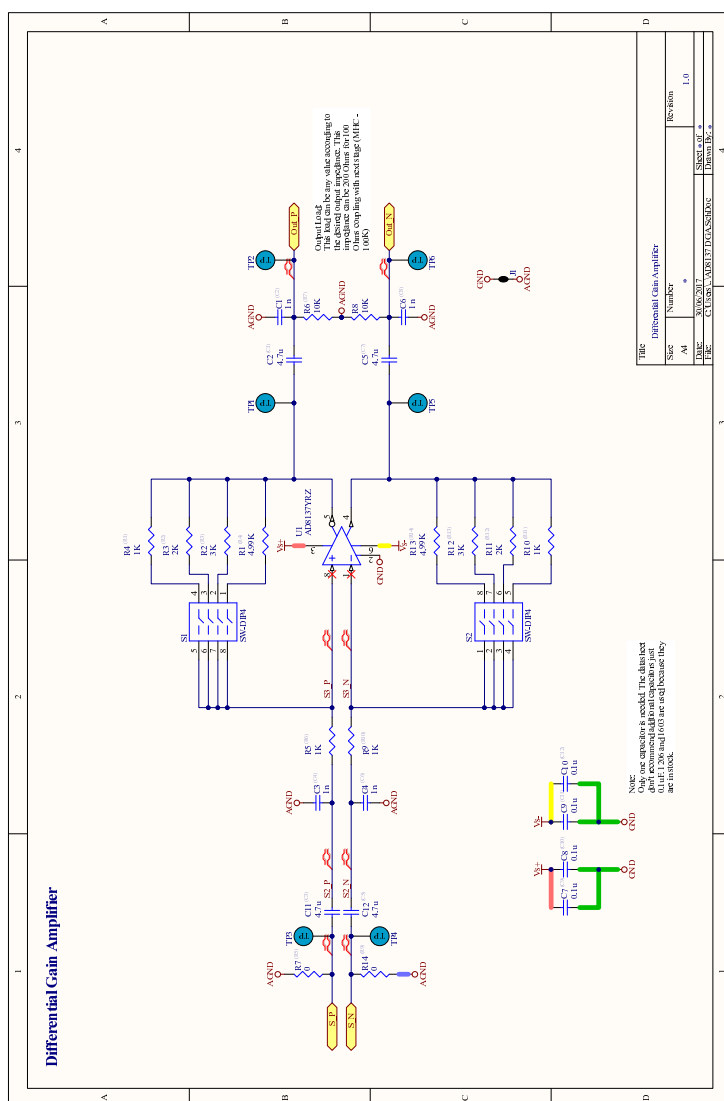


Figure B.7 Differential gain amplifier controlled by 4 position dip-switch adjusting the gain of the signal output.

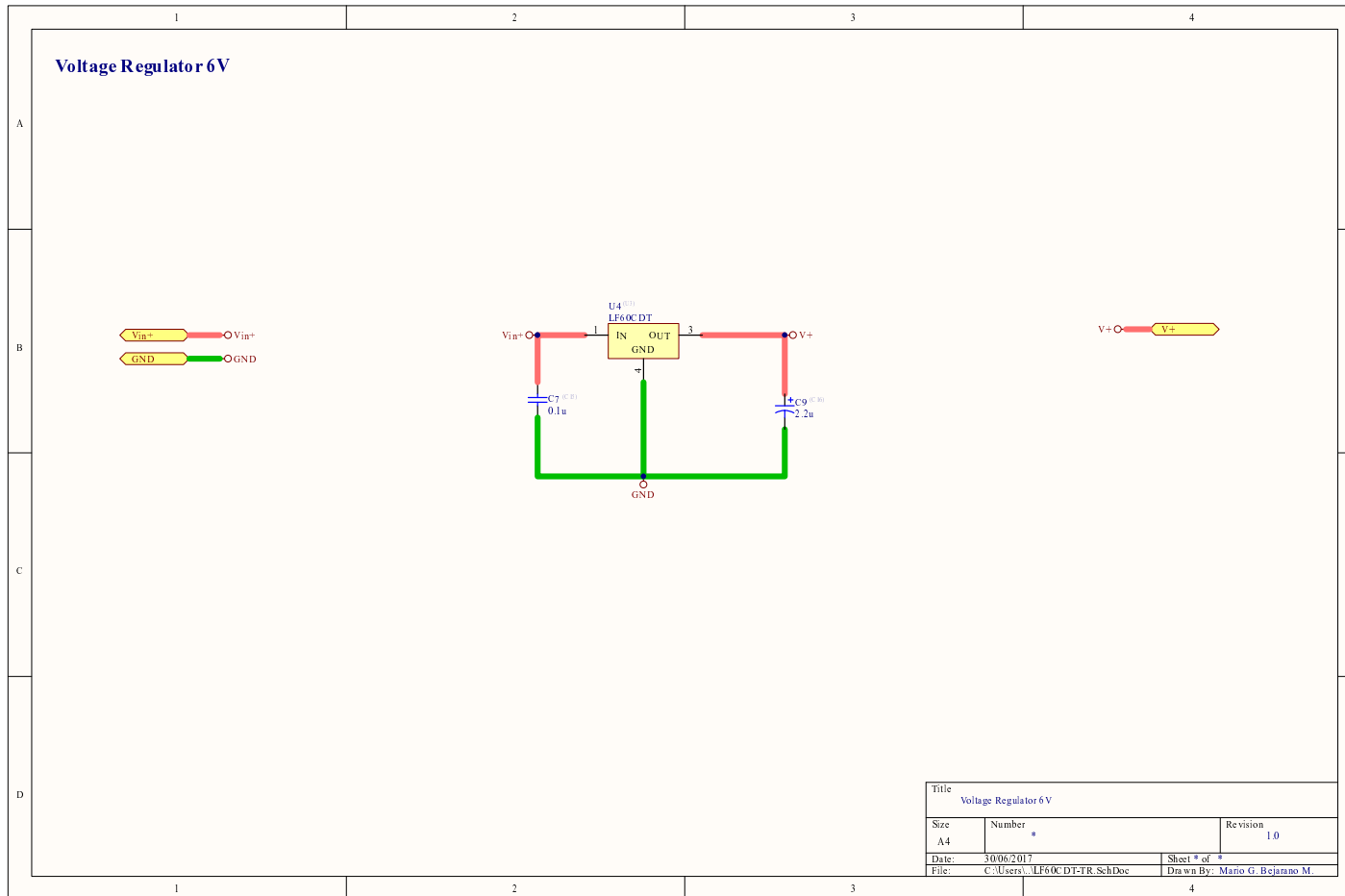


Figure B.8 Power supply circuit based on the IC LF60CDT.

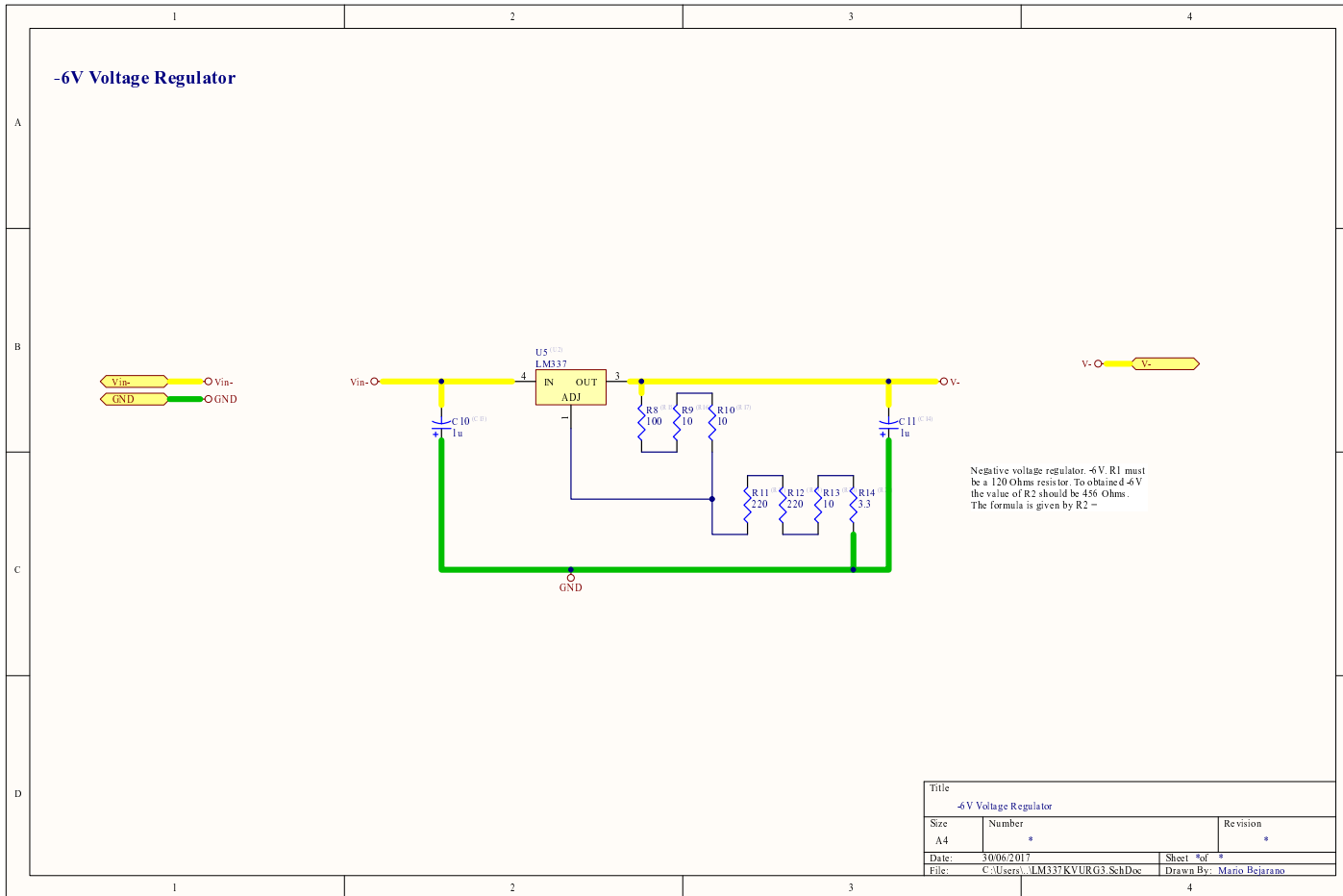


Figure B.9 Power supply circuit based on the IC LM337, the resistors were adjusted to achieve -6 V.

Modified Howland circuit

The Op-Amp selected for this design was the AD8066 [224], a dual Op-Amp that offers high bandwidth of 145 MHz, high input impedance of $1000\text{ G}\Omega @ 4.5\text{ pF}$, low noise of $7\text{ nV}/\sqrt{\text{Hz}}$ at 10 kHz, open loop gain of 113 dB and CMMR of -100 dB [224]. All these characteristics made this Op-Amp an ideal choice to implement a MHC. The design also included a dual power supply of 5 V and -5 V provided by the IC's AP117E50G and L79L05, respectively. The final circuit schematics, which include the MHC and power supplies, are shown in figures B.12, B.10 and B.11. From that design, the PCB was produced using the same manufacturing method of the previous ones.

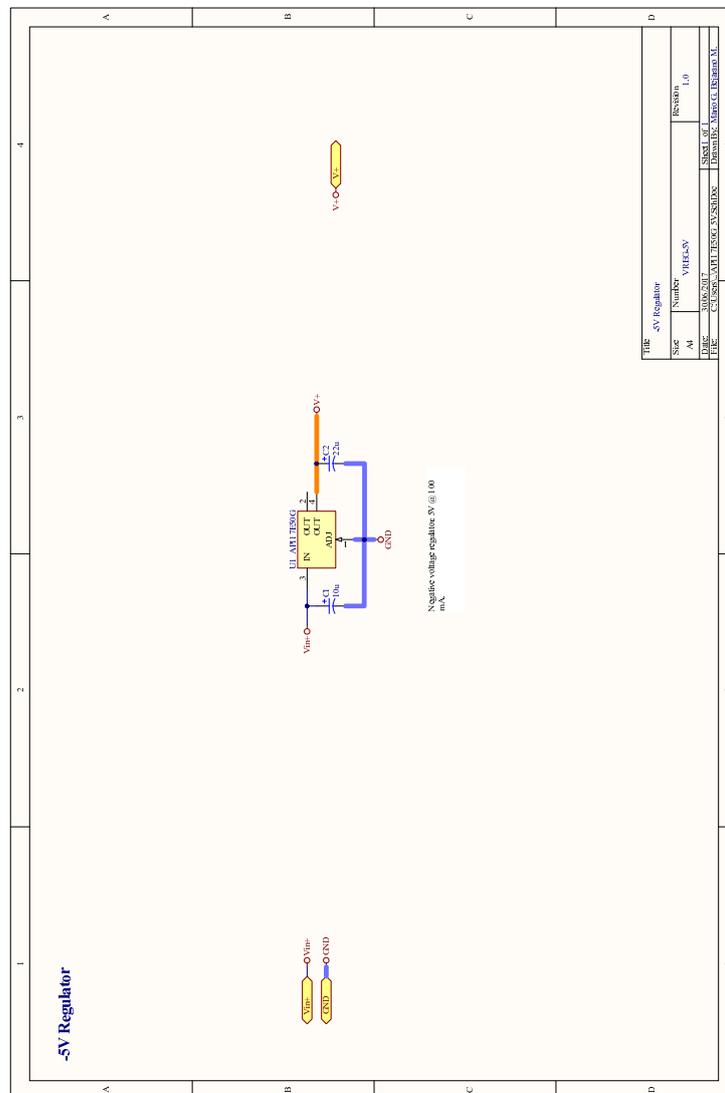


Figure B.10 Power supply circuit based on the IC AP117E50G.

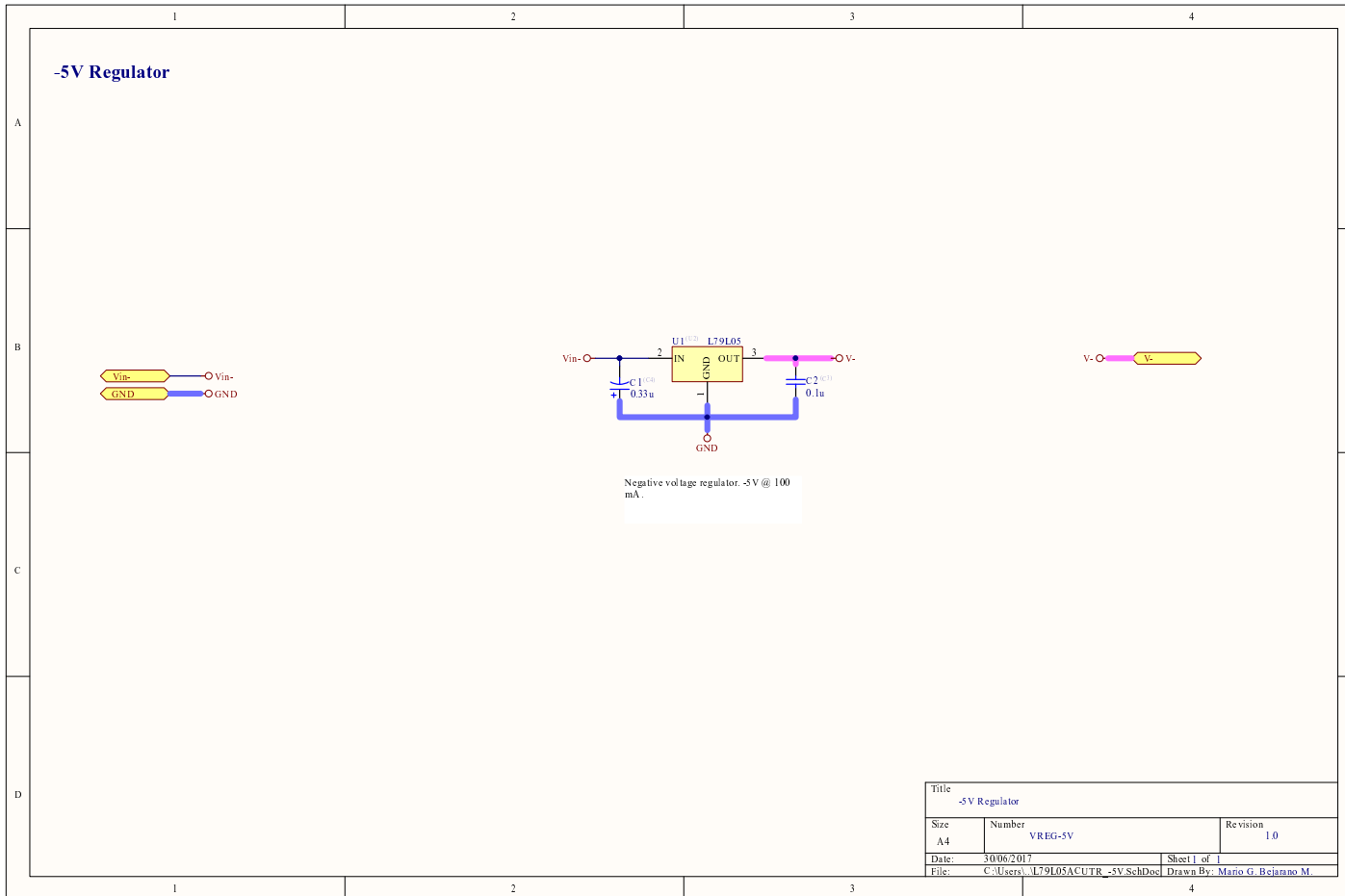


Figure B.11 Power supply circuit based on the fixed voltage regulator (-5 V) IC L79L05.

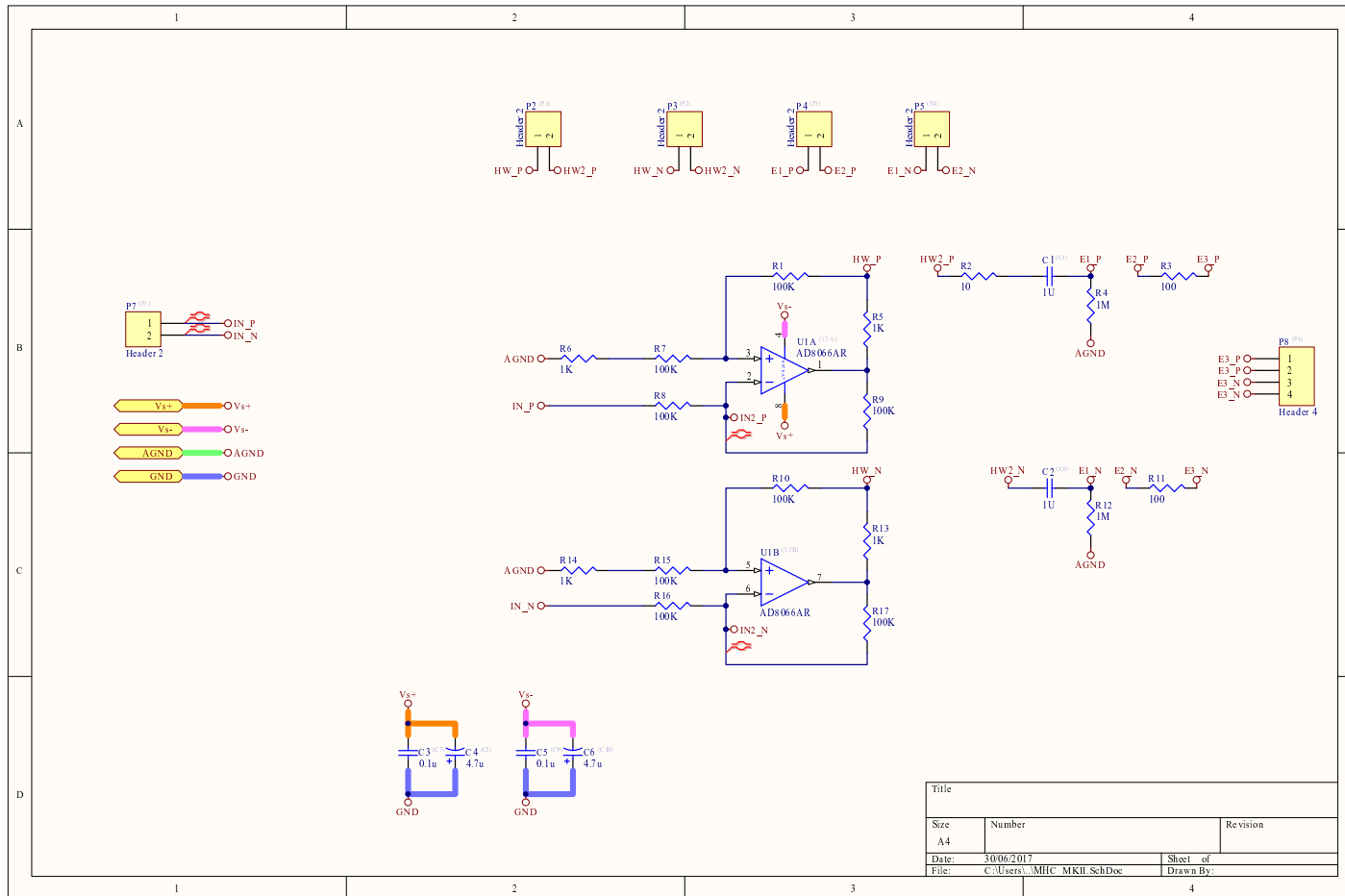


Figure B.12 Differential gain amplifier controlled by 4 position dip-switch adjusting the gain of the signal output.

Envelope detection circuits

The envelope or peak detection is achieved using the combination of an active diode configuration and a hold circuit. The first part of this circuit was created using an Op-Amp TL08XX [225] as well as a diode 1N4148 [226]. The combination creates a "super diode" or "perfect diode" circuit. Thus, the Op-Amp complements the diode's voltage drop when the signal crosses zero. The negative feedback resulting from the output of the diode towards the negative pin of the Op-Amp mitigates the diode's voltage drop. Resultantly, the output signal at the cathode's diode is essentially a half-wave rectified waveform crossing by zero. The figure B.15 shows a model of this circuit.

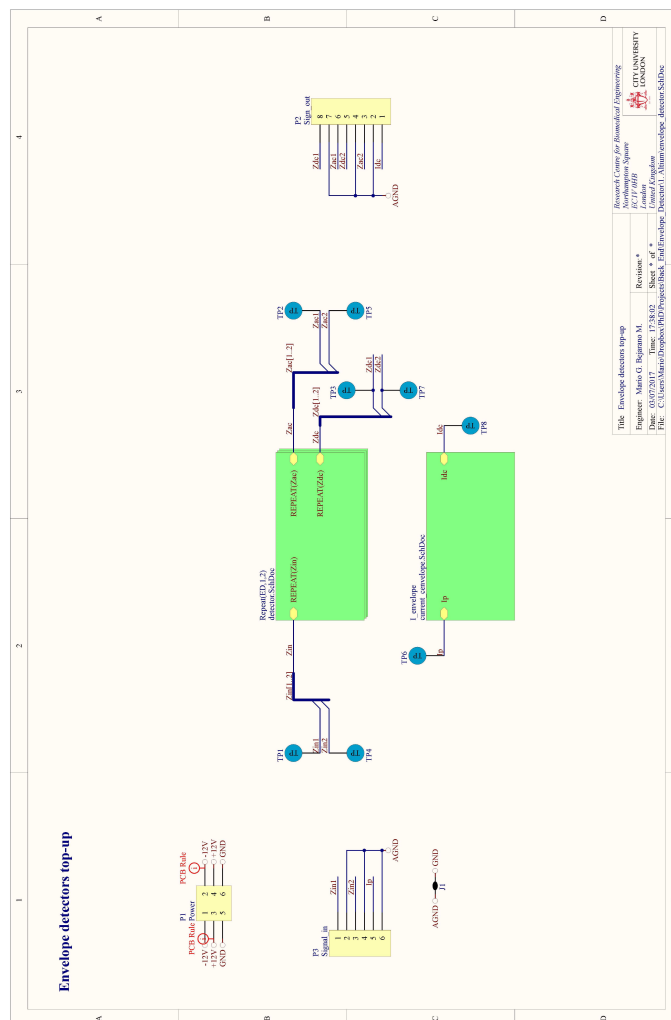


Figure B.14 The iPG device has designed to work with two voltage channels and one current channel sensor. Each envelope detector extracts the peak detection, which output is passed to the output ports of the device.

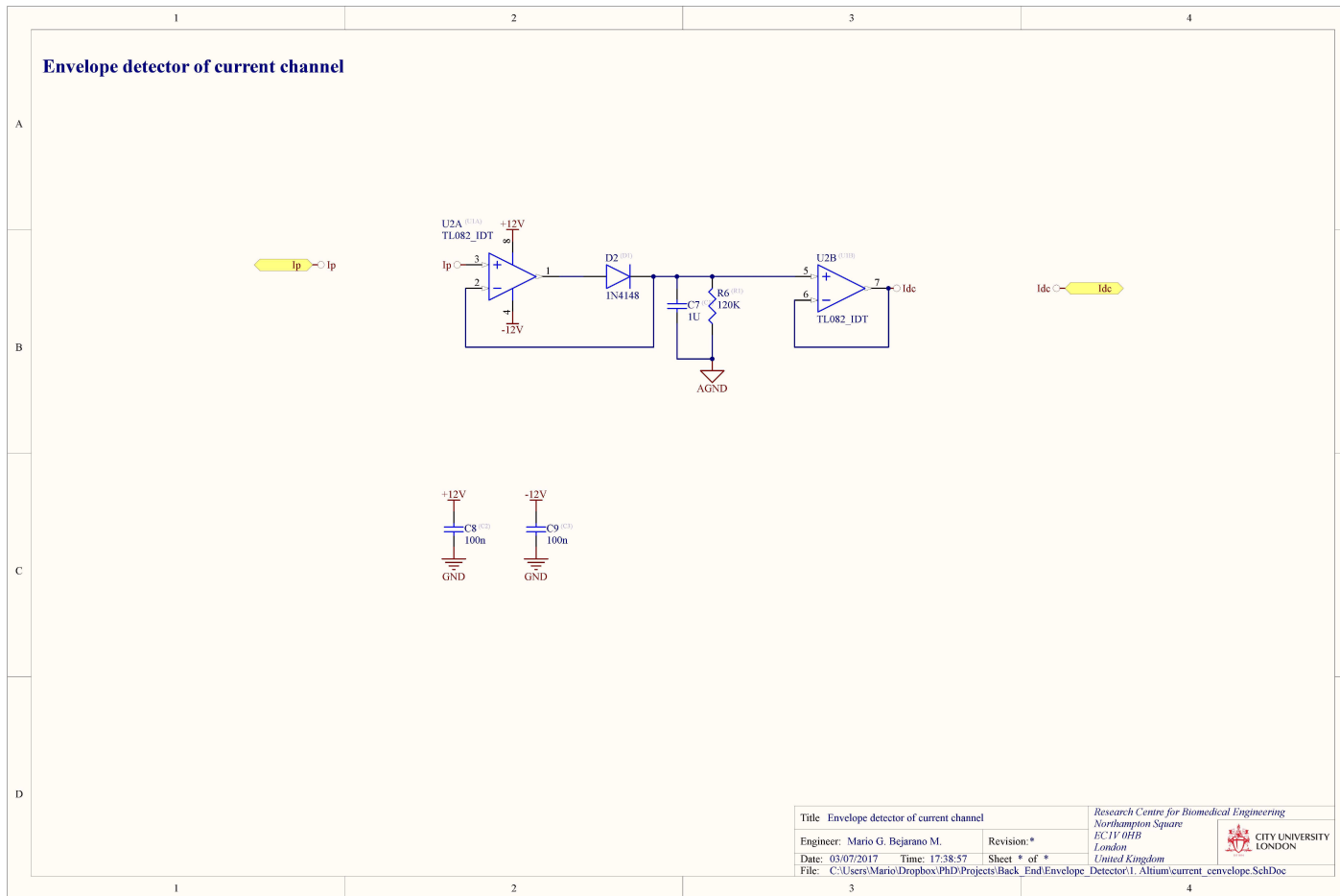


Figure B.15 The current of the MHC is converted to voltage which later can be detected by this circuit. The voltage detected from the current drives consist of a perfect diode configuration based on a TL084 and a diode 1N4148. Then the signal is sampled and hold by a capacitor. The output is buffered to get a low impedance output.

APA waveform isolation

Figure B.16 shows the circuit used to isolate the Arterial Pulse Amplitude waveform. Following that schematic, a high pass filter (HPF) is used to remove the signal's DC components, which is possible by implementing a passive filter composed by capacitor and resistor C_4 and R_5 , respectively. Notably, R_5 is virtually connected to ground (GND) through the negative pin of the Op-Amp. The cutting frequency of the HPF was calculated using the equation B.1 - which demonstrates that this circuit section practically blocks any DC component of the impedance signal.

$$f_c = \frac{1}{2\pi RC} = \frac{1}{2\pi 330K\Omega 4.7\mu f} = 10.26mHz \quad (B.1)$$

Subsequently, a second order active filter eliminates any high-frequency noise occurring within the plethysmography signal. The cut off frequencies were calculated as outlined in equations B.2 and B.3. The first Op-Amp configuration is an inverting amplifier circuit with a frequency cut at 10.61 Hz and a gain in DC of 30.30. The second Op-Amp configuration 10.26 Hz has an amplification factor in DC of 4.70.

In general, the extraction of the APA signal is achieved with a band-pass filter with low-frequency cut at 10.26 mHz with a roll-off of 20 dB/decade as well as a high-frequency cut at 10.26 Hz with a roll-off of 40 dB/decade. Finally, the final output was passed on to a buffer configuring the channel V_{AC} . The APA waveform is then amplified using a fixed gain of 142.41.

$$f_c = \frac{1}{2\pi RC} = \frac{1}{2\pi 10M\Omega 1.5nf} = 10.61Hz \quad (B.2)$$

$$f_c = \frac{1}{2\pi RC} = \frac{1}{2\pi 47K\Omega 330nf} = 10.26Hz \quad (B.3)$$

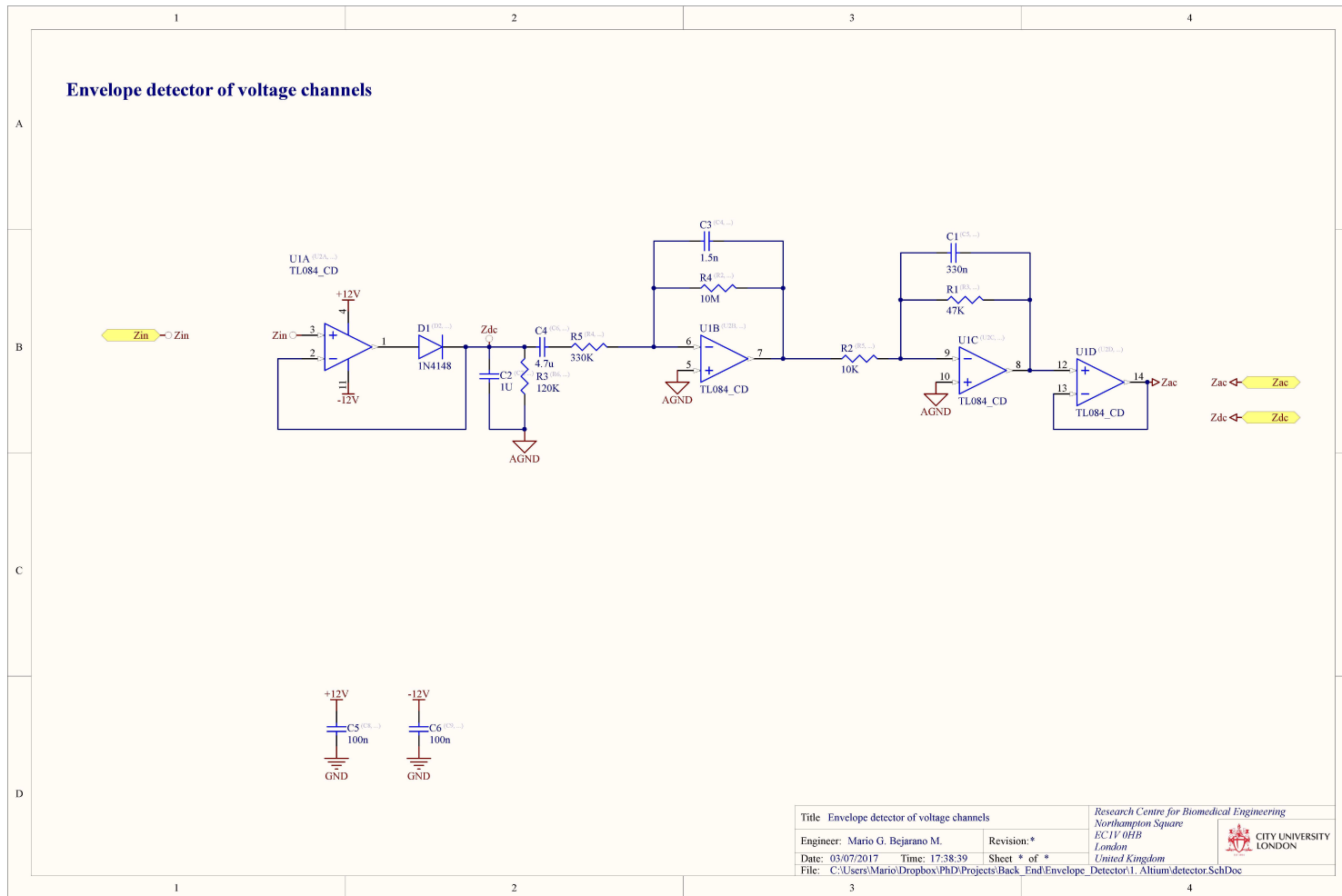


Figure B.16 The voltage detector consist of a perfect diode configuration based on a TL084 and a diode 1N4148. Then the signal is sampled and hold by a capacitor. The output of this signal is later passed to a band-pass filter and a buffer.

Appendix C

Arduino program to control DDS AD5930

```
1 /*
2 AD5930 Controller program
3
4 This program receives instructions via serial USB connection
   from LabView or Matlab.
5 It communicates via SPI portocol to the AD5930.
6
7 The Host PC send commands such as frequency Lock, start/stop
   waveform.
8
9 modified 19 October 2015
10 by Mario Bejarano
11 City University London
12 */
13
14 #include "SPI.h"
15 int ss=10;
16 int del=200;
17 int incomingByte = 0;
18 int CTRL_pin=8;
19 int IPin=4;
20 int VPin=3;
21 int PhasePin=2;
```

Arduino program to control DDS AD5930

```
22 int Bank1 = 0;
23 int Bank2 = 1;
24 int val1=0;
25 int val2=0;
26 int val3=0;
27 int Battery1 = 0;
28 int Battery2 = 0;
29 int LED = 7;
30 String Z;
31 String frequ;
32
33 #define AD5930_F_MCLK 50000000           // 25MHz clock
34 #define AD5930_2POW28 16777216         // 2 to the power of
    24
35
36 void setup()
37 {
38   Serial.begin(115200);
39   pinMode(VPin, INPUT);
40   pinMode(IPin, INPUT);
41   pinMode(PhasePin, INPUT);
42   pinMode(Bank1, INPUT);
43   pinMode(Bank2, INPUT);
44   pinMode(ss, OUTPUT);
45   pinMode(CTRL_pin, OUTPUT);
46   pinMode(LED, OUTPUT);
47   SPI.begin();
48   SPI.setBitOrder(MSBFIRST);
49   SPI.setDataMode(SPI_MODE2);
50   digitalWrite(ss, HIGH);
51   digitalWrite(CTRL_pin, LOW);
52 }
53
54 void setValue(int value)
55 {
```

```

56  digitalWrite(ss, LOW);
57  SPI.transfer(0);
58  SPI.transfer(value);
59  digitalWrite(ss, HIGH);
60 }
61
62 void loop()
63 {
64  delay(100);
65  // send data only when you receive data:
66  if (Serial.available() > 0) {
67  // read the incoming byte:
68  char command = Serial.read();           //Read command
        byte
69  long incomingData = Serial.parseInt(); //Read data
        attached to it
70
71
72  if (Serial.read() == '\n')           //Wait for newline (ENTER)
73  {
74    //Serial.print(command);
75    //Serial.print(incomingData);
76    if (command == 'A')
77    {
78      //Serial.print("Data received:");
79      //Serial.println(incomingData);
80      calc_freq_reg(incomingData);
81    }
82    else if (command == 'B')
83    {
84      CTRL_signal();
85    }
86    else if (command == 'C')
87    {
88      val1 = analogRead(VPin);

```

Arduino program to control DDS AD5930

```
89     Serial.println(val1);
90   }
91   else if (command == 'D') //Low BATTERY Control
92   {
93     val1 = analogRead(VPin);
94     val2 = analogRead(PhasePin);
95     String stringOne = "M";
96     String stringTwo = stringOne + val1;
97     //           Serial.println(stringTwo);
98     String stringThree = "P";
99     String stringFour = stringThree + val2;
100    //           Serial.println(stringFour);
101    String stringFive = stringTwo + stringFour;
102    Serial.println(stringFive);
103    if (val2 < 307)
104    {
105      digitalWrite(LED, HIGH);
106      Serial.println("Low_Bat");
107    }
108    else
109    {
110      digitalWrite(LED, LOW);
111      Serial.println("Good_Bat");
112    }
113  }
114  else if (command == 'E')
115  {
116    val1 = analogRead(VPin);
117    val2 = analogRead(IPin);
118    val3 = analogRead(PhasePin);
119    String stringOne = "V";
120    String stringTwo = stringOne + val1;
121    //           Serial.println(stringTwo);
122    String stringThree = "I";
123    String stringFour = stringThree + val2;
```

```

124     //             Serial.println(stringFour);
125     String stringFive = "P";
126     String stringSix = stringFive + val3;
127     String stringSeven = stringTwo + stringFour;
128     String stringEight = stringSeven + stringSix;
129     Serial.println(stringEight);
130 }
131 else if (command == 'F')
132 {
133     Battery1 = analogRead(Bank1);
134     Battery2 = analogRead(Bank2);
135
136     String stringOne = "B1:";
137     float eq1 = (Battery1*5.0)/1024.0;
138     Serial.println(eq1);
139     float val1 = 3*eq1;
140     String stringTwo = stringOne + val1;
141     //             Serial.println(stringTwo);
142     String stringThree = "B2:";
143     float eq2 = (Battery2*5.0)/1024.0;
144     Serial.println(eq2);
145
146     float val2 = (eq2 - 3.70535)/0.18445;
147     String stringFour = stringThree + val2;
148     //             Serial.println(stringFour);
149     String stringFive = stringTwo + stringFour;
150     Serial.println(stringFive);
151     if (abs(val1) < 12)
152     {
153         digitalWrite(LED, HIGH);
154         Serial.println("Low_Bat_Bank1");
155     }
156     else if (abs(val2) < 12)
157     {
158         digitalWrite(LED, HIGH);

```

Arduino program to control DDS AD5930

```
159     Serial.println("Low_Bat_Bank2");
160 }
161 else
162 {
163     digitalWrite(LED, LOW);
164     Serial.println("Good_Bat");
165 }
166 }
167 else if (command == 'X')
168 {
169     Serial.println("Ok");
170 }
171 else
172 {
173     Serial.println("_is_an_incorrect_command_");
174 }
175 }
176 }
177 }
178
179 void AD5930_Control(uint16_t control)
180 {
181     control = control & 0x3FFF;           // Mask off upper 2
        bits so we are writing to control register
182     control = control | 0x2000;         // Ensure the B28
        control register bit is set
183     Serial.print("Control_command:");
184     Serial.println(control);
185     digitalWrite(ss, LOW);             // Set FSYNC low
186     delayMicroseconds(5);
187     AD5930_Write(control);
188     digitalWrite(ss, HIGH);           // Set FSYNC high
189 }
190
191 void AD5930_Write(uint16_t value)
```

```

192 {
193     SPI.transfer(highByte(value));
194     SPI.transfer(lowByte(value));
195 }
196
197 void AD5930_Phase(uint32_t phase)
198 {
199     digitalWrite(ss, LOW);           // Set FSYNC low
200     delayMicroseconds(5);
201     AD5930_Write(0xC000 | (0x1FFF & (uint16_t)(phase)));
202     AD5930_Write(0xE000 | (0x1FFF & (uint16_t)(phase>>12)));
203     digitalWrite(ss, HIGH);        // Set FSYNC high
204 }
205
206 void AD5930_Raw(uint16_t value)
207 {
208     digitalWrite(ss, LOW);           // Set FSYNC low
209     delayMicroseconds(5);
210     SPI.transfer(highByte(value));
211     SPI.transfer(lowByte(value));
212     digitalWrite(ss, HIGH);        // Set FSYNC high
213 }
214
215 void calc_freq_reg(long freq)
216 {
217     int MSB;
218     int LSB;
219
220     AD5930_Raw(0x0FFF);           // Reset
221     uint32_t AD5930Val = (uint32_t)((freq/(double)
        AD5930_F_MCLK) * (double)AD5930_2POW28);
222     MSB = (0xD000 | ((AD5930Val & 0xFFFF000)>>12));
223     LSB = (0xC000 | (AD5930Val & 0x0FFF));
224     AD5930_Raw(LSB);
225     AD5930_Raw(MSB);

```

Arduino program to control DDS AD5930

```
226 CTRL_signal();
227 }
228
229 void CTRL_signal()
230 {
231     digitalWrite(CTRL_pin, HIGH);
232     digitalWrite(CTRL_pin, LOW);
233 }
```